(1)

ESL-TR-88-02

SORPTION OF SELECTED VOLATILE ORGANIC CONSTITUENTS OF JET FUELS AND SOLVENTS ON NATURAL SORBENTS FROM GAS AND SOLUTION PHASES

P.S.C. RAO, R.D. RHUE, C.T. JOHNSTON, AND R.A. OGUADA

UNIVERSITY OF FLORIDA
INSTITUTE OF FOOD AND AGRICULTURAL SCIENCES
2109 MCCARTY HALL
GAINESVILLE FL 32611

AUGUST 1988

FINAL REPORT

APRIL 1985 - SEPTEMBER 1987

AFESC

ENGINEERING & SERVICES LABORATORY
AIR FORCE ENGINEERING & SERVICES CENTER
TYNDALL AIR FORCE BASE, FLORIDA 32403

UNCLASSIFIED
SECURITY CLASSIFICATION OF THIS PAGE

REPORT DOCUMENTATION PAGE

Form Approved OMB No. 0704-0188

1a. REPORT SECURITY CLASSIFICATION: UNCLASSIFIED	1b. RESTRICTIVE MARKINGS: N/A
2a. SECURITY CLASSIFICATION AUTHORITY: N/A	3. DISTRIBUTION/AVAILABILITY OF REPORT: Approved for public release. Distribution unlimited.
2b. DECLASSIFICATION/DOWNGRADING SCHEDULE: N/A	
4. PERFORMING ORGANIZATION REPORT NUMBER(S)	5. MONITORING ORGANIZATION REPORT NUMBER(S): ESL-TR-88-02
6a. NAME OF PERFORMING ORGANIZATION: University of Florida; 6b. OFFICE SYMBOL (If applicable)	7a. NAME OF MONITORING ORGANIZATION: HQ AFESC/RDVW
6c. ADDRESS (City, State, and ZIP Code): Institute of Food and Agri. Sciences, 2109 McCarty Hall, Gainesville FL 32611	7b. ADDRESS (City, State, and ZIP Code): Tyndall AFB FL 32403-6001
8a. NAME OF FUNDING/SPONSORING ORGANIZATION: Same as Block 7.; 8b. OFFICE SYMBOL (If applicable)	9. PROCUREMENT INSTRUMENT IDENTIFICATION NUMBER: F08635-83-C-0136 T.O. 85-7
8c. ADDRESS (City, State, and ZIP Code)	10. SOURCE OF FUNDING NUMBERS: PROGRAM ELEMENT NO. 62601F; PROJECT NO. 1900; TASK NO. 2077; WORK UNIT ACCESSION NO.

11. TITLE (Include Security Classification)
Sorption of Selected Volatile Organic Constituents of Jet Fuels and Solvents on Natural Sorbents from Gas and Solution Phases.

12. PERSONAL AUTHOR(S)
P. Suresh C. Rao, R. Dean Rhue, Clifford T. Johnston, and Richard A. Oguada

13a. TYPE OF REPORT	13b. TIME COVERED	14. DATE OF REPORT (Year, Month, Day)	15. PAGE COUNT
Final	FROM Apr 85 TO Sep 87	AUG 1988	

16. SUPPLEMENTARY NOTATION
Availability of this report is specified on reverse of front cover.

17. COSATI CODES			18. SUBJECT TERMS (Continue on reverse if necessary and identify by block number)
FIELD	GROUP	SUB-GROUP	Sorption coefficients, soils, mineral surfaces, aquifer materials, organic chemical transport, sorption equilibrium, spectroscopic techniques, JET FUELS, WATER POLLUTION (JES)
07	01		
07	04		

19. ABSTRACT (Continue on reverse if necessary and identify by block number)
Sorption of selected volatile organic constituents (VOC) of jet fuels and solvents on several natural sorbents from the gas and aqueous phases was investigated. The sorbates studied were trans-1,2-dichloroethylene; 1,2-dichloroethane; trichloroethylene; 1,1,2,2-tetrachloroethane; toluene; ethylbenzene; p-xylene; o-xylene; and cyclohexane. The sorbents used included clays (kaolin, montmorillonite, SAz-1), soils (Webster and Oldsmar), and aquifer materials (Borden and Lula). Sorption from the vapor phase was studied using three techniques: the headspace analysis method, dynamic flow method, and a gas chromatographic method. Sorption of VOC on anhydrous sorbents and sorbents in equilibrium with water at different relative humidities was examined. The energetics of sorption were characterized by measuring VOC sorption at several temperatures. Miscible displacement techniques were used to measure effluent breakthrough curves (BTC) for trichloroethylene (TCE) and p-xylene displacement in saturated columns of Lula and Borden aquifer materials. The BTC measured at two velocities were used to evaluate the utility of bicontinuum model for predicting sorption nonequilibrium during
(Continued on reverse.)

20. DISTRIBUTION/AVAILABILITY OF ABSTRACT	21. ABSTRACT SECURITY CLASSIFICATION
☒ UNCLASSIFIED/UNLIMITED ☐ SAME AS RPT. ☐ DTIC USERS	UNCLASSIFIED
22a. NAME OF RESPONSIBLE INDIVIDUAL: RICHARD A. ASHWORTH, Capt, USAF, BSC	22b. TELEPHONE (Include Area Code): (904) 283-4628; 22c. OFFICE SYMBOL: HQ AFESC/RDVW

DD Form 1473, JUN 86 — Previous editions are obsolete. — SECURITY CLASSIFICATION OF THIS PAGE

UNCLASSIFIED

19. ABSTRACT (continued).

transport. BTC measured for displacement of binary mixtures (TCE plus p-xylene) and single solute (TCE or p-xylene) were identical, suggesting no competitive sorption. Methods were developed for molecular-level investigations of sorption on clays using Fourier Transform Infrared (FT-IR) spectroscopic techniques. These methods were used to observe IR spectra of clay minerals as dry powders, thin self-supporting films, and aqueous slurries. IR spectra were obtained for kaolinite and montmorillonite clays as well as for p-xylene adsorbed on homoionic montmorillonite, both in the presence and absence of water. The application of FT-IR methods to study the p-xylene-clay complex provided a sensitive in-situ method to observe the surface-mediated transformation of the p-xylene on the Cumontmorillonite sample as the clay was dehydrated. Such a transformation was not noted on Na-montmorillonite.

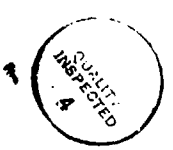

EXECUTIVE SUMMARY

BACKGROUND AND STUDY OBJECTIVES

The Air Force Installation Restoration Program has identified several sites of soil and groundwater pollution requiring remedial action. The most commonly reported organic contaminants at these Air Force sites and at other hazardous waste disposal/spill sites are volatile organic constituents of fuels and solvents. The current knowledge base is inadequate to fully understand the environmental behavior of numerous organic contaminants found at these sites. Lacking this knowledge, it is often difficult to develop and implement cost-effective technologies for cleanup and restoration of the contaminated sites. Therefore, it is necessary that an understanding of the processes and factors that govern the environmental transport and transformations of the organic contaminants be developed.

The purpose of the research was to study the sorption of several volatile organic components of jet fuels and solvents on model sorbents, soils, and aquifer solids. The focus of this study was not to develop an extensive data base of sorption parameters. Rather, the emphasis was on a characterization of kinetics, engergetics, and mechanisms of organic contaminant sorption using innovative experiemental approaches. Under Task 1, a literature search for publications dealing with organic contaminant sorption was conducted. The following is a brief description of the three specific tasks pertaining to experimental work done under this Task Order:

Task 2: The purpose of this task was to determine the sorptive capacities of anhydrous and hydrated sorbents for volatile organic contaminants. Those sorbate-sorbent systems showing appreciable adsorption were carried forward into Task 3 for further study.

Task 3: Under this task gas- and liquid-chromatographic techniques were adapted for measuring energetics and kinetics of volatile organic contaminant adsorption on natural sorbents.

Task 4: A single sorbate-sorbent system among those studied in Tasks 2 and 3 was selected for an investigation of sorption processes at the molecular-scale using Fourier Transform Infrared (FT-IR) spectroscopic techniques.

This report presents the results obtained under Tasks 2, 3, and 4. Data collected under Task 2 are discussed in Section II, while findings under Task 3 are presented in Sections III and IV. Finally, Section V of this report presents development and assessment of FT-IR techniques to study vapor sorption (Task 4).

SYSTEMS INVESTIGATED

The following alkyl benzenes and chlorinated alkanes and alkenes were selected for inclusion in this study: trans-1,2-dichloroethylene (t-DCE); 1,2-dichloroethane (DCA); trichloroethylene (TCE); 1,1,2,2-tetrachloroethane (PCA); toluene; ethylbenzene; p-xylene; m-xylene; o-xylene; and cyclohexane. These compounds represent common volatile organic constituents of jet fuels and solvents. These chemicals represent a broad spectrum of aqueous solubilities and volatiles. The sorbents studied included clays (kaolin, bentonite, and SAz-1), silica gel, soils (Webster and Oldsmar), and aquifer materials (Borden and Lula). These materials were selected as representatives of sorbents with low organic carbon content (<1 percent) and low surface areas ($<5 m^2 g$) commonly found in subsoils and aquifers. Pure clay mineral specimens were also used to represent the major clay species found in soils, sediments, and aquifer solids. Finally, the Webster surface soil was used as a reference sorbent with high organic carbon content (about 3 percent organic carbon content). The sorbents used exhibited a broad range in chemical and physical properties and the data gathered in this study permitted evaluation of sorption of organic compounds of interest at Air Force sites on a variety of sorbents.

SUMMARY OF KEY FINDINGS

Sorption of organic contaminants was studied using three techniques: a headspace analysis method, a dynamic flow method, and a gas chromatographic method. Since water has been shown to affect sorption of organics on polar sorbents, in this study we characterize sorption on sorbents with water contents ranging from complete saturation (i.e., aqueous suspensions) to near zero (i.e., anhydrous sorbents). These studies facilitated an evaluation of the competitive sorption of volatile organics and water on clays and soils, such that the sorption capacities of these sorbents in the unsaturated regions (vadose zone) and saturated regions (aquifers) can be assessed.

Adsorption on anhydrous and hydrated sorbents was studied at several temperatures in order to estimate the heats of sorption (ΔH_{ads}). With the exception of water adsorption on bentonite and alkylbenzene adsorption on Oldsmar soil, the measured isotherms for adsorption on anhydrous sorbents from vapor-phase conformed to type-II isotherms which were adequately described by the BET model. Sorbent surface areas calculated from the BET monolayer capacities indicated that, except for silica gel, the surface available for alkylbenzene adsorption was essentially that measured by nitrogen adsorption; adsorption on silica gel was lower than expected based on nitrogen surface area. The areas available for water adsorption were larger than those for alkylbenzene adsorption on all sorbents except silica gel which adsorbed more alkylbenzene than water. Plots of relative adsorption (i.e., the amount adsorbed divided by the BET monolayer capacity value) versus relative vapor pressure (P/P_o) showed that relative adsorption of water and p-xylene were similar for several diverse sorbents used both in this study and in the literature.

Competitive adsorption of water and p-xylene on kaolin and silica gel was

measured using several mixed-vapor systems where the relative humidities (RH) ranged from 10 to 70 percent and the relative vapor pressures varied from 0.1 to 0.5. Water adsorption on kaolin and silica gel appeared not to be affected by the presence of p-xylene over the entire range of P/P_o studied. Adsorption of p-xylene on silica gel and kaolin appeared to be only slightly affected by water at low relative humidities (RH <20 percent), but was dramatically reduced at higher RH. Strong dipole interactions of water with polar surfaces of the sorbents probably accounts for the observed suppression of p-xylene adsorption on hydrated sorbents.

The adsorption isotherms for anhydrous sorbents measured using the headspace method agreed closely with those obtained using the dynamic flow method. While the latter method has a practical working range of P/P_o from 0.03 to 0.9, the former technique permits adsorption measurements at lower vapor pressures ($P/P_o \sim 0.001$). Thus, using both methods, adsorption isotherms may be obtained over a board range of P/P_o.

The heats of adsorption (ΔH_{ads}) for several volatile organics were measured using the headspace method and a gas chromatographic (GC) method. By measuring adsorption isotherms at a minimum of two temperatures using the headspace method, ΔH values can be estimated as a function of surface coverage. The GC method facilitates rapid and more precise measurement of vapor adsorption at several temperatures and the estimation of ΔH_{ads} values at surface coverages approaching zero. The estimated values for heats of adsorption were, within the experimental errors, similar in magnitude to the heats of vaporization (ΔH_{vap}) and about 5 kJ/mole larger than the heats of solutions (ΔH_{sol}). Small heats of adsorption suggest nonspecific (physical) adsorption of these volatile organics on the sorbents studied. In the absence of compound-specific data, it is recommended that ΔH_{vap} values be used as the first-best estimates of ΔH_{ads}.

Batch equilibrium and miscible displacement studies were conducted to investigate the sorption and transport of trichloroethylene (TCE) and p-xylene in two aquifer materials. The utility of a bicontinuum sorption model to describe the extent of sorption nonequilibrium during transport through water-saturated columns of the aquifer solids was investigated. The effluent breakthrough curves (BTC) for tritiated water (used as a nonadsorbed tracer), TCE and p-xylene were measured at two pore-water velocities (v=6 and 24 cm/hr). The BTC measured at the high velocity were used to estimate the model parameters and were then used to successfully predict BTC obtained at the lower velocity. The BTC obtained at the lower velocity could also be described well using an equilibrium sorption model coupled to the convective-dispersive model. On the basis of model parameters, it was suggested that solute diffusion within the organic matter matrix was the rate-limiting step for sorption on these aquifer solids. First-order rate constants estimated using the column data were about 1000-times larger than those reported on the basis of <u>in situ</u> measurements for organic contaminant transport measured in natural-gradient field studies. Thus, at flow velocities typical in most aquifers the physical and chemical heterogeneities (e.g., layering) and mass transfer between domains of widely different flow velocities may have a more dominant impact on sorption nonequilibrium.

Three FT-IR sample presentation techniques were evaluated in order to determine the optimum noninvasive sampling techniques for vapor-phase adsorption of volatile organics on natural sorbents. FT-IR spectra of clay minerals obtained using diffuse reflectance (DR), cylindircal internal reflectance (CIR), and controlled-environment transmission (CE-TR) presentation methods were compared. The CE-TR method provided the highest signal-to-noise ratio (SNR) of the three methods investigated. The CIR and DR spectra obtained in this study represent the first reported application of these spectroscopic sampling methods to studies of clay minerals and clay-organic complexes. A controlled desorption study of p-xylene on sodium- and copper-saturated SAz-1 clay was performed. It was shown that a small amount of p-xylene was irreversibly sorbed on the sodium-saturated clay and that more water than the organic vapor was adsorbed. As the water content of the clay film was decreased, transformation products of p-xylene were formed on the copper-saturated clay, but not on the sodium-saturated clay. These results demonstrate the potential for using FT-IR spectroscopic techniques for noninvasive, molecular-scale investigations of sorbent-sorbate interactions. FT-IR techniques also offer increased sensitivity in comparison to earlier infra-red spectroscopic methods.

PRACTICAL APPLICATIONS OF FINDIINGS

With increasing concern over groundwater contamination, research on contaminant transport and fate, contaminant transport modeling, and groundwater remediation technology has grown rapidly. Knowledge of the various physical, chemical, and biological processes that affect contaminant behavior in groundwater is essential for such research. Of the various processes, sorption is one of the most important and can have profound effects on contaminant transport, fate, and dissipation.

Work done under the present Task Order focused on furthering our knowledge of sorption of organic contaminants on sorbents typically found in subsoils and aquifers. Adsorption of organic vapors was investigated on anhydrous sorbents and on hydrated sorbents equilibrated at a range of relative humidities. These studies coupled with those for sorption from aqueous solutions provide data covering the entire range of water contents likely to be encountered in surface soils, subsoils and aquifers. Under anhydrous conditions, similar to those likely to be found in dry soils in the upper few centimeters near ground surface, organic vapor sorption is determined primarily by the available surface area; the chemical characteristics of the sorbent surface seem to play only a secondary role. On hydrated sorbents, like those found in the vadose zone and in aquifers, the aqueous solubility of the contaminant and the organic carbon content of the solids play a dominant role in determining organic contaminant sorption.

In many groundwater contamination studies, the description of the sorption process is simplified by assuming the existence of local equilibrium. This assumption greatly simplifies contaminant transport modeling and may be quite adequate for certain situations. The validity of this approach has been questioned by a number of researchers as experimental data that challenge the local equilibrium assumption have been reported. The

impact of sorption nonequilibrium is twofold. First, the contaminant will be detected at a groundwater monitoring point earlier than that estimated on the basis of local equilibrium assumption. Second, contaminant desorption will take longer than that expected. The first effect means that down-gradient areas will be contaminated sooner, while the second effect implies that aquifer remediation by flushing (i.e., pump and treat) will probably take longer because of slow desorption. Column experiments we conducted allowed for an evaluation of the extent of nonequilibrium sorption of organic contaminants. While contaminant diffusion within the organic matter matrix was shown to be an important rate-limiting step, mass transfer limitations resulting from aquifer heterogeneities may have an even more significant impact on sorption nonequilibrium at the field-scale. Contaminant sorption and retardation parameters estimated using batch equilibrium and column displacement techniques in this study were in close agreement. However, the column displacement techniques are preferred because additional quantitative information on sorption nonequilibrium could be obtained.

The FT-IR spectroscopic techniques provided information at the molecular-scale enabling determination of organic contaminant sorption mechanisms. This noninvasive technique seems to offer considerable promise in the future, especially for characterizing sorption in the presence of water, a ubiquitous solvent.

(The reverse of this page is blank)

PREFACE

This report was prepared by the Soil Science Department, Institute of Food and Agricultural Sciences, University of Florida, Gainesville, Florida 32611, under Contract Number F08635-83-C-0136, Task Order Number 85-7, for the Air Force Engineering and Services Center, Engineering and Services Laboratory (AFESC/RDVW), Tyndall Air Force Base, Florida 32403-6001.

This report summarizes work done between 30 April 1985, and 30 September 1987. HQ AFESC/RDVW project officer was Capt Richard A. Ashworth.

The authors are indebted to the following colleagues who contributed to the successful completion of the work reported here: Mr Sture Edvardsson, for the gas chromatographic measurements of heats of sorption; Ms Linda Lee, for performing the miscible displacement studies; Mr Rick Smith and Mr Bill Reev for conducting the dynamic flow equilibration sorption experiments; Messrs Bruce Kreis, Randy McGrady, and Kurt Pennel, for assistance in gas chromatographic analyses; Mr Mark Brusseau, for literature review of nonequilibrium sorption models; Mr Ron Jessup, for assistance in statistical analysis and sorption model parameter estimation; and Profs Martin Walla and Willis Person, and Ms LeeAnn Applewhite, for assistance in FT-IR investigation. Mr Mark Sawka and Mr Bruce Kreis drafted most of the figures. Ms Brenda Clutter typed the revisions to this report.

Mention of trademarks and trade names of material and equipment does not constitute endorsement or recommendation for use by the Air Force, nor can the report be used for advertising the product.

This report has been reviewed by the Public Affairs Office (PA) and is releaseable to the National Technical Information Service (NTIS). At NTIS, it will be available to the general public, including foreign nationals.

This technical report has been reviewed and is approved for publication.

Richard A. Ashworth
RICHARD A. ASHWORTH, Capt, USAF, BSC
Project Officer

Thomas J. Walker
THOMAS J. WALKER, Lt Col, USAF, BSC
Chief, Environics Division

F. Thomas Lubozynski
F. THOMAS LUBOZYNSKI, Maj, USAF, BSC
Chief, Environmental Engineering Branch

Lawrence D. Hokanson
LAWRENCE D. HOKANSON, Colonel, USAF
Director, Engineering and Services Laboratory

(The reverse of this page is blank)

TABLE OF CONTENTS

TABLE OF CONTENTS
(Concluded)

LIST OF FIGURES

LIST OF FIGURES
(Continued)

LIST OF FIGURES
(Continued)

LIST OF FIGURES
(Continued)

LIST OF FIGURES
(Continued)

LIST OF FIGURES
(Concluded)

LIST OF TABLES

LIST OF TABLES

(Concluded)

SECTION I

INTRODUCTION

A. OBJECTIVES

The Air Force's Installation Restoration Program has identified several sites of soil and subsurface pollution requiring remedial action. Current knowledge is insufficient to understand the environmental fate of numerous organic pollutants found at these locations. Lacking this knowledge, it is difficult to develop technologies that are more cost-effective than current cleanup methods. In addition, there is a need to focus on research to predict organic contaminant transport. The purpose of this Task Order was to study the sorption of several organic chemicals on model sorbents, soils, and aquifer materials and to characterize the kinetics, energetics, and mechanisms of the sorption processes.

The objectives of the research conducted under the Task Order 85-7 were as follows:

1. Evaluate the contribution of nonhydrophobic (polar) interactions to equilibrium sorption of nonionic organic chemicals by model sorbents, soils, and aquifer materials.
2. Evaluate the applicability of gas-solid (GSC) and high-pressure liquid chromatographic (HPLC) techniques for measuring kinetics and energetics of nonionic organic chemical sorption on model sorbents, soils, and aquifer materials.
3. Investigate the mechanisms of sorption of nonionic organic chemicals on model sorbents, soils, and aquifer materials using Fourier Transform Infrared (FT-IR) and Laser-Raman spectroscopy.

B. BACKGROUND

1. Sorption of Organic Contaminants

The most commonly used model for the sorption of nonpolar organic chemicals is that of hydrophobic partitioning. Karickhoff (Reference 1) presented a comprehensive review of sorption of hydrophobic organic chemicals

(HOC) on soils and other natural sorbents. He discusses the limitations of the hydrophobic sorption concept and presents approaches to deal with the additional contributions of other sorptive mechanisms (e.g., polar) when present.

As with gas-solid sorption, sorption of HOC from liquid is characterized by equilibrium sorption isotherms. A linear sorption model [$S = K_d C$, where S and C are sorbed (μg/g) and solution (μg/mL) concentrations, and K_d is the sorption or partition coefficient (mL/g)], appears to describe HOC sorption from water by soils and other natural sorbents. The K_d value depends on three factors: the amount of nonpolar or lipophilic surface available on the sorbent; sorbate lipophilicity; and solvent surface tension (τ) or a related parameter.

Soil organic carbon content (OC) is an excellent measure of the amount of lipophilic surface area available for sorption of HOC. Thus, a close linear relationship is found between K_d and OC. This allows for calculation of OC-normalized sorption coefficient K_{oc} ($= K_d/OC$). For a given HOC, K_{oc} may vary only by a factor of 2 or 3 (Reference 1). Various indices of solute lipophilicity have been investigated. Among these, aqueous solubility (X_s), octanol-water partition coefficient (K_{ow}), nonpolar molecular surface area (HSA), and molecular connectivity indices (χ_1) have been successfully correlated with K_{oc} values.

In dissolving a nonpolar organic solute, a "cavity" will be created in the solvent to accommodate the solute. With increasing solute size (i.e., HSA) or the solvent surface tension (τ), the energy required to create the cavity increases, which leads to increased sorption. Addition of inorganic salts to aqueous solutions increases τ, while the addition of water-miscible organic cosolvents decreases τ. This explains "salting out" of hydrophobic solutes (increased sorption) on addition of salts, and a decrease in sorption in the presence of organic cosolvents (References 2 and 3). Several authors have also shown that HOC sorb independently (i.e., noncompetitive sorption) from complex solute mixtures (References 4, 5, 6).

Reversed-phase liquid chromatography (RPLC) has been used successfully as a surrogate model for HOC sorption on soils. Wauchope and co-workers (References 7, 8) have examined the thermodynamic basis for sorption of organic compounds by soils. Woodburn (Reference 9) presented the most recent and comprehensive theoretical and experimental basis for the use of RPLC. He

also reviewed the available chromatographic literature on energetics of sorption and collected extensive data for retention of a number of HOC on RPLC sorbents and Webster soil. The use of soils as packings in chromatographic columns has been attempted recently.

The use of miscible displacement (MD) techniques to measure equilibrium and kinetic parameters, however, has been the topic of debate among soil scientists for the past decade. Rao and Jessup (Reference 10) and Brusseau and Rao (Reference 11) have critically reviewed this literature and discussed the theoretical difficulties in estimating equilibrium and kinetic parameters for sorption using this method. Goerlitz (Reference 12) used the MD technique to measure sorption coefficients for phenol, pentachlorophenol (PCP), and naphthalene for an aquifer sediment sample. He fitted the measured solute breakthrough curves (BTC) to an analytical solution of the solute transport model (convection-dispersion plus equilibrium, linear, reversible sorption) to estimate the sorption coefficients (K_d). The limitations of this approach, attributed to sorption nonequilibrium, were more evident for naphthalene displacement than for phenol or PCP. Nkedi-Kizza et al. (Reference 13) have recently shown that K_d values measured by the batch equilibrium method and the MD technique were not different. They used a frontal analysis technique, based on the area above the solute BTC, to estimate sorption coefficients for two herbicides (atrazine and diuron). Condor and Young (Reference 14) also give a theoretical basis for the method used by Nkedi-Kizza et al. (Reference 13). This method can be used even if sorption equilibrium is not attained during displacement through the soil column, but the method has not been used by others. The use of batch suspension methods to characterize sorption kinetics has been presented by Karickhoff and Morris (Reference 15), extending earlier work by Karickhoff (Reference 16).

Gas chromatographic (GC) techniques can also be used to measure equilibrium sorption and related rate processes. The theory behind physicochemical measurements using GC has been detailed by Laub and Pecsok (Reference 17), Conder and Young (Reference 14), and Conder (Reference 18). The former involves the measurement of a chromatographic retention volume, while the latter involves examining the broadening of the chromatographic pulse. Conder (Reference 18) stated that while the application of GC to the study of equilibrium sorption has received considerable attention, its use to

study rate processes is the subject of continuing controversy because of uncertainty in the nature of rate equations needed to describe processes and/or factors leading to sorption nonequilibrium (intraparticle diffusion, kinetics, etc.). Conder (Reference 14) and Conder and Young (Reference 18) describe in detail a number of specific GC methods for measuring equilibrium sorption parameters.

The eluted pulse (EP-GC) technique applied to the Henry's law region allows for the calculation of the equilibrium sorption coefficient, K, as follows:

$$K_{GLC} = (V_N / V_L) \quad (1)$$

$$K_{GSC} = (V_N / A_s) \quad (2)$$

$$K_{GSC} = V_g = (V_N / m) \quad (3)$$

where V_N is the net retention volume for the sorbate (mL), V_L is the volume of the stationary phase (mL), A_s is the total surface area of the solid phase (m^2), m is the total mass of the solid phase (g), and the subscripts GLC and GSC indicate, respectively, gas-liquid chromatography and gas-solid chromatography. The Henry's region is identified chromatographically as that region for which (1) the chromatogram peaks are symmetrical, and (2) retention times, t_r, are independent of injected pulse volume.

The free energy of adsorption (ΔG_a°) is related to the equilibrium constant K through,

$$\Delta G_a^\circ = - RT \ln K \quad (4)$$

where ΔG_a° is the free energy change that occurs when 1 mole of sorbate in the gas phase in its standard state is transferred to the sorbent surface at some other specified standard state, and R is the gas constant (L·atm/mole·K). It can be shown that the enthalpy standard state (ΔH_a°) and the standard state entropy (ΔS_a°) changes for the adsorption process are calculated from:

$$\ln V_g = [-\Delta H_a^\circ / RT] + \text{constant}. \quad (5)$$

$$\Delta G_a^\circ = \Delta H^\circ - T \Delta S^\circ \quad (6)$$

where T is absolute temperature (K), and V_g is the specific retention volume (mL/g) of the sorbate at T. Note that Equation (5) was obtained from Equation (4) by the use of the Gibbs-Helmholtz equation:

$$\frac{\partial}{\partial T}\left(\frac{\Delta G^{\circ}_a}{T}\right) = -\left(\frac{\Delta H^{\circ}_a}{T^2}\right) \qquad (7)$$

By measuring V_g at several temperatures, i.e., several isothermal elutions, the energetic parameters may be calculated. Miller and Lee (Reference 19) described a novel experimental method for measuring heats of physical adsorption. Their method is based on thermal desorption of the gaseous sorbate in a continuous flow sorptometer and facilitates the estimation of the heats of sorption from a single experiment rather than several determinations as discussed in the foregoing paragraphs.

For nonlinear isotherms, i.e., outside the Henry region, the eluted pulse (chromatogram) is asymmetric and the retention times vary with eluted pulse volume or concentration. Under these conditions, the frontal analysis (FA-GC) is recommended for obtaining an adsorption isotherm over an extended range of sorbate partial pressures, (P). The enthalpy of adsorption is given by the Clausius-Clapeyron equation:

$$\ln P = [\Delta H_a / RT] + \text{constant} \qquad (8)$$

where ΔH_a is the isosteric heat of adsorption, and corresponds to the enthalpy change associated with the transfer of 1 mole of the adsorbate from the gas phase in equilibrium with the interface to the adsorbed phase at a fixed coverage, θ.

There are a number of published papers where the EP-GC and the FA-GC techniques have been used to evaluate the energetics of adsorption of volatile organics on synthetic sorbents, Gale and Beebe (Reference 20) gave a concise derivation of the enthalpies of adsorption from GSC retention data. They also derived equations which relate the surface coverage, θ, to known column and elution curve (chromatogram) parameters. Gale and Beebe (Reference 20) compared the enthalpies of sorption measured using GSC and calorimetry for a number of volatile sorbates on carbon blacks and bone mineral. The agreement in enthalpy values measured by the two methods was considered good, especially

considering the fact that the calorimetric values had to be extended to zero coverage ($\theta = 0$) in order to compared with those measured by the EP-GC method. Gale and Beebe (Reference 20) thoroughly investigated the usefulness of GSC techniques to evaluate the sorption energetics on well-characterized sorbents.

Flour and Paplrer (Reference 21) used the FA-GC technique to measure the adsorption isotherms for benzene and n-decane over a wide range of sorbate partial pressures (P/P_o) and calculated the surface free energy of short glass fibers. Their paper demonstrated the use of GSC techniques to evaluate the surface characteristics of the sorbent.

In contrast to the work done with synthetic sorbents, very little seems to have been published on the application of the GC techniques for characterizing the sorption of volatile organics on natural sorbents. The work by Bohn et al. (Reference 22) demonstrates the use of EP-GC to evaluate sorption of volatile hydrocarbons on soils. Bohn et al. (Reference 22) packed 1.83 and 3.3 m long (4 mm i.d.) columns with < 2 mm size fraction of several soils. These soil-GC columns were "baked" at 200°C to remove water and any organics before injecting the volatile hydrocarbons. Retention data were collected in the temperature range of 28 to 200°C and the specific retention volumes (V_g) at T = 15°C were determined by extrapolating the linear plots of ln V_g versus 1/T. The temperatures were selected to give symmetric elution peaks and t_r < 10 minutes. Two limitations in this paper are evident. First, it is not clear how the authors corrected the measured retention volumes for the column dead volume. Second, the authors did not investigate the effects of column packing reproducibility or the column diameter on their results, although there was evidence that V_g was affected by column packing. In spite of these limitations, however, Bohn et al. (Reference 22) found that for the volatile organics with the same number of carbons, t_r values decreased with branching of the carbon chains and increased with number of unsaturated bonds. Benzene and toluene had considerably larger t_r than did alkanes or alkenes. Bohn et al. (Reference 22) reported that these GC results were the opposite of those obtained for VHC sorption on semctite clay from dilute aqueous suspensions.

The work by Okamura and Sawyer (Reference 23) complimented the work of Bohn et al. (Reference 22) in that they studied sorption of volatilize organics on "water-modified" sorbents including soils (hydrated sorbents containing several layers of water). Okamura and Sawyer (Reference 23)

measured the specific retention volumes of alkanes and halomethanes on Gila silt loam, Rosita very fine sandy loam, Chromosorb W, Porosil C, and Porosil B at temperatures between 24 and 25°C. An important aspect of their study was that they attributed the measured retention volume to two factors: adsorption at the gas-water interface and partitioning into the sorbed water. They ruled out any significant sorption at the solid-water interface at the water contents they used. Water-modified Chromosorb W and Porosil C were evaluated as surrogate models for a moist soil. They concluded that water adsorbed on Chromosorb W was a good model for characterizing halomethane sorption by moist soils. At water contents approaching that of a very dry soil, sorption of both alkanes and halomethanes by Gila silt loam increased dramatically, indicating that water is a strong competitor for adsorption on the sorbent surfaces. In moist soil, adsorption onto water (i.e., at water-gas interface) was the dominant mechanism for retention of alkanes, while partitioning into the water phase was the dominant mechanism for halomethanes. These results are important because of their work with water-modified sorbents in GC, and because their results suggest that sorbent surfaces in natural systems may have little or no effect in retarding the transport of volatile organics.

An innovative variation of the "batch slurry" technique is the "headspace analysis" method for measuring sorption of volatile organics by soils with moisture contents ranging from a few percent to complete saturation. Garbarini and Lion (Reference 24) and Urano and Murata (Reference 25) have demonstrated the utility of this method. Chiou and Shoup (Reference 26) have investigated the sorption of a number of HOC by one soil at various relative humidities. Their findings confirm Okamura and Sawyers' (Reference 23) GC findings that water effectively out competes the HOC on mineral surfaces. This results in dramatic reductions (compared to anhydrous gas-solid systems) in HOC sorption by soils. For several chloroethanes, Urano and Murata (Reference 25) reported that K_d was proportional to OC and X_s. They also reported that the sorption of chloroethanes on sand, montmorillonite, and kaolinite was too small ($\leq$ 2 ng/g soil) to be measured by their technique. Friesel et al. (Reference 27) presented data for sorption of several volatile organics by soils, and these results were in general agreement with those of Urano and Murato (Reference 25). These finding are consistent with the hydrophobic model and suggest that the leaching of these compounds in aquifers (with low OC) would not be significantly retarded.

A potential problem with the headspace analysis method is the adsorption of the volatile organics at the water-gas interface, which can be misinterpreted as sorption on soil (at the soil-water interface). Drozd et al. (Reference 28) discussed the significance of this experimental artifact, while Okamura and Sawyer (Reference 23) explicitly accounted for it in their GC study.

2. Spectroscopic Investigations

Recent advances in the development and application of new vibrational spectroscopic methods (Reference 29), such as Fourier transform infrared (FT-IR), and laser Raman spectroscopic techniques are providing clay mineralogists with powerful tools to aid in the elucidation of solute interactions with natural substrates. Recent applications of advanced vibrational spectroscopic methods to the study of nonhumic organic solute behavior in the interfacial region will be briefly reviewed here.

Within the realm of optical absorption spectroscopy, the principal complementary techniques for investigating vibrational modes are infrared (IR) and Raman spectroscopy. The vibrational state transitions probed by IR spectroscopy must involve changes in dipole moment, whereas those probed by Raman spectroscopy must involve changes in polarizability (Reference 30). In principle, each technique can give a different picture of the vibrational spectrum. Hence, more complete characterization of the modes of atomic motion should result from applying both methods.

Infrared spectroscopy has long been one of the primary tools used for identification of molecular systems. Recent advances in the past 10 years in molecular microspectroscopy, laser technology, and computer data acquisition systems have led to the increased popularity of Raman techniques as complementary methods to IR absorption spectroscopy. One of the attractive aspects of Raman spectroscopy, insofar as its application to clay minerals is concerned, results from the fact that liquid water is much less Raman active than IR active. Water possesses this property because the fundamental vibrations of the water molecule induce a large change in its dipole moment but only a small change in its polarizability. As a result, Raman spectroscopy is uniquely suitable for studying the vibrational spectra of clay minerals in aqueous suspension, which better simulates natural conditions than

the sample presentation techniques used in IR studies of clay minerals (Reference 31). In addition, Raman spectroscopy can easily measure low-frequency vibrational modes which are difficult to measure using IR spectroscopy.

The Raman spectrum of kaolinite, a clay mineral commonly found in soil environments, was reported recently by Johnston et al. (Reference 32). The Raman spectra of a Georgia kaolin were studied in aqueous suspension as a function of clay solids concentration and pH and compared to IR spectra of dry kaolin samples. Several unique spectral bands were observed in the IR spectrum. Nonhumic organic molecules interact with environmental substrates through relatively weak chemical bonding mechanisms such as hydrogen bonding, ion-dipole, and protonation (Reference 33). Consequently, observation of low-frequency vibrational modes in the Far-IR and low-frequency Raman spectra of organic-solute:surface complexes should provide additional insight into the chemical mechanism(s) of solute behavior in the interfacial region. To date there have been no reported Raman or Far-IR studies of solute-surface interactions.

Raman and IR methods were combined by Johnson et al. (Reference 34) in a vibrational spectroscopic study of the kaolinite:dimethyl-sulfoxide (DMSO) complex. The structural framework modes of clay minerals are much less Raman-active than IR-active; thus, interference from these modes, such as Al-O and Si-O stretching and bending, is minimized in Ramam spectroscopy. In contrast, IR spectra of clay minerals and hydrous metal oxides below 1200 cm^{-1} are dominated almost entirely by the strong IR-active structural framework modes. Observing low-frequency vibrational modes of adsorbed species using IR methods is often not possible because the structural modes of the substrate completely obfuscate the lower-frequency spectral region (< 1200 cm^{-1}). The low-frequency Raman spectra of the kaolinite:DMSO complex were dominated by the spectral contributions from adsorbed DMSO rather than from the kaolinite substrate. To date, this study has been the only reported Raman and IR study of a clay-organic complex; however, because of the minimal interference present in Raman spectroscopy this technique should provide useful information in future studies.

Previous IR studies of clay mineral and hydrous metal oxide interactions with organic solute species have been limited to the severe sample presentation restrictions of conventional-IR spectroscopy. Virtually

all of the reported conventional-IR studies of clay/oxide-organic complexes used transmission sample presentation methods (Reference 35). Thus, samples were presented either as Nujoll mulls, thin, self-supporting films, thin films deposited on IR windows (AgCL, NaCl, KBr); or as KBr pellets. Results obtained using Nujoll mulls and KBr pellet presentation methods in particular are highly suspect as a result of interference from the Nujoll or KBr matrix, respectively.

Recent advances in solid state IR detectors, computerized data acquisition systems, IR optics, and laser technology have all contributed to the popularity of Fourier Transform Infrared spectroscopy during the past 10 years. The four principal advantages of FT-IR spectroscopy over conventional dispersive IR spectrometers are (Reference 36):

1. Fellgett (or multiplexing) advantage. Radiation of all wavelengths reaches the detector simultaneously. Thus, more energy reaches the detector at any given time.
2. Jacquinot (or throughput) advantage. The product of the solid angle and area of the beam at any focus is greater for an interferometer than for a monochromator.
3. Extremely high wavenumber precision. All modern FTIR spectrometers use a laser-referencing system for frequency calibration.
4. Digital file-handling capability of the data acquisition systems. FT-IR data files can easily be stored, compared, ratioed, and subtracted from other files.

To date, no reported FT-IR studies of clay- or hydrous metal oxide-organic complexes have been reported. Conventional, dispersive IR spectroscopy, however, has been a principal method of characterizing organic solute interactions with clay minerals and hydrous metal oxides. Moreale et al. (Reference 37) recently reported dispersive-IR spectra of the Fe(III)- and Cu(II)-montmorillonite-aniline complex. Aniline is rapidly adsorbed by montmorillonite clay minerals and the resulting complex undergoes dramatic color changes depending on the exchangeable cation. IR spectra of the clay-aniline complexes were obtained as thin films using a dispersive instrument; although the IR bands of the aniline are relatively strong, interference from the intense structural modes of the clay makes unambiguous

spectral interpretations of their data very difficult. Their data indicate that aniline can form a Type-II complex or polymerize, depending on the solution concentration of aniline and the type of exchangeable cation present on the surface of the clay.

The chemisorption of anisole (methyoxy-benzene) on Cu(II) hectorite has been studied (Reference 38) using IR and electron-spin resonance (ESR) spectroscopy. In addition to physical adsorption, methoxybenzene forms two distinct types of chemically distinct surface complexes. Dispersive, transmission IR spectra of thin films were obtained; however, the lower-frequency vibrational modes of the hectorite clay obfuscate a large portion of the low-frequency region. The methoxybenzene-hectorite complex appears to polymerize and form a very stable complex on the surface of the clay which is proposed to be 4,4'-dimethoxybiphenyl. Additional spectroscopic information is needed before conclusive band assignments can be made. The digital file-handling capability of FT-IR methods should provide a powerful method to reduce the background interference from structural clay modes by spectral subtraction.

Aochi et al. (Reference 39) reported the IR spectra of hydrous oxide coated montmorillonite-picloram (4-amino-3,5,6-trichloropicolinic acid) complexes. For Al- and Fe- exchanged montmorillonite-picloram complex, the IR data indicated the presence of the monomeric acid on the mineral surface. The Cu exchanged montmorillonite-picloram complex information was quite distinct from that observed for the Al- or Fe- systems indicating that the type of exchangeable cation on the surface plays a major role in determining organic solute interactions with mineral surfaces.

Several recent developments in sample presentation methods designed specifically for high-throughput FT-IR spectrometers have greatly increased the sampling capability of IR spectroscopy. Diffuse reflectance (DR) FT-IR methods have been developed over the past 10 years (Reference 40) and commercial DR attachments are currently available. Diffuse reflectance FT-IR methods provide a powerful means for observing the infrared spectra of powdered solids. Hamadeh et al. (Reference 41) have reported recently DR FT-IR spectra using a heatable evacuable diffuse reflectance cell designed for studying adsorbed species. Application of DR FT-IR methods to the study of organo-clay and oxide complexes should provide a useful means of better understanding the physical and chemical mechanisms of surface interactions.

C. APPROACH

A sound theoretical approach and an extensive experimental data base currently exist for describing organic chemical sorption in soils and sediments when hydrophobic interactions are dominant. In sharp contrast to this, only limited data are available describing HOC sorption on predominantly polar mineral sorbents such as those usually encountered in subsurface soil horizons and aquifer materials. Focus of the research in this task order is to study HOC sorption on sorbents having low organic carbon contents (OC), such as those found in subsoils and aquifer materials. In addition, pure clay mineral specimens representing the major clay species present in soils, natural sediments, and aquifer media will be used.

Since water has been shown to affect sorption of organics on polar sorbents, HOC sorption in systems ranging in water content from near zero to complete saturation (i.e., systems consisting of aqueous suspensions) will be evaluated. Emphasis in this research effort is on evaluating specific sorption processes and sorption theories rather than on extensive data collection. The data generated will be useful in the development and/or evaluation of theoretical approaches to HOC sorption.

The following is a brief description of these tasks found in Task Order 85-7:

Task 2: The purpose of this task was to determine the ability of a variety of sorbents such as clays, metal oxides, aquifer materials, and soil samples of varying OC to adsorb the nine nonionic chemical compounds in Table 1. Those systems showing appreciable sorption were carried forward into Task 3 for further study.

Task 3: The purpose of this task was to evaluate GSC and HPLC techniques for measuring sorption of volatile organics on natural sorbents. In addition, the techniques were evaluated for their ability to measure the energetics of HOC sorption on synthetic and natural sorbents.

Task 4: A single sorbate/sorbent system among those used in Task 3 was selected and the sorption processes occurring at the molecular level at the solid-solution interface were studied, using a variety of spectroscopic techniques such as FT-IR and Laser-Raman spectroscopy.

TABLE 1. VOLATILE ORGANIC COMPOUNDS SELECTED FOR USE IN TASK ORDER 85-7.

Compound	Chemical formula	Molecular weight, g	Boiling point, C°	Specific gravity	Aqueous solubility, mg/L
trans-1,2-di chloroethylene	CHClHCl	96.95	48.0	1.260	600 (20°C)
Cyclohexane	C_6H_{12}	84.16	81.0	0.779	55 (20°C)
1,2-dichloro-ethane	CH_2ClCH_2Cl	99.00	83.5	1.257	8,690 (25°C)
Trichloro-ethylene	CCl_2=CHCl	131.50	86.7	1.460	1,100 (25°C)
Toluene	$C_6H_5CH_3$	92.10	110.8	0.867	515 (20°C)
Ethylbenzene	$C_6H_5C_2H_5$	106.16	136.2	0.867	206 (25°C)
p-Xylene	$(CH_3)_2C_6H_4$	106.17	138.4	0.860	198 (25°C)
m-Xylene	$(CH_3)_2C_6H_4$	106.17	139.0	0.864	---
o-Xylene	$(CH_3)_2C_6H_4$	106.17	144.4	0.880	175 (20°C)
1,1,2,2, tetra-chloroethane	$CHCl_2CHCl_2$	167.86	146.4	1.600	2,900 (20°C)

Task 1 of this Task Order called for a critical review of key papers and reports available in the published literature on sorption of organic contaminants by soils, sediments, clay minerals, and synthetic media. A report summarizing our literature review was submitted to HQ/AFESC/RD, Tyndall Air Force Base.

This report presents results obtained under Tasks 2, 3, and 4. Experimental data for adsorption of several volatile organic chemicals (VOC) anhydrous and hydrated clays, soils, and aquifer materials from the vapor phase are discussed in Section II. The utility of gas chromatographic (GC) methods for characterizing the energetics of VOC sorption on several sorbents is discussed in Section III. A preliminary assessment of the GC methods to measure VOC adsorption isotherms is also presented in this section. Miscible displacement studies were conducted to examine nonequilibrium sorption of VOC in water-saturated columns packed with aquifer materials. The data from these studies and evaluation of a bicontinuum model to describe sorption nonequilibrium are presented in Section IV. Development and application of Fourier Transform Infrared (FT-IR) spectroscopic techniques for molecular-

level characterization of adsorption on natural sorbents are presented in Section V. For the ease of the readers, each section of this report contains a description of the experimental methods used to accomplish the task and a listing of the literature cited within each section.

D. REFERENCES

1. Karickhoff, S. W., "Organic Pollutant Sorption in Aqueous Systems," 1984, Amer. Soc. Civil Eng., J. Hydraulic Eng., Vol. 110, pp. 707-735.

2. Rao, P. S. C., Hornsby, A. G., Kilcrease, D. P., and Nkedi-Kizza, P., "Sorption and Transport of Hydrophobic Organic Chemicals in Aqueous and Mixed Solvent Systems: Model Development and Preliminary Evaluation," 1985, J. Environ. Qual., Vol. 14, pp. 376-383.

3. Nkedi-Kizza, P., Rao, P. S. C., and Hornsby, A. G., "Influence of Organic Cosolvents on Sorption of Hydrophobic Organic Chemicals by Soils," 1985, Environ. Sci. Tech., Vol. 19, pp. 975-979.

4. Chiou, C. T., Porter, P. E., and Schnedding, D. W., "Partitioning Equilibria of Nonionic Organic Compounds Between Soil Organic Matter and Water," 1983, Environ. Sci. Tech., Vol. 17, pp. 227-231.

5. Karickhoff, S. W., Brown, D. S., and Scott, T. A., "Sorption of Hydrophobic Organic Pollutants on Natural Sorbents," 1979, Water Res., Vol. 13, pp. 241-248.

6. MacIntyre, W. G., and deFur, P. O., "The Effect of Hydrocarbon Mixtures on Adsorption of Substituted Naphthalenes by Clay and Sediment," 1985, Chemosphere, Vol. 14, pp. 103-112.

7. Wauchope, R. D., and Koskinen, W. C., "Adsorption-Desorption Equilibria of Herbicides in Soils: A Thermodynamic Perspective," 1983, Weed Sci., Vol. 31, pp. 504-512.

8. Wauchope, R. D., Savage, K. E., and Koskinen, W. C., "Adsorption-Desorption Equilibria in Soils: Naphthalene as a Model Compound for Entropy-Enthalpy Effects," 1984, Weed Sci., Vol. 31, p. 744-751.

9. Woodburn, K. B., "Thermodynamics and Mechanisms of Sorption for Hydrophobic Organic Compounds on Natural and Artificial Sorbent Materials," Ph.D. Dissertation, University of Florida, pp. 350.

10. Rao, P. S. C., and Jessup, R. E., "Sorption and Movement of Toxic Organic Substances in Soils," in: Chemical Mobility and Reactivity in Soil Systems, (Eds.) D. W. Nelson, K. K. Tanji, and D. E. Elrick, 1983, Amer. Soc. Agron., Madison, WI, pp. 183-201.

11. Brusseau, M. L., and P. S. C. Rao, "Evaluation of Models for Sorption Nonequilibrium During Transport in Porous Media," 1987, CRC Critical Reviews in Environ. Control., (Manuscript in Review).

12. Goerlitz, D. F., "A Column Technique for Determining Sorption of Organic Solutes on the Lithologic Structure of Aquifers," 1984, Bull. Environ. Contam. Toxicol., Vol. 32, pp. 37-44.

13. Nkedi-Kizza, P., Rao, P. S. C., and Hornsby, A. G., "Influence of Organic Cosolvents on Leaching of Hydrophobic Organic Chemicals in Soils," 1987, Env. Sci. Techn., Vol. 21, pp. 1107-1111.

14. Condor, J. R., and Young, C. L., Physicochemical Measurements by Gas Chromatography, John Wiley and Sons, Inc., NY, 1979.

15. Karickhoff, S. W., and Morris, K. R., "Sorption Dynamics of Hydrophobic Pollutants in Sediment Suspensions," 1985, Environ. Toxicol. Chem., Vol. 4, pp. 469-477.

16. Karickhoff, S. W., "Sorption Kinetics of Hydrophobic Pollutants in Natural Sediments," in: Processes Involving Contaminants and Sediments, (Ed.) R. A. Baker, Ann Arbor Sci. Publ., Inc., MI, 1980, pp. 193-205.

17. Laub, R. J., and Pecsok, R. L., Physicochemical Applications of Gas Chromatography, John Wiley & Sons, NY, 1978.

18. Condor, J. R., "Physical Measurements by Gas Chromatography," in: Advances in Analytical Chemistry and Instrumentation. Vol. 6. Progress in Chromatrography, (Ed.) J. H. Purnell, Interscience Publishers (John Wiley and Sons, Inc), NY, 1967, pp. 209-270.

19. Miller, D. J., and Lee, H. H., "An Experimental Method for Determining Theat of Physical Adsorption," 1983, J. Catalysis, Vol. 81, pp. 281-290.

20. [illegible]e, R. L., and Beebe, R. A., "Determination of Heats of Adsorption on [illegible]bon Blacks and Bone Material by Chromatography Using the Eluted Pulse T[illegible]nique," 1964, J. Phys. Chem., Vol. 68, pp. 555-567.

21. Flour C. S., and Paplrer, E., "Gas-Solid Chromatography, A Method of Meas[illegible]ing Surface Free Energy Characteristics of Short Glass Fibers: 1. Through Adsorption Isotherms," 1982, Ind. Eng. Chem. Prod. Res. Dev., Vo[illegible]21, pp. 337-341.

22. Bohn, H. L., Prososki, G. K., and Eckhardt, J. G., "Hydrocarbon Adsorption by Soils as the Stationary Phase of Gas-Solid Chromatography," 1980, J. Environ. Qual., Vol. 9, pp. 563-565.

23. Okamura, J. P., and Sawyer, D. T., "Gas-Chromatographic Studies of Sorptive Interactions of Normal and Halogenated Hydrocarbons with Water-Modified Soil, Silica, and Chromosorb," 1973, J. Anal. Chem., Vol. 45, pp. 80-84.

24. Garbarini, D. R., and Lion, L. W., "Evaluation of Sorptive Partitioning of Non-ionic Pollutants in Closed System by Headspace Analysis," 1985, Env. Sci. Tech., Vol. 19, pp. 1122-1128.

25. Urano, K., and Murata, C., "Adsorption of Principle Chlorinated Organic Compounds on Soils," 1985, Chemosphere, Vol. 14L, pp. 293-299.

26. Chiou, C. T., and Shoup, T. D., "Soil Uptake of Organic Vapors and Effect of Humidity on Sorptive Mechanisms and Capacity," 1985, Env. Sci. Tech., Vol. 19, pp. 1196-1200.

27. Friessel, P., Milde, G., and Steiner, B., "Interactions of Halogenated Hydrocarbons with Soils," 1984, Fresenius Z. Anal. Chem., Vol. 319, pp. 160-164.

28. Drozd, J., Vejrosta, J., and Novak, J., "Spurius Adsorption Effects in Headspace-Gas Determination of Hydrocarbons in Water," 1982, J. Chromat., Vol. 245, pp. 185-192.

29. Bell, A. T., and Hair, M. L., "Vibrational Spectroscopies for Adsorbed Species," 1980, ACS Symposium Series No. 137, pp. _____.

30. Long, D. A., Ch. 3 in Raman Spectroscopy, McGraw Hill, 1977.

31. Farmer, V. C., "The Layer Silicates: Ch. 15," in: The Infrared Spectra of Minerals, (Ed.) V. C. Farmer, Mineralogical Society London, 1974, pp. 331-336.

32. Johnston, C. T., Sposito, G., and Birge, R. R., "Raman Spectroscopic Study of Kaolinite in Aqueous Suspensions," 1985, Clays and Clay Min., Vol. 33, pp. 483.

33. Mortland, M. M., "Clay-Organic Complexes and Interactions," 1970, Adv. Agron., Vol. 22, pp. 75.

34. Johnston, C. T., Sposito, G., Bocian, D. F., and Birge, R. R., "Vibrational Spectroscopic Study of the Interlamellar Kaolinite-Dimethyl Sulfoxide Complex," 1984, J. Phys. Chem., Vol. 88, pp. 5959.

35. Pinnavaia, T. J., "Intercalated Clay Catalysts," 1983, Science, Vol. 220. pp. 365.

36. Griffiths, P. R., "Fourier Transform Infrared Spectroscopy," 1983, Science, Vol. 222, pp. 297.

37. Moreale, A., Cloos, P., and Badot, C., "Differential Behavior of Fe(III)- and Cu(II)-Monmorillonite with Aniline: I. Suspensions with Constant Solid:Liquid Ratio," 1985, Clay Minerals, Vol. 20, pp. 29.

38. Fenn, D. B., Mortland, M. M., and Pinnavaia, T. J., "The Chemisorption of Anisole on Cu(II) Hectorite," 1973, Clays and Clay Min., Vol. 21, pp. 315.

39. Aochi, Y., and Farmer, W. J., "IR Spectroscopy of Picloram Interactions with Al(III)-, Fe(II)- and Cu(II)-Saturated and Hydrous Oxide Coated Montmorillonite," 1981, Vol. 29, pp. 191.

40. Fuller, M. P., and Griffiths, P. R., "Diffuse Reflectance Measurements by Infrared Fourier Transform Spectrometry," 1978, Anal. Chem., Vol. 50, pp. 868.

41. Hamadeh, I. M., King, D., and Griffiths, P. R., "Heatable-Evacuable Cell and Optical System for Diffuse Reflectance FT-IR Spectrometry of Adsorbed Species," 1984, J. Catalysis, Vol. 88, pp. 264.

(The reverse of this page is blank)

SECTION II

VAPOR-PHASE SORPTION OF VOLATILE ORGANICS

A. MATERIALS AND METHODS

1. Sorbents

Seven sorbents, which exhibited a range in chemical and physical properties, were selected for this study The sorbents and a listing of some of these properties are shown in Table 2. The bentonite and kaolin samples were obtained from Fisher Scientific, Fort Lawn, NJ., and were used as received without any pretreatment. The silica gel was micron size amorphous silica supplied by Davison Chemical, Baltimore, MD, intended for use as a chromatographic sorbent in liquid chromatography. The Oldsmar soil (Arenic Haplaquod) was a sample from the spodic horizon located approximately 1.1 m below the surface taken from a site in Collier County, FL. The Webster soil (Typic Haplaquod) was a sample from the surface horizon (0-30 cm) taken from a site in Iowa. The SAz-1 Montmorillonite was a reference clay obtained from the clay depository in Clay Bank, NE. The Lula aquifer material was taken from the top layer of the saturated zone on the Johnson ranch near Lula, OK.

Organic matter (OM) was measured using the Walkley-Black heat of dilution method (Reference 1). Total surface area was measured using the ethylene glycol monoethyl ether (EGME) procedure of Carter et al. (Reference 2). EGME forms a monolayer on all external mineral surfaces as well as a bilayer in the interlayer regions of Ca-saturated 2:1 layer silicate clays such as montmorillonite. Thus, the EGME method measures the total surface area which is accessible to polar molecules like water, and may overestimate the surface area accessible to nonpolar organics such as ethylbenzene and toluene since they are unable to expand the interlayers and enter the interlamellar regions of smectite clay. The surface area procedure of Carter et al. (Reference 2) calls for the use of a 60-mesh fraction of Ca-saturated soil treated with H_2O_2 to remove OM. The sorbents in Table 2 were used without this modification. Some uncertainty is introduced when the EGME method is used on sorbents that contain oxides and OM or exchangeable cations other than Ca since the surface area occupied by an EGME molecule on these surfaces is assumed to be the same

TABLE 2. PHYSCIAL AND CHEMICAL CHARACTERISTICS OF THE SORBENTS USED IN TASK ORDER 85-7.

Sorbent	Organic carbon	Surface Area		Texture			Clay mineralogy	Cation exchange capacity	NH_4Cl Extractable Bases			
		EGME	N_2	Sand	Silt	Clay			Na	Ca	Mg	K
	%	m^2/g		%				cmol(-)/kg	cmol(+)/kg			
Bentonite	0.48(±0.01)*	690(±4)	14.4	1	7	92	smectite	93.3(±2.0)	63.0(±1.5)	46.8(±1.2)	4.3(°0.1)	1.8(±0.1)
Kaolin	0.065(±0.002)	30.9(±0.3)	13.6	0	15	85	kaolinite	5.0(±0.6)	7.3(±0.2)	0.5(±0.1)	0.0	0.5(±0.1)
Silica Gel	0.045(±0.008)	395(±3)	238	--	--	--	amorphous	---	---	---	---	---
Webster Soil	3.02(±0.23)	101(±2)	4.2	55	20	25	smectite, vermiculite, mica, kaolinite	37.4(±1.1)	0.0	32.1(±1.0)	1.7(±0.1)	0.6(±0.1)
Oldsmar Soil	1.09(±0.04)	3.8(±0.4)	0.18	96	2	2	amorphous	5.2(±0.2)	0.0	4.4(±0.1)	0.3(±0.1)	0.4(±0.1)
Lula <60 mesh	0.012(±0.003)	10.5(±0.8)	7.7	93	4	3	smectite, kaolinite	---	---	---	---	---
Montmorillonite Arizona (SAz-1)	NA	810	97.42±0.58	--	--	--	---	120	---	---	---	---
Borden Aquifer Material	0.01	NA	0.3±0.0	--	--	--	---	NA	---	---	---	---

*Standard errors of determination are shown in parenthesis.

as that on Ca-saturated smectite. However, surface areas were measured on the untreated sorbents, since the untreated sorbents were used to measure sorption of water and organics. External surface areas were measured by N_2 adsorption at the Advanced Materials Research Center Analytical Division, University of Florida, Gainesville, FL.

Crystalline clays in the <2 μm clay fraction were identified using X-ray diffraction analysis as described by Jackson (Reference 3). Exchangeable cations were measured by extracting a known oven-dried (110°C) mass of each sorbent with five 10 mL aliquots of 1.0M NH_4Cl. The five 10 mL extractions were composited and diluted to 100 mL volume with deionized water. Calcium, Mg, K, and Na in the extracts were measured using a Jarrell-Ash Model 9000 ICAP. After the sediments were extracted with 1.0M NH_4Cl, they were Ca saturated by resuspending the sorbent in 20 mL of 0.05M $CaCl_2$, centrifuging, discarding the supernate, and resuspending in fresh $CaCl_2$ solution. This step was repeated five times. After the fifth time, the tubes were centrifuged, the supernates were discarded, and the tubes were weighed to obtain a measure of the salt solution entrained in the sediment. The sediment with entrained solution was then extracted with five 10 mL aliquots of $Mg(NO_3)_2$, the extractions composited and taken to 100 mL volume with deionized water, and Ca measured as above. Chloride was also measured in the $Mg(NO_3)_2$ extract and used to estimate the amount of Ca in the entrained solution. Exchangeable Ca was taken as the difference between total Ca in the $Mg(NO_3)_2$ extract and entrained Ca and was used as a measure of the cation exchange capacity (CEC) of the sorbent.

The bentonite and kaolin contained some free salts which can be seen by comparing the CEC with the sum of extractable Na, Ca, Mg, and K. These were apparently Na salts in the case of kaolin and perhaps a combination of Na and Ca salts in the bentonite. The Oldsmar soil was predominantly Ca saturated with no evidence of free salts. The sum of exchangeable bases was less than the CEC for the Webster soil, indicating the presence of some exchangeable acidity (H^+ and/or Al^{+3}) in the sample.

2. Sorbates

The sorbates used in this study consisted of water, ethylbenzene, toluene, p-xylene, trichloroethane (TCE), and cyclohexane. These chemicals

were reagent grade obtained from Fisher Scientific, Inc., and were used as received from the vendor.

3. Gas-Phase Sorption Studies

a. Dynamic Flow Method

(1) Apparatus

The apparatus used for measuring adsorption of water and the alkylbenzenes is shown in Figure 1. A carrier gas stream consisting of prepurified N_2 gas was used and the gas flow rate was regulated by the three needle valves, V1, V2, and V3. V2 controlled N_2 flow through a gas-washing bottle containing water; V3 controlled N_2 flow through a gas washing bottle containing liquid organic. By controlling the flow rates with the three valves, both the relative humidity and the relative vapor pressure (P/P_o) of the organic could be varied independently over a wide range of P/P_o values with the constraint that the sum of the two P/P_o values could not exceed one.

(2) Measuring Adsorption

The adsorbents were oven-dried at 140°C before use. This temperature was deemed high enough to remove all of the adsorbed water but not high enough to cause any irreversible alteration of the clay. Differential scanning calorimetry and thermal gravimetric analyses of the bentonite and kaolin indicated no loss of structural water at this temperature. Oven-drying the bentonite at this temperature did reduce the d(001) spacing to about 1.0 nm, as expected, but the spacing returned to about 1.5 nm on exposure to water vapor.

Approximately 1 gram of adsorbent was placed in oven-dried glass centrifuge tubes and sealed with screw caps fitted with Teflon^R-backed silicone rubber septa while both the tubes and clay were still hot. A total of four tubes containing clay and four blank tubes were placed in a series arrangement on the flow stream. The gas stream was then passed through the tubes via hypodermic needles punched through the septa. The gas flow rate was generally in the range of 0.75 to 1.1 mL/sec. The apparatus was housed in an

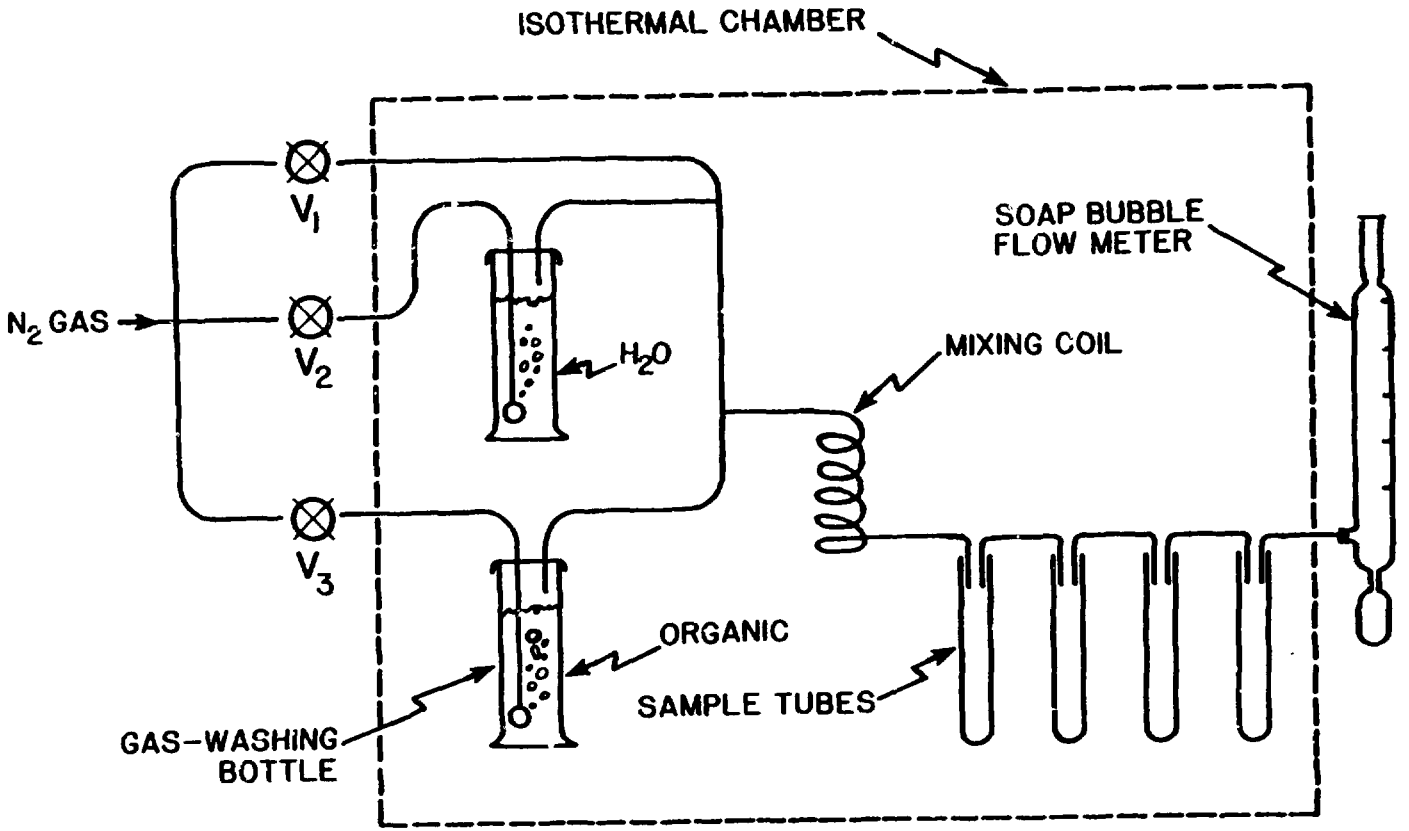

Figure 1. Schematic of the Dynamic Flow Equilibration Apparatus Used to Measure Sorption of Water and Volatile Organics.

insulated chamber and the temperature-controlled to ±0.1°C or less with a circulating, refrigerated water bath.

(3) Measuring Vapor Concentrations

To measure water vapor concentrations, approximately 20 mL of methanol were added to each of two 35 mL glass centrifuge tubes and the methanol titrated to a visual endpoint using the Karl Fischer (KF) reagent (Reference 4). All titrations were conducted while slowly purging the gas phase within the titration vessel with N_2 to prevent contact of the methanol solution with air. This preliminary titration removed water initially present in the methanol. The flow stream was then bubbled through the pretitrated methanol for a measured time. The solutions were then removed from the flow stream and immediately retitrated. A small amount of titer was always required by the second trap in the series, presumably caused by loss of volatile compounds from the KF reagent. This titer volume was subtracted from the titer consumption by the first trap and this corrected value was then used to calculate the amount of water trapped by the methanol.

Alkylbenzene vapors were trapped by bubbling the flow stream through 20 mL of methanol in each of two glass centrifuge tubes placed in series on the flow stream. The concentration of the alkylbenzene in these trap solutions was then measured with a Perkin Elmer Model 320 UV-VIS spectrophotometer by scanning the wavelength region between 230 and 320 nm at a rate of 120 nm/min and using a slit width of 1 or 2 nm. Maximum absorbance was compared to that obtained with alkylbenzene standards prepared in methanol in accordance with EPA Test Method 602 (Reference 5). The trap solutions were also analyzed by HPLC, using a CM 4000 pump and equipped with a Waters Model 490 UV detector. Samples were eluted isocratically using an 85:15 methanol-water solution flowing at 1.6 mL/min through a 25 cm C-18 RVP column. Peak areas were recorded with an HP 3392 integrator and compared to those obtained by injection of the appropriate alkylbenzene standards. Agreement between the spectrophotometric and HPLC methods was generally within a few percent. The amount of alkylbenzene found in the second trap was generally much less than 1 percent of that in the first trap, indicating that methanol was very efficient in trapping the alkylbenzene vapors.

Since the efficiency of methanol for trapping water and alkylbenzene vapors was not known, the results obtained with the methanol traps were compared with those obtained by trapping the vapor on activated charcoal. Activated charcoal was placed in polyethylene drying tubes and the traps were conditioned on a pure N_2 stream until they had achieved a constant weight. Two traps were then placed in series on the flow stream. The mass of vapor trapped was taken as the difference between the initial and final trap weights.

Vapor concentrations were calculated from the mass of water or alkylbenzene trapped and the total volume of carrier gas that had passed through the trap. Gas volumes were calculated from the average flow rate and total trap time and were not corrected for the volume of water or alkylbenzene vapor removed from, or for the volume of methanol vapor introduced into, the N_2 stream. These two sources of error were offsetting and both were found to be within the experimental error associated with the volume measurements. The vapor concentrations were converted to vapor pressure (P) assuming ideal gas behavior and the relative vapor pressure, P/P_o, was calculated using saturated vapor pressure (P_o) data from the Handbook of Chemistry and Physics (Reference 6).

(4) Measuring Adsorbed Phase Concentrations

Adsorbed phase concentrations of water and alkylbenzene were measured by extracting the adsorbents with 20 mL methanol containing $CaCl_2$. The $CaCl_2$ was necessary to flocculate the clays in the methanol suspensions. The $CaCl_2$-methanol solutions were made by adding 10 mL of a saturated $CaCl_2$-methanol solution to 1 L of pure methanol. The suspensions were shaken intermittently for about 2 hours and centrifuged at 1500 g for 10 minutes. Extraction times between 2 and 48 hours were found to have no effect on the amount of water or alkylbenzene extracted. Water in the methanol extracts was measured by KF titration; alkylbenzenes in the methanol extract were measured by HPLC and spectrophotometric methods. The alkylbenzene concentrations obtained by the two analytical methods were found to agree within a few percent except for Webster soil. Webster soil apparently contained methanol soluble compounds that interfered with the direct spectrophotometric analysis of the alkylbenzenes. The coefficient of

variation for adsorbed phase concentrations of water and the alkylbenzenes was generally on the order of one to two percent.

Adsorbed phase concentrations were also measured gravimetrically. In this latter method, the glass centrifuge tubes were weighed before and after exposure to vapor. The difference in weight, corrected for the weight change of the blank tubes, was taken as a measure of the amount of adsorbed water or alkylbenzene.

b. Static Headspace Method

Adsorption of p-xylene and TCE on Webster soil, kaolin, montmorillonite (SAz-1), and Lula aquifer material was evaluated. Adsorption experiments were carried out using both air-dry and oven-dry sorbents weighed into either 5 mL or 158 mL glass vials, respectively. Because of the low amount of adsorption by the air-dry sorbents, (2.5 to 4 percent gravimetric water content), 50 to 1000 µL of TCE or p-xylene vapor were taken from the headspace over the corresponding pure liquid in a 1-mL flask. These aliquots were then delivered to the 5 mL hypo-vials each containing 1 gram of the air-dry sorbent sample. A blank for each gas concentration in this study received the vapor but not the sorbent. Sorption on oven-dry sorbents (dried at 100°C for 48 hours) called for slight modification to the procedure used for air-dry sorbents. The sorption capacities for the oven-dry sorbents were so much higher than those for air-dry sorbents that the total mass of vapor contained in 2 mL of saturated vapor was insufficient to produce measurable vapor concentrations after equilibration. Hence, 158 mL vials were employed in this phase of the study. A 0.5 to 2.5 µL aliquot of pure liquid TCE or p-xylene was delivered to the vials containing 2 grams of sorbent. The syringe volume used was initially calibrated using two independent methods (gravimetric and spectrophotometric methods). After delivering the liquid compound to the vial, the vial was immediately sealed with Teflon^{R}-lined rubber septum in an aluminum crimp top.

Studies on air-dry and oven-dry sorbents were done in 3 and 2 replicates, respectively. The samples were equilibrated overnight in a 24 or 40°C water bath. Gas-phase analysis from the headspace of these samples and blanks was then performed by gas chromatography (GC). The Perkin Elmer Sigma 2000 gas chromatograph equipped with photoionization detector was used. The

column used was 100/120 supelcoport. Helium (grade 5) was employed as the carrier gas at a flow rate of 20 mL/min. The injector and the column were equilibrated at 225°C and 90°C, respectively.

Standard curves for TCE or p-xylene were made from the analysis of the vapor of the compound contained in 158 mL vials. To prepare the standards, various small aliquots (0.5, 1, 1.5, 2, 2.5 μL) of a pure liquid compound were introduced into each of the five 158 mL vials. The aliquots were delivered using a precalibrated airtight syringe. The mass of the compound contained in each aliquot was therefore known. After introducing an aliquot, the vial was immediately sealed and equilibrated under similar conditions as the sample before gas analysis by the GC. The equilibrium concentrations of both the samples and the controls were computed from the chromatographic peak areas using the standard curves. The amount of the compound adsorbed by the air-dry or oven-dry sorbent was calculated as the difference between the gas phase concentrations, the compound in the control and sample vials.

B. RESULTS

1. Dynamic Flow Method

a. Evaluation of Procedures

Table 3 compares methanol trap data for water and ethylbenzene vapor concentrations with those obtained using activated charcoal. Agreement between the two methods was quite good. However, trapping with methanol was much faster because of the shorter trap times required and the precision was equally as good as that obtained with the charcoal traps. In other studies, methanol was found to be as efficient as hexane for trapping alkylbenzene vapor and as efficient as molecular sieve for trapping water vapor.

Table 4 compares the gravimetric water content of several hydrated adsorbents with that obtained by methanol extraction and KF titration. The agreement between the two methods was quite good for bentonite and kaolin but not for silica gel. Silica gel retained water when dried at 140°C that was removed by methanol extraction. Bryant et al. (Reference 7) also found that the KF titration of air-dried silica gel measured more adsorbed water than was removed by oven-drying.

TABLE 3. COMPARISON OF TWO METHODS FOR MEASURING ETHYLBENZENE AND WATER VAPOR CONCENTRATIONS IN THE FLOW STREAM.

Compound	P/P_o	Trap Method	
		Carbon trap	Methanol trap
		mg/L	
Ethylbenzene	0.09	4.5 (±0.2)*	4.5 (±0.1)
	0.11	5.5 (±0.1)	5.2 (±0.1)
	0.24	11.5 (±0.2)	11.4 (±0.1)
	0.31	15.1 (±0.1)	14.9 (±0.2)
Water	0.14	3.1 (±0.1)	3.1 (±0.2)
	0.24	5.2 (±0.2)	5.20 (±0.07)
	0.38	8.2 (±0.1)	7.70 (±0.05)
	0.84	18.34 (±0.06)	17.58 (±0.10)

*Numbers in parenthesis are values for standard error of mean.

TABLE 4. COMPARISON OF GRAVIMETRIC AND METHANOL-EXTRACTABLE WATER CONTENTS OF HYDRATED ADSORBENTS.

Adsorbent	Method	
	Gravimetric	Methanol
	mg/g	
Bentonite	86.8 (±0.2)*	87.0 (±0.2)
Kaolin	7.4 (±0.2)	7.6 (±0.2)
	7.7 (±0.4)	6.46 (±0.06)
	4.3 (±0.2)	4.85 (±0.04)
Silica Gel	42.3 (±0.5)	58.8 (±3.2)
	46.8 (±0.8)	60.2 (±0.7)

*Numbers in parenthesis are values for standard error of mean.

Table 5 compares the data obtained using the gravimetric and methanol extraction methods for several other adsorbate-adsorbent combinations. The data for water plus p-xylene on kaolin were obtained by exposing the clay to a N_2 stream containing both vapors. In general, the agreement between the gravimetric and methanol extraction methods was quite

TABLE 5. COMPARISON OF GRAVIMETRIC AND METHANOL EXTRACTION METHODS FOR MEASURING ADSORBED PHASE CONCENTRATIONS.

Adsorbate	Adsorbent	Method	
		Gravimetric	Methanol
		----------mg/L----------	
Ethylbenzene	Bentonite	5.4 (±0.6)*	5.5 (±0.1)
		6.5 (±0.4)	5.6 (±0.2)
		7.9 (±0.5)	9.1 (±0.1)
		15.6 (±0.3)	14.2 (±0.2)
p-Xylene	Lula	1.9 (±0.4)	1.77 (±0.02)
Water plus p-xylene	Kaolin	8.7 (±0.2)	8.6 (±0.1)
		5.2 (±0.4)	5.08 (±0.06)
		19.3 (±0.6)	19.5 (±0.4)

*Numbers in parenthesis are for standard errors for the means.

good for the alkylbenzenes and the water plus alkylbenzene combinations. In other comparisons, complete isotherms for bentonite and kaolin, obtained using only carbon traps and gravimetric methods, were found to agree within experimental error with those obtained using only methanol traps and methanol extraction procedures. All isotherm data presented in the following section were obtained using the methanol trapping and extraction procedures.

b. Single Sorbate Isotherms

Figure 2 shows data for toluene, ethylbenzene, and p-xylene adsorption on bentonite, kaolin, silica gel, and Lula aquifer material. Alkylbenzene adsorption on Webster soil was similar in magnitude to that on Lula; adsorption on Oldsmar soil was very low and barely detectable over much of the range of relative vapor pressures shown in Figure 2. Differences in the amounts of the three alkylbenzenes adsorbed on a given adsorbent were generally quite small. The isotherms in Figure 2 conform to the Type II isotherms described by Sing et al. (Reference 8). The amounts of alkylbenzene adsorption on bentonite, kaolin, and silica gel show that mineral surfaces have a sizeable adsorption capacity for organic vapors when water is absent from the system.

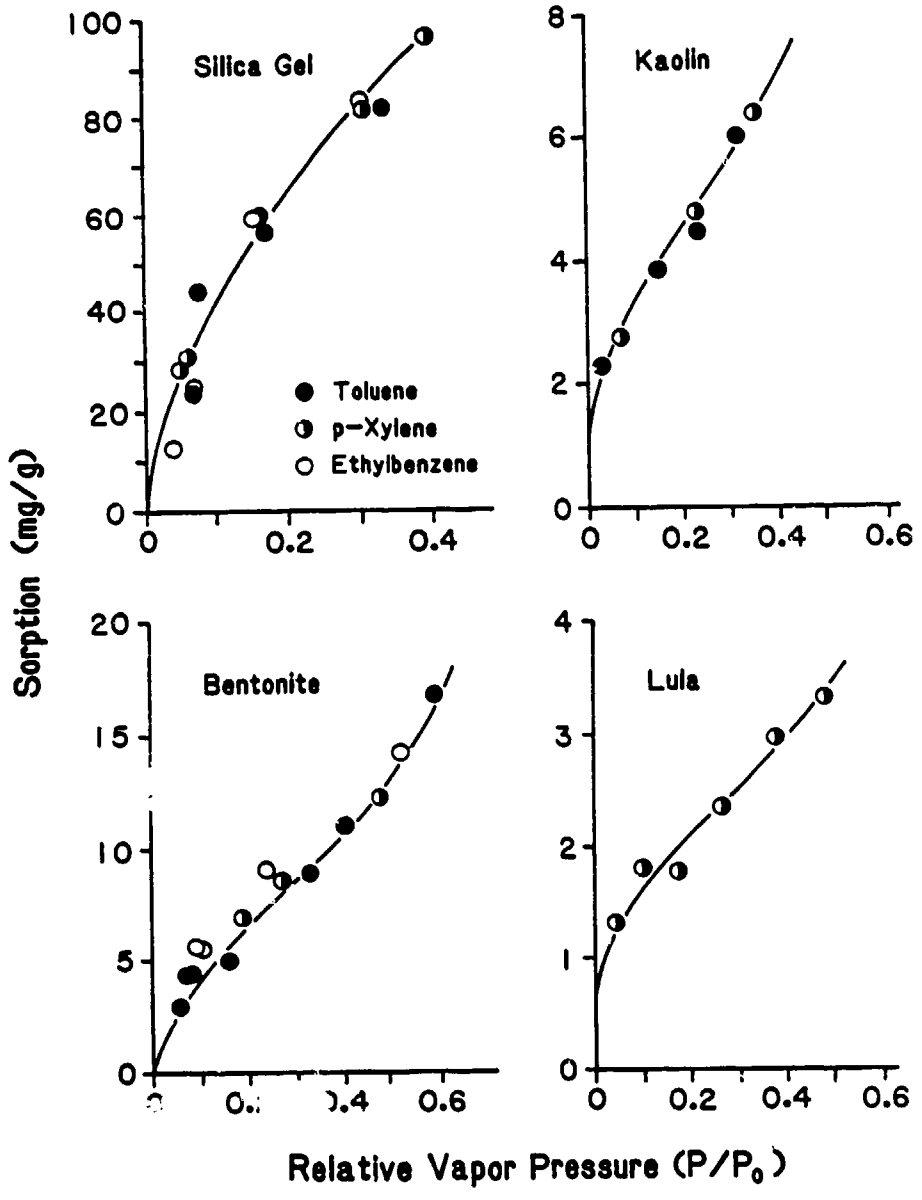

Figure 2. Adsorption Isotherms for Toluene, p-Xylene, and Ethylbenzene on Several Sorbents at 24°C.

Adsorption of water vapor on five of the adsorbents in Table 1 is shown in Figure 3. Water adsorption on Lula was very similar to that on Oldsmar soil. With the exception of bentonite, the isotherms for water adsorption were also Type II isotherms. Type II isotherms for water adsorption on soils and clays, including smectites, have been reported by others (References 9,10,11,12,). However, the water adsorption isotherm for bentonite in this study was distinctly different from that for the other adsorbents. Mooney et al. (Reference 13) obtained a water adsorption isotherm on Wyoming bentonite which was similar to the one in Figure 3, which they described as a combination of Type I and Type II isotherms. They attributed the unusual shape of the isotherm at relative humidities less than 60 percent to the complex processes of interlayer expansion of the clay platelets and the formation of a single layer of water molecules on the internal surfaces. Silica gel was unique among the six adsorbents in this study in that it adsorbed much less water than it did alkylbenzene. Van Voorhis et al. (Reference 14) observed that the monolayer adsorption capacity for water on an amorphous silica with a N_2 surface area of 309 m^2/g was about half that for benzene and toluene, which is consistent with the observations made here. In addition, the water adsorption data for the silica gel used in this study agreed well with the manufacturer's reported water adsorption capacity at these relative humidities.

Studies were conducted to determine the effect of equilibration times on the amount of sorption. Isotherm data corresponding to different equilibration times for sorption of toluene on bentonite are shown in Figure 4. Equilibration times ranged from as low as 7 hours to as long as 30 hours. The data indicate that exposure times longer than 7 hours had no measurable effect on the isotherm. Overnight equilibration times were adopted for convenience which generally resulted in sorbents being exposed to the vapors for 18 to 24 hours. In work to be reported below for ethylbenzene and water sorption on bentonite, exposure times of up to 10 days resulted in the same amount of water sorption as that measured in an 18- to 24-hour exposure. Thus, it is believed that the sorption data given in this section represent equilibrium sorption values.

Both adsorption and desorption isotherms were measured for some of the sorbents in Table 2. Figure 5 shows both adsorption and desorption isotherms for toluene sorption by kaolin and bentonite. Hysteresis is a term

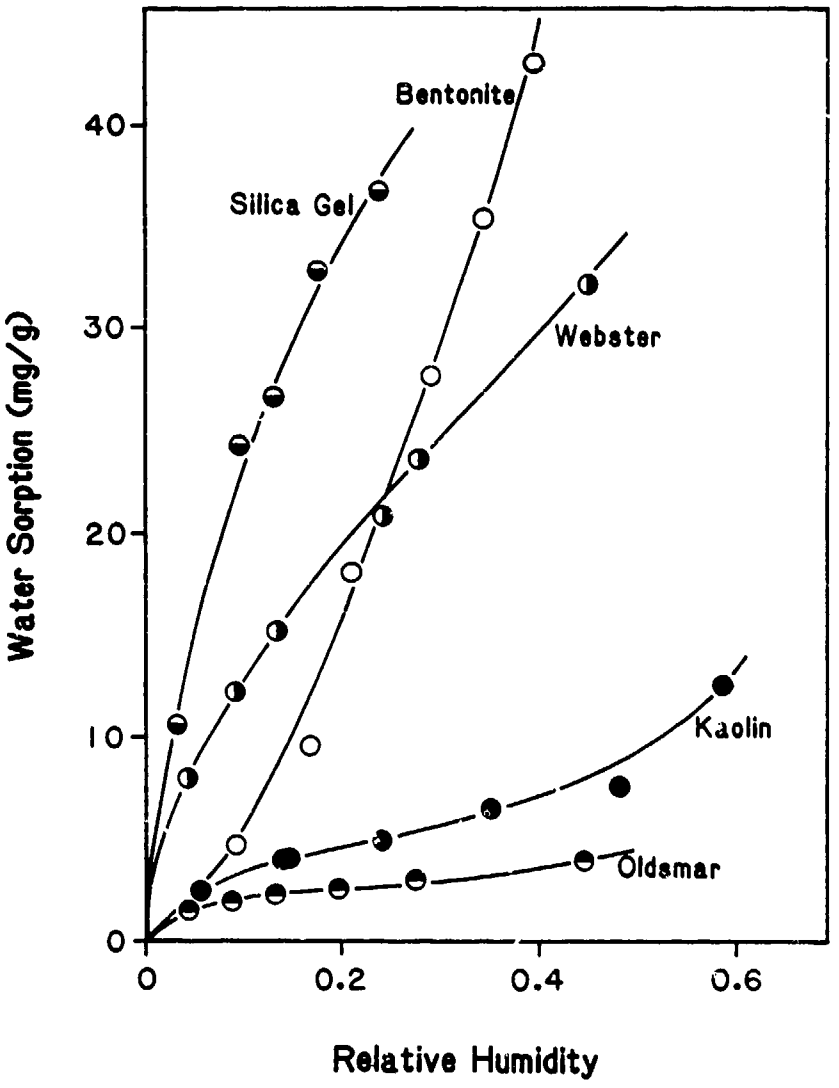

Figure 3. Adsorption Isotherms for Water Vapor on Several Sorbents at 24°C.

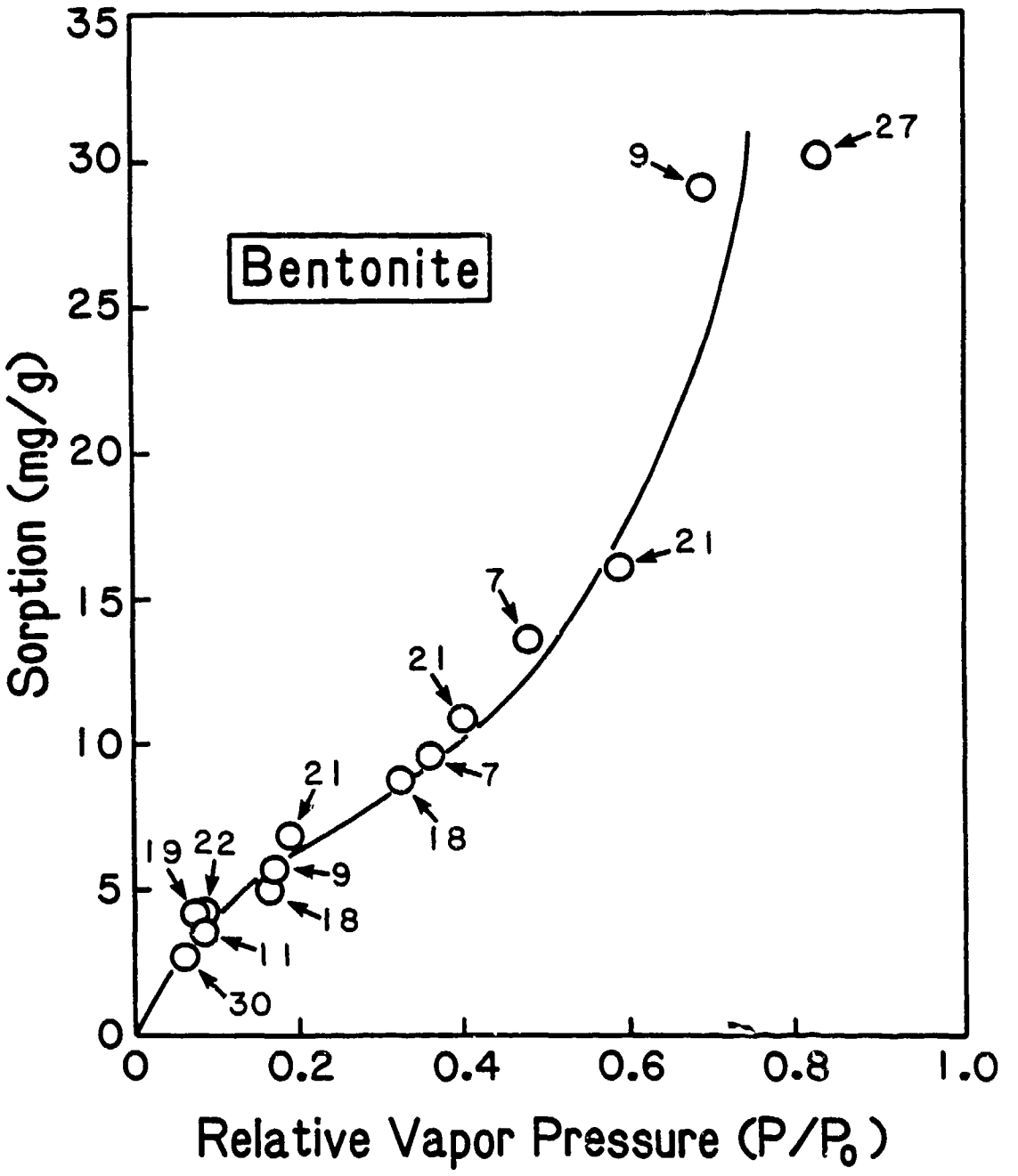

Figure 4. Adsorption Data for Different Equilibration Times (Numbers Shown Are in Hours) for Toluene on Bentonite.

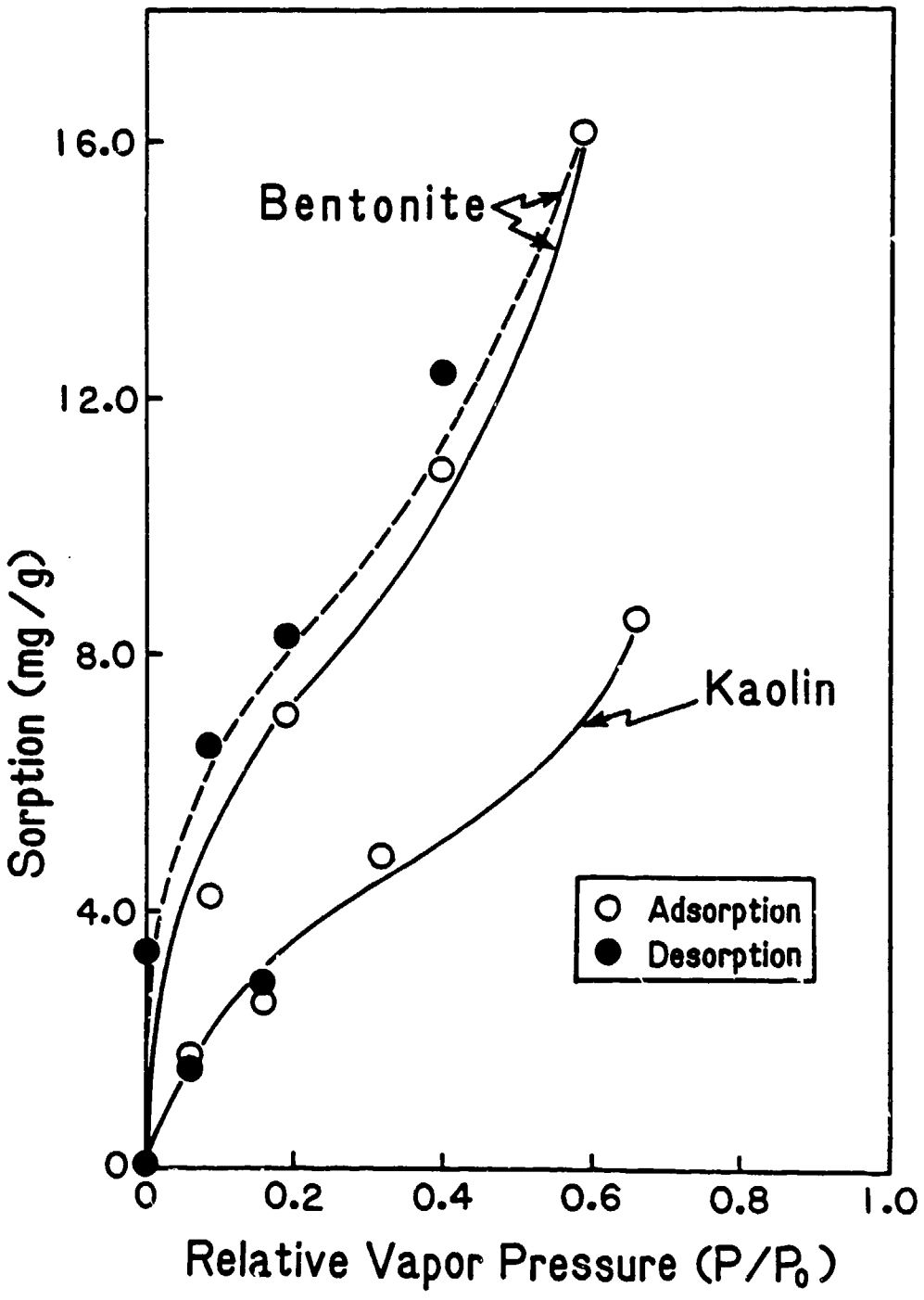

Figure 5. Adsorption-Desorption Isotherms for Tcluene on Two Clays at 24°C.

which describes the failure of the adsorption and desorption isotherms to coincide. Hysteresis was not observed with any sorbate on kaolin but was observed with all other sorbate-sorbent combinations studied. The desorption isotherms generally indicated a slightly higher amount of sorption than the corresponding adsorption isotherm. The hysteresis shown for toluene on bentonite was typical of that exhibited by the other sorbate-sorbent systems. Oven-drying the sorbents at 110°C following a desorption isotherm measurement restored the sorbent to the initial oven-dry weight it had before exposure to the vapors, showing that sorption in these instances was not completely irreversible. The HPLC analyses of the methanol trap solutions taken during the isotherm measurements did not reveal any degradation products of the organic vapors or indicate the presence of other volatiles coming from the sorbents. The isotherms presented in this section are adsorption isotherms only.

The adsorption data in Figures 2 and 3 were analyzed by a least squares procedure for fit to the linear form of the BET equation,

$$\frac{P/P_o}{S(1-P/P_o)} = \frac{1}{S_m C} + \frac{C-1}{S_m C}\ (P/P_o) \qquad (9)$$

where S and S_m are the amount adsorbed and the monolayer adsorption capacity, (mg/g), respectively; and C is a parameter related to the heat of adsorption. BET plots for several sorbate-sorbent combinations are shown in Figures 6 through 10. Estimates of S_m and C are shown in Table 6 along with the coefficients of determination (R^2) obtained from the regression analyses and an estimated P/P_o value associated with S_m. Application of BET theory to the water adsorption data on bentonite did not give any meaningful results, which might have been expected based on the unusual shape of the isotherm. Although the BET model is generally assumed to provide reliable estimates of the monolayer capacity for systems showing Type II behavior, the C values obtained from the theory do not provide quantitative measures of heats of adsorption (Reference 8). However, they do indicate the relative magnitude of the adsorbent-adsorbate interactions. The C values in Table 6 are indicative of the low interaction energies associated with physical adsorption processes.

C values of the magnitude shown in Table 6 are associated with Type II isotherms which do not have the sharp knees signifying completion of a monolayer prior to the onset of multilayer adsorption. The physical

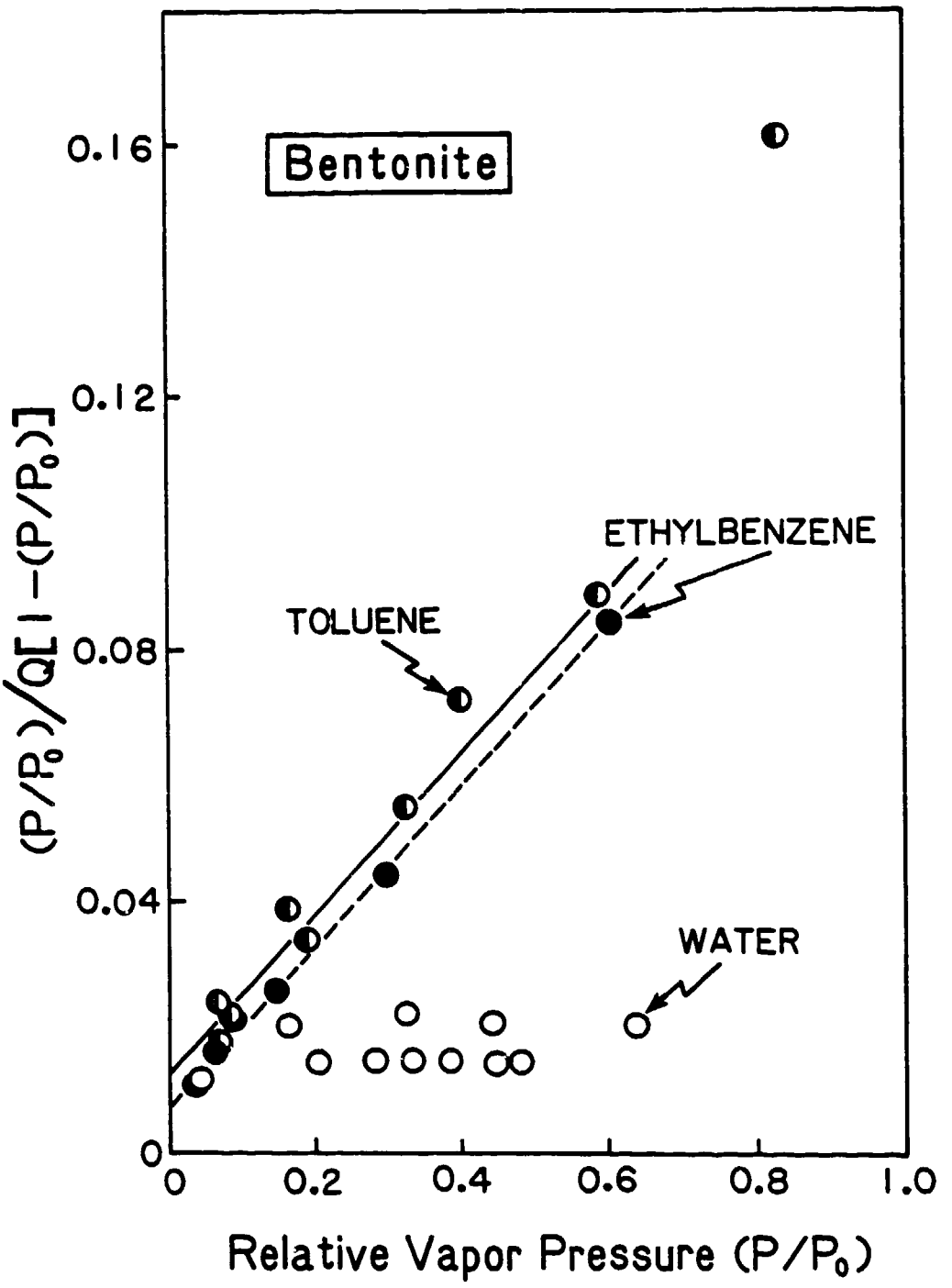

Figure 6. Linearized BET Plots for Water, Ethylbenzene, and Toluene Adsorption on Bentonite at 24°C.

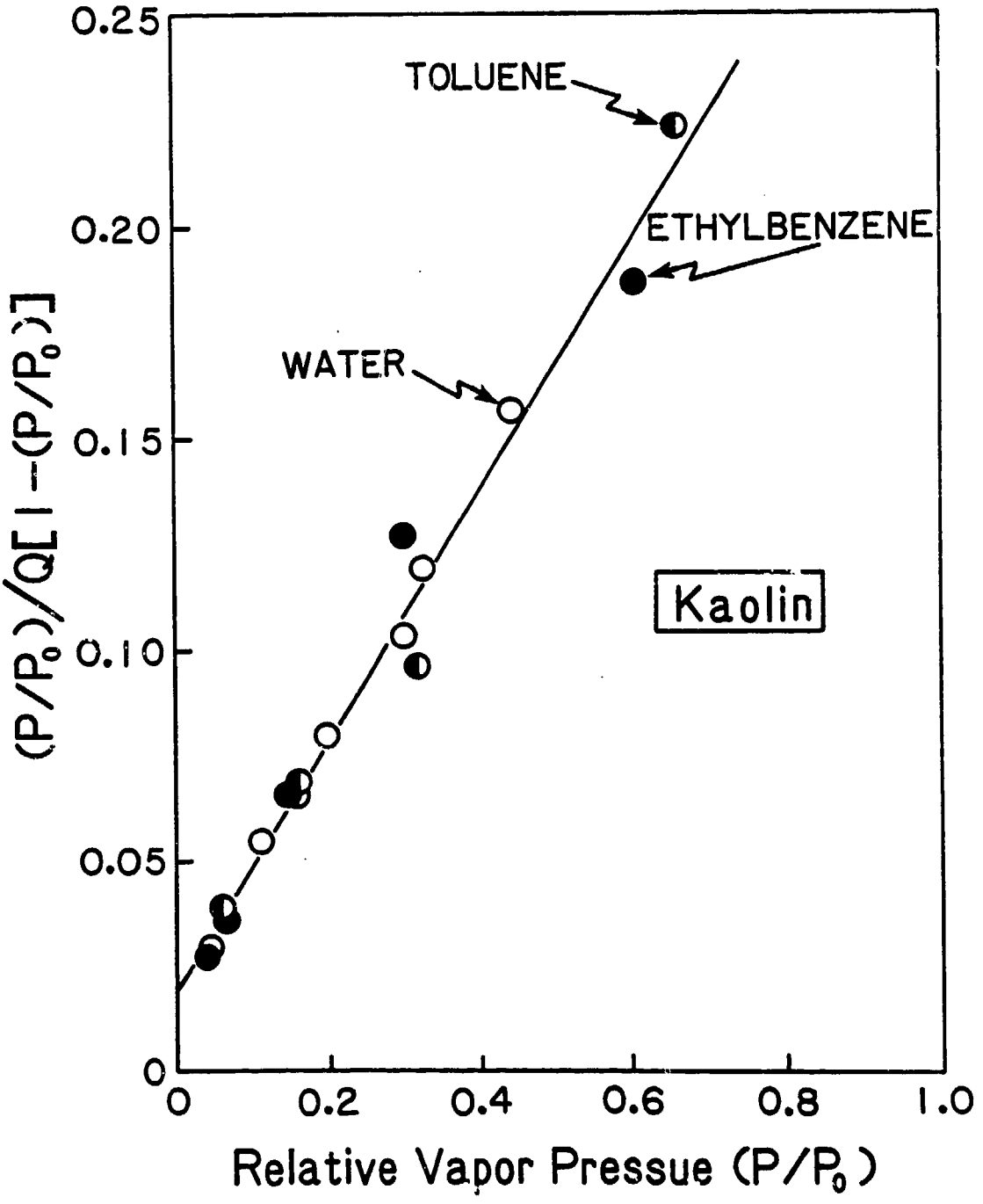

Figure 7. Linearized BET Plots for Water, Ethylbenzene, and Toluene Adsorption on Kaolin at 24°C.

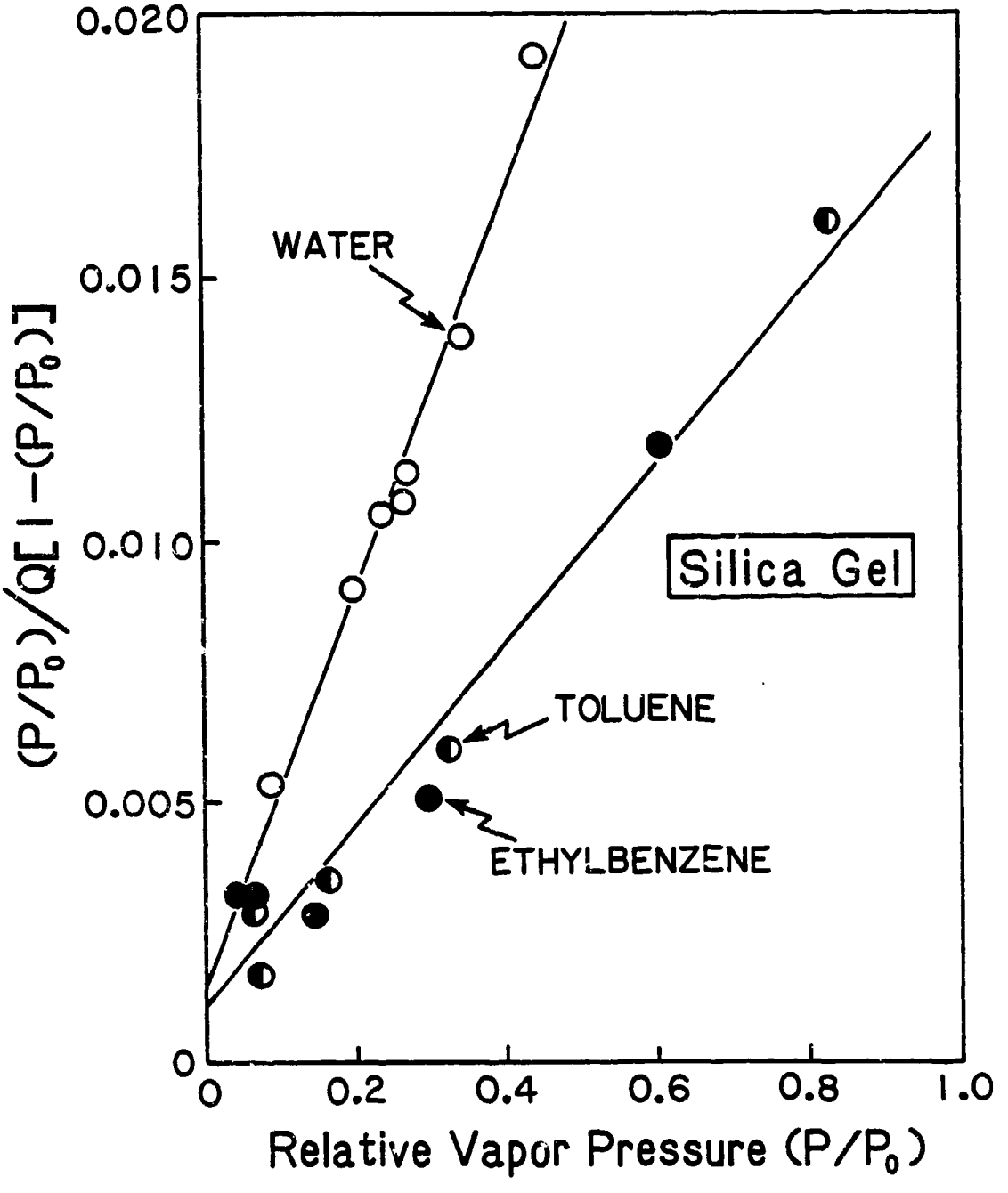

Figure 8. Linearized BET Plots for Water, Ethylbenzene, and Toluene Adsorption on Silica Gel at 24°C.

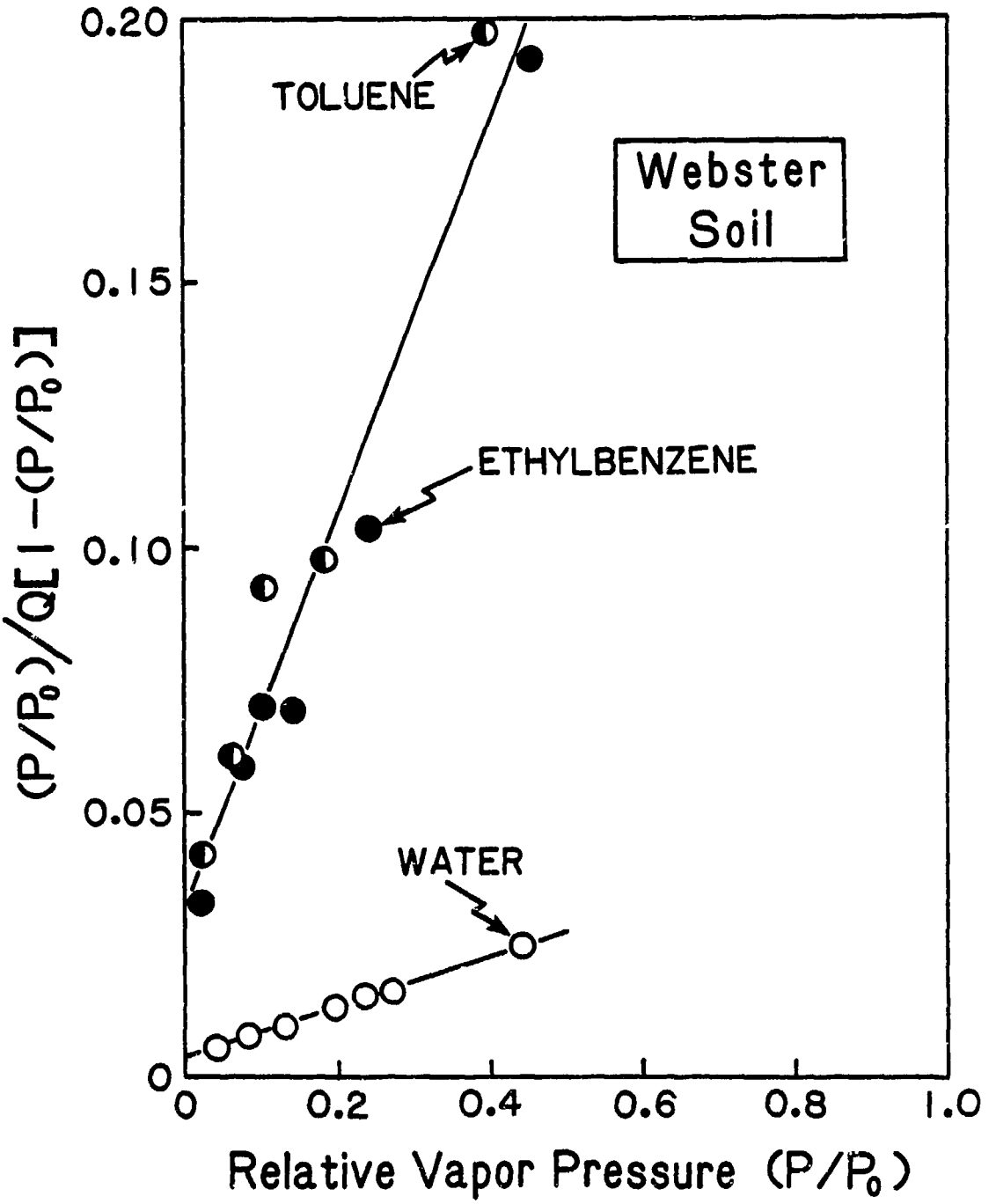

Figure 9. Linearized BET Plots for Water, Ethylbenzene, and Toluene Adsorption on Webster Soil at 24°C.

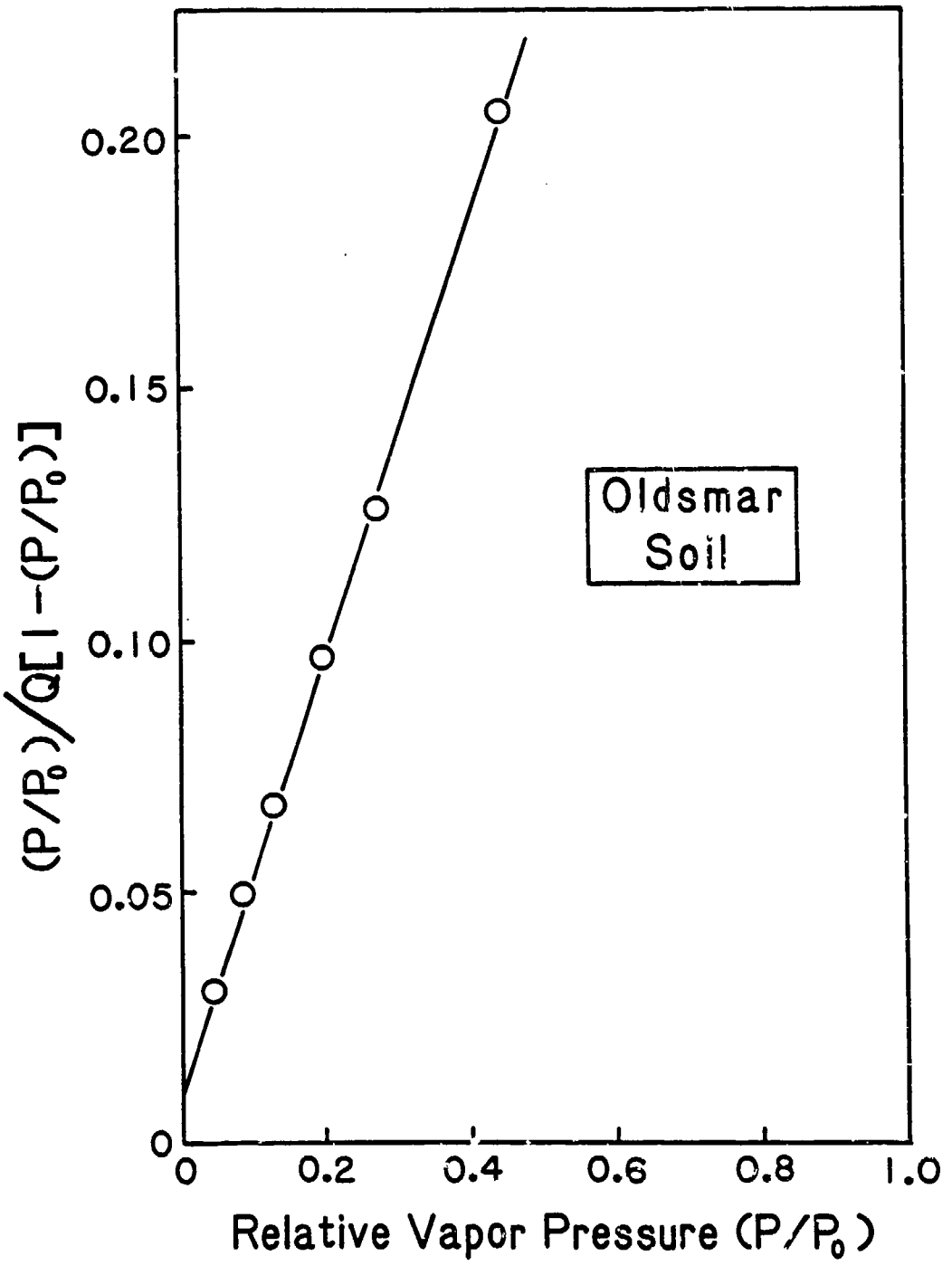

Figure 10. Linearized BET Plots for Water Adsorption on Oldsmar Soil at 24°C.

TABLE 6. PARAMETERS CALCULATED FROM ADSORPTION ISOTHERMS USING BET THEORY AND THE BET SURFACE AREAS CALCULATED FROM MONOLAYER COVERAGES

Adsorbent	Adsorbate	S_m	C	P/P_o	R^2	BET Surface area
		mg/g				m^2/g
Bentonite	Toluene	7.3	10	0.23	0.956	16
	Ethylbenzene	7.8	17	0.21	0.989	17
	p-Xylene	7.9	10	0.23	0.999	17
Kaolin	Toluene	4.2	27	0.17	0.968	9
	p-Xylene	4.6	18	0.19	0.998	10
	Water	4.2	22	0.17	0.990	15
Silica Gel	Toulene	65.3	12	0.21	0.918	146
	p-Xylene	64.7	17	0.20	0.997	139
	Water	33.8	18	0.18	0.998	119
Webster Soil	Toulene	2.3	12	0.19	0.976	5
	Ethylbenzene	2.6	14	0.18	0.984	6
	Water	19.5	14	0.20	0.998	69
Oldsmar Soil	Water	2.3	38	0.17	0.999	8
Lula Aquifer Material (<60 mesh)	p-Xylene	1.8	45	0.12	0.991	4
	Water	2.7	14		0.993	10

significance of S_m in these systems becomes uncertain in that a single layer of adsorbate covering the entire surface does not exist at any value of P/P_o. In these systems, multilayer adsorption is presumed to begin at surface coverages much less than one (Reference 8). Jurinak and Volman (Reference 15) concluded from thermodynamic studies that multilayer adsorption of ethylene dibromide (EDB) occurred on Ca-montmorillonite and Ca-kaolin at fractional surface coverages of only 0.65 and 0.35, respectively. C values for their montmorillonite and kaolinite systems were about 24 and 14, respectively.

Using the values for S_m in Table 6, along with estimates of the areas occupied by the adsorbate molecules, one can calculate the amount of surface area available for adsorption of a given compound. The adsorbate molecular areas for the alkylbenzenes and water were calculated, using the formula (References 16,17):

$$a_m = 1.091(M/\tau A)^{2/3} \quad (10)$$

where M is the adsorbate molecular weight, τ is the liquid density, and A is Avogadro's number. Equation (10) assumes a hexagonal close packing of adsorbate molecules at a density similar to that in the bulk liquid. The error introduced into surface area calculations by making the assumption of hexagonal close-packing has been discussed by Karnaukhov (Reference 16) and by McClellan and Harnsberger (Reference 17). The adsorbate molecular areas obtained with Equation (10) for water, toluene, ethylbenzene, and p-xylene were 0.105, 0.343, 0.375, and 0.380 nm^2, respectively. Surface areas calculated from the BET monolayer capacities and the above estimates of adsorbate molecular areas are shown in Table 6.

The BET surface areas in Table 6 indicate that the areas available for alkylbenzene adsorption on bentonite, kaolin, Webster soil, and Lula aquifer material were similar to those measured by N_2 adsorption. Jurinak and Volman (Reference 18) concluded that the surface area available for EDB adsorption in soil was that measured by N_2 adsorption. The interlamellar surface of smectite clay was inferred by Jurinak and Volman (Reference 18) to be inaccessible to EDB vapor and it appears from this study that it is also inaccessible to alkylbenzene vapors. For silica gel, the surface area available for alkylbenzene adsorption would appear to be only about 59 percent of that measured with N_2. Van Voorhis et al. (Reference 14) found that the adsorbate molecular area for toluene on their amorphous silica had to be 0.584 nm^2 in order for the BET surface area measured with toluene to agree with that measured with N_2. It is interesting to note that if a value of 0.584 nm^2 is assumed for the area per toluene molecule adsorbed on the silica gel used in this study, the toluene BET surface area would be 249 m^2/g, which is very close to the N_2 surface area shown in Table 1. The monolayer capacity of p-xylene on Oldsmar soil, estimated from its N_2 surface area, would be only about 0.08 mg/g. This is one to two orders of magnitude below that of the other adsorbents in Table 6 and explains why so little adsorption was detected.

The BET surface areas estimated from water adsorption data were similar to those measured with EGME for koalin, Oldsmar soil, and Lula aquifer material; they were much lower for silica gel and Webster soil. Makrides (Reference 20) concluded, after a detailed study of sorption on silica gels,

that surface areas estimated from water adsorption on silica gel were not reliable and argued that the N_2 surface area should more nearly reflect the true area of the gel. The molecular area for water adsorbed on silica gel in this study, calculated from the N_2 surface area, was 0.210 nm^2 which is well within the range of values reported in the literature.

N_2 surface areas of organic soils or of OM extracted from soil are typically a small fraction of those measured with water or other polar adsorbates. Jurinak and Volman (Reference 18) found that the EDB surface area of a muck soil (35 percent OM) was only about 8 percent of that measured by ethylene glycol adsorption. Chen and Schnitzer (Reference 9) reported that the BET surface areas measured by water adsorption on humic and fulvic acids were about 210 m^2/g while the N_2 surface areas were only about 2.5 m^2/g. These results suggest that soil OM has a much lower adsorption capacity for organic vapors than it does for water. This would explain why water adsorption on Oldsmar spodic material, with its low clay and relatively high OM content, was considerably greater than alkylbenzene adsorption. Both the relatively high OM content and the presence of smectite clay in the Webster soil would contribute to the high water adsorption relative to alkylbenzene adsorption. In contrast, alkylbenzene adsorption on kaolin and silica gel, which had little or no OM, equalled or exceeded water adsorption.

Figure 11 shows the relative water adsorption, S/S_m, as a function of relative vapor pressure, P/P_o, for three of the adsorbents in Table 2. The use of relative adsorption allows a comparison of the adsorptive capacity of various adsorbents on a per unit of surface area basis. Coincidence of the relative adsorption curves for several adsorbents can then be taken as evidence that the adsorbent-adsorbate interactions are similar in each case. Although the relative water adsorption was very similar for these three adsorbents, there was a slight increase in relative adsorption corresponding to an increase in the value of C. Thus, Oldsmar (C=38) exhibited higher relative adsorption than kaolin (C=22), which, in turn, exhibited higher relative adsorption than Webster soil (C=15). Included in Figure 3 are data for water adsorption on kaolin at 10°C by Jurinak (Reference 19), and on Woodburn soil at 25°C by Chiou and Shoup (Reference 21). The sample of Woodburn soil used by Chiou and Shoup (Reference 21) contained 1.9 percent OM, 21 percent clay, and had kaolin and mica as the dominant clay minerals.

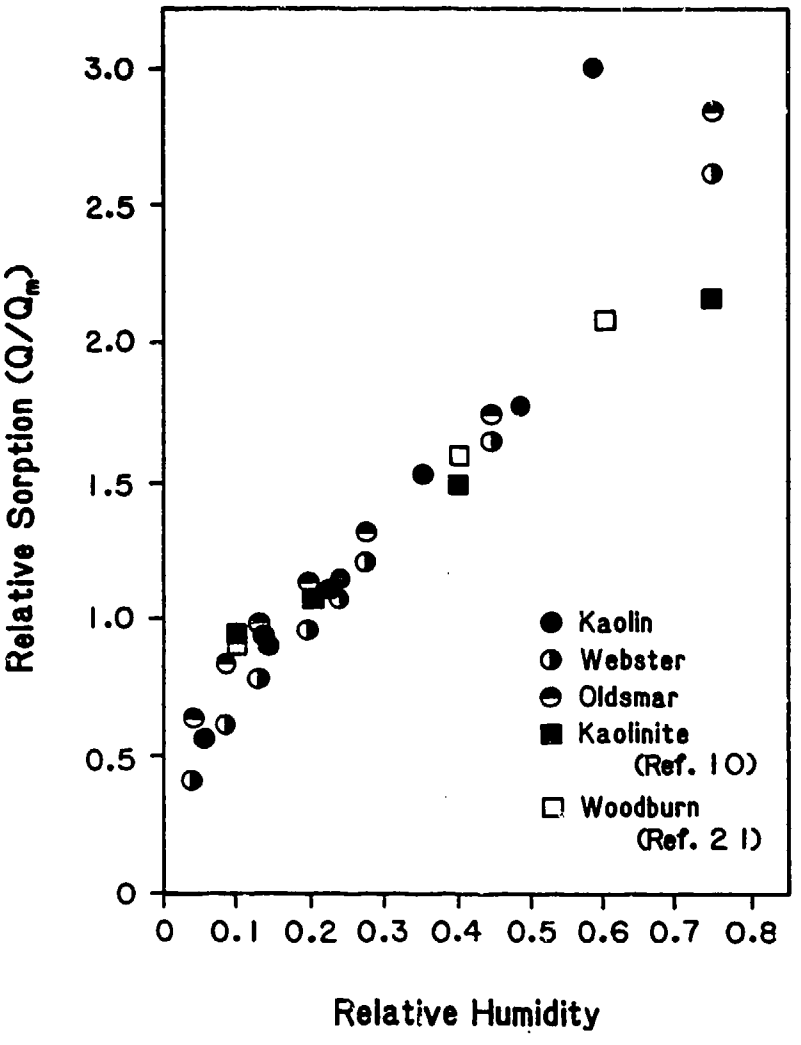

Figure 11. Relative Adsorption of Water on Several Adsorbents as a Function of Relative Humidity.

Relative adsorption of p-xylene is shown in Figure 12. The increase in relative adsorption with an increase in C is also apparent with the p-xylene data. No data were found in the literature for alkylbenzene adsorption on soils with which to compare the results found here. However, Chiou and Shoup's (Reference 21) data for benzene adsorption on Woodburn soil are shown in Figure 5 and appear to fall within the range of relative adsorption obtained for p-xylene in this study. The general agreement among the various sources of data in Figures 11 and 12 suggests that water and alkylbenzene adsorption by soils and clays is controlled primarily by the available surface area and is much less affected by the specific mineral and organic surfaces present.

Vapor-phase adsorption of cyclohexane onto kaolin was also measured and is shown in Figure 13. Adsorption of this organic differed from that of the alkylbenzenes in that it showed Type III adsorption behavior, indicating that the heat of adsorption onto kaolin was less than the heat of condensation onto the pure liquid. However, this is purely speculative since sorption did not conform to the BET theory in that a plot of Equation (9) for this system did not result in a straight line.

c. Competitive Sorption of Water and Organic Vapors

(1) Ethylbenzene and Water on Bentonite

Table 7 gives the relative vapor pressures of water and ethylbenzene and the resulting values for water and ethylbenzene sorption on bentonite. The results are shown in Figures 14 and 15 along with the sorption isotherms obtained on the corresponding single sorbate systems.

Sorption of ethylbenzene was not affected by water at 23 percent RH (Figure 14). Compared to sorption measured in the absence of water, ethylbenzene sorption at 50 percent RH was reduced 15 percent at the highest ethylbenzene vapor pressure and 58 percent at the lowest ethylbenzene vapor pressure. Thus, the effect of water was more pronounced at lower ethylbenzene vapor pressures. In contrast, ethylbenzene at relative vapor pressures as high as 0.48 had no measurable effect on water sorption (Figure 15). The data show that, above 23 percent RH, water competes strongly with ethylbenzene for sorption on bentonite.

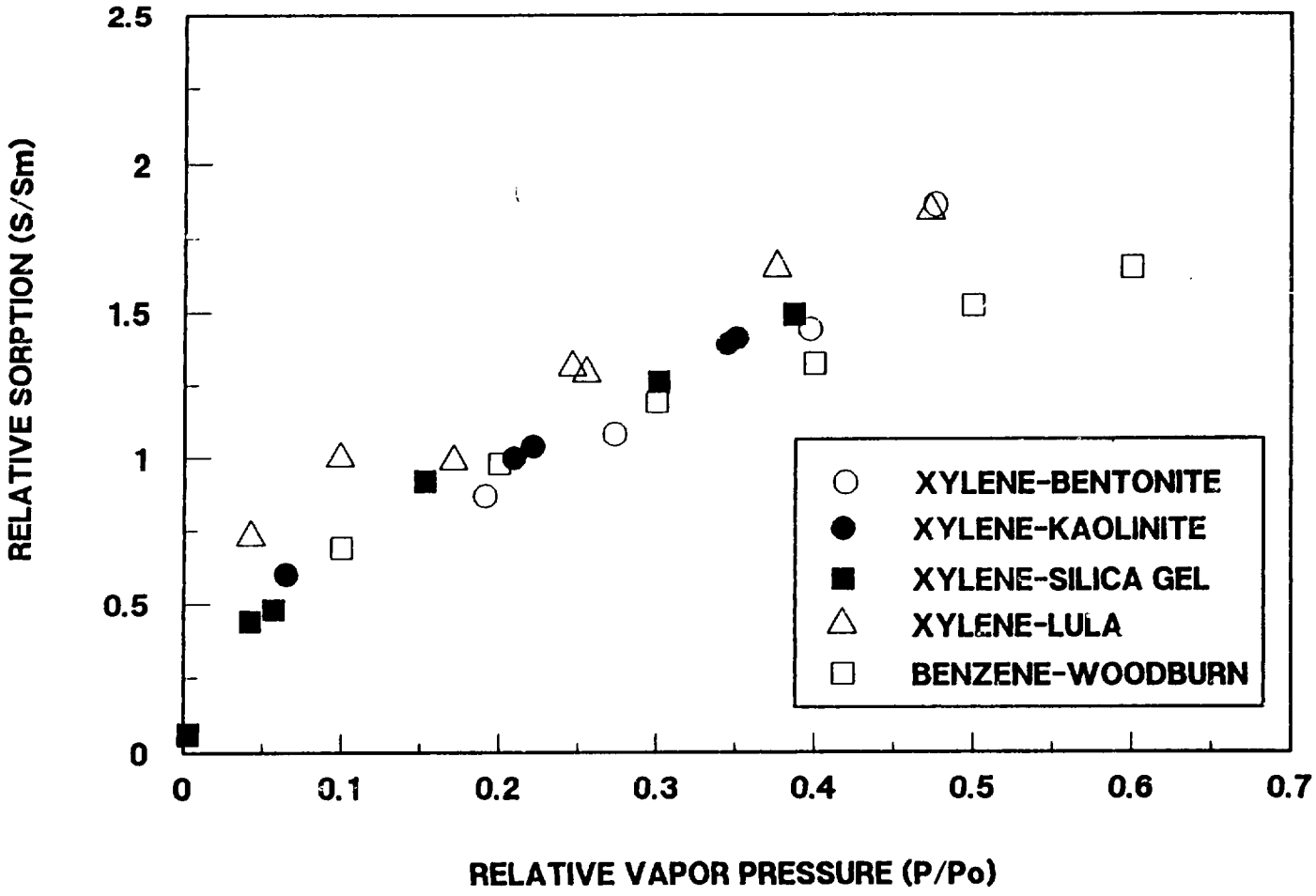

Figure 12. Relative Adsorption of p-Xylene on Several Adsorbents as a Function of Relative Vapor Pressure.

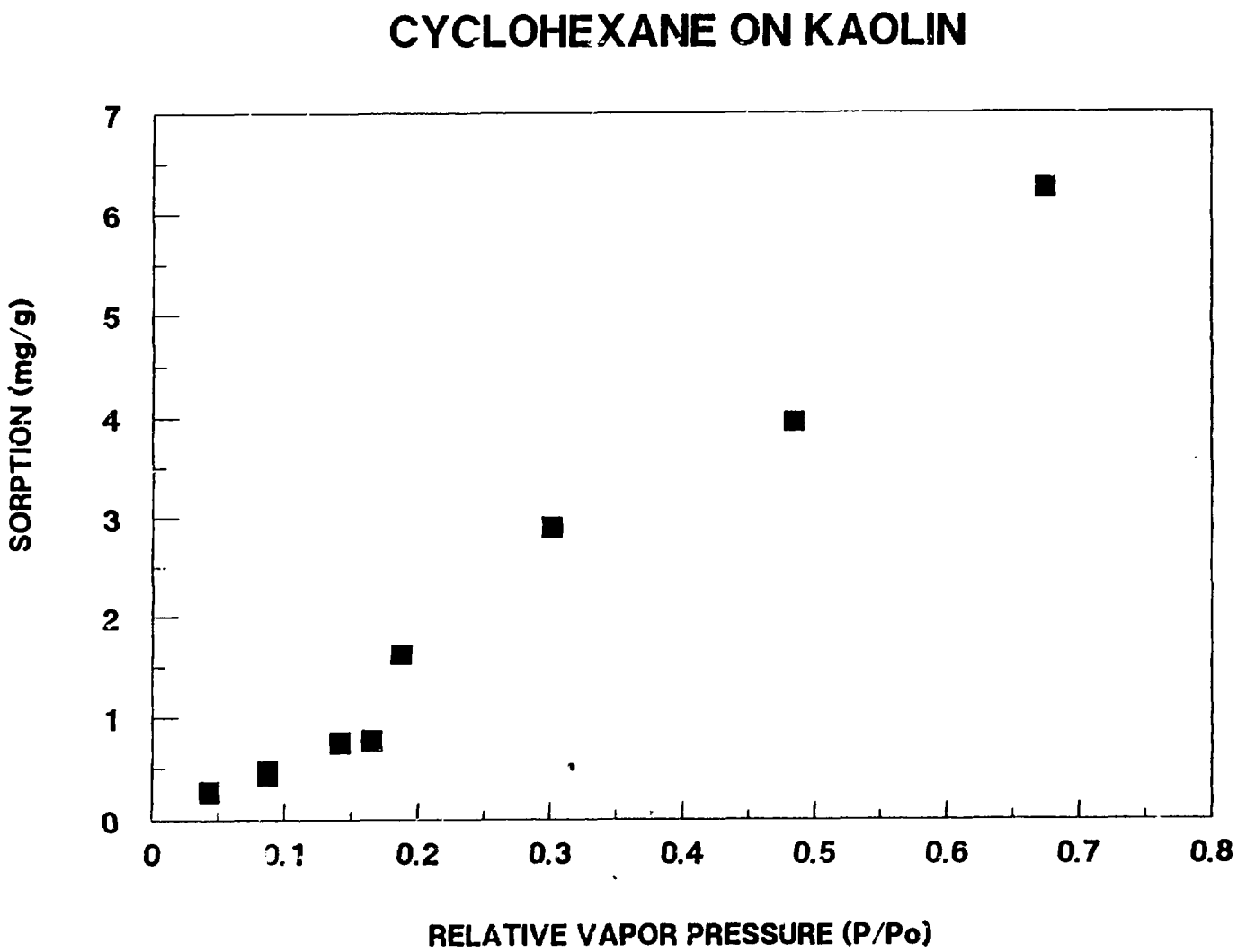

Figure 13. Isotherm for Adsorption of Cyclohexane on Kaolin at 24°C.

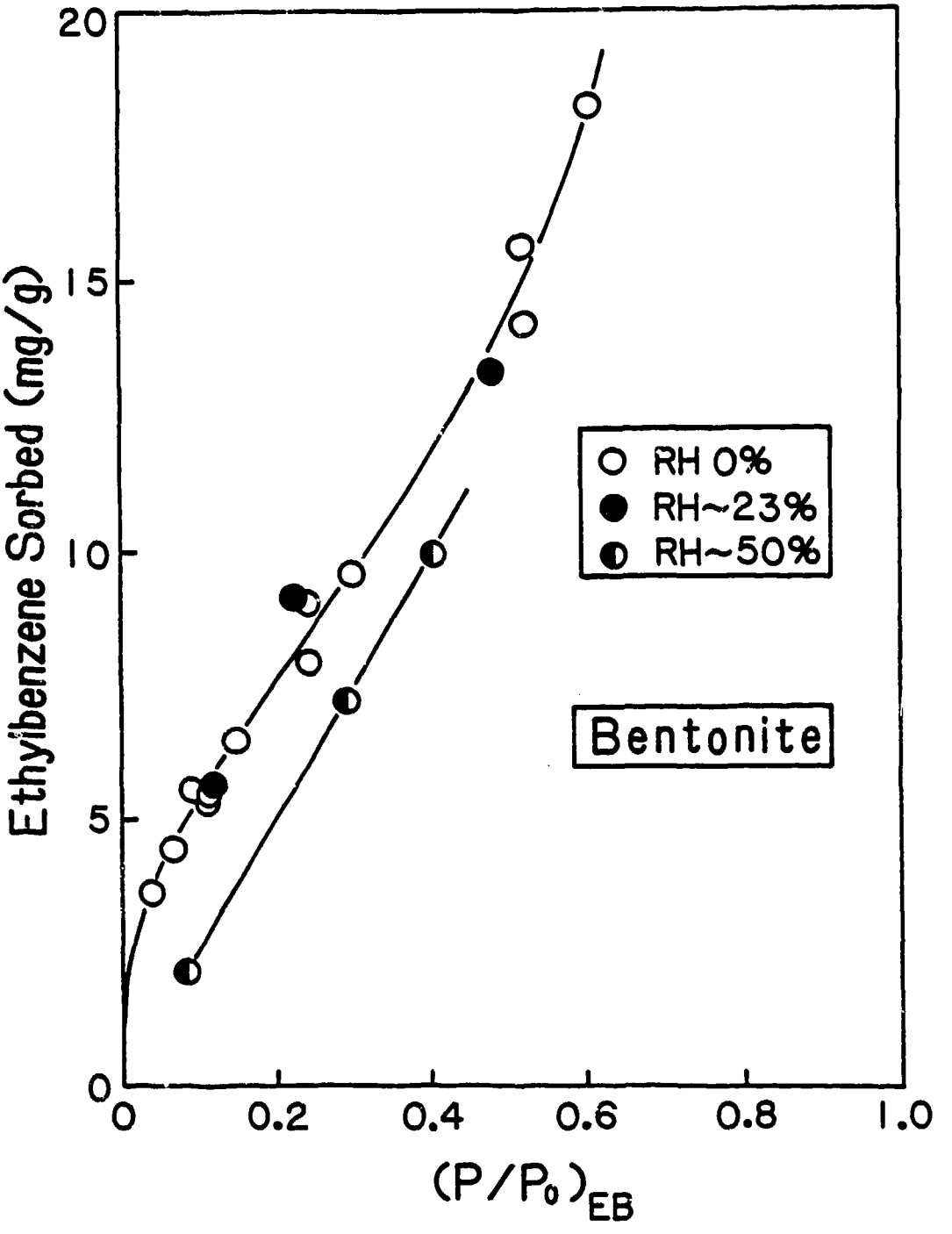

Figure 14. Isotherms for Ethylbenzene Adsorption on Bentonite at Several Relative Humidities (RH)

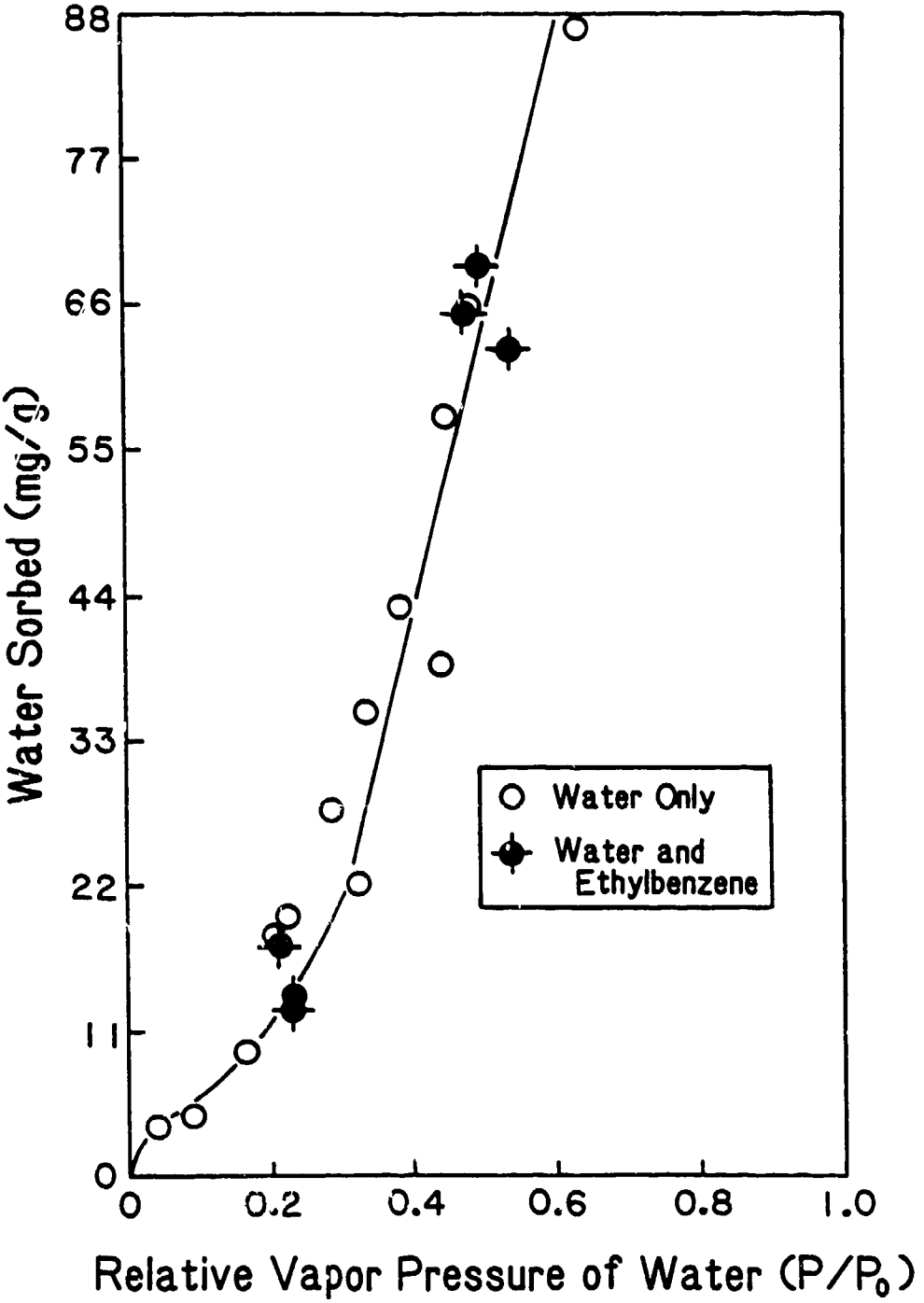

Figure 15. Isotherms for Water Adsorption on Bentonite in the Presence of Ethylbenzene.

TABLE 7. COMPETITIVE SORPTION OF ETHYLBENZENE AND WATER ON BENTONITE AT SEVERAL RELATIVE VAPOR PRESSURES (P/P_o) AND THE RELATIVE SORPTION (S/S_m).

Ethylbenzene			Water		
P/P_o	Sorption	S/S_m*	P/P_o	Sorption	S/S_m*
	mg/g			mg/g	
0.482	13.38 (±0.17)**	1.81	0.215	17.5 (±1.6)	0.17
0.220	9.14 (±0.24)	1.24	0.230	12.7 (±2.0)	0.13
0.115	5.65 (±0.06)	0.76	0.230	13.7 (±0.8)	0.14
0.403	9.98 (±0.05)	1.35	0.542	62.6 (±1.0)	0.62
0.291	7.24 (±0.06)	0.98	0.479	65.3 (±2.2)	0.65
0.082	2.15 (±0.02)	0.29	0.500	69.1 (±2.4)	0.69

*S_m for ethylbenzene taken as 7.4 mg/g and for water taken as 100.8 mg/g.
**Numbers in parentheses are standard errors for the means.

The relative sorption values in Table 7 were calculated for ethylbenzene using the S_m given in Table 6. To obtain an estimate of S_m for water sorbed on bentonite, an area of 0.106 nm^2 per water molecule on the surface was assumed. The S_m value of 100.8 mg/g corresponds to a single layer of water on the external surfaces and in the interlayer region of the clay (Reference 19). Using the surface area for bentonite shown in Table 2, S_m was estimated to be about 100 mg/g. The relative sorption values for water and ethylbenzene in Table 7 sum to values ranging from about 1.0 to values near 2.0. The similarity in the values for the summed relative sorption at both 23 and 50 percent RH's indicates that the total relative sorption has no significance with regard to competitive effects of water on ethylbenzene sorption. For example, a total relative sorption for ethylbenzene and water of 1.98 at 21.5 percent RH was associated with no reduction in ethylbenzene sorption. At 50 percent RH, a total relative sorption of 0.98 was associated with a 58 percent reduction in ethylbenzene sorption compared to that measured in the absence of water.

The first water sorbed by dry smectite clay is associated with hydration of the exchangeable cations. Since most of the exchange sites are associated with the interlayer region of the clay, most of the water sorbed at low RH would be located in the interlayer. It is believed that

divalent cations on hydrated smectites at low RH contain primary solvation shells of 6 to 8 water molecules in octahedral or cubic coordination with the cation (Reference 19). Because of the lower hydration energy on monovalent cations, Li^+ and Na^+ contain only about 3 water molecules in the primary hydration shell at low RH.

The bentonite sample had about 116 cmol(+) of extractable cations per kilogram of clay which was mostly Ca^{++} and Na^+ (Table 2). Calculations using the amount of water sorbed and the cation composition shown in Table 2 showed that, at 23 percent RH, the number of water molecules per cation was less than sufficient to form a primary solvation shell around all the cations. At 50 percent RH, the amount of water sorbed was sufficient to form a primary solvation shell around each cation with a small amount left over. These data suggest that the inhibition of ethylbenzene sorption by water may have been associated with the completion of the primary solvation shell around cations in the bentonite sample The amount of water required to complete the primary solvation shell around just the exchangeable cations (93.3 cmol(+)/kg) would be about 50 mg H_2O/g clay which would correspond to a RH of about 44 percent (Figure 15).

X-ray diffraction data have shown that the initial water sorption at low RH increases the interlayer spacing of smectites by about 0.3 nm (Reference 22) which is about the van der Waals radius of a water molecule. It is conceivable that, once the interlayer spacing has increased but before the cation hydration shells are completed, ethylbenzene and toluene could sorb in the interlayer regions near the clay edges. The surface functional groups in the interlayer region of smectite clays are the siloxane ditrigonal cavities which are considered to be Lewis base sites (Reference 19). Complexes between the siloxane ditrigonal cavities and ethylbenzene and toluene would probably be very weak, if they formed at all, since the aromatic ring is considered to be a soft Lewis base (Reference 23). A more likely sorption site might be the Lewis acid sites located on the edges of the clay particles, or exchangeable cations (which are Lewis acids) located on external surfaces.

(2) Water and p-Xylene Sorption on Kaolin

The competitive adsorption of p-xylene and water on kaolin was measured in nine different mixed vapor systems where RH ranged from 10 to

68 percent and the relative vapor pressure of p-xylene ranged from 0.13 to 0.42 (Table 8). Sorption of water and p-xylene in these mixed systems are shown in Figures 16 and 17. Sorption of water and p-xylene measured in the single sorbate systems are also shown for comparison. p-Xylene adsorption on kaolin was not affected by water at RH of 10 percent or less, and appeared to be only slightly affected by RH as high as 26 percent. At RH of 68 percent and a p-xylene relative vapor pressure of 0.14, p-xylene adsorption was only about 10 percent of that obtained on oven-dry clay. Water adsorption on kaolin appeared to be relatively insensitive to p-xylene at relative vapor pressures as high as 0.42 (Table 8, Figure 17).

(3) Water and p-Xylene Sorption on Silica Gel

The competitive adsorption of p-xylene and water on silica gel was measured in eight different mixed vapor systems where RH ranged from

TABLE 8. ADSORPTION OF WATER AND p-XYLENE VAPORS ON KAOLIN AND SILICA GEL IN MIXED VAPOR SYSTEMS.

Sorbent	No.*	P/P_o		Sorption (mg/g)	
		p-Xylene	H_2O	p-Xylene	H_2O
Kaolin	1	0.132	0.100	3.96 (±0.30)	2.53 (±0.06)
	2	0.136	0.682	0.41 (±0.01)	20.20 (±0.39)
	3	0.156	0.390	2.34 (±0.02)	6.94 (±0.04)
	4	0.171	0.262	3.50 (±0.02)	4.62 (±0.05)
	5	0.180	0.220	3.87 (±0.01)	4.01 (±0.03)
	6	0.187	0.517	1.85 (±0.02)	8.84 (±0.08)
	7	0.281	0.239	5.23 (±0.02)	4.15 (±0.12)
	8	0.390	0.084	7.11 (±0.02)	2.06 (±0.02)
	9	0.424	0.228	7.04 (±0.07)	3.98 (±0.04)
Silica Gel	1	0.103	0.346	24.11 (±0.09)	45.40 (±0.37)
	2	0.131	0.112	44.33 (±0.85)	21.81 (±0.18)
	3	0.132	0.243	36.03 (±0.06)	39.35 (±0.16)
	4	0.135	0.082	51.48 (±1.09)	18.86 (±0.20)
	5	0.151	0.439	27.69 (±0.51)	46.72 (±0.18)
	6	0.227	0.146	63.29 (±0.42)	27.63 (±0.20)
	7	0.344	0.170	82.67 (±0.49)	35.87 (±0.17)
	8	0.479	0.098	133.43 (±1.73)	26.89 (±0.12)

*These numbers refer to data points shown in Figures 16 through 19.

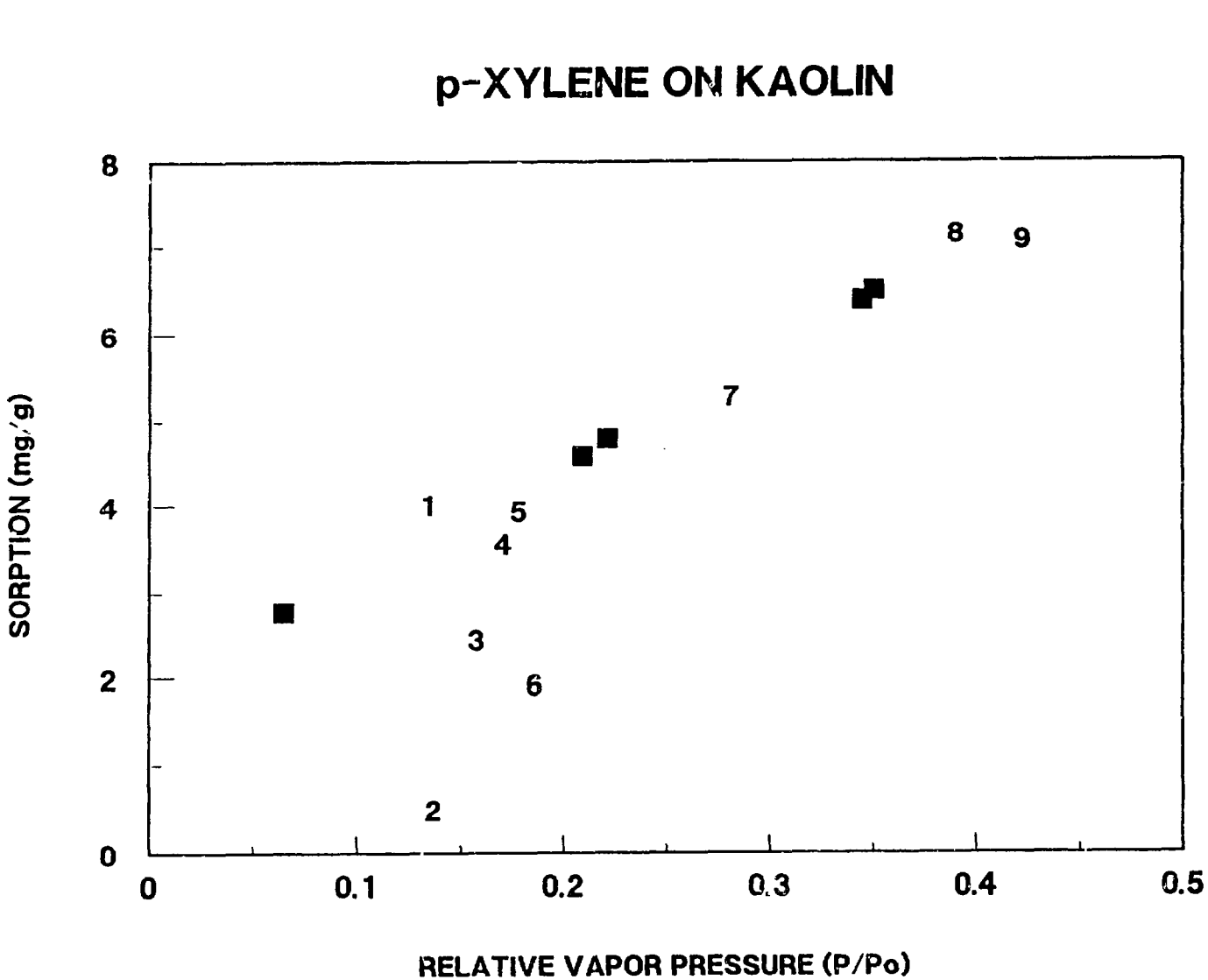

Figure 16. Adsorption of p-Xylene on Kaolin in Anhydrous ( ) Systems and in Systems Containing Water Vapor (Numbers Refer to Mixed-Vapor System Identified in Table 8).

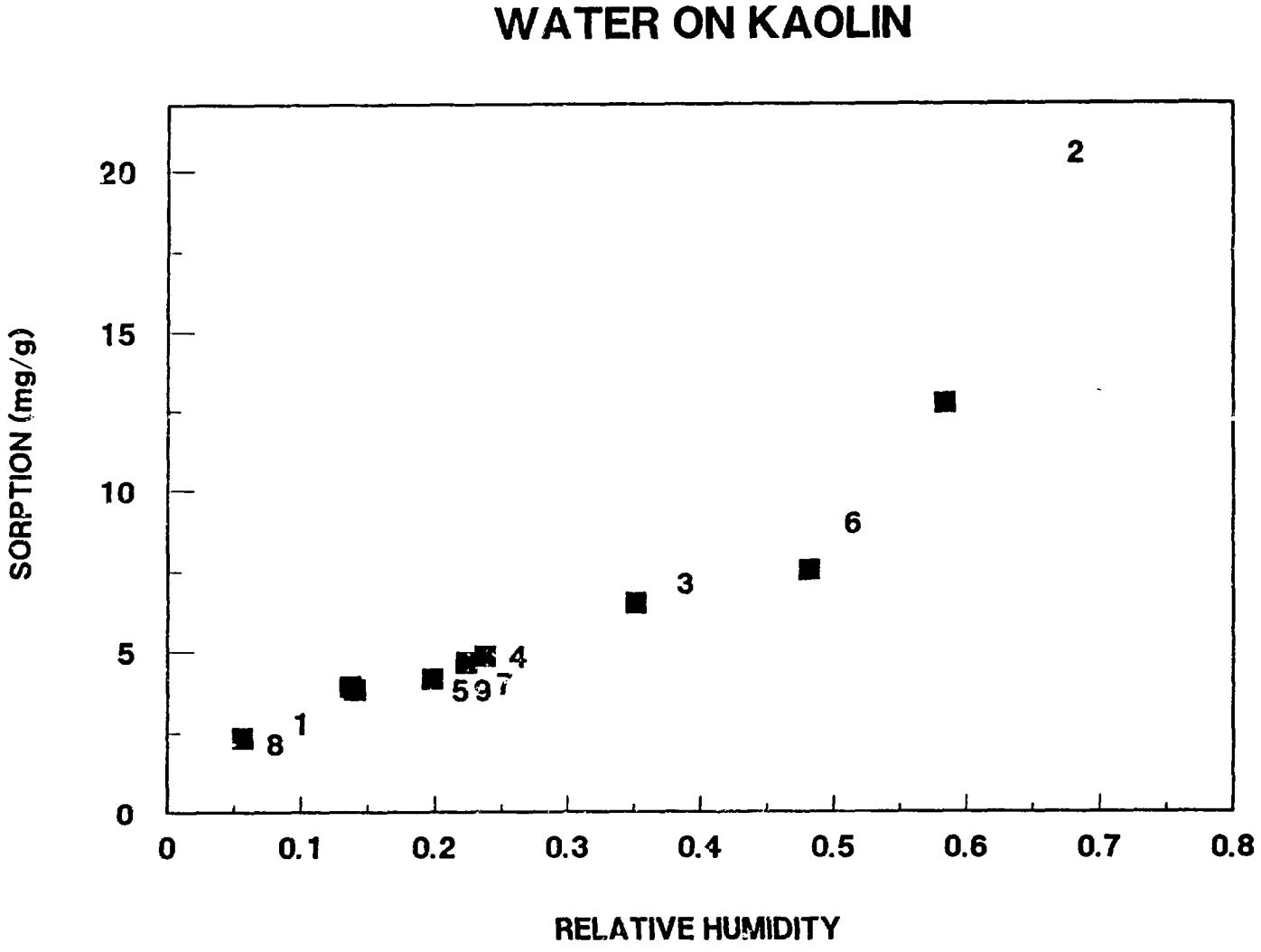

Figure 17. Adsorption of Water on Kaolin in the Absence of p-Xylene ( ) and in Systems Containing p-Xylene Vapor (Numbers Refer to Mixed-Vapor Systems Identified in Table 8).

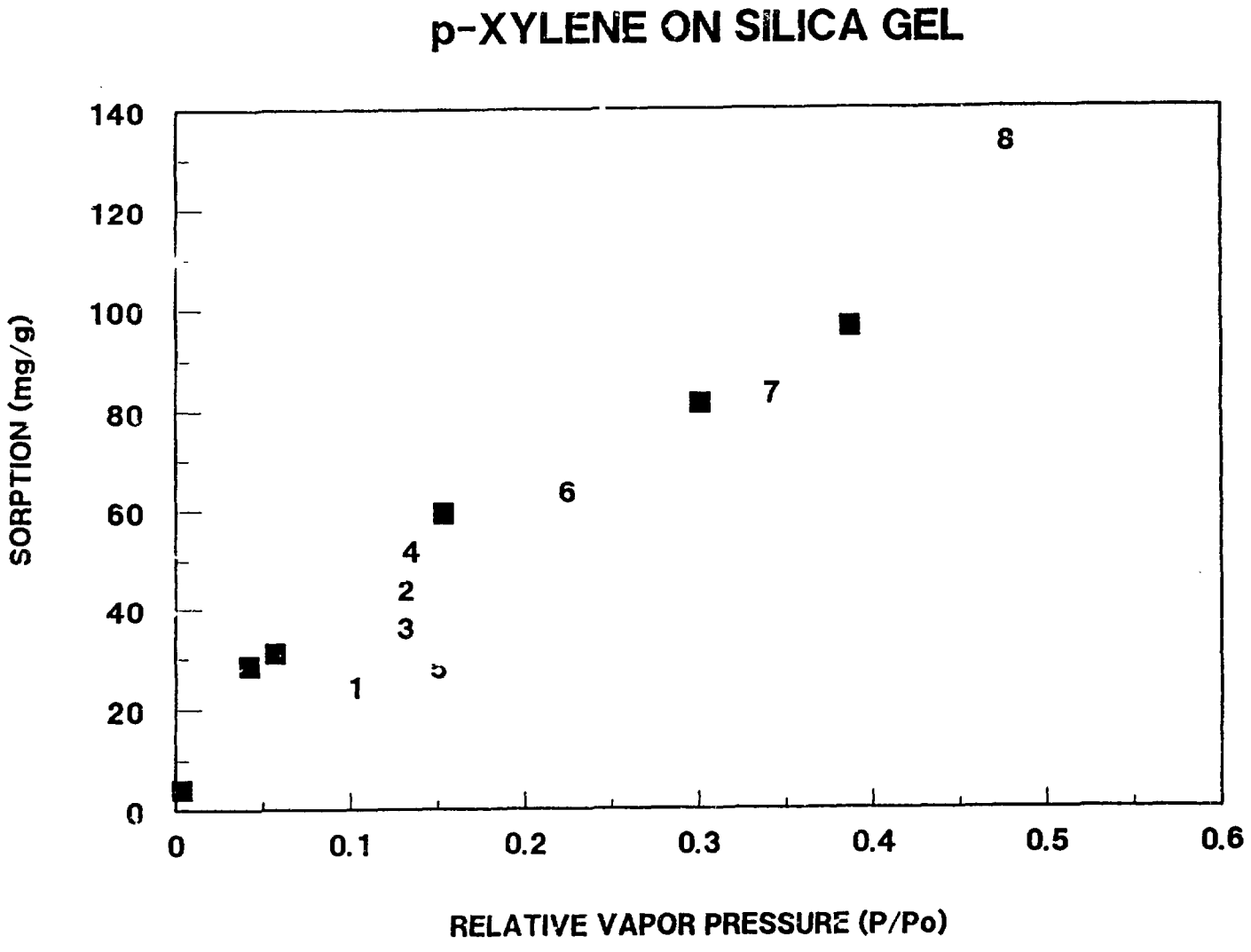

Figure 18. Sorption of p-Xylene on Silica Gel in Anhydrous ( ) Systems and in Systems Containing Water Vapor (Numbers Refer to the Mixed-Vapor Systems Identified in Table 8).

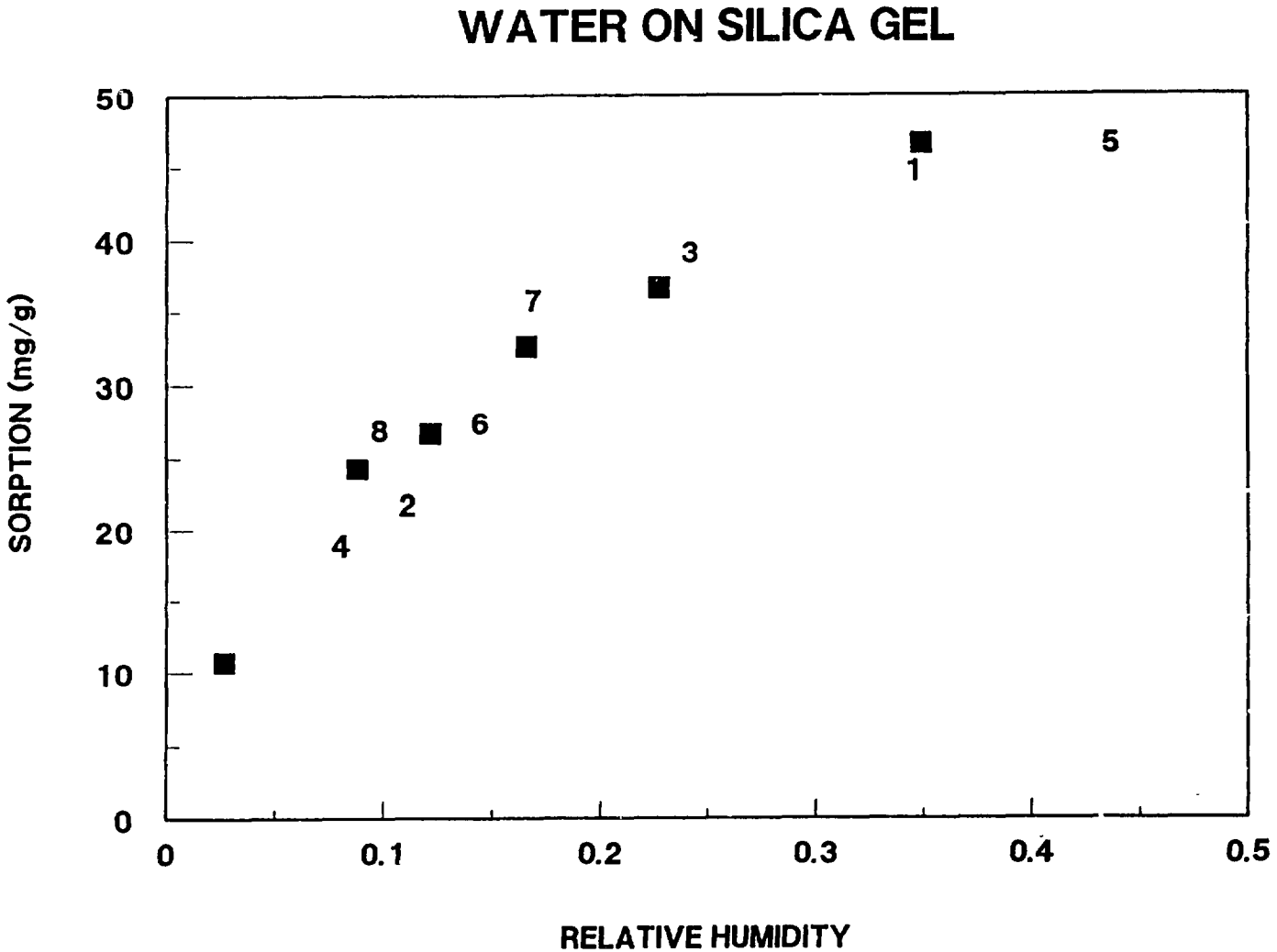

Figure 19. Sorption of Water on Silica Gel in the Absence of p-Xylene ( ) and in Systems Containing p-Xylene Vapor (Numbers Refer to the Mixed-Vapor Systems Identified in Table 8).

10 to 44 percent and the relative vapor pressure of p-xylene ranged from 0.10 to 0.48 (Table 8). Sorption of water and p-xylene in these mixed systems are shown in Figures 18 and 19. Adsorption of p-xylene on silica gel appeared to be relatively insensitive to water at RH below 20 percent (Table 4, Figure 11). RH above 20 percent reduced p-xylene adsorption by as much as 50 percent compared to adsorption on oven-dry clay. Water adsorption on silica gel was not affected by p-xylene at relative vapor pressures as high as 0.48 (Table 8, Figure 17).

2. Headspace Method

a. Evaluation of Procedures

Results obtained using the headspace method were compared with those obtained with the dynamic flow and eluted pulse gas chromatographic methods. A preliminary study was conducted to ensure that p-xylene relative pressures (P/P_o) measured by the headspace and the dynamic flow methods agreed. The initial results in this comparison were poor. The discrepancy between these two equilibrium methods was attributed to compression of the vapor sample in the syringe barrel during on-column injection into the GC. In the headspace analysis procedure, the analyzed sample is in the gaseous phase. Since the pressure in the injection port of the GC is above atmospheric pressure, the gas being injected is compressed and some vapor sample could remain in the syringe. This results in an underestimation of the actual ass of vapor removed from the sample vial headspace, especially when liquid standards in methanol were used in c.. ulating gas concentrations. In the methanol trap technique, the samples to be analyzed are in methanol and since the samples are injected as liquids, they are less subject to errors that occur with gas injection. When vapor standards were used instead of liquid standards, excellent agreement between the GC headspace and the dynamic flow method was observed.

Sorption data obtained using the two methods for p-xylene on oven-dry kaolin and Lula aquifer material are given in Figures 20 and 21, respectively. The data produced by the headspace method, in the P/P_o range of 0.017 to 0.27, agreed well with those obtained by the dynamic flow method. By using both methods, adsorption isotherm data can be obtained over a wide range

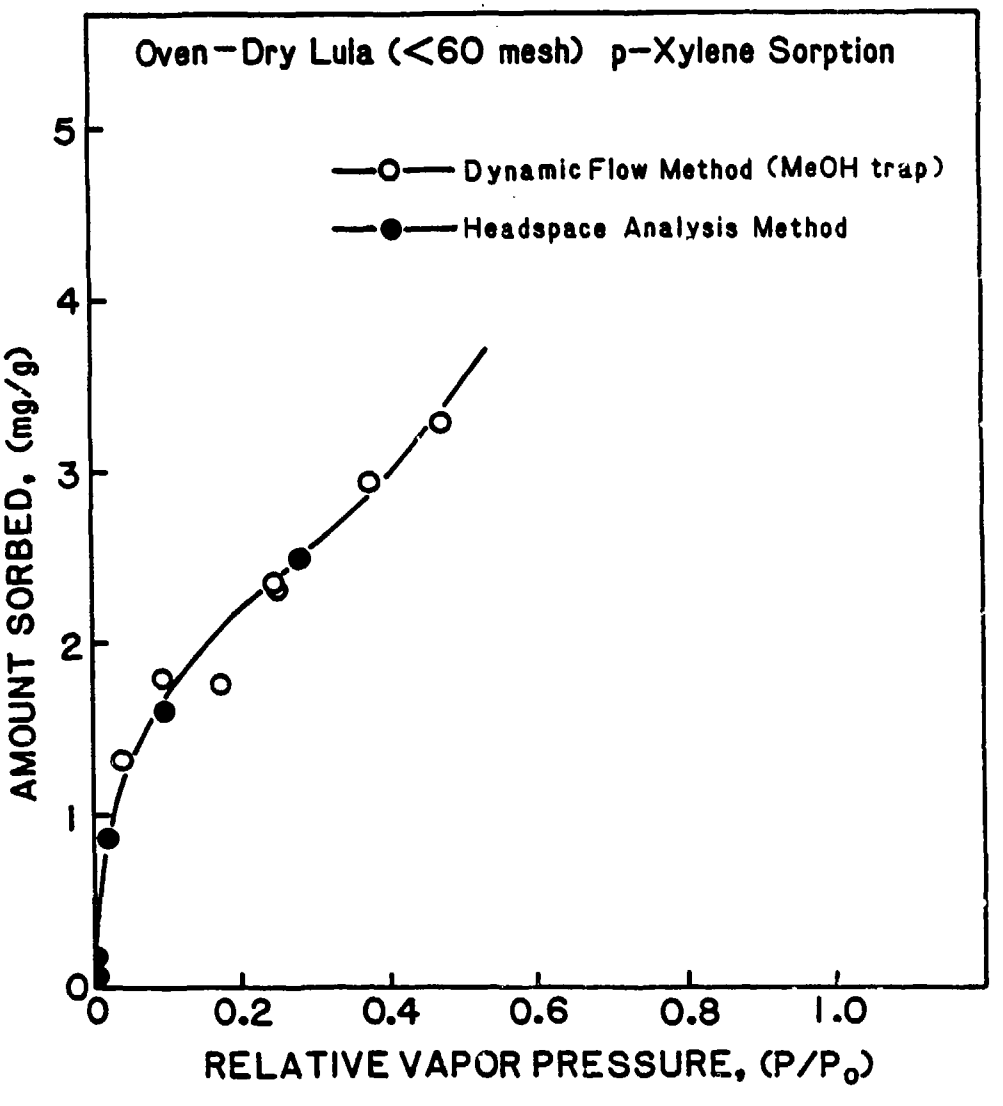

Figure 20. Comparison of Dynamic Flow and Headspace Analysis Methods for Measuring p-Xylene Adsorption on Oven-Dry Lula Aquifer Material at 24°C.

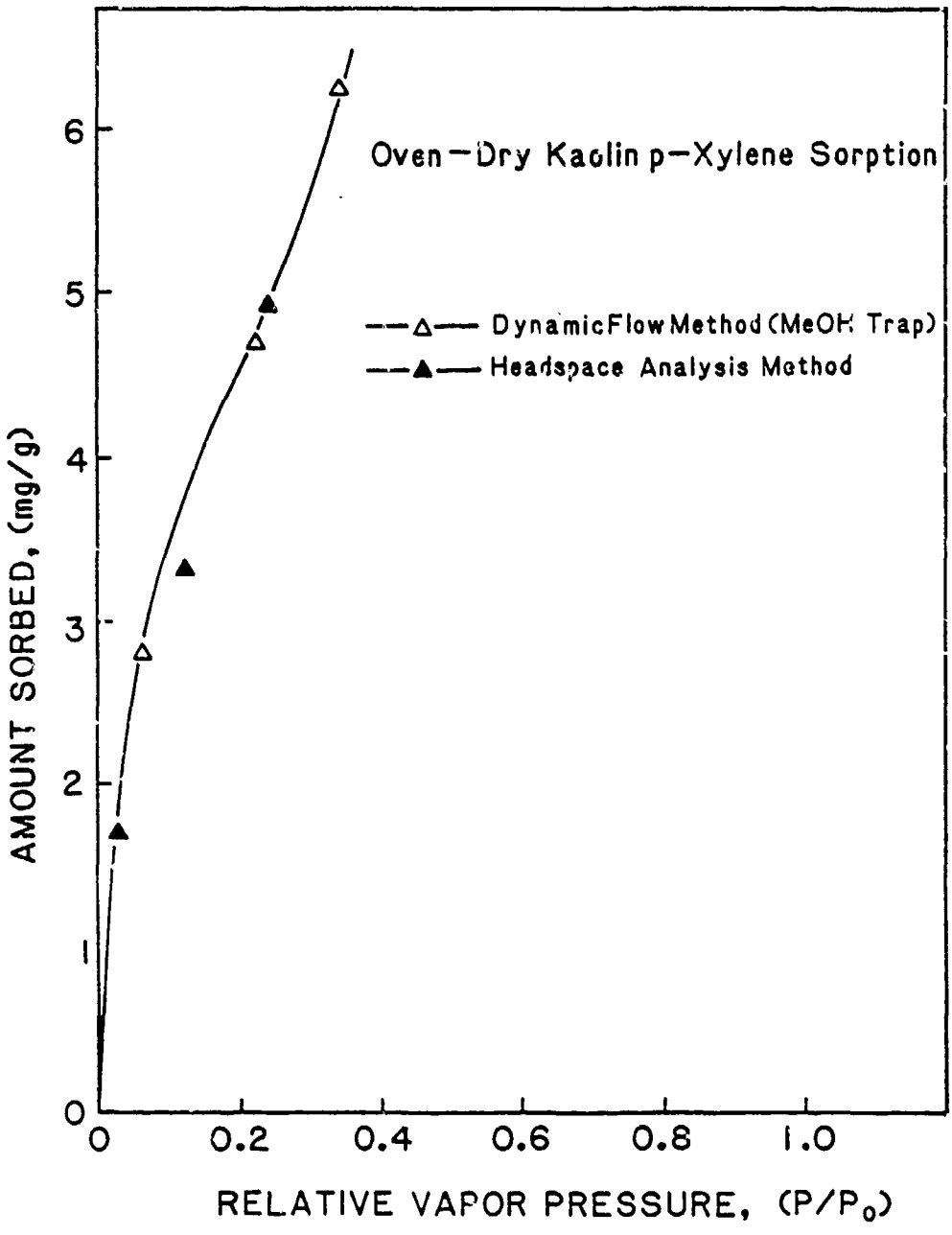

Figure 21. Comparison of Dynamic Flow and Headspace Analysis Methods for Measuring p-Xylene Adsorption on Oven-Dry Kaolin at 24°C.

of P/P_o values. The headspace method can be used at P/P_o values as low as 10^{-4}, while the dynamic flow method has a working range of P/P_o from 0.03 to 0.9.

b. Adsorption on Oven-Dry Sorbents

Isotherms for adsorption of p-xylene and TCE on oven-dry sorbents at 24°C are presented in Figures 22 and 23. The data conform to Type II BET adsorption isotherms. Vapor-phase adsorption of both solutes was the largest on the SAZ-1 clay and the lowest on the Lula material and the kaolin clay; vapor adsorption on the Webster soil was intermediate. These trends are generally consistent with the differences in N_2 specific surface areas of these sorbents (Table 2). Nominal monolayer coverage (S_m, mg/g) values were estimated by fitting the adsorption data to BET equation. These S_m values were then used to normalize the sorbed concentrations (S, mg/g) and plot these S/S_m values versus relative gas-phase concentrations (C/C_o, which is equivalent to P/P_o). These plots, shown in Figure 24, suggest that for a given solute adsorption data for different sorbents collapse essentially into a single isotherm. This is consistent with the trends observed for p-xylene adsorption data obtained using the dynamic flow method (see Figure 12). Available sorbent surface area is apparently the dominant factor controlling the adsorption of p-xylene and TCE on anhydrous sorbents. Variations in the nature of the specific mineral and organic surfaces of these sorbents seem to play a secondary role in the adsorption of organic vapors.

c. Adsorption on Air-Dry Sorbents

Data for adsorption of p-xylene on air-dry sorbents are shown in Figure 25. The gravimetric water contents for these sorbents were: 30 mg/g for Webster soil, 25 mg/g for Lula material, and 25 mg/g for kaolin. These values correspond to sorbents in equilibrium at relative humidities larger than 50 percent. Note that the isotherms are linear and that the adsorbed concentrations are about 1000-times less in comparison to oven-dry sorbents (Figure 25 versus Figure 22 and 23). Linearity of sorption isotherms is in agreement with the results of Chiou and Shoup (Reference 21) for benzene adsorption on Woodburn soil at high relative humidities. Strong dipole

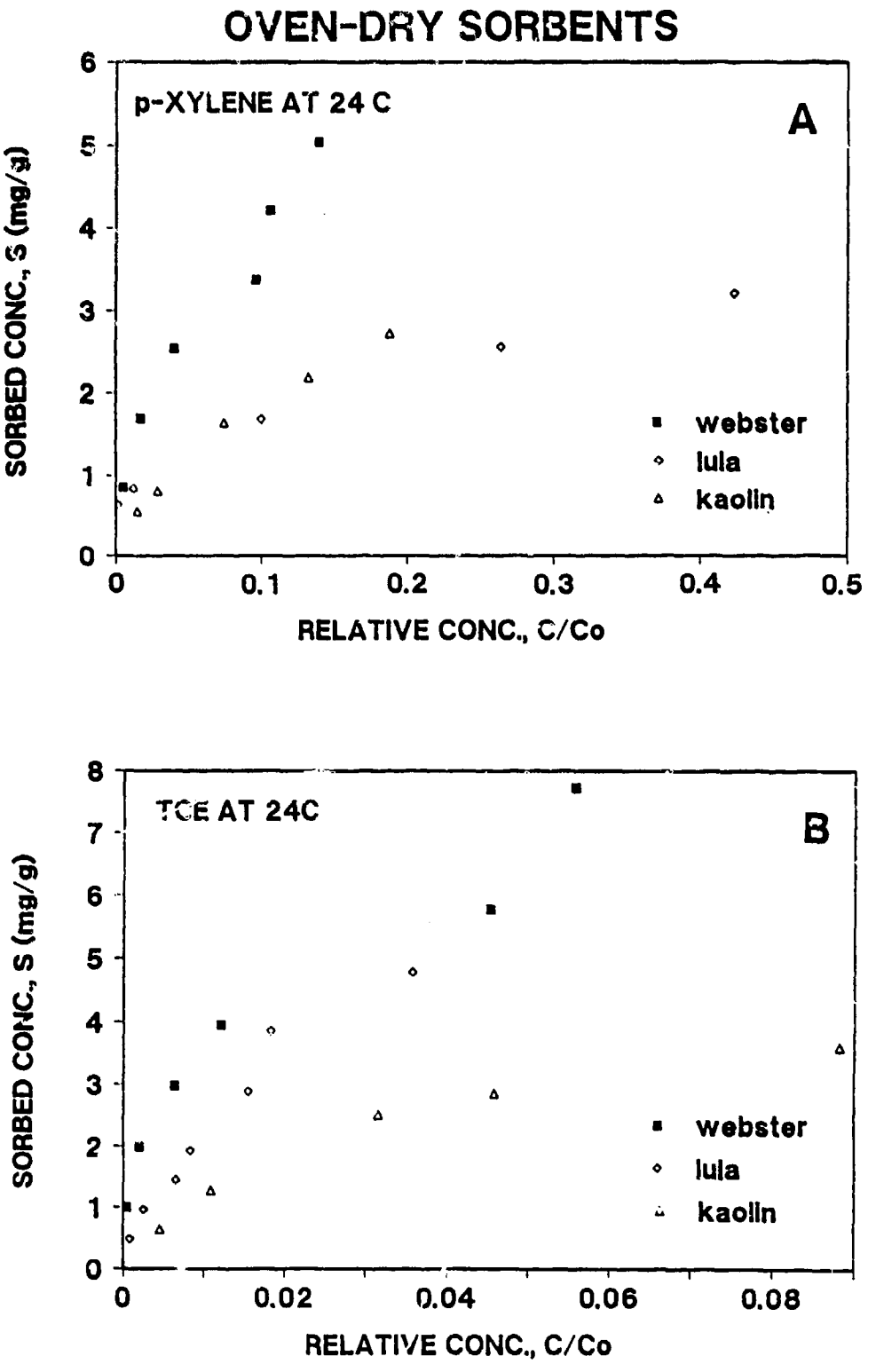

Figure 22. Adsorption Isotherms for p-Xylene and TCE on Several Oven-Dry Sorbents at 24°C.

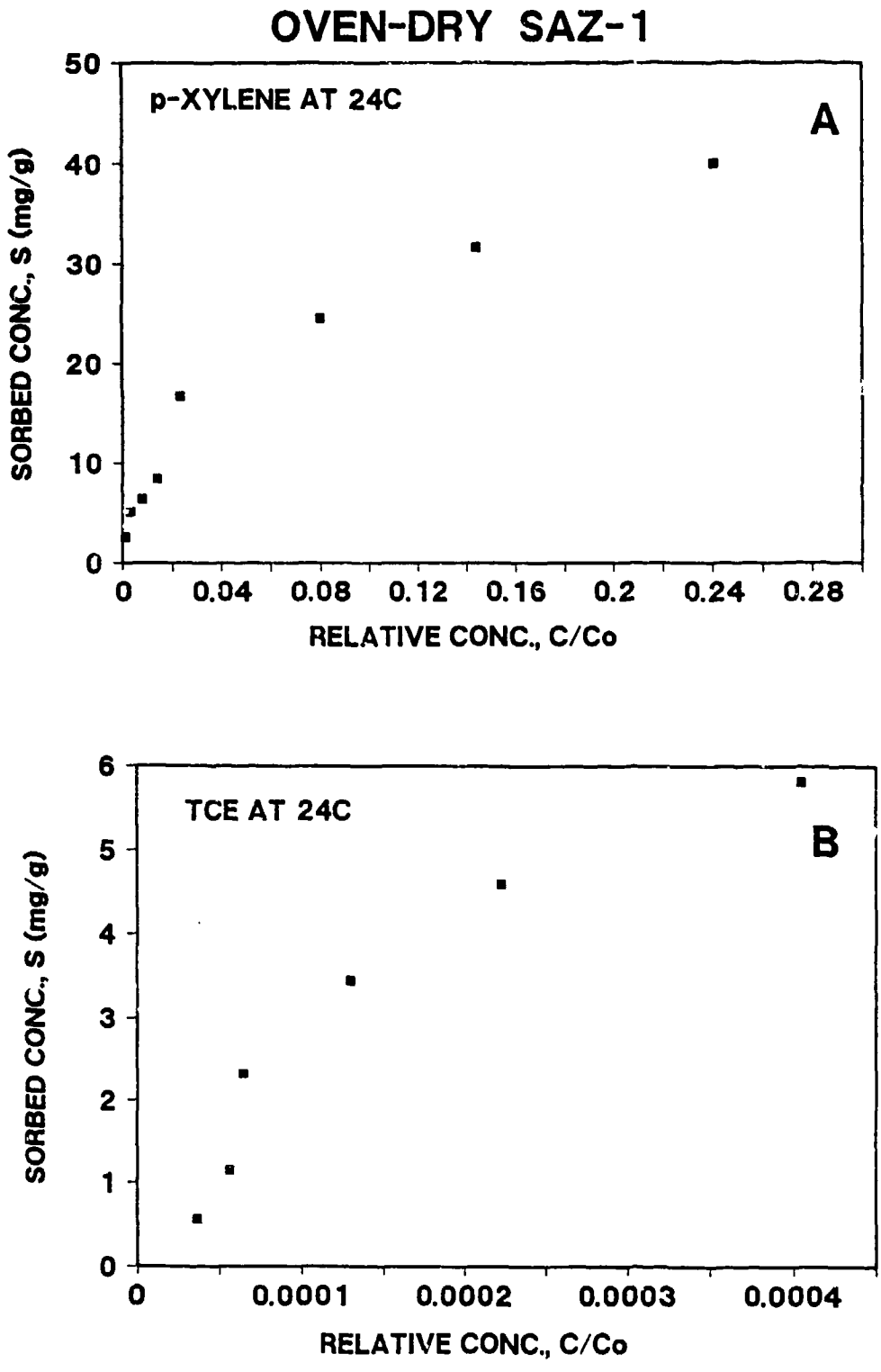

Figure 23. Adsorption Isotherms for p-Xylene and TCE on Oven-Dry SAz-1 Clay at 24°C.

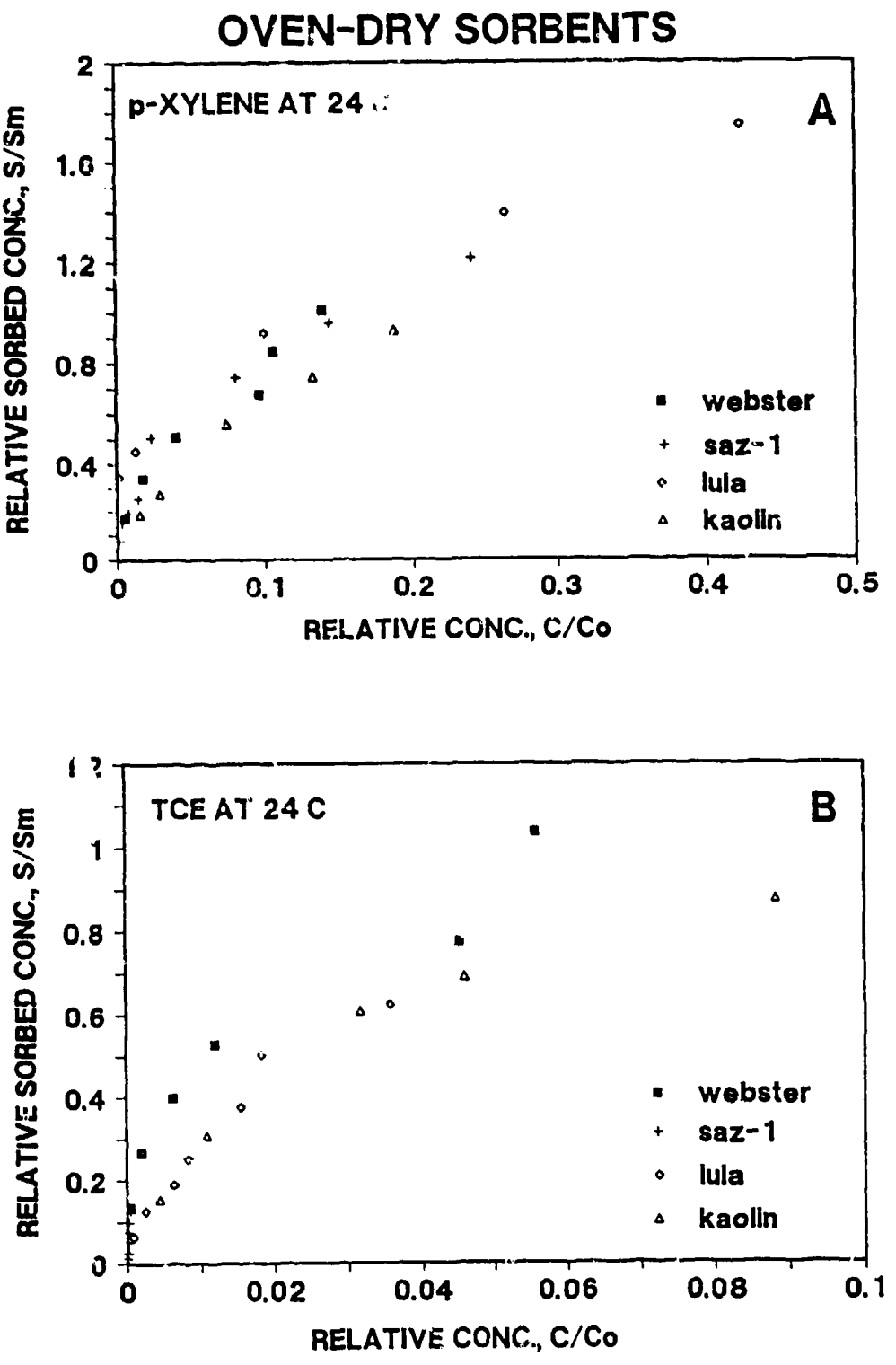

Figure 24. Relative Adsorption of p-Xylene and TCE on Several Oven-Dry Sorbents at 24°C.

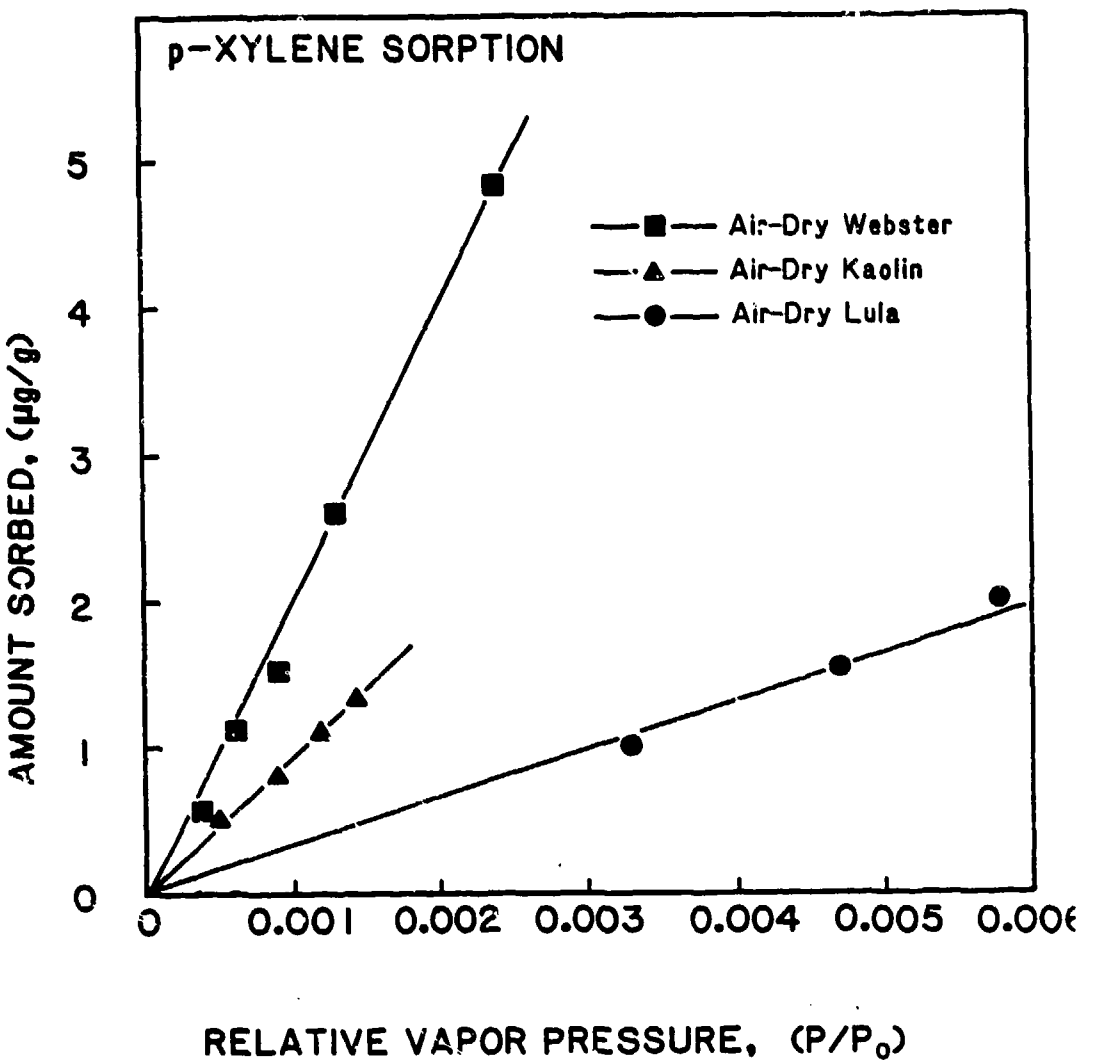

Figure 25. Isotherms for Adsorption of p-Xylene on Air-Dry Sorbents at 24°C.

interaction of water with the polar surfaces of the sorbents probably account for the inhibition of organic vapor sorption on the air-dry sorbents (Reference 24). Suppression of p-xylene adsorption in the presence of water is consistent with data collected using the dynamic flow method (see Figure 16 and Table 8).

d. Heats of Adsorption

Heats of adsorption, (ΔH_{ads}), may be obtained from adsorption isotherms measured at several temperatures. The derivation of ΔH_{ads} from adsorption isotherm data is based on the Claussius-Clapeyron equation and is analogous to the derivation of the heat of vaporization, ΔH_{vap}, from the temperature dependence of the saturation vapor pressure. In the case of adsorption, ΔH_{ad} is given by the following equation:

$$\ln P = [\Delta H_{ads} / RT] + \text{constant} \qquad (11)$$

where P is the vapor pressure of adsorbate in equilibrium with the adsorbed phase, T is the temperature in °K, R is the ideal gas constant, and ΔH_{ads} is the heat of adsorption corresponding to the transfer of one mole of adsorbate from the vapor phase to the surface at a fixed surface coverage. ΔH_{ads} as defined here is usually negative since it is defined as $\overline{H}_{ads} - \overline{H}_{vap}$ and $\overline{H}_{ads}$ is generally less than $\overline{H}_{vap}$.

From a series of adsorption isotherms (i.e., plots of amount adsorbed versus vapor pressure) obtained at different temperatures, paired values of ln P and 1/T corresponding to specific surface coverages can be plotted. The slope of this plot will be $\Delta H_{ads}/R$.

It can be shown that if the amount of adsorption decreases with increasing temperature, then $[d\ln P/dt] > 0$, $-\Delta H_{ads} > 0$, thus requiring $\Delta H_{ads} < 0$. As indicated above, this is more often the case since adsorption generally results in the loss of kinetic energy. By the same reasoning, if a system shows increasing sorption with increasing temperature, ΔH_{ads} would have to be positive.

Adsorption isotherms are more commonly plotted using the reduced vapor pressure, P/P_o, where P_o is the saturated vapor pressure (i.e.,

the vapor pressure of pure liquid adsorbate). The corresponding equation for condensation of adsorbate onto the pure liquid is as follows:

$$\ln P_o = [\Delta H_{vap} / RT] + \text{constant} \quad (12)$$

where ΔH_{vap} replaces ΔH_{ads}. To maintain consistency, ΔH_{vap} is defined as $\overline{H}^\circ_{liq} - \overline{H}^\circ_{vap}$ and is generally less than zero (i.e., $\overline{H}^\circ_{liq} < \overline{H}^\circ_{vap}$). If Equation [12] is subtracted from Equation [11], the following is obtained:

$$\ln P - \ln P_o = \ln (P/P_o) = [(\Delta H_{ads} - \Delta H_{vap})/RT] + \text{constant} \quad (13)$$

From Equation (13), it can be seen that if the amount of adsorption, as now measured in the reduced pressure plots, decreases with increasing temperature, then $[d\ln(P/P_o)/dt] > 0$, $-(\Delta H_{ads} - \Delta H_{vap}) > 0$, $(\Delta H_{ads} - \Delta H_{vap}) < 0$, and $\Delta H_{ads} < \Delta H_{vap}$. Thus, if ΔH_{vap} is negative, which is the usual case, then ΔH_{ads} must be more negative and, therefore, have a larger absolute value.

By similar reasoning, if the amount of adsorption in the reduced pressure plots increases with increasing temperature, then $[d\ln(P/P_o)/dT] < 0$, and $\Delta H_{ads} > \Delta H_{vap}$. Thus, if ΔH_{vap} is negative, then ΔH_{ads} must be less negative and, therefore, have a smaller absolute value.

Another way of describing this behavior is shown below for the case where adsorption decreases with increasing temperature when plotted against P/P_o:

$$\Delta H_{ads} < \Delta H_{vap} \quad (14)$$

$$[\overline{H}_{ads} - \overline{H}_{vap}] < [\overline{H}^\circ_{liq} - \overline{H}^\circ_{vap}] \quad (15)$$

In the derivation of the Classius-Clapeyron equation, the assumption was made that the vapor behaved as an ideal gas. This requires that $\overline{H}_{vap} = \overline{H}^\circ_{vap}$. This results in the following:

$$\overline{H}_{ads} < \overline{H}^\circ_{liq} \quad (16)$$

Thus, the molar enthalpy in the adsorbed phase is less than that of the pure liquid. Conversely, if the amount of adsorption increases with temperature,

then

$$\overline{H}_{ads} > \overline{H^{\circ}}_{liq} \qquad (17)$$

The headspace method was used to measure the adsorption of p-xylene and TCE on oven-dry sorbents at 24 and 40°C (except for p-xylene on SAZ-1 where the higher temperature was 33°C). These isotherm data are shown in Figures 26 through 29 as plots of amount adsorbed versus relative concentration (C/C_o) in the gas phase (which is equivalent to reduced vapor pressure, P/P_o). In most cases, these isotherms show considerable overlap, particularly at the lower surface coverages. In these cases, ΔH_{ads} and ΔH_{vap} must be presumed to be of equal magnitude within experimental errors. The two notable exceptions to this trend are p-xylene adsorption on Lula material and TCE adsorption on kaolin. In both cases, the amount adsorbed decreases at the higher temperature, suggesting that $\Delta H_{ads} < \Delta H_{vap}$. In some cases (e.g., TCE on Webster), the amount adsorbed at higher relative concentrations appears to increase with increasing temperature; this implies that $\Delta H_{ads} > \Delta H_{vap}$, an unlikely situation for organic vapor sorption on anhydrous sorbents.

The headspace method was also used to measure temperature-dependence of TCE adsorption on air-dry Webster soil (water content 30 mg/g). These data are presented as plots of amount adsorbed versus equilibrium gas-phase concentration (C, μg/mL) in Figure 30A and versus relative concentration (C/C_o) in Figure 30B. Note that the isotherms are linear and the adsorption coefficient (K_D, mL/g), calculated as the slope of the isotherm, decreases with increasing temperature. Within the experimental errors, the isotherms obtained at three temperatures are indistinguishable when plotted against relative concentration. A van't Hoff plot of ln K_D versus 1/T is shown in Figure 31, and ΔH_{ads} calculated from the slope of this plot was -38.2 kJ/mole. This value is similar to ΔH_{sol} = -30.8 kJ/mole, estimated on the basis of temperature-dependence of Henry's-law constant for TCE, and ΔH_{vap} = -34.5 kJ/mole calculated based on TCE vapor pressure dependence on temperature.

Heats of adsorption were calculated for sorption of several other volatile organic solutes on air-dry Webster soil and air-dry Oldsmar soil as well as on oven-dry Oldsmar soil. These ΔH_{ads} values are summarized in Table 9, and are compared with corresponding ΔH_{vap} and ΔH_{sol} values. Calculated ΔH_{ads} values are in good agreement with ΔH_{vap}.

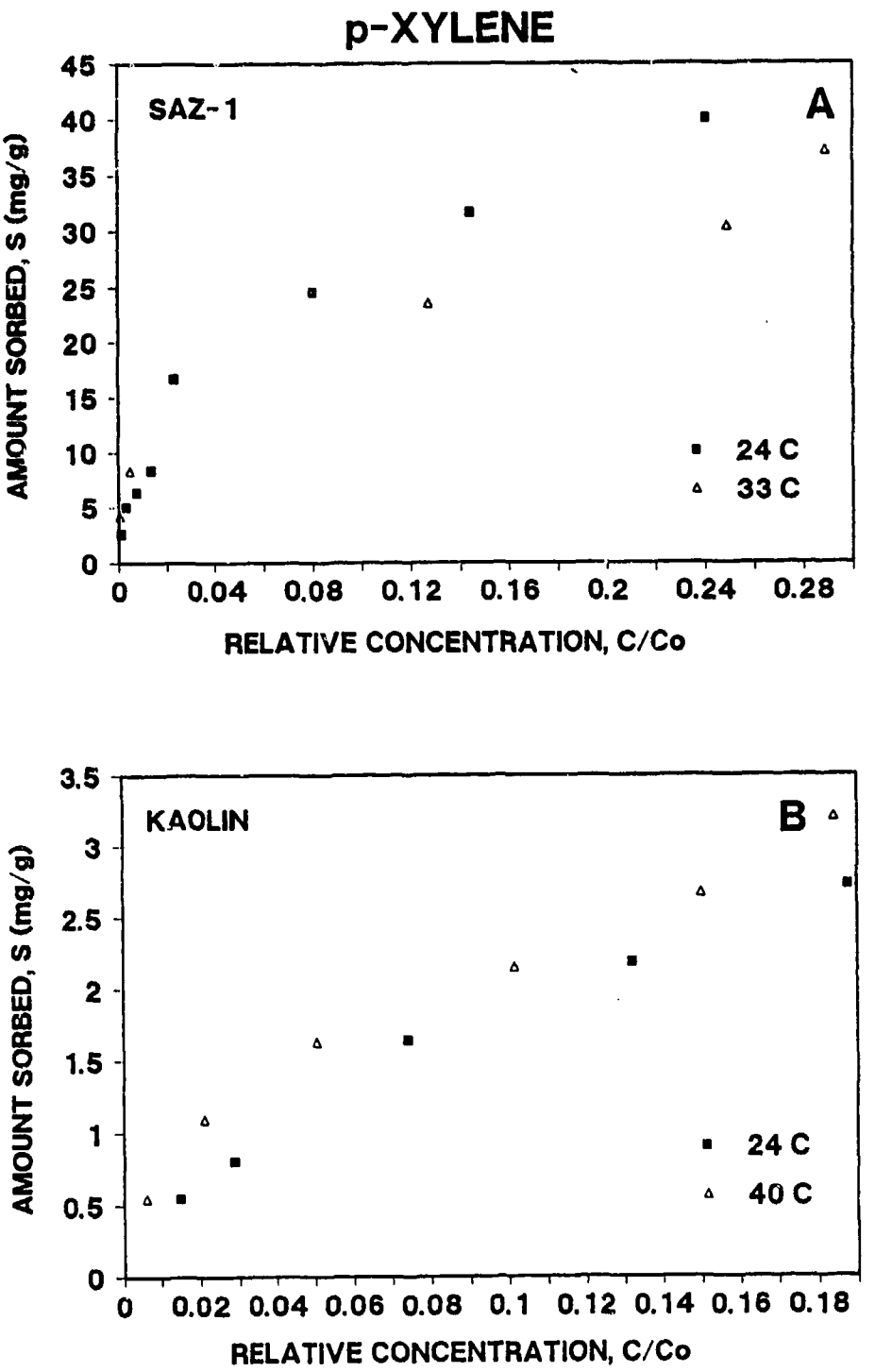

Figure 26. Isotherms for p-Xylene Adsorption on Oven-Dry SAz-1 and Kaolin Clays at Two Temperatures.

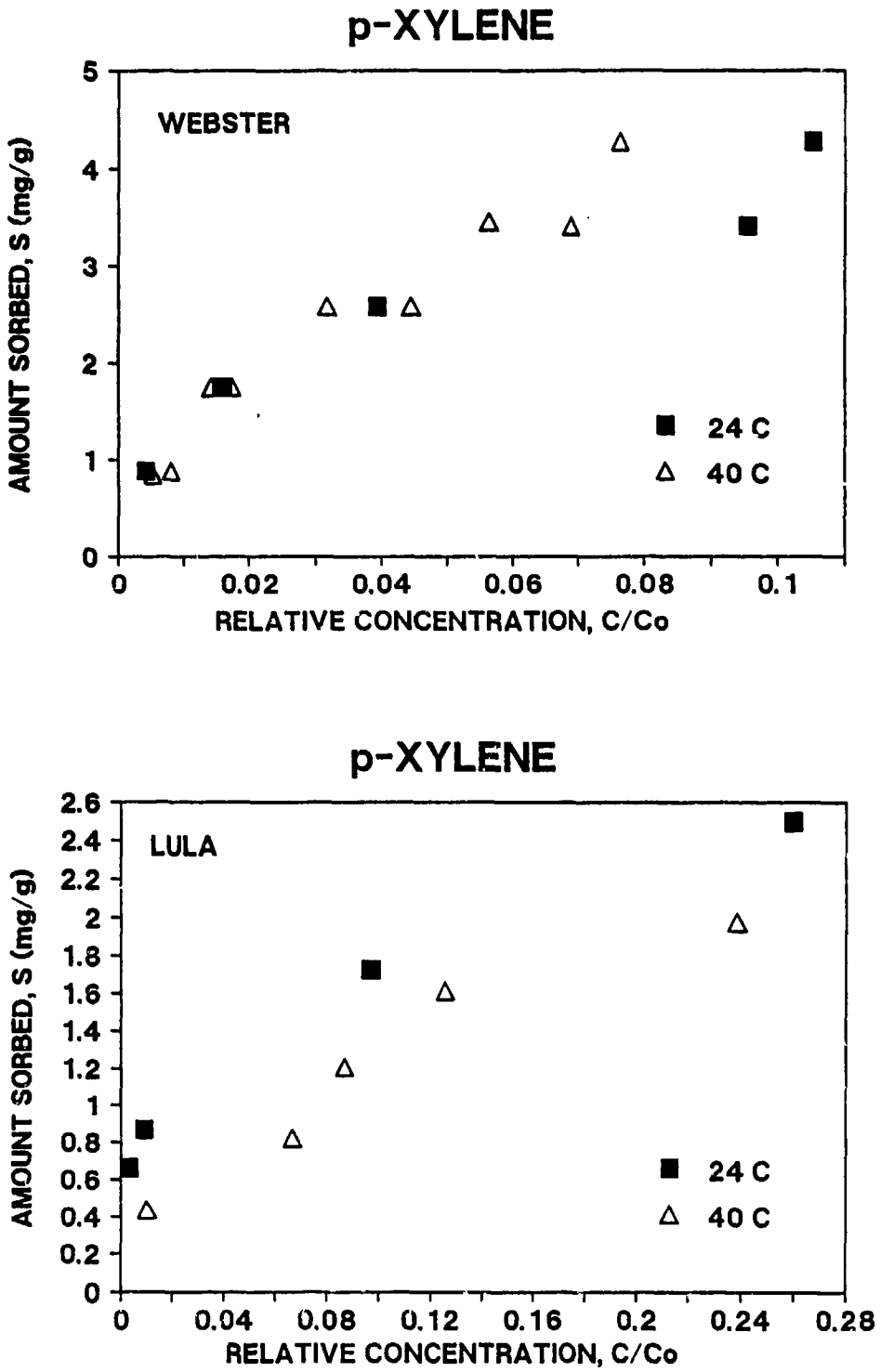

Figure 27. Isotherms for p-Xylene Adsorption on Oven-Dry Webster Soil and Lula Aquifer Material at Two Temperatures.

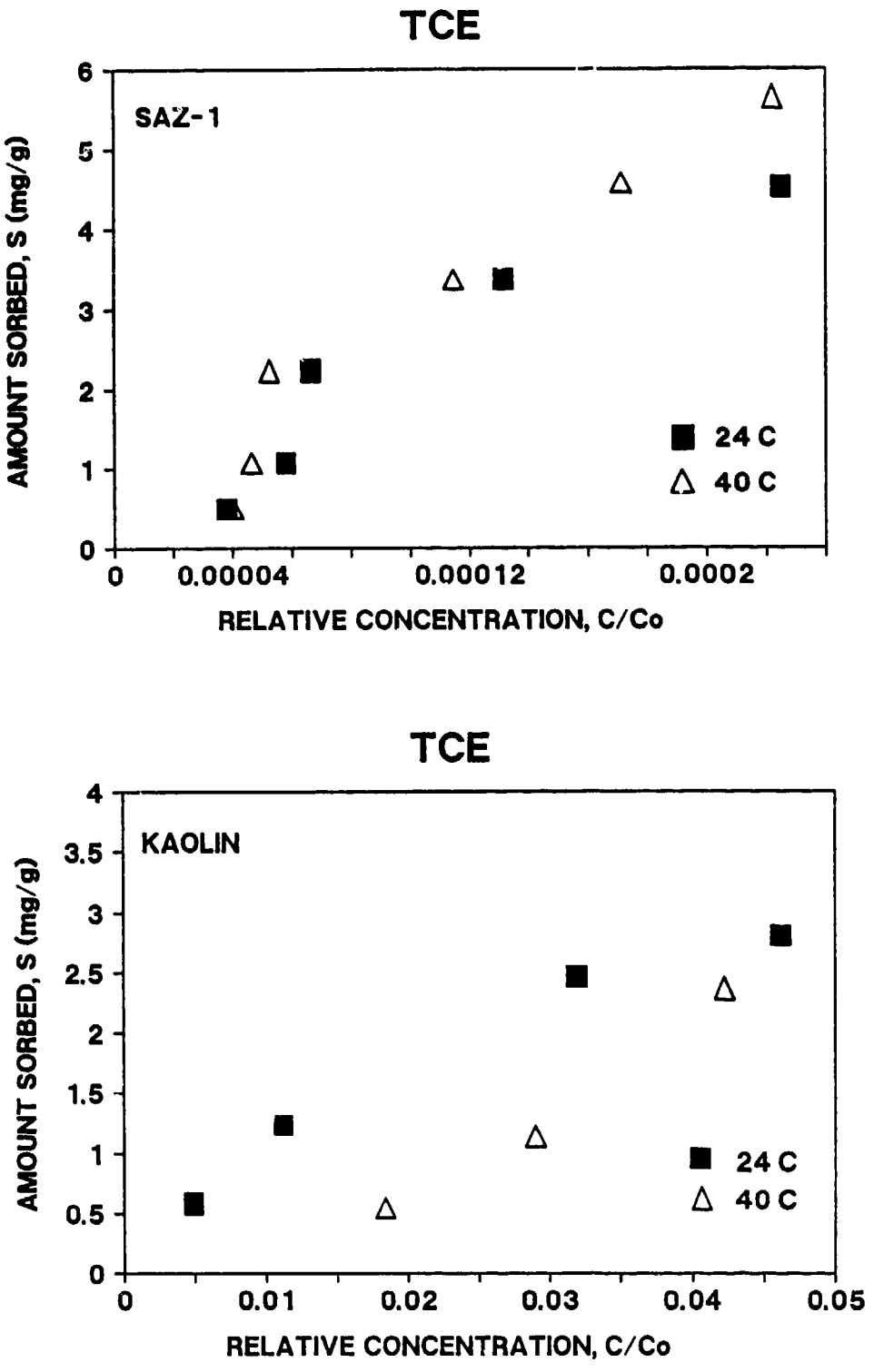

Figure 28. Isotherms for TCE Adsorption on Oven-Dry SAz-1 and Kaolin Clays at Two Temperatures.

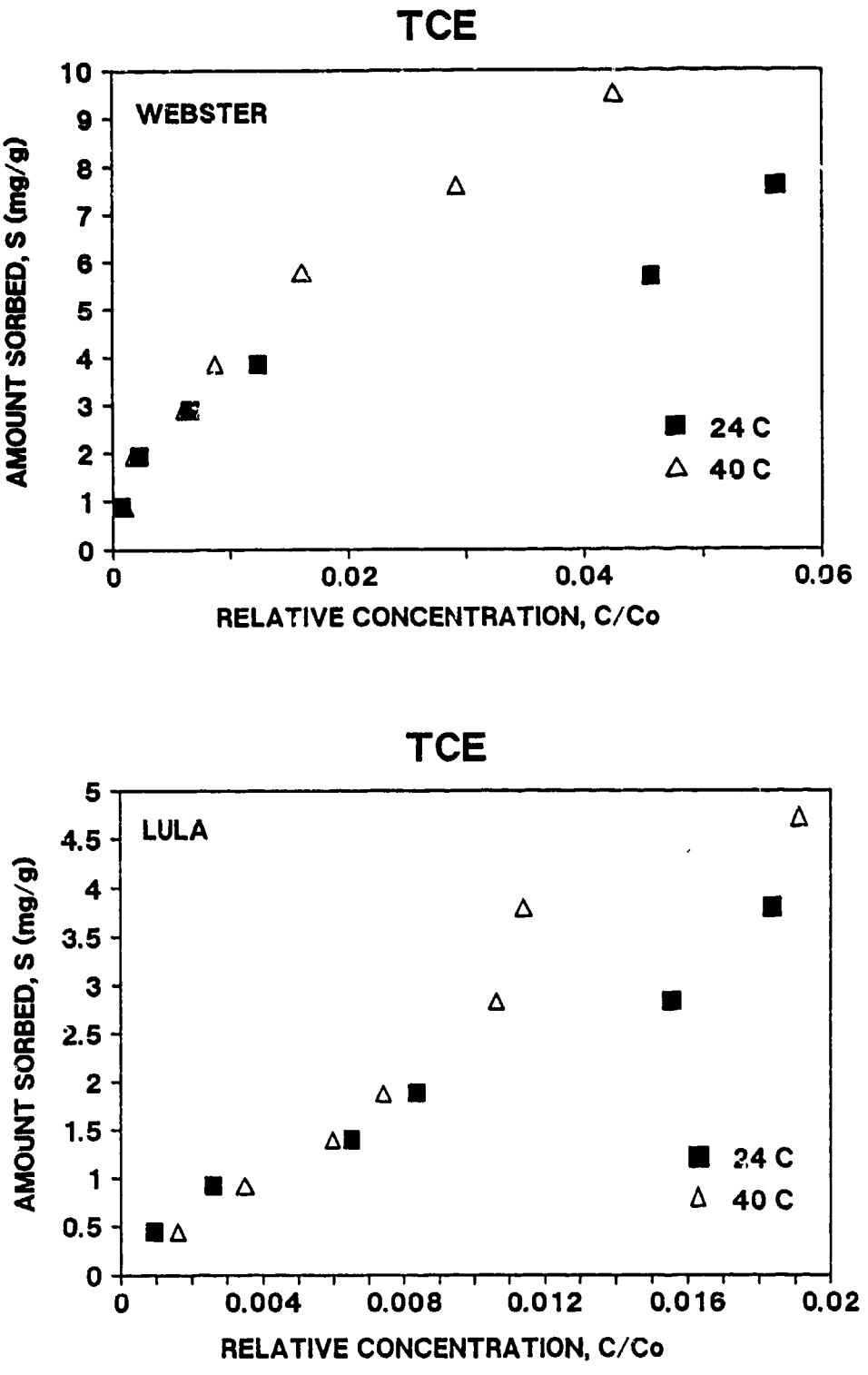

Figure 29. Isotherms for TCE Adsorption on Oven-Dry Webster Soil and Lula Aquifer Material at Two Temperatures.

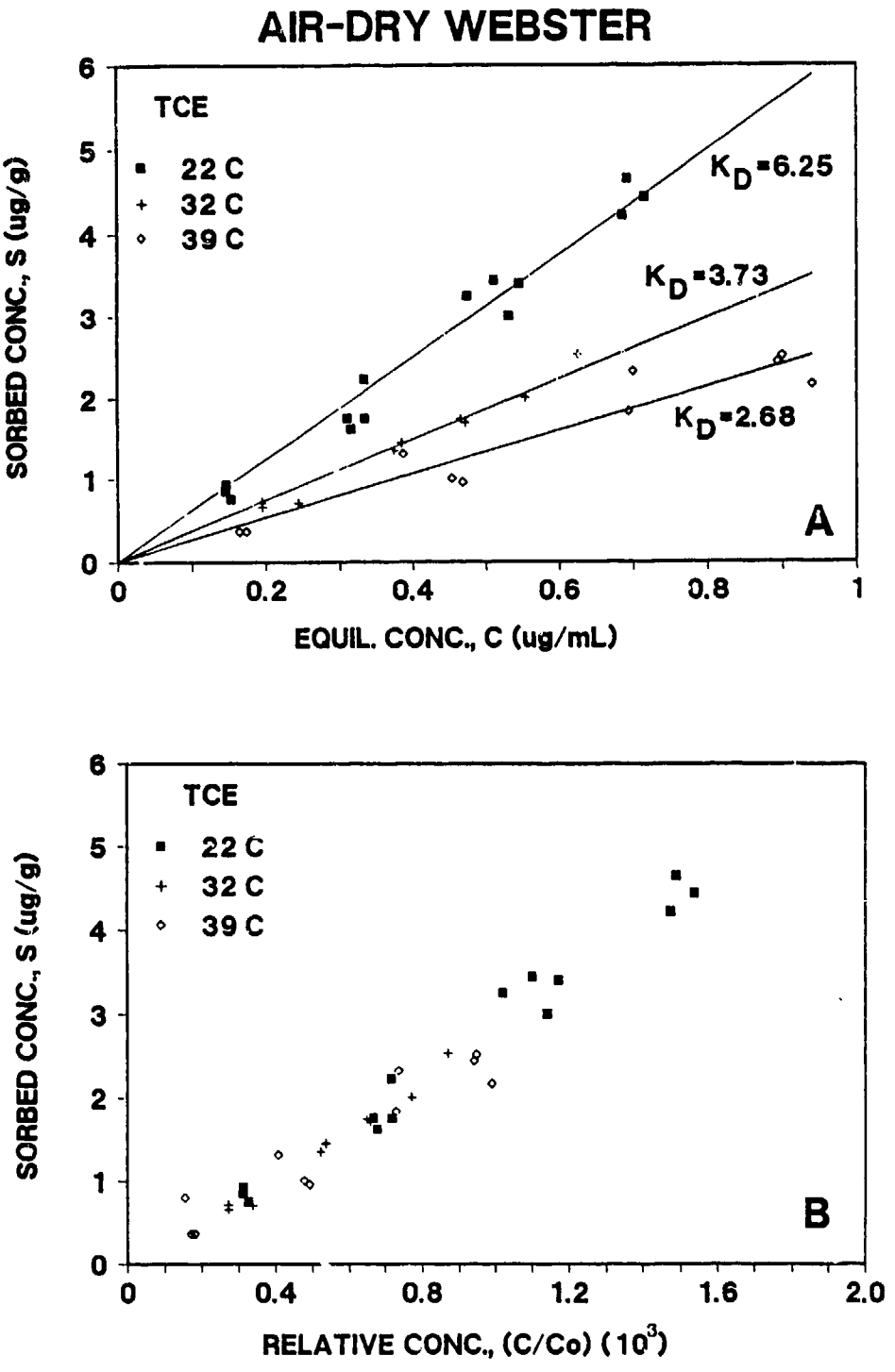

Figure 30. Isotherms for Adsorption of TCE on Air-Dry Webster Soil at Three Temperatures.

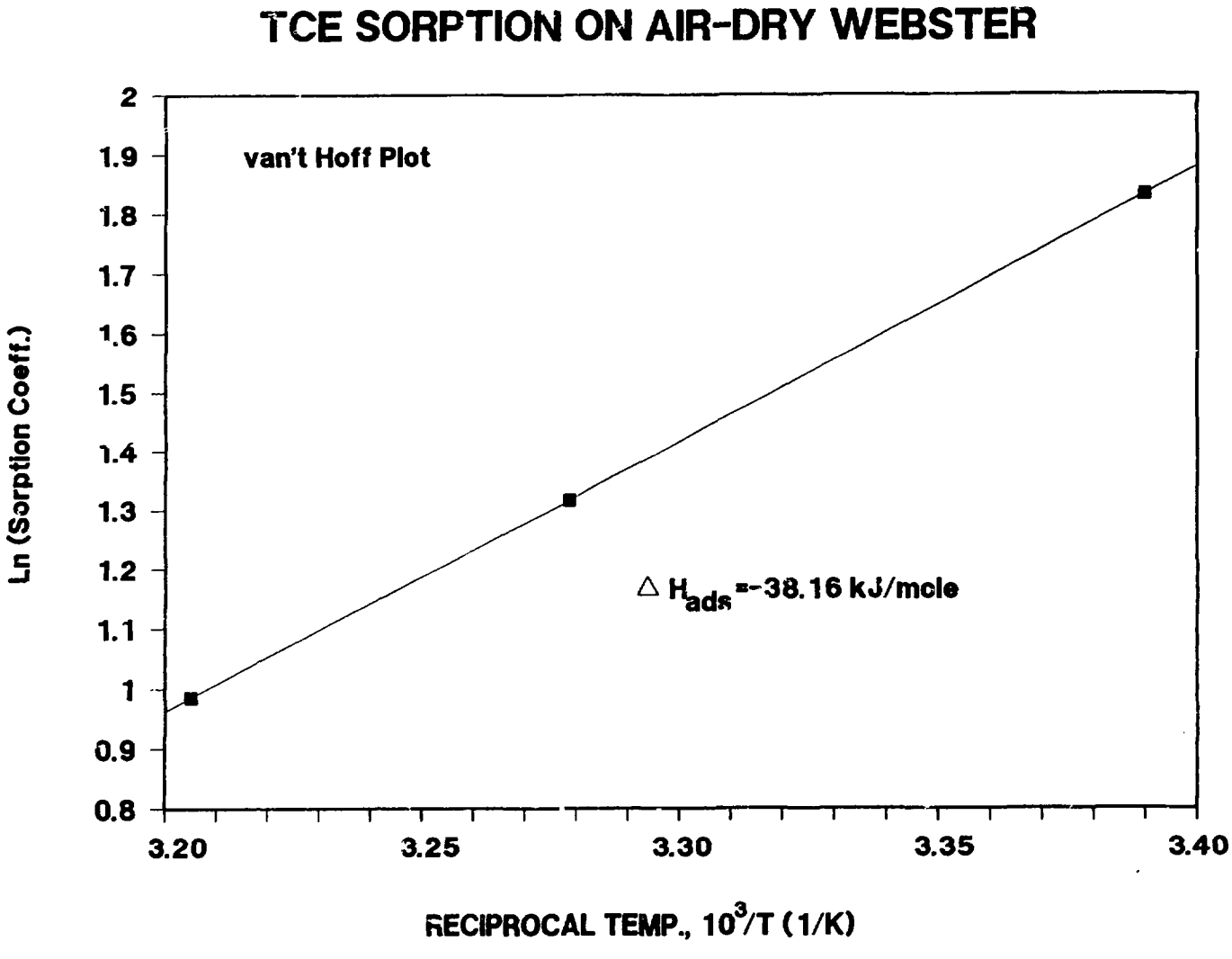

Figure 31. van't Hoff Plot of TCE Adsorption Coefficient Dependence on Temperature.

TABLE 9. HEATS OF ADSORPTION (ΔH_{ads}) MEASURED USING THE HEADSPACE METHOD COMPARED WITH HEATS OF VAPORIZATION (ΔH_{vap}) AND HEATS OF SOLUTION (ΔH_{sol}).

Solute	$-\Delta H_{ads}$ (kJ/mole) Air-Dry Webster	Air-Dry Oldsmar	Oven-Dry Oldsmar	$-\Delta H_{vap}$ (kJ/mole)	$-\Delta H_{sol}$ (kJ/mole)
Cyclohexane	35.8	ND	34.2	32.9	26.9
Toluene	32.8	ND	37.2	36.5	25.1
Ethylbenzene	33.6	40.4	ND	40.6	26.9
o-Xylene	38.6	39.9	ND	42.6	26.8
p-Xylene	37.1	40.7	ND	41.7	29.1
Trichloroethylene	38.2	ND	23.2	34.5	30.8

C. SUMMARY

Two experimental techniques were used to measure adsorption isotherms for volatile organic compounds on soils and clays. The dynamic flow method was an open system through which a gas stream containing the organic vapor at a constant vapor pressure was passed for a certain equilibration period. Organic compounds adsorbed on soils and clays were extracted into methanol and the concentrations were assayed using direct UV or HPLC techniques. The headspace method was a closed system into which known masses of the organic liquid (or saturated vapor) were injected and the system was allowed to equilibrate. Gaseous samples of the headspace were analyzed using GC techniques. Adsorption isotherms obtained by the dynamic flow and headspace methods for p-xylene adsorption on kaolin clay and Lula aquifer material were in excellent agreement provided that p-xylene vapor standards and not p-xylene standards in methanol were used to obtain the GC calibration curve. The combination of the dynamic flow and headspace methods allow the measurement of adsorption isotherms for volatile organics over a relative vapor pressure range from about 10^{-4} to 0.8 or more.

The surface areas available for alkylbenzene adsorption on soils and clays appeared to be those measured by N_2 adsorption. Silica gel was an exception, adsorption being lower than expected based on the N_2 surface area. The surface areas available for water adsorption were generally greater than those for alkylbenzene adsorption. However, silica gel was again unique among the adsorbents in that it adsorbed much more alkylbenzene than it did water.

Plots of relative adsorption, S/S_m, against relative vapor pressure, P/P_o, showed that relative adsorption of water, p-xylene, and TCE were similar for several diverse adsorbents used in this study. These results suggest that the amount of adsorption is primarily a function of available sorbent surface area and that the effects of specific surface interactions are minimal.

Competitive adsorption of water and an alkylbenzene (p-xylene or ethylbenzene) was measured at low relative vapor pressures using the dynamic flow system. In mixed-vapor systems, water at relative humidities up to about 0.20 had little or no effect on the adsorption of the alkylbenzenes. Increases in relative humidity above 0.20 decreased alkylbenzene adsorption markedly. Adsorption of p-xylene and TCE on air-dry sorbents, measured with the headspace method, showed that p-xylene and TCE adsorption were about three orders of magnitude below that obtained on the corresponding anhydrous sorbents. In contrast to the effect of water on alkylbenzene adsorption, the alkylbenzene had little or not effect on water adsorption at alkylbenzene relative vapor pressures as high as 0.48.

The Classius-Clapeyron equation was applied to organic adsorption on oven-dry sorbents at different temperatures in order to calculate isosteric heats of adsorption. The overlapping of the adsorption isotherms, when plotted against relative vapor concentration, particularly at the lower P/P_o values, indicated that heats of adsorption, ΔH_{ads} were not very different from the heat of vaporization, ΔH_{vap}. Similar data obtained for air-dry sorbents, containing several times the monolayer capacity for water, showed that ΔH_{ads} in these systems was more like ΔH_{vap} than ΔH_{sol}. The amount of organic adsorbed onto the air-dry sorbents was calculated to be well below the solubility limit in the adsorbed water, assuming that the solution properties of bulk and adsorbed water were similar. These results suggest that interactions of volatile organic compounds, like p-xylene and TCE, with adsorbed water may be quite different from those involving bulk water.

D. REFERENCES

1. Nelson, D. W., and Sommers, L. E., "Total Carbon, Organic Carbon, and Organic Matter," Chapter 29, in: Methods of Soil Analysis, Part 2, Agronomy Monograph No. 9, American Society of Agronomy, Madison, WI, 1982, pp. 585-571.

2. Carter, D. L., Heilman, M. D., and Gonzalez, C. L., "Ethylene Glycol Monoethyl Ether for Determining Surface Area of Silicate Minerals," 1965, Soil Sci., Vol. 100, pp. 356-360.

3. Jackson, M. L., "Soil Chemical Analysis-Advanced Course," 2nd Ed., 9th Printing, Published by the author, Dept. of Soil Science, University of Wisconsin, Madison, WI, 1974.

4. Mitchell, J., Jr., and Smith, D. M., "Aquametry-Part III," (The Karl Fischer Reagent), A Treatise on Methods for the Determination of Water, Chem. Anal., Vol. 5, Sec. Ed., John Wiley & Sons, NY, 1980.

5. Longbottom, J. E., and Lichtenberg, J. J. (eds.), Test Method 602-Purgeable Aromatics, U. S. Environmental Protection Agency, Environmental Monitoring and Support Laboratory, Cincinnati, OH, 1982.

6. Weast, R. C. (ed.), Handbook of Chemistry and Physics, 63rd ed., The Chemical Rubber Company, 1982-1983.

7. Bryant, W. M. D., Mitchell, Jr., J., Smith, D. M., and Ashby, E. C., "Analytical Procedures Employing Karl Fischer Reagent. VIII. The determination of water of hydration in salts," 1941, J. Am. Chem. Soc., Vol. 63, pp. 2924-2927.

8. Sing, K. S. W., Everett, D. H., Haul, R. A. W., Moscou, L., Pierotti, R. A., Rouquerol, J., and Siemieniewska, T., "Reporting Physisorption Data for Gas/Solid Systems with Special Reference to the Determination of Surface Area and Porosity," 1985, Appl. Chem., Vol. 57, pp. 603-619.

9. Chen, Y., and Schnitzer, M., "Water Adsorption on Soil Humic Substances," 1976, Can. J. Soil Sci., Vol. 56, pp. 521-524.

10. Jurinak, J. J., "Multilayer Adsorption of Water on Kaolinite," 1963, Soil Sci. Soc. Am. Proc., Vol. 27, pp. 269-272.

11. Keenan, A. G., Mooney, R. W., and Wood, L. A., "The Relation Between Exchangeable Ions and Water Adsorption on Kaolinite," 1951, J. Phys. Chem., Vol. 55, pp. 1462-1474.

12. Orchiston, H. D., "Adsorption of Water Vapor: II. Clays at 25 C," 1954, Soil Sci., Vol. 78, pp. 463-489.

13. Mooney, R. W., Keenan, A. G., and Wood, L. A., "Adsorption of Water by Montmorillonite: I. Heat of Desorption and Application of BET Theory," 1952, J. Am. Chem. Soc., Vol. 74, pp. 1367-1371.

14. Van Voorhis, J. J., Craig, R. G., and Bartell, F. E., "Free Energy of Immersion of Compressed Powders with Different Liquids: II. Silica Powder," 1957, J. Phys. Chem., Vol. 61, pp. 1513-1519.

15. Jurinak, J. J., and Volman, D. H., "Thermodynamics of Ethylene Dibromide Vapor Adsorption by Ca-Montmorillonite and Ca-Kaolinite," 1958, Soil Sci., Vol. 86, pp. 6-12.

16. Karnaukhov, A. P., "Improvement of the Methods for Surface Area Determinations," 1985, J. Coll. I. Sci., Vol. 103, pp. 311-314.

17. McClellan, A. L., and Harnsberger, H. F., "Cross-Sectional Areas of Molecules Adsorbed on Solid Surfaces," 1967, J. Coll. Int. Sci., Vol. 23, pp. 577-599.

18. Jurinak, J. J., and Volman, D. H., "Application of the Brunauer, Emmett, and Teller Equation to Ethylene Dibromide Adsorption by Soils," 1957, Soil Sci., Vol. 83, pp. 487-496.

19. Sposito, G., The Surface Chemistry of Soils, Oxford University Press, NY, 1984.

20. Makrides, A. C., "Thermal Aging of Silica Gels," 1959, J. Phys. Chem., Vol. 63:1789-1791.

21. Chiou, C. T., and Shoup, T. D., "Soil Sorption of Organic Vapors and Effects of Humidity on Sorptive Mechanism and Capacity," 1985, Environ. Sci. Technol., Vol. 19, pp. 1196-1200.

22. Norrish, K., "The Swelling of Montmorillonite," 1954, Disc. Far. Soc., Vol. 18, pp. 120-134.

23. Moeller, Therald, Inorganic Chemistry - A Modern Introduction, John Wiley & Sons, NY, 1982.

24. Chiou, C. T., Porter, P. E., and Schmedding, D. W., "Partition Equilibria of Non-ionic Organic Compounds Between Soil Organic Matter and Water," 1983, Environ. Sci. Technol., Vol. 17, pp. 227-231.

(The reverse of this page is blank)

SECTION III

EVALUATION OF GAS CHROMATOGRAPHIC TECHNIQUES FOR MEASURING VAPOR-PHASE ADSORPTION

A. REVIEW OF THEORETICAL BASIS

1. Energetics of Vapor Sorption

Recent rapid advances in chromatographic instrumentation and theory have renewed interest in the adaptation of gas- and liquid- chromatographic methods for measuring sorption of organic pollutants by natural and synthetic sorbents. These methods offer the distinct advantages of speed, reproducibility, and precision compared to the more conventional batch equilibration methods. Gas chromatography (GC) has been used essentially in two ways to study physical adsorption of volatile organic compounds on solid surfaces: (1) the retention time of very small samples of the vapor yields the initial slope (Henry's-law constant) of the sorption isotherm, and (2) chromatographic studies at higher concentrations of the vapor can be used to determine adsorption isotherms at higher surface coverages.

The use of the eluted-pulse gas chromatographic (EP-GC) techniques to determine thermodynamic parameters of vapor-phase adsorption of volatile organic compounds on model sorbents will be evaluated in this section. The use of other GC techniques to measure complete adsorption isotherms for VOC will be discussed in Section IV.

Gale and Beebe (Reference 1) presented a thorough derivation of the determination of ΔH_{ads} by the chromatographic method from basic concepts of adsorption equilibrium processes. More recently this technique was refined and applied to soils and clays (References 2,3,4,5). Boudreau and Cooper (Reference 4) described the method of computing the complete distribution of submonolayer adsorbate-adsorbent interaction energies from a single chromatographic peak.

The change in Gibb's free energy of adsorption for any given initial and final condition, ΔG_{ads}, is given by,

$$\Delta G_{ads} = \Delta H_{ads} - T_c \Delta S_{ads} \qquad (18)$$

where ΔH_{ads} = change in enthalpy of adsorption (kJ/mole), ΔS_{ads} = change in entropy of adsorption (kJ/mole °K), and T_c is soil column temperature (°K). If the reaction is considered to occur under standard-state conditions, then

$$\Delta G^\circ_{ads} = - R\ T_c\ \ln\ V_g \tag{19}$$

where ΔG°_{ads} = change in standard-state Gibb's free energy for the sorption reaction (kJ/mole); V_g = specific retention volume (mL/g); and R = gas constant (0.0821 L·atm/mole·K).

The change in standard-state enthalpy for the adsorption reaction, ΔH°_{ads}, can be determined by from Equation (19) and use of the Gibbs-Helmholtz relation (i.e., $\partial/\partial T\ [\Delta G^\circ_{ads}/T] = [-\Delta H^\circ_{ads}/T^2]$)

$$\ln\ V_g = [-\Delta H^\circ_{ads}/RT] + \text{constant} \tag{20}$$

The change in standard-sta entropy can be determined from an equation analogous to Equation (18):

$$\Delta G^\circ_{ads} = \Delta H^\circ_{ads} - T\ \Delta S^\circ_{ads} \tag{21}$$

Using Equation (20), the ΔH°_{ads} value can be calculated from the slope of a van't Hoff plot of $\ln V_g$ versus the reciprocal of temperature (1/T), and the ΔS°_{ads} value can be determined from Equation (21). It was assumed when deriving Equation (20) that ΔH°_{ads} was independent of temperature, thus any temperature dependence in ΔG° must be assumed to result from the temperature dependence of ΔS°.

The standard state of the adsorbate in the gas phase is defined as the partial pressure of 1 atm at 273.15°K and the adsorbate vapor assumed to behave as an ideal, perfect gas. For the adsorbed phase the standard state is defined such that the mean distance between the adsorbed molecules is equivalent to the intermolecular distance in the three-dimensional gas phase standard state (Reference 1).

2. Measurement of Adsorption Isotherms

a. Linear, Ideal Chromatography

In this region, the adsorption isotherm is assumed to be linear with the sorption coefficient being given by one of the three Equations, (1), (2), or (3). As indicated previously, use of these equations with chromatographic measurements of retention times requires one to be in the infinitely dilute region with respect to both solute concentrations and surface coverages. However, as pointed out by Valentin and Guichon (Reference 6), isotherms derived from GLC systems can have curvature even at concentrations approaching the detection limits of modern gas chromatographs. The major limitation in this region seems to be accounting for the effects of a finite pressure drop along the column on the computed retention volumes. However, it is usually assumed that the Martin-James compressibility factor (j), defined below, adequately accounts for the pressure drop

$$j = \frac{3[(P_i/P_o)^2 - 1]}{2[(P_i/P_o)^3 - 1]} \tag{22}$$

where P_i and P_o are the inlet and outlet pressures.

b. Nonlinear, Finite Concentration Chromatography

Several factors must be taken into account when attempting to measure sorption isotherms from gas chromatographic retention data. The first of these is the so-called sorption effect. The sorption effect becomes significant as solute concentration increases and causes the gas flow rate in the solute zone to be greater than that in the pure carrier gas. The increased flow results from the flux of solute across the phase boundary and the fact that the partial specific volume of the solute in the vapor phase is many times greater than that in the adsorbed phase. The sorption effect results in eluted pulses with relatively sharp front boundaries and diffuse rear boundaries. Thus, the sorption effect on peak asymmetry is the same as the isotherm effect when the isotherm is concave to the x-axis.

Another factor is the thermal effect. Since adsorption often is exothermic and desorption endothermic, there is always the likelihood of temperature gradients across the solute zone. The thermal effect is believed to be secondary to the sorption effect on peak shape and solute retention times and is usually ignored.

Pressure gradients are still a problem in finite concentration GC and must be accounted for if accurate isotherms are to be derived from chromatographic retention data. Two divergent approaches have been used in accounting for pressure gradients in column GC work and both appear to have been used with success to obtain sorption isotherms from GC retention data. Conder and Purnell (Reference 7) and, later, Conder (Reference 8), derived expressions which relate the retention volumes associated with a particular solute concentration in the solute zone to the isotherm slope. This expression is given as follows (Reference 8):

$$V_R = V_m + V_L (1-y) \frac{dq}{dc} \tag{23}$$

Equation (23) gives the retention volume, V_R, of a point of constant concentration, c, on the frontal boundary. The sorption effect results in the factor (1-y), where y is the solute mole fraction corresponding to the concentration, c. V_m is the retention volume of a nonadsorbed solute and V_L is the volume of the stationary phase. In deriving this equation, a zero pressure gradient along the column was assumed. According to Conder (Reference 8), the equation remains valid for finite pressure drops if the retention volume and solute mole fraction, y, are modified by multiplying by the Martin-James compressibility factor (Equation 22). Allowing for gas compressibility, the equation becomes

$$V_R^o = V_m^o + V_L (1-jy_o) \left(\frac{dq}{dc}\right)_p \tag{24}$$

where y_o is the mole fraction of solute measured at outlet pressure. The isotherm slope, dq/dc, refers to a mean pressure given by

$$P = \frac{3P_o}{4} \left[\frac{(P_i/P_o)^4 - 1}{(P_i/P_o)^3 - 1}\right] \tag{25}$$

Equation (25) is equivalent to multiplying the outlet pressure, P_o, by the compressibility factor, J_3^4.

Conder (Reference 8) cautions that the correct outlet flow rate must be used in calculating V_R. As indicated earlier, the flow rate measured in the solute zone is greater than that for the carrier gas alone. The correct flow rate for calculating V_R is that associated with the solute concentration, c, corresponding to y_o. F(y) is related to the flow rate of the pure carrier gas as follows:

$$\frac{F(y)}{F(o)} = \left[\frac{1 + k}{1 + k\ (1-y)}\right] \tag{26}$$

where k is the mass distribution coefficient, the ratio of the amount of solute in the stationary phase to the amount in the equilibrated mobile phase at concentration, c. Thus, the correct measure of retention volume, according to Conder (Reference 8), is

$$jV_R = V_R^o = jF(jy_o)t_R \tag{27}$$

The above theory can be applied to eluted pulse GC data using a method to which Conder (Reference 8) refers as 'Elution by Characteristic Point', or ECP. A single, large pulse is injected on column and the isotherm is then derived from the retention times associated with the various concentrations along the pulse boundary. A typical ECP chromatogram showing a diffuse rear boundary is shown in Figure 32.

When both the sorption effect and pressure gradient are taken into account, the equation relating the stationary phase concentration to the solute mole fraction in the mobile phase, y_o, is as follows:

$$qV_L = \frac{P_o}{RT}\left[\frac{(\alpha + \beta)\ (1 + k)\ F(o)}{y_o}\ \ln\left(1 + \frac{jy_o}{(1 + k)\ (1 - jy_o)}\right)\right.$$

$$\left. + V_m \ln\ (1 - jy_o) - \beta F\ (0.8\ y_o)\right] \tag{28}$$

where α is measured from the instant of injection on the column ($t = 0$), and β is the triangular area bounded by the chromatogram and the time axis. If k is replaced by the expression, $(q/c)(V_1/jV_m)$, the equation relating q to c can be

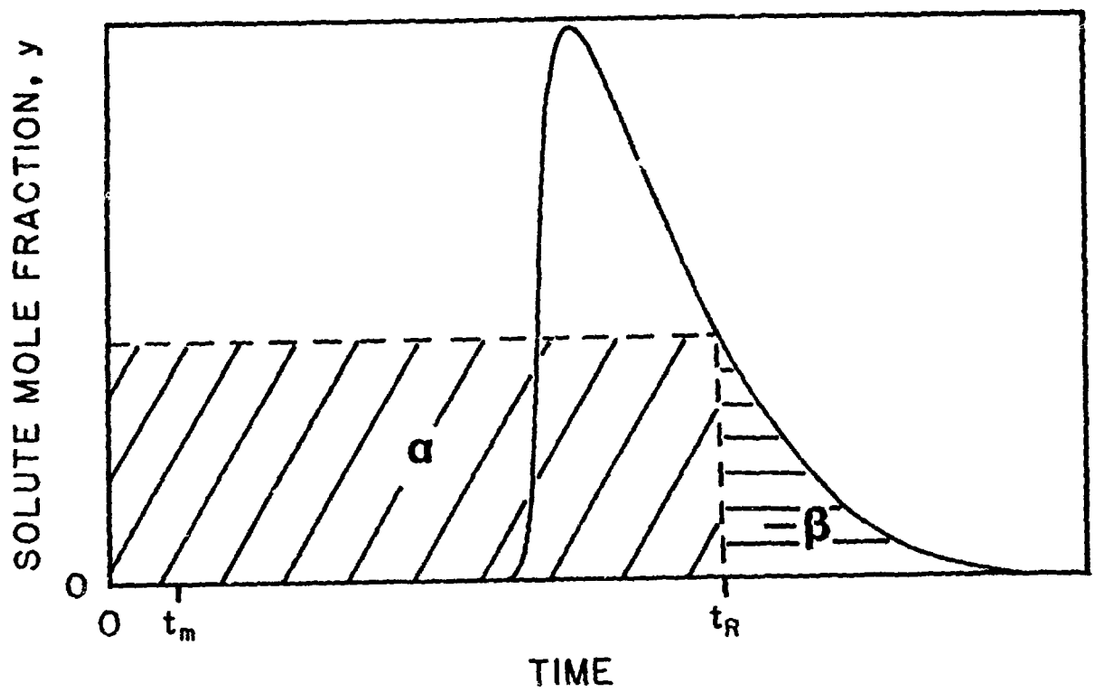

Figure 32. Schematic Representation of a Chromatographic Peak Suitable for the Elution by Characteristic Point (ECP) Method Showing a Diffuse Rear Boundary.

solved, giving a single point on the isotherm. Several points can be obtained by selecting different concentrations along the diffuse boundary of the chromatogram. Thus, an entire isotherm can be derived from a single injection of a sufficiently large pulse.

Conder (Reference 8) cautions that other sources of error must be considered before attempting to derive isotherm from ECP retention data. Obviously, the pressure drop must not be too large since the original derivation of the flow equation was made assuming a zero pressure drop along the column. Another source of error, according to Conder, is that because of nonideal peak spreading which causes the derived an isotherm to deviate from the true isotherm, the sign of the deviation depending on whether the isotherm is initially concave or convex to the concentration axis. Conder recommends using columns of at least 2 meters in length and also using a gas flow rate that minimizes the theoretical plate height. Another problem with short columns is that peak shape measured at the column outlet depends greatly on the shape of the injection band.

A different approach was taken by Valentin and Guichon (Reference 6) in that the flow equation they used to describe the movement of a solute down a column took the finite pressure gradient explicitly into account. They recognized that a negligible pressure gradient, as assumed by Conder and Purnell, was not very realistic when one considers that relatively fine particles are needed to enhance the kinetics of mass transfer and that the resulting pressure drops will generally exceed 1 atmosphere. They also indicate that pressure gradients of this magnitude have a strong influence on the band shape which must be taken into account when deriving the adsorption isotherm. However, they did assume that the pressure gradient was independent of time or solute concentration. The pressure gradient within the column was assumed to be given by the following equation for all times:

$$p(z)^2 = Pi^2 - \frac{z}{L}(P_i^2 - P_o^2) \qquad (29)$$

where z is a coordinate along the column length and L is the column length.

According to Valentin and Guichon (Reference 6), pressure variation directly affects the retention by changing the equilibrium constant when the isotherm is nonlinear. Furthermore, the effect of the pressure

gradient is a function of the adsorption isotherm itself. In agreement with Conder (Reference 8), Valentin and Guichon (Reference 5) also stressed that the calculation of retention volume from retention time requires the use of the actual local flow rate as opposed to the pure carrier gas flow rate. They point out that retention volume cannot be derived simply from t_R in finite concentration chromatography and it losses most of the significance it has under linear, ideal chromatography conditions. The full set of simultaneous equations required to describe the chromatographic system of Valentin and Guichon (Reference 6) is given in Table 10 along with the boundary conditions.

Although the system of equations in Table 10 does not have an analytical solution, Valentin and Guichon (Reference 5) used the Method of Characteristics (Reference 9) to derive certain relationships that describe the peak geometry as it moves down a column. One aspect of the system of equations in Table 10 is that it predicts the formation of concentration discontinuities on either the front, rear, or both sides of a solute zone as it moves down the column. Since concentration discontinuities are physically impossible, the interpretation given to them is that the concentration gradient at the point where a discontinuity is indicated is essentially infinite. The important point made by Valentin and Guichon (Reference 6) is that any region of the chromatogram which results from the interaction of these discontinuities, or shocks, cannot be used to derive information about the isotherm. Many times, the tail of an elution peak cannot be used because it results from the degradation of a shock. The method known as 'Step and Pulse' is particularly advantageous in this respect since no shock can occur to complicate the retention data.

Another result derived from the Valentin and Guichon (Reference 6) model is that the pressure gradient enhances the isotherm effect (the peak asymmetry due to nonlinearity of the sorption isotherm). According to these authors, the pressure gradient impacts on peak broadening and deformation and it cannot be accounted for by the use of an average column pressure as was done by Conder and Purnell (Reference 7). The coupling of the isotherm effect and the pressure gradient invalidates most methods of determining isotherms by using GC retention data.

An equation derived by Valentin and Guichon (Reference 6) which relates GSC retention times to the slope of the isotherm assuming that some

TABLE 10. THE SYSTEM OF EQUATIONS DERIVED BY VALENTIN AND GUICHON (RRFERENCE 6) TO DESCRIBE THE MOVEMENT OF A GASEOUS SOLUTE ZONE ALONG A CHROMATOGRAPHIC COLUMN.

I. F, X Continuous

$$P \left(\frac{\partial X}{\partial t}\right) [1 + k' (1 - x)] = -F \left(\frac{\partial X}{\partial z}\right)$$

$$P \left(\frac{\partial X}{\partial t}\right) k' = -\frac{\partial F}{\partial z}$$

$$F = uP$$

$$k' = (\partial n_L / \partial n_G)_P \quad \text{(Capacity factor)}$$

$$P = P_i^2 - z/L \, (P_i^2 - P_o^2)$$

II. F, X Discontinuous

$$V_{12} = \frac{u_1}{1 + \frac{k_2 - k_1}{X_2 - X_1} (1 - X_2)} = \frac{u_2}{1 + \frac{k_2 - k_1}{X_2 - X_1} (1 - X_1)}$$

$$k_1 = \int_0^{X_1} k' \, dX \qquad k_2 = \int_0^{X_2} k' \, dX \quad \text{(Retardation factor)}$$

II. Boundary Conditions

$u(0,t) \equiv U_o$ (gas velocity)

$t = 0 \qquad X(z,0) \equiv 0$

$0 < t \leq \zeta \qquad X(0,t) = X(t)$

$t > \zeta \qquad X(0,t) = 0$

Note that this is different from the Conder (Reference 8) method since the latter method gives direct estimates of Γ [referred to as q by Conder (Reference 8)] and does not require one to choose any particular model of the adsorption process.

portion of the chromatogram can be found which has not interacted with shocks is as follows:

$$\left[\frac{t_x - t_m}{1 - y}\right]\left[\frac{P^{\circ}_A V_o}{jRTSm_s}\right] = \int_{P_o}^{P_i} \left(\frac{d\Gamma}{d\pi}\right) \frac{3p^2 dp}{P_i^3 - 1} \qquad (30)$$

where Γ is the number of moles per unit mass or area of adsorbent, π is the dimensionless ratio of solute vapor pressure to the saturated vapor pressure. P^{o}_{A}, $d\Gamma/d\pi$ is the slope of the sorption isotherm, P_o is outlet pressure, and P_i is the inlet pressure. Note that it is not possible to directly plot an isotherm from measurement of retention times. Instead, one uses retention data to optimize the parameters of a model isotherm. The isotherm is then plotted using these optimized parameters. Actual experimental data points used to verify the GC derived isotherm must be provided by other methods such as those used in batch sorption experiments.

B. MATERIALS AND METHODS

1. Chromatographic Soil Columns

The energetics of sorption of various VOC was studied in packed soil columns using the EP-GC method. The physicochemical characteristics of the soils used in this study are given in Table 2 (see Section II). With the exception of the Oldsmar fine sand collected from the spodic soil horizon, all other soils were sieved to pass through a 60-mesh screen (0.25 mm) before packing in the columns. The soils judged as having low sorption capacities (based on low surface areas and batch sorption data) were packed in the columns without dilution, while those with large sorption capacities were diluted with treated sand. This sand to be used as a diluent was prepared by first digesting it in concentrated HCl for 24 hours, then in 30 percent H_2O_2 to remove the organic matter. The sand was then washed with 1N HCl and deionized water before igniting at 550°C for 6 hours. The physical conditions of the column packing materials are shown in Table 11.

All columns used in this study were made from 15 cm lengths of glass tubing with 0.32 cm o.d. and 0.155 cm i.d. The packed sorbent bed length was approximately 10 cm, and the two ends of the column were plugged with

TABLE 11. SUMMARY INFORMATION ON THE CHROMATOGRAPHIC SOIL COLUMNS

Column name	Sorbent	Sorbent mass	Soil bulk density	Surface area
		g	g/cm^3	m^2
O-100	Oldsmar spodic	0.43	1.82	1.63
B-101	Borden sand, <60-mesh	0.41	1.74	1.14
LCI-005	3.4 percent Lula, <60-mesh; w/sand	0.65 total 0.022 Lula		2.63 Lula
Sand V	treated Eustis sand, <60-mesh	0.38	2.67	1.75
W-025	25 percent Webster, <60-mesh; w/sand	0.34 total 0.085 Webster		8.10 Webster

silanized glass wool. Sorbents were oven-dried at 160°C before packing into the columns. Diluted packing materials were dried as separate components and weighed before mixing and packing to be certain of the composition.

The VOC sorption studies in packed soil columns were carried out using a Tracor Model 220 gas chromatograph equipped with a flame ionization dector (FID). Zero-grade hydrogen and oxygen (<0.1 ppm total hydrocarbon) were used for the FID, and zero-grade nitrogen was the carrier gas. The packed column was initially conditioned at 160°C overnight or until no change in column weight was detected. The temperature was then adjusted to the required experimental level and allowed to equilibrate. The temperature was monitored by a thermocouple with a digital readout device (Bailey model BAT-8) and maintained within 0.1°C of the desired set temperature.

2. Experimental Parameters

Under a predetermined set of conditions, measurements of specific retention volumes for several sorbates were collected over a range of temperatures (40-140°C). The inlet pressure (1.0-1.3 atmospheres) depended on the temperature used. The outlet was at atmospheric pressure. The ambient pressure was measured with a mercury barometer and the inlet pressure by

difference, using an open-end mercury manometer fitted with a syringe needle for piercing the inlet septum. The carrier gas flow rate was 2.97 mL/min, as determined with a soap-film and buret flowmeter and maintained by means of a digital flow controller. The injection pulse size was 10 μL and the retention time was recorded directly on the chromatogram by an HP 3390A recording integrator. Relative retention times for the target compounds were calculated by subtracting the retention time for methane (t_o) from the retention times of the compounds under identical injection conditions (t_r), as in Equation (31).

$$t'_r = (t_r - t_o) \tag{31}$$

Standardized injections of the vapor pulses were made as follows: (1) 100 μL gas tight syringe filled with saturated vapor; (2) vapor expelled; (3) needle volume diluted to 100 μL; (4) all but 10 μL expelled; and (5) 10 μL injected.

Retention volumes (V_s) were then calculated from:

$$V_s = [t'_r F_a (T_c/T_a) j] A^{-1} \tag{32}$$

where, F_a is the carrier gas flow rate (mL/min) determined at ambient temperature T_a (K), T_c is the column temperature (K), A is the total N_2-surface area of the sorbent in the column (m^2), and j is the James-Martin compressibility factor [Equation (22)].

Initially, retention volumes were reported relative to the mass of sorbent in the column, but as the sorbent specific area information has become available, retention volumes were reported on the surface area basis. Also, for the diluted column studies the retention volumes were corrected for the surface area of the sorbent of interest.

3. Effects of Sample Size and Flow Rate

To use the equations given in the previous section to determine the sorption thermodynamic parameters, two conditions must be met. One is that the amount of vapor injected must be small enough so that the data obtained correspond to the linear portion of the adsorption isotherm (i.e., the Henry's law region). The second condition is that the interstitial gas flow velocity

must be small enough to assure equilibrium adsorption during transport of the vapor pulse through the chromatographic soil column. If these conditions are not met, the values for the sorption thermodynamic parameters obtained by the EP-GC technique have no meaning. Validity of both these assumptions was examined by measuring the retention volumes at several flow rates and for injections of several pulse sizes.

The effect of pulse size and concentration on retention time was evaluated to satisfy the first condition mentioned above. The vapor samples were injected on-column using a gas tight syringe. Using the standardized injections described above, Steps 1-5 were repeated several times to give a statistical sample of retention times. Following the last such injection, several more were made repeating only Steps 3-5. This process was continued until the signal was lost in the baseline.

The effect of carrier gas flow rate on the effective retention volume of a target compound was evaluated on the diluted Webstar column. For this purpose the most highly retained sorbate, 1,1,2,2-tetrachloroethane, was studied at the lowest temperature used for this column, 75°C.

4. Evaluation of Sorption by Hydrated Sorbents

To investigate the energetics of sorption of the target compounds in the presence of water, the carrier gas delivery system was modified to allow for the addition of water vapor at different relative humidities (RH). A schematic of the plumbing diagram is shown in Figure 37. In this application, the bubbler was filled with water and the system allowed to equilibrate until the column outlet showed a constant RH. Different RH levels were accomplished by varying the relative settings of dry and water-saturated carrier gas.

The actual RH level at different flow settings was determined by trapping the system effluent in a series of carbon traps. The carbon traps were degassed on a stream of dry N_2 overnight or until they had been brought to constant mass. Two carbon traps were then placed in series at the column outlet for a timed interval and the mass gained related to the water vapor contained in the calibrated gas flow. The failure of the second trap to show a mass gain would serve to demonstrate the efficiency of the technique.

After evaluating the Borden column (B-101) at three RH levels, the other columns listed in Table 10 were investigated at only the lowest setting.

This was done in order to maximize our ability to measure any sorption under these conditions.

5. Measurement of Adsorption Isotherms

a. GC Column

The column used to evaluate the utility of the gas chromatographic methods for measuring vapor adsorption isotherms was packed with a mixture of SAz-1 clay and treated sand used as a diluent. Both the clay and the sand were oven-dried at 160°C. In order to minimize subsampling errors in packing the column, 2.33 mg of SAz-1 clay and 0.39905 grams of treated sand were mixed, and this entire sample was then packed in to a 15 cm long glass column (0.15 cm i.d.). Both ends of the column were packed with silanized glass wool. Prior to use, the packed column was conditioned in the GC oven at 160°C under a continuous flow of anhydrous N_2 gas.

b. Sorbates

The compounds used in this study were: n-hexane, cyclohexane, p-xylene, and trichloroethene (TCE). Cyclohexane was obtained from Eastman Chemicals, while all others were purchased from Fisher Scientific, Inc. All chemicals were reagent-grade and used as received from the vendor without purification.

c. Eluted-Pulse Technique

Following the development by Valentin and Guichon (Reference 6), several different sized injections were made and overlayed such that the tails of the decaying chromatographic peaks produced a collection of peak heights traced as a function of retention time. The detector was calibrated by replacing the column with a minimum volume capillary tube and injecting volumes larger than the dead volume in order to achieve a plateau response to a known concentration of vapor.

Isotherms were calculated for p-xylene and n-hexane assuming that the BET model is appropriate. With detector response being related to

the mole fraction (X) of the solute in the vapor, it is possible to tabulate values of R_x as a function of X and t_x from:

$$R_x = \left[\frac{(t_x - t_m)}{t_m}\right] \left[\frac{1}{(1 - X)}\right] \tag{33}$$

where t_x is the retention time associated with the mole fraction of solute in the vapor, X; and t_m is the retention time associated with an unretained vapor, methane. This value of R_x relates to the derivative form of the sorption isotherm slope integrated over the pressure differential of the column.

$$R_x = \int_{P_{out}}^{P_{in}} k' \left[\frac{3p^2}{p^3 - 1}\right] dp \tag{34}$$

$$\text{where } k' = S\, m_s \left[RT/V_g\, P_A^\circ\right] \cdot \left[d\alpha/d\pi\right] \tag{35}$$

$$\text{and } \pi = P_A/P_A^\circ = \left[pX/P_A^\circ\right] \tag{36}$$

$$\text{From the BET:} \quad \frac{d\alpha}{d\pi} = \frac{\alpha_m C \left[1 + \pi^2 (C-1)\right]}{\{(1-\pi) \left[1 + \pi (C-1)\right]\}^2} \tag{37}$$

$$\text{and defining} \quad a = \frac{X}{P_A^\circ} \tag{38}$$

$$b = \left[\frac{3\, S\, m_s\, RT}{V_G\, P_A^\circ\, (p^3-1)}\right] \tag{39}$$

We rewrite Equation (34) as follows:

$$R_x = b\, \alpha_m C \int_{P_{out}}^{P_{in}} \frac{1 + p^2\, a^2\, (C-1)\, p^2}{\{(1-pa) \left[1 + pa\, (C-1)\right]\}^2}\, dp \tag{40}$$

where the remaining terms are defined as follows: α = moles solute sorbed per m^2; S = specific surface area in m^2/g; m_s = mass of sorbent in the column in grams; α_m = monolayer capacity in moles/m^2; C = constant related to heat of adsorption; and p = local pressure in the column.

d. Step-and-Pulse Technique

In order to avoid complications by several factors on the shape of the degrading tail of an eluted pulse, an attempt was made to measure retention times of small pulses superimposed on the plateau of a concentration "step." This is accomplished by maintaining a given concentration of solute through the system and measuring the retention times of small pulses of air (negative peaks) or solute (positive peaks). To achieve the steps of solute concentration, the carrier gas delivery system was modified as shown in Figure 33. By adjusting the relative flows of dry and saturated carrier gas, different concentrations of solute were achieved. The concentration was determined by trapping the column effluent in methanol traps for a timed interval and assaying aliquots of the methanol solution by HPLC analysis in the same manner as described earlier (see Section II.A.3.a.3).

C. RESULTS AND DISCUSSION

1. Energetics of Adsorption

a. Effect of Sample Pulse Size and Flow Rate

A sample of retention times for dilute injections (dil.-t_r) compared to their initial values (t_r) is presented in Table 12. At column temperatures of 45°C and above, no effect on t_r values as a result of sample dilution was observed. Chromatograms for various volumes of cyclohexane saturated headspace injected on the Oldsmar column are presented in Figure 34. These data indicate that variation of pulse size had no measurable effect on retention times. Similar experiments were carried out on each column prior to collection of temperature-dependent data to verify that the first such injection was already dilute enough to satisfy the condition of linearity.

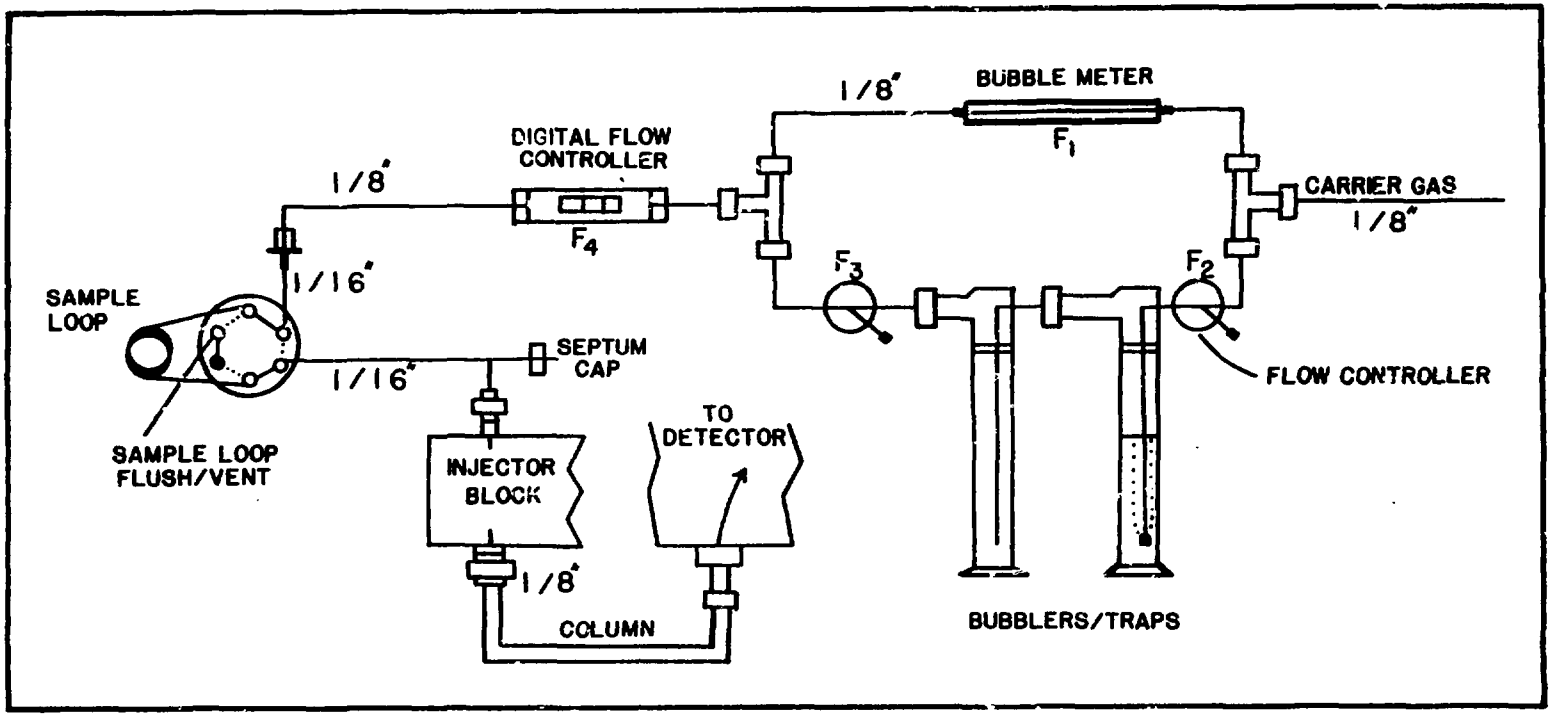

Figure 33. Schematic of the Gas Chromatographic Apparatus Used to Measure Sorption.

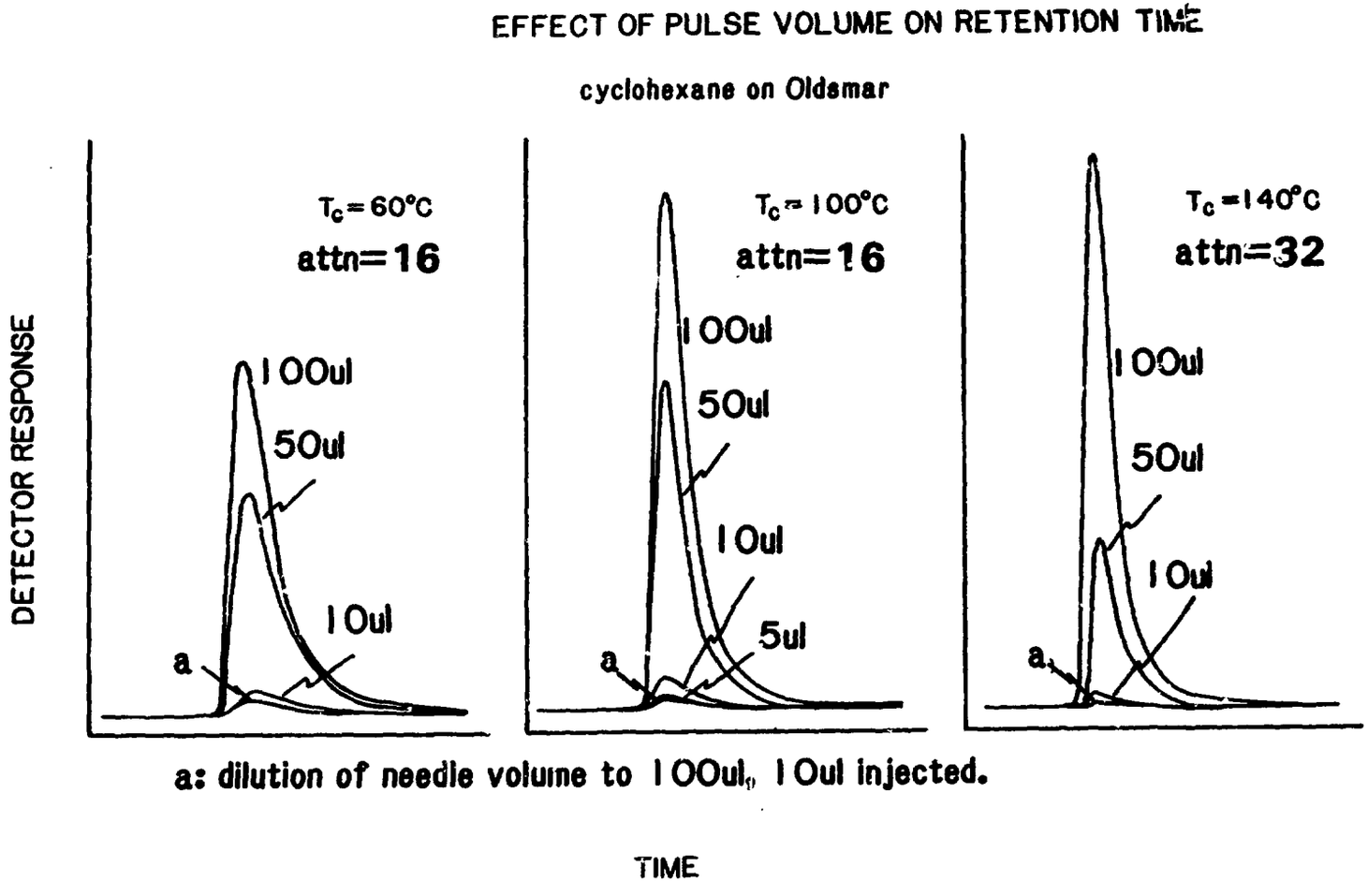

Figure 34. Chromatograms for Various Pulse Sizes of Cyclohexane Saturated Headspace Injected on the Oldsmar Column.

TABLE 12. RETENTION TIMES (t_r, SECONDS) AS A FUNCTION OF INJECTED PULSE CONCENTRATION

Compound	Column Temperature (°C) 110 t_r	110 dil-t_r	100 t_r	100 dil-t_r	90 t_r	90 dil-t_r
ethane	a	a	a	a	0.07	0.06
butane	a	a	a	a	0.13	0.17
pentane	a	a	0.24	0.15	0.13	0.12
hexane	0.12	a	0.27	0.07	0.27	0.25
heptane	0.25	0.10	0.58	0.40	0.58	0.53
cyclohexane	0.22	0.04	0.26	0.32	0.31	0.23
toluene	0.68	0.57	0.73	0.63	1.34	1.41
ethylbenzene	1.30	1.09	1.63	1.55	2.83	2.93
o-xylene	1.86	1.80	2.22	2.05	3.60	3.76
m-xylene	1.55	1.36	1.90	1.78	3.17	3.34
p-xylene	1.37	1.56	1.88	1.74	3.21	3.34
1,2-dichloroethane	0.50	0.26	0.47	0.28	0.69	0.79
1,1,2,2-tetrachloroethane	1.90	2.25	2.76	2.75	4.64	4.76
t-dichloroethane	0.18	0.09	0.14	0.09	0.16	0.15
trichloroethene	0.35	0.30	0.42	0.34	0.54	0.52

a) These values are smaller than the standard errors in the original t_r values.

The results of flow velocity studies are presented in Table 13. The measured retention times for 1,1,2,2-tetrachloroethane are variable with an average value of 6.8 ∓ 0.2 mL/g; however, a trend of increase in V_g with decreasing flow rate is not apparent. This indicates that the chromatographic conditions of the experiment allowed for sorption equilibrium to be attained.

b. Enthalpies of Adsorption

Gale and Beebe (Reference 1) found that ΔH_a values obtained by the EP-GC method showed excellent agreement with those measured by other techniques. In Table 14 the ΔH_a data derived from the EP-GC method are compared with heats of vaporization (ΔH_v) data. The ΔH_a values presented in Table 14 were determined from van't Hoff plots using retention data obtained over a wide range of temperatures (40°-140°C). This assumes that total heats of adsorption are not greatly dependent upon temperature over a considerable

TABLE 13. RETENTION VOLUMES (V_g, mL/g) AS A FUNCTION OF CARRIER GAS FLOW RATE[1].

Flow rate	P_{atm}	P_{inlet}	t_r	t_0	t'_r	j	V_g'
mL/min	mm Hg	mm Hg	---------sec----------				mL/g
6	762	828	8.32	3.82	4.50	0.958	6.8
7.2	763	826	7.77	3.80	3.97	0.960	6.3
18.1	762	913	3.36	1.66	1.70	0.907	6.4
41.0	762	1038	1.74	0.84	0.90	0.840	7.2
75.0	762	1214	1.06	0.50	0.56	0.758	7.3
						Average	6.8±0.2

[1]Column temperature (T_c) was 351 K.

TABLE 14. COMPARISON OF ΔH_{ads} VALUES MEASURED USING EP-GC METHOD WITH ΔH_{vap} VALUES[1].

Compound	ΔH_{vap} (25°C)[2]	ΔH_{vap} (25°C)[3]	ΔH_{vap} (BP)[4]	ΔH_{ads} by EP-GC Method			
				Webster	Oldsmar	Borden	Lula
	----------kJ/mole[1]----------						
Cyclohexane	33.04	32.76	29.96	42.7	20.4	13.7	21.37
Benzene	33.84	34.09	30.73	--	18.1	14.2	27.67
Toluene	37.99	35.09	33.18	15.1	21.7	17.3	33.77
Ethylbenzene	42.25	38.92	35.20	24.7	26.1	21.4	38.02
o-Xylene	43.43	41.83	36.82	29.3	27.6	20.5	39.01
m-Xylene	42.66	41.44	36.36	27.6	27.6	20.2	39.78
p-Xylene	42.38	41.05	35.98	27.6	26.9	20.2	38.37
Propylbenzene	--	43.61	--	--	30.9	24.4	41.45
Butylbenzene	51.05	46.24	39.25	--	35.9	25.4	44.86
1,2-Dichloroethane	34.27	33.26	32.02	20.1	16.6	16.4	31.88
1,1,2,2-Tetrachloroethane	44.98	41.50	38.64	29.3	32.5	24.5	43.56
trans-Dichloroethene	30.04	34.79	28.89	12.1	12.8	14.1	19.66
Trichloroethene	34.27	34.79	31.47	29.3	21.2	14.1	24.32

[1]All ΔH values are negative
[2]Reference 9.
[3]Reference 10.
[4]Reference 11.

range of temperature. However, because the heats of vaporization (ΔH_{vap}) are temperature-dependent, ΔH_{ads} values may also be expected to vary with temperature. In Figures 35-37, note that, at intermediate temperatures, the data points were sufficiently close to the regression line (close to linearity), but those for the highest and the lowest temperatures showed a slight deviation from the straight line. On this basis, heats of adsorption at the two lowest temperatures were estimated using the Clausius-Clapeyron equation. These ΔH_{ads} estimates are presented in Table 15.

The ΔH_{ads} values obtained over the entire temperature range were consistently lower than those derived from the headspace method. The ΔH_a values calculated from the two lowest temperature points, were much larger (negative values) than those calculated from the data over the entire temperature range. This is important when one considers that the headspace sorption techniques generated data only in the 25°-40°C temperature range. The ΔH_{ads} values measured by the EP-GC method at lower temperatures and the headspace method are in reasonable agreement with ΔH_{vap} values.

TABLE 15. COMPARISON OF THE ΔH_{ads} VALUES COMPUTED USING CHROMATOGRAPHIC DATA FOR THE LOW (40°-60°C) AND HIGH (40°-140°C) TEMPERATURE RANGES.*

Compound	EP-GC Method		HS Method
	Oldsmar High T	Oldsmar Low T	Oldsmar T=24°C
	----------kJ/mole----------		
Cyclohexane	20.4	34.8	34.2
Benzene	18.1	30.3	--
Toluene	21.7	26.8	37.2
Ethylbenzene	26.1	25.8	--
o-Xylene	27.6	34.7	--
m-Xylene	27.6	35.6	--
p-Xylene	26.9	39.1	--
Propylbenzene	30.9	19.2	--
Butylbenzene	35.9	43.4	--
1,2-Dichloroethane	16.6	32.2	--
1,1,2,2-Tetrachloroethane	32.5	46.0	--
trans-Dichloroethene	12.8	38.9	--
Trichloroethene	21.2	35.5	23.3

*All ΔH_{ads} values are negative.

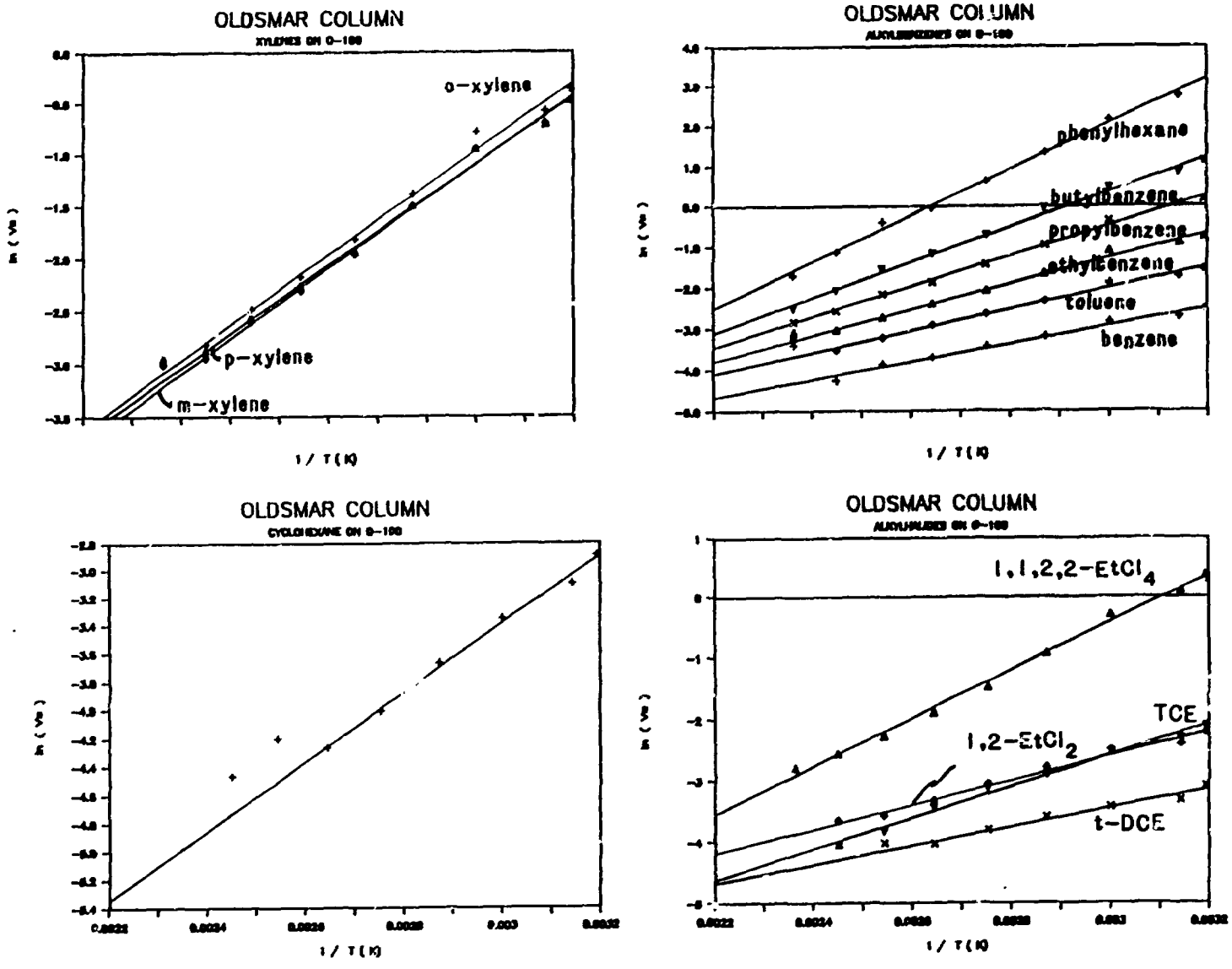

Figure 35. van't Hoff Plots of the Chromatographic Data Obtained Using the Oldsmar Column.

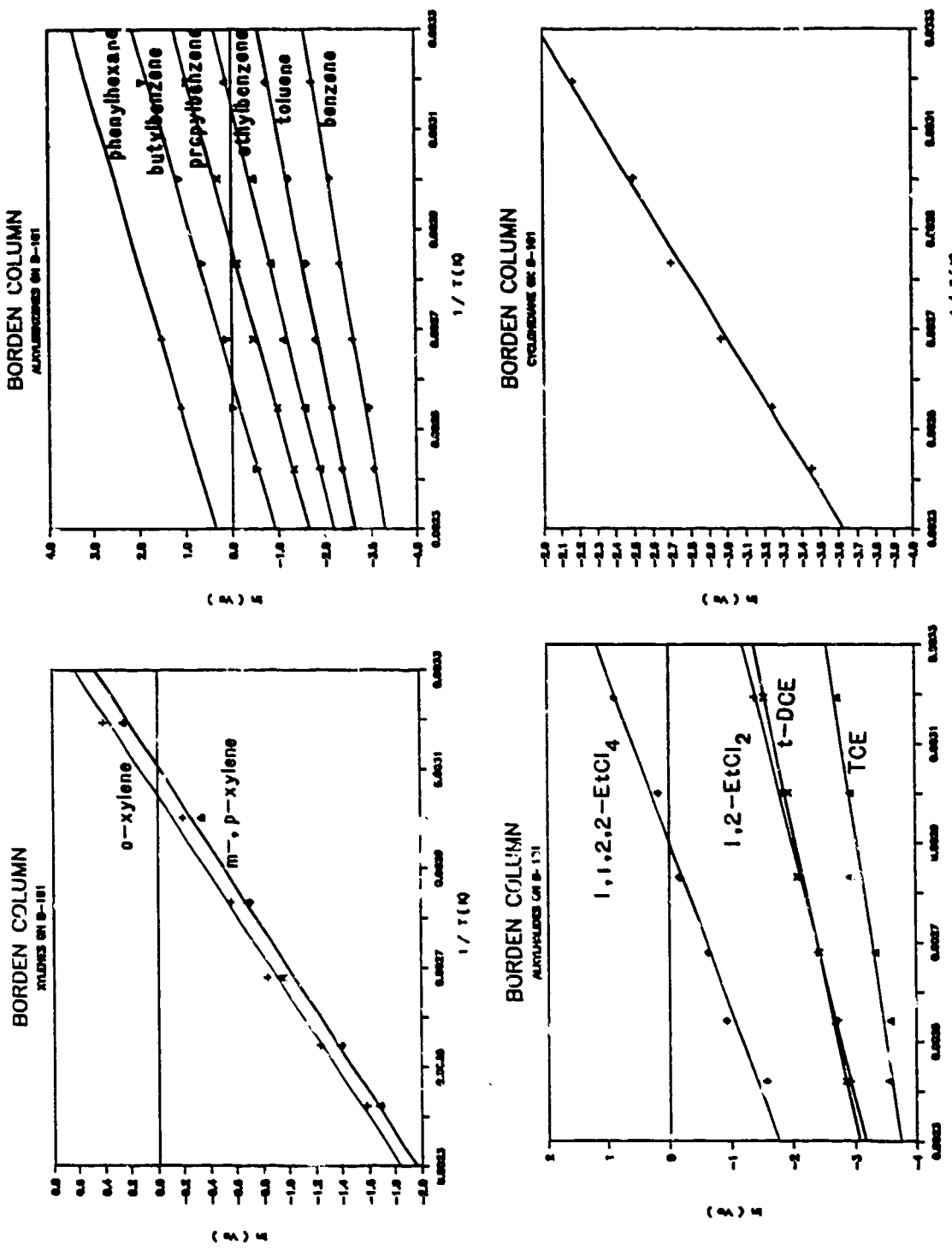

Figure 3 BORDEN

Figure 36. van't Hoff Plots of the Chromatographic Data Obtained Using the Borden Column.

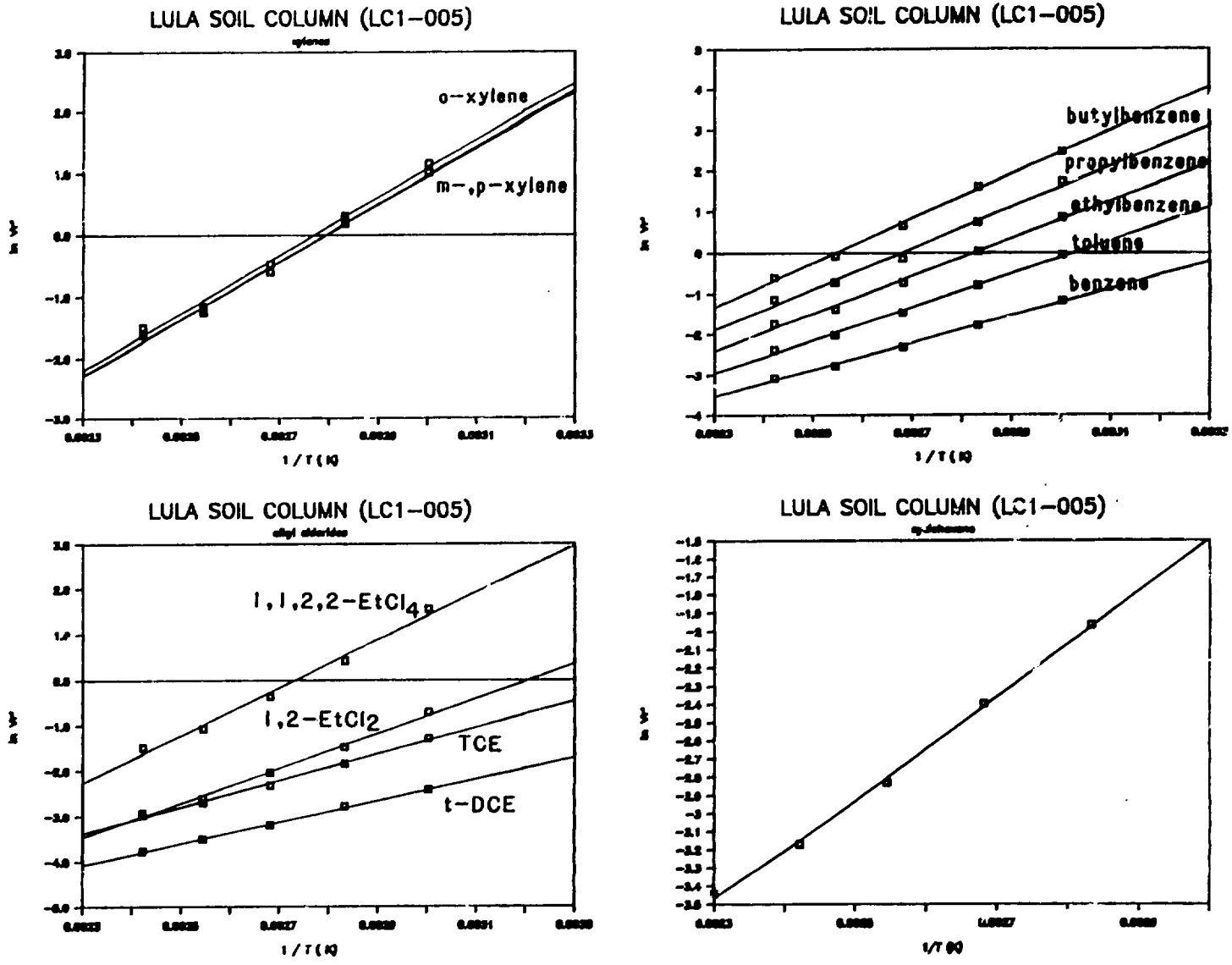

Figure 37. van't Hoff Plots of the Chromatographic Data Obtained Using the Lula Column.

c. Sorption on Hydrated Sorbents

The investigation of the energetics of sorption of organic vapors in the presence of water vapor was an attempt to parallel the work of Okamura and Sawyer (Reference 5). RH levels of 48, 21, and 10 percent were investigated for the Borden column (B-101) at three temperatures, 140°, 100°, and 60°C. Even at the lowest temperature, there was no measurable sorption for any of the target compounds under these conditions. Only the 10 percent RH study was attempted for the other columns listed in Table 11, with the intention to expand to higher RH values for those systems in which a retention greater than dead volume could be observed.

The Borden, Oldsmar, and Webster columns all showed similar results at 10 percent RH. None of the compounds showed any measurable retention in the presence of water vapor. The results for the Lula column (LCI-005) were very inconsistent. Because of these results, this part of the research effort was discontinued due to time constraints.

2. Measurement of Adsorption Isotherms

a. Eluted-Pulse Technique

Optimal values for α_m and C were obtained by a mathematical fitting procedure. The integration and curve-fitting procedures were performed using a twelve-point Gaussian integration scheme (Reference 13) and a nonlinear curve fitting procedure called PROC NLIN available on SAS (Reference 14). The estimated values of α_m and C are summarized in Table 16.

TABLE 16. SUMMARY OF BET ISOTHERM PARAMETERS ESTIMATED USING THE ELUTED PULSE TECHNIQUE.

Compound	Column temp. (°C)	α_m (moles/m^2)	C
n-hexane	28.3	9.6×10^{-8}	16.035
p-xylene	28.5	8.4×10^{-8}	16.49
	43.6	5.1×10^{-8}	26.95
	44.0	6.1×10^{-8}	23.31
	80.2	4.9×10^{-8}	73.27
	120.0	1.8×10^{-8}	698.7

The calculated values of a_m for p-xylene (at T = 28.5°C) are about 5-10 times smaller than those estimated using the dynamic flow method, while the C values are in agreement. The reasons for this disparity have not been thoroughly investigated. However, it was noted that all degrading peak tails looked alike near the baseline and we were concerned that a mechanical system response was interfering with the observation of the isotherm effect. To overcome this we need to recalculate the isotherms using only the steeper portion of the tail, and the revised parameter estimates should be compared with those from other methods.

b. Step-and-Pulse Technique

The work here has progressed only far enough to indicate that equilibrium state measurements are possible, but the adsorption isotherm parameters have not been calculated. At three different concentrations of p-xylene, for each of three different temperatures, both positive and negative peaks gave similar retention times. These data were averaged and are summarized in Table 17.

D. CONCLUSIONS

The data reported here lead to the conclusion that in addition to the interest in its established use as a method of analysis and separation, gas-solid chromatography offers a promising technique for the determination of thermodynamic data for the retention of organic vapors by natural sorbents.

TABLE 17. STEP-AND-PULSE RETENTION TIMES FOR p-XYLENE ON THE SAz-1 CLAY COLUMN.

P/P_o	Retention Times (t_r, min)		
	44°C	80°C	120°C
0.38	1.12	0.81	0.18
0.18	2.34	1.04	0.26
0.06	3.81	1.84	0.64

This corroborates the findings of others who have used the technique to measure heats of adsorption (References 1,2,3,5,15). The EP-GC technique is reliable, straightforward, fast and capable of producing a large body of thermodynamic data in a relatively short period of time. Additional work is needed to expand the use of this technique to determine the adsorption energy distribution functions. Despite the numerous attributes of gas chromatographic techniques, there are a few limitations. For instance, because of the possibility of gas condensation, the desired parameters at low temperatures are obtained by extrapolation from data obtained at higher temperatures. Such parameters may not necessarily give the correct picture of sorption processes at lower temperatures, which are typical for most environmental applications relevant to groundwater contamination.

Within measurement errors, the measured heats of adsorption values are similar to heats of vaporization for the compounds examined in this study. The heats of solution (ΔH_{sol}), estimated based on temperature-dependence of Henry's-law constant, are usually within 5-10 kJ/mole of ΔH_{vap}. Thus, either ΔH_{vap} or ΔH_{sol} may be used as a first-best estimate of ΔH_{ads}.

Efforts to measure sorption in the presence of water vapor points out the need for modification in column design. Whenever a small amount of water decreases sorption of organic vapors by orders of magnitude, one needs to investigate the system with a much longer column in order to magnify the effect. The resultant increase in pressure gradient across the column and added dispersion may be equally difficult to overcome. This aspect needs to be further evaluated.

Our preliminary evaluation of the eluted-pulse and the step-and-pulse GC methods for determining vapor sorption identified a number of experimental and design modifications that are needed before additional data are collected. We used the same columns as those used to measure the energetics of adsorption. Column lengths, the amount of sorbent packed (in case of diluted sorbents), and the pulse sizes injected need to be optimized to enable the measurement of the adsorption effects. The shapes of the measured asymmetrical peaks, as recorded on the integrator, can be influenced by the lag-time in mechanical and electronic response of the instrument. Additional work is needed to improve column design and data collection techniques.

E. REFERENCES

1. Gale, R. L., and Beebe, "Determination of Heats of Adsorption on Carbon Blacks and Bone Material by Chromatography Using the Eluted Pulse Technique," 1964, J. Phys. Chem., Vol. 68, pp. 555-567.

2. Bohn, H. L., Prososki, G. K., and Eckhardt, J. G., "Hydrocarbon Adsorption by Soils as the Stationary Phase of Gas-solid Chromatography," 1980, J. Environ. Qual., Vol. 9, pp. 563-565.

3. Boudreau, S. P., Smith, P. L., and Cooper, W. T., "HGSC: A New Approach to Inverse Chromatography," 1987, Chromatography, Vol. 2, pp. 31-35.

4. Boudreau, S. P., and Cooper, W. T., "Determination of Surface Polarity by Heterogeneous Gas-solid Chromatography," 1987, Anal. Chem., Vol. 59, pp. 353.

5. Okamura, J. P., and Sawyer, D. T., "Gas-chromatographic Studies of Sorptive Interactions of Normal and Halogenated Hydrocarbons with Water-modified Soil, Silica, and Chromosorb W.," 1973, Anal. Chem., Vol. 45, pp. 80-84.

6. Valentin, P., and Guichon, G., "Determination of Gas-liquid and Gas-solid Equilibrium Isotherms by Chromatography: II. Apparatus, Specification, and Results," 1976, J. Chrom. Sci., Vol. 14, pp. 132-139.

7. Conder, J. R., and Purnell, J. H., "Gas Chromatogrpahy at Finite Concentration: 2. A Generalized Retention Theory," 1968, Trans. Far. Soc., Vol. 64, pp. 3100-3111.

8. Conder, J. R., "Thermodynamic Measurement by Gas Chromatography at Finite Solute Concentration," 1974, Chromatographia, Vol. 7, pp. 387-394.

9. Aris, R., and Amundson, N. R., Mathematical Methods in Chemical Engineering, Vol. 2, Prentice-Hall, Englewood Cliffs, New Jersey, 1973.

10. Riddick, J. A., Bunger, W. B., and Sakano, T. K., "Organic Solvents: Physical Properties and Methods of Purification, 4th edition," in: Techniques in Chemistry, Volume III, John Wiley and Sons, Inc., New York, 1986.

11. Weast, R. C. (ed.), CRC Handbook of Physics and Chemistry, 51st edition, CRC Press Inc., Boca Raton, Florida, 1983.

12. Research Triangle Park Institute.

13. Scheid, Francis, "Schaum's Outline of Theory and Problems of Numerical Analysis," Chapt. 15, in: Schaum's Outline Series, McGraw-Hill, pp. 135.

14. SAS version 5, SAS Institute

15. Ross, S., Saelens, J. K., and Olivier, J. P., "On Physical Adsorption: XVIII. Limiting Isosteric Heats of Adsorption of Gases on Graphitized Carbon by the Chromatographic Method," 1962, J. Phys. Chem., Vol. 66, pp. 696.

SECTION IV

NONEQUILIBRIUM SORPTION DURING TRANSPORT

A. EQUILIBRIUM AND NONEQUILIBRIUM SORPTION

The local equilibrium assumption (LEA) is a major component of the conventional convective-dispersive solute transport equation. This model, referred to as the CD model here, can be stated as follows:

$$R \frac{\partial C}{\partial p} = \frac{1}{P} \frac{\partial^2 C}{\partial X^2} - \frac{\partial C}{\partial X} \tag{41}$$

$$P = (vL/D); \qquad R = [1 + (\rho K_d / \theta)] \tag{42a}$$

$$X = (x/L); \qquad p = (vt/L) \tag{42b}$$

where C is the pore-fluid concentration (mg/L); x is the distance (cm); t is the time (hr); P is the Peclet number; v is the pore-water velocity (cm/hr); L is column length (cm); D is the hydrodynamic dispersion coefficient (cm^2/hr); R is the retardation factor; ρ is the bulk density (g/cm^3); K_d is the sorption coefficient (mL/g) measured as the slope of the linear sorption isotherm; θ is the volumetric water content (mL/cm^3); X is dimensionless distance; and p is dimensionless time, which is equivalent to pore volumes.

If the LEA is to be valid the rate of sorption process must be fast, relative to the other processes affecting solute concentration (e.g., convection, and hydrodynamic dispersion) in the porous medium so that equilibrium may be established between the sorbent and the pore fluid. Because of the generally slow movement of water in subsurface, equilibrium conditions might be expected to prevail and, therefore, the LEA should be valid. Detailed laboratory and field investigations, however, have revealed that in many cases this assumption is invalid.

Sorption data from batch experiments have been found to exhibit a two stage approach to equilibrium: a short initial phase of fast uptake followed by an extended period of much slower uptake. This pattern is followed by most, if not all, sorption reactions (References 1,2). Generally, roughly 50

percent of the sorption occurs within the first few minutes or hours, with the remainder occurring over periods of days or months (References 3,4,5,6,7,8).

Assuming that isotherm nonlinearity and nonsingularity effects are negligible and that hydrodynamic dispersion induced asymmetry is small, the solute breakthrough curves (BTC) for a sorbed solute measured from miscible displacement experiments using packed columns should be symmetrical if the LEA is valid. Data from many laboratory experiments, however, exhibit asymmetrical BTC characterized by earlier breakthrough, increased time to reach complete breakthrough (i.e., breakthrough front tailing), increased time for complete desorption (i.e., elution front tailing), and decreased solute peak height (Reference 9).

The impact of sorption nonequilibrium on solute transport is two-fold. First, solute will be detected at a given monitoring point earlier than that calculated using the LEA model. Second, desorption will take longer than expected as a result of the tailing effect. These two components can have considerable impact on groundwater contamination and restoration efforts. Early breakthrough results in the arrival of the contaminant earlier than expected; i.e., downgradient areas will be contaminated sooner. Aquifer remediation by flushing will take longer than that predicted by models based on LEA because of the tailing effect.

1. Models for Sorption Nonequilibrium

Over the past decade, a number of authors have examined the experimental and the theoretical aspects of sorption nonequilibrium. Brusseau and Rao (Reference 10) have critically reviewed the published literature on this topic. A brief summary of their review is presented here.

Early attempts to model sorption kinetics involved simple one-site first-order models in which the sorption rate is a function of the concentration difference between the sorbed and solution phases. Such models have failed to predict experimental data well. A bicontinuum model of some type has been used to conceptualize sorption kinetics. The bicontinuum approach may take one of two general forms, either chemical or physical, depending on which mechanism is hypothesized as being the rate-limiting step for sorption nonequilibrium. These two categories of models will be briefly discussed below.

a. Chemical Nonequilibrium Models

For these models, nonequilibrium is a result of a time-dependent sorption reaction at the sorbent-solution interface. Sorption may be represented by two reactions, occurring either in series or in parallel, but the latter has been the more common bicontinuum conceptualization. The sorbent is hypothesized as having two classes of sorption sites, where sorption is assumed to be instantaneous for one class, and rate-limiting for the other. Sorption on the kinetic-controlled sorption sites is assumed to be described by a first-order rate equation, while the other class is represented by the equilibrium sorption isotherm model. Two-site models were developed by Selim et al. (Reference 11), Cameron and Klute (Reference 13), and Karickhoff and Morris (Reference 8). The one-site model mentioned previously is a special case of the two-site model, where all sorption sites are assumed to be of the time-dependent class (Reference 13). The two-site model has generally been able to represent nonequilibrium data better than the one-site model.

b. Physical Nonequilibrium Models

For these models, the sorption reaction at the sorbent-liquid interface is assumed to be instantaneous; the rate at which the solute is transported to and from this interface controls the sorption rate. The bicontinuum model is developed by designating two pore-water domains -- a "mobile" region and a "stagnant" or "immobile" region. The immobile region has been variously conceptualized as intraaggregate microporosity, dead end pores, adsorbed water films (i.e., surface films), and matrix porosity of fractured media. Convective-dispersive transport occurs in the immobile region. Solute transfer between the two regions causes the immobile region to act as a sink/source component. Nonequilibrium is a result of the noninstantaneous nature of the solute transfer. Solute transfer between the mobile and immobile regions can be accounted for in three ways (References 14,15): (1) explicitly, with the use of Fick's law to describe the physical mechanism of diffusive transfer; (2) explicitly, but with the use of an empirical first-order kinetic expression, in place of Fick's law to approximate mass transfer; (3) implicitly, with the use of an effective or lumped dispersion coefficient that includes the effects of the sink/source

diffusion, as well as hydrodynamic dispersion and axial diffusion. This coefficient replaces the usual dispersion coefficient in the CD model.

The increased accuracy obtained by explicitly accounting for the actual solute diffusion process (Item 1 above) is countered by a concomitant increase in the model complexity. To use Fick's equation for solute diffusion, a complete geometric description of the mobile and the immobile regions would be required. For the sake of conceptual simplicity and mathematical tractability, most models have assumed that the immobile domains can be represented by uniformly-sized, spherical regions (intraparticle or intraaggregate regions). Geometry of most porous media, however, is usually far from such an idealization with a wide distribution of both sizes and shapes of the particles or aggregates. A model that includes explicit provisions for aggregate size distribution and aggregate shape variations in the CD model was proposed by Rasmuson (Reference 16). However, in most experimental studies, it is usually difficult to provide the values for the parameters defining the statistical distributions assumed for the size and shape variations of the particles or aggregates. To overcome such difficulties, methods have been developed to represent the nonspherical aggregates by "equivalent" spherical aggregates by the use of a shape factor (References 17,18), and to represent a size distribution by a nominal average size (Reference 19). Mathematical expressions have also been derived (References 18,19) for relating the empirical mass transfer coefficient used in approach (2) above to the physical parameters (e.g., aggregate radius, flow velocity, etc.) defining the porous medium.

The phenomenon attributed to physical nonequilibrium is a transport component, and that the sorption reaction itself is not involved. If the definition of sorption is limited to the processes occurring at the solid-liquid interface, perhaps it would be better to label this case as nonequilibrium transport, rather than nonequilibrium sorption.

This effect of physical nonequilibrium for conservative solutes may be used to assist in delineating which nonequilibrium mechanism is causing an observed nonideality (i.e., BTC asymmetry). As opposed to the physical nonequilibrium case, conservative solute BTC are not affected when chemical nonequilibrium is operating. Hence, cases where sorbing solute BTC exhibit asymmetry but not the conservative solute BTC, this suggests a chemical, rather than physical, mechanism causing the observed sorption nonequilibrium.

In addition to physical and chemical nonequilibrium mechanisms, some evidence suggests the existence of another rate-limited mass transfer mechanism. Considering the predominance of organic matter (OM) as a sorbent for hydrophobic organic chemicals (HOC), there is a strong probability that OM participates in this proposed mechanism. Diffusion into the OM matrix is one such possible mechanism, and would be an alternate explanation for nonequilibrium phenomena. An intraorganic matter solute diffusion model would be similar in theory to the physical diffusion model, except that the OM matrix replaces porous aggregates as the immobile domain. The two-stage sorption phenomenon is now explained as sorption to external OM surfaces during the initial rapid phase and subsequent diffusion into the OM during the longer, rate-controlled phase. As sorption is rate-controlled, not all solute is sorbed instantaneously; some solute may short-circuit the sorption process, thereby, resulting in an early breakthrough. The BTC tailing effect is a result of slow diffusion into and out of the OM.

2. Equivalence of Equilibrium and Nonequilibrium Models

The occurrence of sorption nonequilibrium increases solute dispersion. Hence, under such conditions, solute dispersion is a result of the combined effects of hydrodynamic dispersion and nonequilibrium induced dispersion. The relative importance of these two dispersion mechanisms depends on the conditions eliciting their effect. Hydrodynamic dispersion will tend to dominate under conditions of low pore-water velocities and in fine-grained, poorly aggregated media; whereas nonequilibrium dispersion will tend to predominate for larger velocities and large scale aggregation (References 20,21). While hydrodynamic dispersion may be most important at low Peclet numbers, nonequilibrium dispersion dominated the high Peclet number domain (Reference 22). This is supported by model sensitivity analyses (References 21,21) and experimental data, where, for Peclet numbers in the range of 20, nonequilibrium contributions to dispersion were of similar or greater magnitude as the contributions of hydrodynamic dispersion (References 21,24).

Temporal moments provide quantitative descriptors of the solute BTC. For example, the first, second, and third moments describe the mean breakthrough time, the degree of spreading, and the degree of asymmetry,

respectively. These moments may be used to evaluate the impact of nonequilibrium upon solute transport and to assess the differences between nonequilibrium and equilibrium models. To aid in such analyses, nonequilibrium transport parameters equivalent to LEA parameters may be developed by equating the transport impacts of the models. Such equivalent parameters were developed by Valocchi (Reference 25) and Parker and Valocchi (Reference 15) by equating the second moments. As the second moment describes the extent of solute dispersion, equating the second moments results in exact expressions for "effective" Peclet numbers (P_{eff}) that include a term for the usual hydrodynamic dispersion and an additional term for the nonequilibrium induced dispersion component. These effective P values are equivalent to P values that would be derived by curve-fitting the LEA-based CD model (Equations 41 and 42) directly to measured BTC data. The utility of this approach will be evaluated here.

3. Model Parameter Estimation

The usefulness of a predictive model for sorption nonequilibrium is dependent upon the ease with which the model parameter values can be determined. Models based on empirical representations of the sorption processes and whose parameters need to be estimated by calibration with measured data would be of somewhat limited use for predictive purposes. Conversely, physically-based mechanistic models whose parameters can be estimated by independent experimentation or by correlations to more easily measured properties have a greater utility for predictions of the system behavior. Most of the models developed for describing sorption nonequilibrium suffer from the limitation that methods are generally lacking to independently measure or estimate the required parameter values. This limitation is perhaps more evident in the chemical nonequilibrium models, where the values for sorption rate constants and the fraction of equilibrium sites are difficult to measure or to relate to other system parameters. Model calibration by curve-fitting to measured data has been a common approach to overcome this difficulty. As pointed out by Rao et al. (Reference 9) and others, the model parameter values estimated in this manner must be evaluated by testing their ability to predict data obtained under a different set of experimental conditions (e.g., flow velocities, column lengths, etc.). A

bicontinuum nonequilibrium sorption model will be evaluated here using BTC data obtained from columns packed with aquifer materials.

B. MATERIALS AND METHODS

1. Equilibrium Sorption Isotherms

Equilibrium isotherms for the sorption of TCE and p-xylene on the Lula and the Borden aquifer materials, Webster surface soil, and SAz-1 montmorillonite clay were determined using a headspace analysis technique. This method was proposed by Lincoff and Gossett (Reference 26) to measure vapor-liquid partitioning of volatile organic chemicals. The specifics of the technique used are as those described by Garbarini and Lion (Reference 27). The method involves measuring the solute concentration in the headspace of sealed bottles in which a known mass of the sorbent is equilibrated with a known volume of solution of a given solute concentration. The amount sorbed is calculated by comparison of the headspace concentrations in bottles which contain only the solutions of known initial concentrations. Given the value of the Henry's constant (K_h) for gas-liquid partitioning of the volatile solute, the total solute mass introduced, the volumes of the gas and liquid phases, and the sorbent mass, the sorbed concentration can be calculated.

Samples of the headspace were analyzed using gas chromatography (GC) techniques. A Perkin-Elmer Sigma 2000 gas chromatograph equipped with a photoionization detector (PID) was employed. A 1.83 meter long column (0.32 cm i.d.) packed with 100/200-mesh Supelcoport (5 percent each of SP-1200 and Bentone34) was used for headspace analysis. Grade 5 helium was used as the carrier gas at a flow rate of 20 mL/min. The injector and the column temperatures were 225°C and 90°C, respectively. On-column injections of 25 µL gas samples were made using a 25 µL Precision Sampling gas-tight syringe. The PID response was monitored with a Perkin Elmer LCI-100 integrator. Gas concentrations were determined by comparing peak areas against calibration curves.

In this study, sorption isotherms were measured by adding to the sorbents only TCE or p-xylene or a binary mixture of both solutes. Sorbent to solution ratio used was 5 for the aquifer materials and 3 for the Webster soil and the clay. For each sorbent-solute combination, sorption was determined up

to 5 concentrations. The samples were equilibrated for 24 hours in 26-mL glass bottles sealed with Teflon^{R}-lined crimp tops. All experiments were conducted at a temperature of 22°C ($\pm$ 1°C).

2. Miscible Displacement Studies

Miscible displacement studies were conducted using the Lula and Borden aquifer materials. The Lula material was collected on the Johnson Ranch near Ada in south central Oklahoma from the 5 m depth in a shallow unconfined sandy aquifer. This material has been used in other studies reported by Banerjee et al. (Reference 28) and Bouchard et al. (Reference 29). The Borden material was collected from an unconfined sand aquifer underlying an inactive sand quarry on the Canadian Forces Base, Borden, Ontario, Canada. At this site large-scale field experiments have been conducted on natural gradient transport of inorganic tracers and organic contaminants in groundwater (References 30,31,32,33,34,35). The Lula material was supplied by Dr. Marvin Piwoni of the R.S. Kerr Environmental Research Laboratory, U.S. Environmental Protection Agency, Ada, OK. A sample of the Borden material was furnished by Dr. Robert Gillham, Institute of Groundwater Research, University of Waterloo, Waterloo, Ontario, Canada. Both materials were received air-dried and were used without further pretreatment except that <500 um size fractions of the Lula material were used in all studies, while the unsieved Borden material was used.

Stauffer (Reference 36) has recently used the Lula and the Borden materials along with several other aquifer materials, hydrous oxides, and clay minerals to measure equilibrium sorption isotherms for four organic contaminants. He determined the physical, chemical, and mineralogical characteristics of these aquifer materials. Both the aquifer materials are very sandy (93 and 96 percent sand, respectively) and have low organic carbon contents (OC of 0.025 and 0.034, respectively). These properties would suggest a low retention of hydrophobic organic contaminants on these sorbents.

Miscible displacement techniques, similar to those described by Zhong et al. (Reference 37) and Bouchard et al. (Reference 29), were used to study the sorption and transport of a nonreactive tracer ($^{3}H_{2}O$) and two volatile organic contaminants (TCE and p-xylene). The column apparatus used was an Altex/Beckman preparative chromatography column made of precision bore

borosilicate glass, 2.5 cm in diameter, with an adjustable shaft such that the packed bed length can be varied up to 25 cm. Bed supports on both ends consist of a woven FEP Teflon^R diffusion mesh in contact with a porous Teflon^R filter disk of 30-60 μm pore size. The diffusion mesh enhances radial distribution of the influent solution and reduces dispersion in the effluent end. The column was designed to have a minimum void volume in the end plates. Two single-piston HPLC pumps from Gilson Medical Electronics (Model 302) were connected to the column through a Rheodyne switching valve (Model 7060) to facilitate easy switching between the electrolyte solution (0.01 N $CaCl_2$) with and without the tracers. All tubing used throughout the experimental apparatus was either stainless steel or Teflon^R. The solution reservoirs used for the volatile compounds were Teflon^R gas sampling bags (20 cm X 30 cm) from Alltech with stainless steel fittings for attachment to the pumps.

The effluent fractions were collected using the automated ISIS fraction collector from ISCO. The ISIS allows sample fractionation in sample vials below a solvent surface which is necessary for the collection of volatile compounds. Sample vials were immediately capped with Teflon^R-lined screw caps to further minimize volatile losses. Glass vials (5 mL) from Kimble with a known volume of methanol were used in the collection process of TCE and p-xylene. All vials were sequentially numbered and weighed before and after the addition of methanol, and following effluent collection.

Both the Lula and the Borden columns were packed with air-dried aquifer material sterilized using 2450 MHz microwave radiation. The columns were saturated by pumping the electrolyte solution at a flow rate equivalent to the estimated saturated conductivity of the column until steady-state, water-saturated conditions were established in the columns. Column weights were monitored periodically throughout the miscible displacement studies. All solutions used were filter-sterilized using 0.45 μm Gelman membrane filters.

A pulse of electrolyte solution containing tritiated water (^3H_2O) was displaced through the columns at pore-water velocities (v) of 6 and 24 cm/hr. These two velocities will be referred to as "slow" and "fast." respectively, in the remainder of this discussion. Following the tritium displacements, various pulses of electrolyte solutions containing a binary mixture of TCE and p-xylene, only p-xylene, and only TCE, respectively, were displaced through the columns at the two velocities. The specific activity of ^3H in the displacing solution was about 5 nCi/mL. The influent solution

concentrations were in the range of 170-400 mg/L for TCE and 15-85 mg/L for p-xylene.

^3H activity in effluent fractions was assayed by liquid scintillation methods using a Searle Delta 300 liquid scintillation counter. Capillary GC methods were used to analyze for TCE and p-xylene in the effluent samples. The GC method consisted of a linear temperature program with a gradient from 60° to 125°C using a Perkin-Elmer Sigma-3B gas chromatograph equipped with a flame ionization detector (FID) and a Supelco VOCOL wide bore capillary column (0.75 mm x 60 m, 1.5 μm film thickness). One microliter splitless injections were made using a 10 μL Hamilton syringe and the FID response was monitored with a HP 3392 integrator. Ratios of the peak areas of the effluent samples and input solution samples were used to calculate the relative effluent concentrations. TCE and p-xylene concentrations in the influent (stock) solutions were determined by comparing peak heights against calibration curves.

C. RESULTS AND DISCUSSION

1. Equilibrium Sorption Isotherms

The measured isotherms for sorption from aqueous solutions of TCE and p-xylene on four sorbents are presented in Figures 38 and 39. The isotherms are linear over the concentration range used. The sorption coefficients (K_d) estimated using linear regression techniques and the coefficients of determinations (r^2) are also indicated in the figures. The sorption isotherms for single-solute (only TCE or p-xylene) and binary mixtures are not statistically different, suggesting no competitive sorption. These results are consistent with reports of earlier workers (References 38,39,40,41). The order of TCE and p-xylene sorption on the four sorbents was: SAz-1 > Webster > Lula > Borden. Except for the clay, this order is consistent with the organic carbon content of the natural sorbents. Note that in all cases K_d values for p-xylene are larger than those for TCE; this is consistent with the differences in aqueous solubilities and hydrophobicities of the two solutes (Table 1).

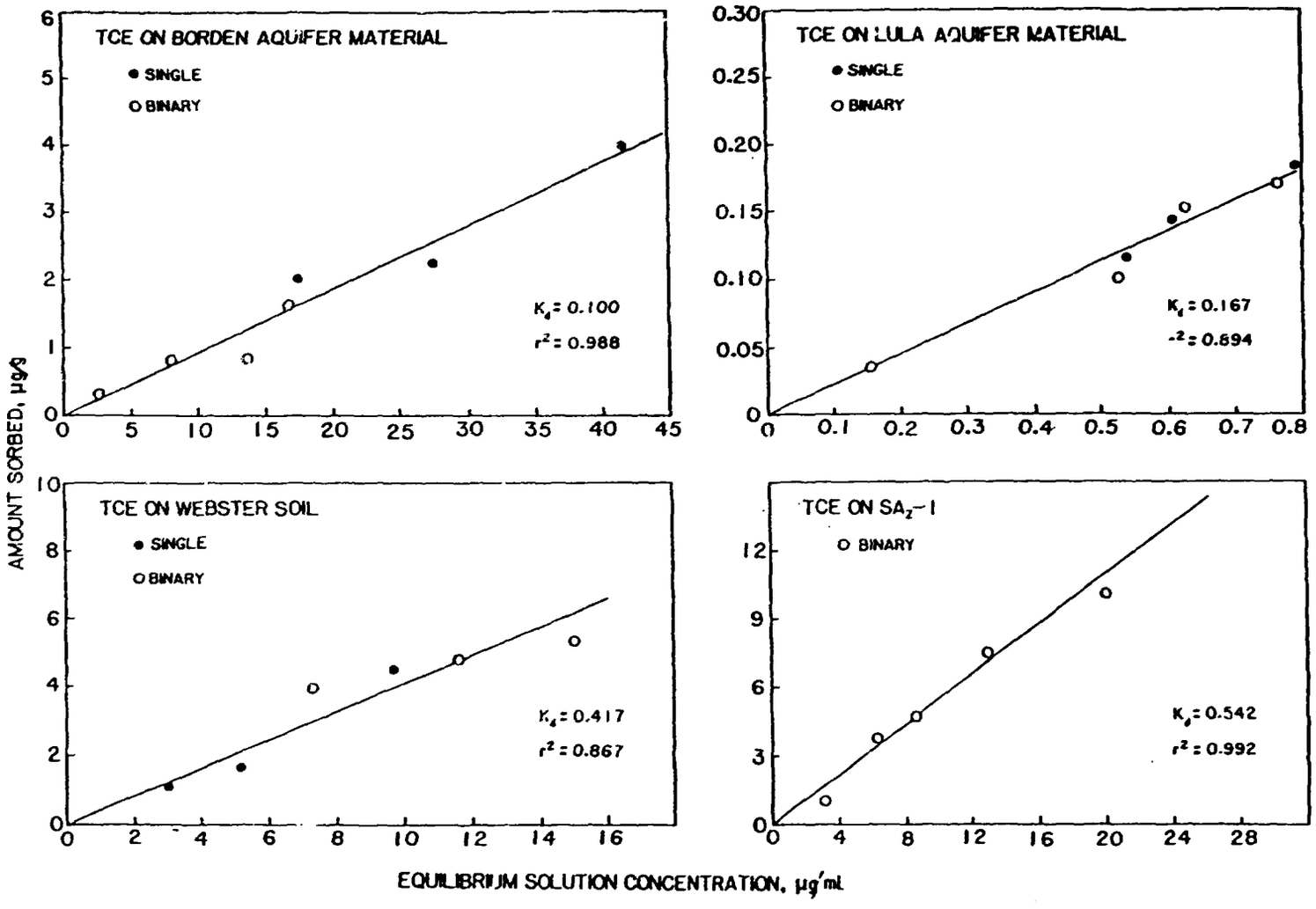

Figure 38. Equilibrium Isotherms for Sorption of TCE from Aqueous Solutions.

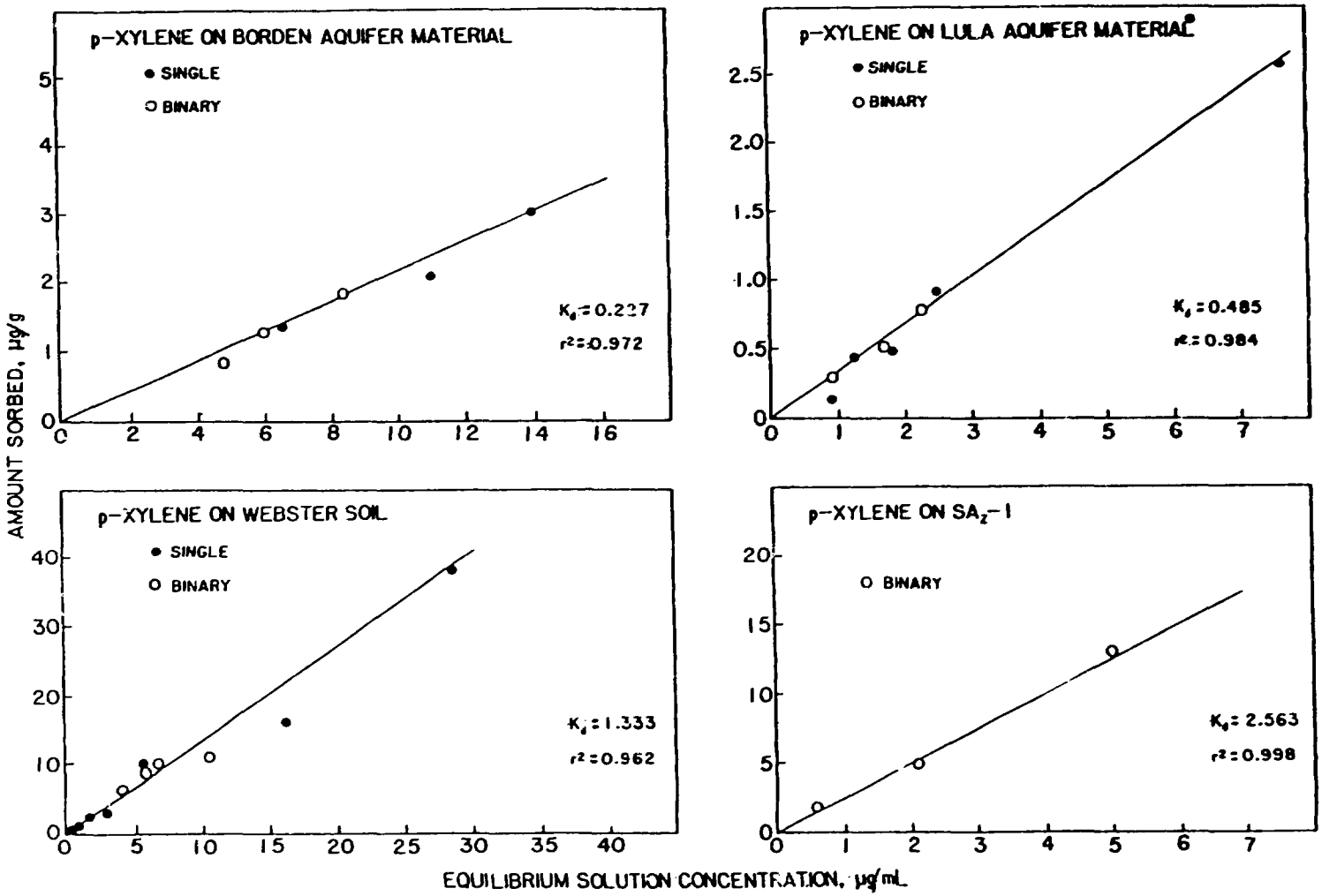

Figure 39. Equilibrium Isotherms for Sorption of p-Xylene from Aqueous Solutions.

2. Miscible Displacement of ^3H_2O

The ^3H_2O effluent breakthrough curves (BTC) measured at the two velocities in each of the columns were symmetrical and sigmoidal in shape (Figures 40 and 41). The fronts of the BTC measured at two velocities were identical; the distal portions of the BTC are shifted only because the pore volumes of the tritium pulse displaced was different in each case.

The measured BTC were fitted to the analytical solution of CD model [Equation (41) and (42)] to estimate the values of the Peclet Number (P), which is a measure of hydrodynamic dispersion during flow, and the retardation factor (R). As expected, these BTC do not indicate any retardation (R = 1) due to sorption of tritium on the aquifer materials. The estimated P values for the Lula and Borden columns were 94 and 193, respectively (Table 18). It has been shown by a number of other workers that D is directly proportional to v, such that it may be assumed that $D = \alpha v$, where α is called the dispersivity (cm). Thus, $P (= L/\alpha)$ is independent of v suggesting that tritium BTC measured at two velocities in a given column should be invariant. This was found to be true for the ^3H_2O BTC measured at two velocities (6 and 24 cm/hr) in both Lula and Borden columns (Figures 40 and 41). The calculated α values for the Lula and the Borden columns were 0.06 and 0.05 cm, respectively (Table 18). Such small values of α are expected for well packed homogeneous columns of sandy aquifer materials. These results suggest that hydrodynamic dispersion during transport through these columns was minimal and that "mobile" and "immobile" soil-water regions are nonexistent in these columns.

TABLE 18. SUMMARY OF PHYSICAL PARAMETERS FOR THE COLUMNS USED IN MISCIBLE DISPLACEMENT STUDIES.

Column	θ	ρ	L	P	$\alpha = (L/P)$
	mL/cm^3	g/cm^3	cm		cm
Lula	0.422	1.683	6.0	94	0.06
Borden	0.399	1.771	8.8	193	0.05

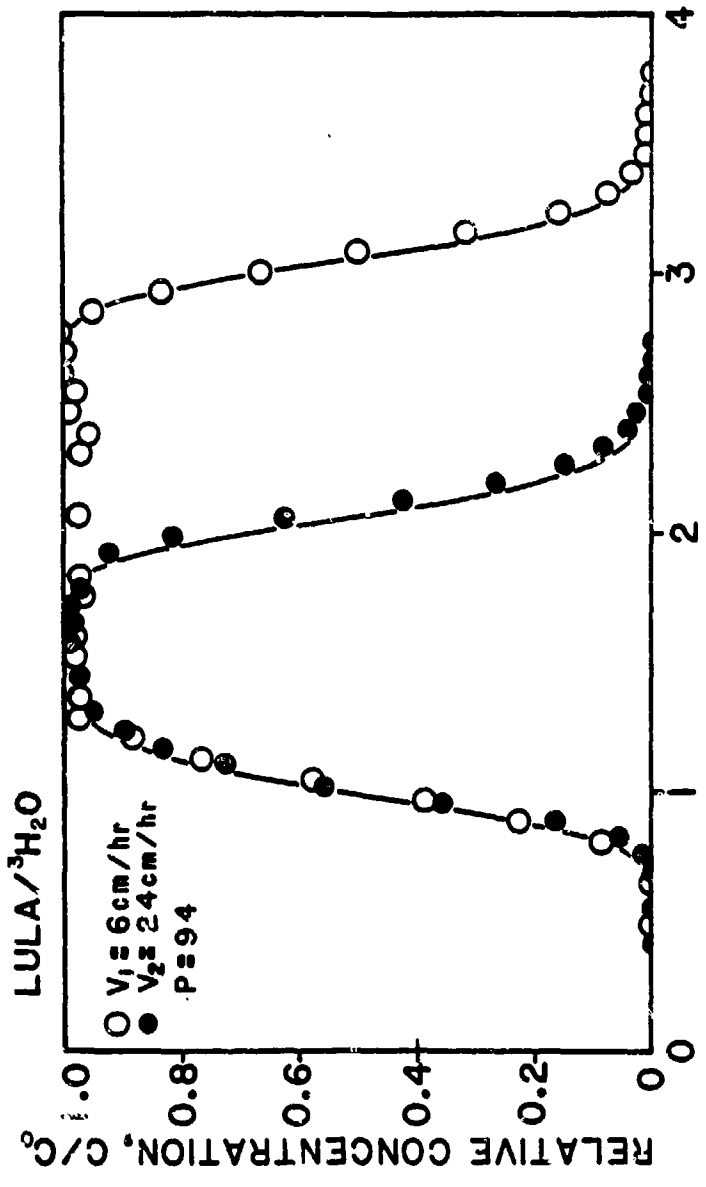

Figure 40. BTC for Displacement of ^3H_2O at Two Velocities Through the Lula Column.

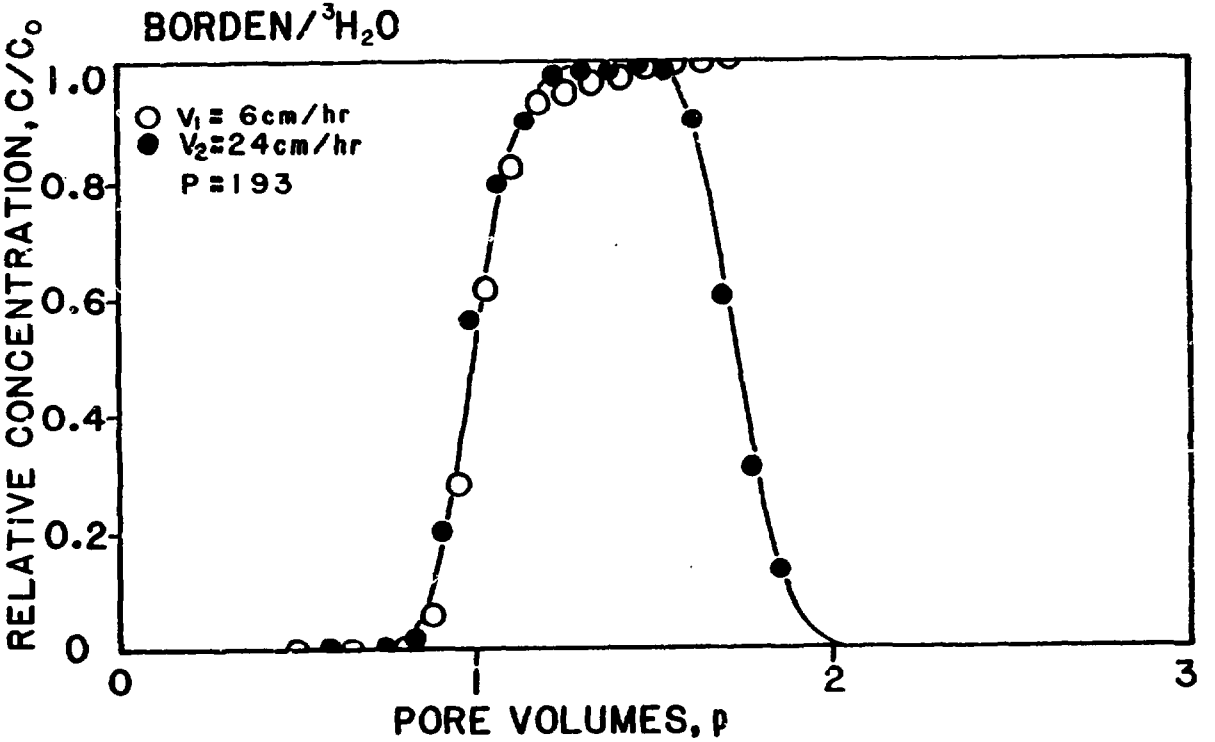

Figure 41. BTC for Displacement of ^3H_2O at Two Velocities Through the Borden Column.

3. Miscible Displacement of Binary Mixtures

The BTC measured for the displacement of a binary mixture TCE and p-xylene through the Lula and the Borden columns at the high velocity (v = 24 cm/hr) are shown in Figures 42 and 43. The rightward displacement of the p-xylene BTC relative to that of TCE in both columns is consistent with the larger sorption coefficients (hence, greater retardation) for the less soluble and the more hydrophobic aromatic solute. The measured BTC are strongly asymmetric in shape with a considerable tailing with a slow approach to C/C_o = 1.0 on the frontal end and in reaching C/C_o = 0 on the distal end of the BTC. Such BTC asymmetry is indicative of sorption nonequilibrium during transport through the columns.

In order to assess the extent of sorption nonequilibrium, the measured BTC for TCE and p-xylene were fitted to the two-site sorption model (References 9, 11, and 12) to estimate unknown model parameters. This model assumes that sorption occurs simultaneously on two groups of "sites"; the instantaneous equilibrium type and the kinetic type, where sorption on the latter sites is assumed to be described by first-order reversible kinetics. In the model, sorption on both types of sites is assumed to follow linear sorption isotherms with K_1 and K_2 as the sorption coefficients (mL/g).

The two-site model parameters can be grouped into five dimensionless parameters as defined below :

$$P = (vL/D);\ D = \alpha v;\ \text{and}\ P = (L/\alpha) \tag{43}$$

$$R_T = [1 + \rho\ K_d/\theta];\quad K_d = (K_1 + K_2) \tag{44}$$

$$R_1 = [1 + \rho\ F\ K_1/\theta];\quad F = (K_1/K_d) \tag{45}$$

$$\beta = (R_1/R_T) \tag{46}$$

$$\omega = [k(1-\beta)R_T\ L/v] \tag{47}$$

where K_1 and K_2 are, respectively, the sorption coefficients (mL/g) for the equilibrium and the kinetic sites; K_d is the total sorption coefficient (mL/g); F is the fraction of the equilibrium-type sorption sites; ω is the

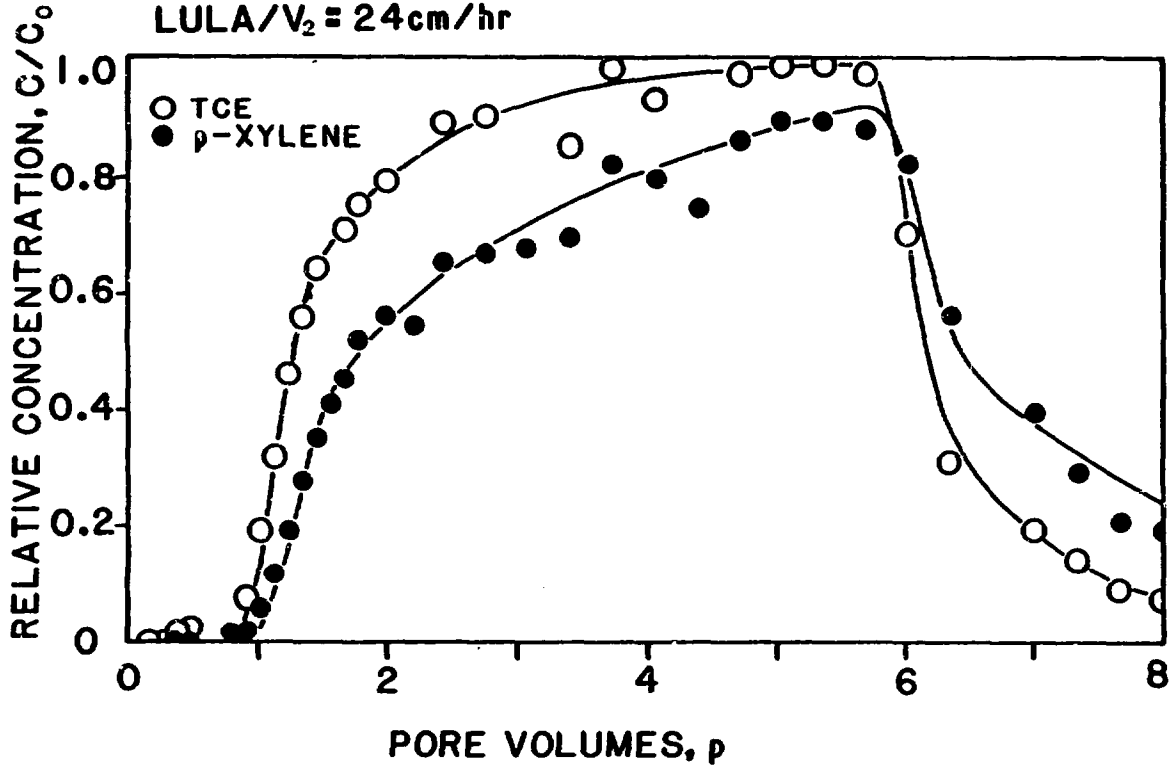

Figure 42. BTC for Displacement of TCE and p-Xylene at High Velocity (v = 24 cm/hr) Through the Lula Column.

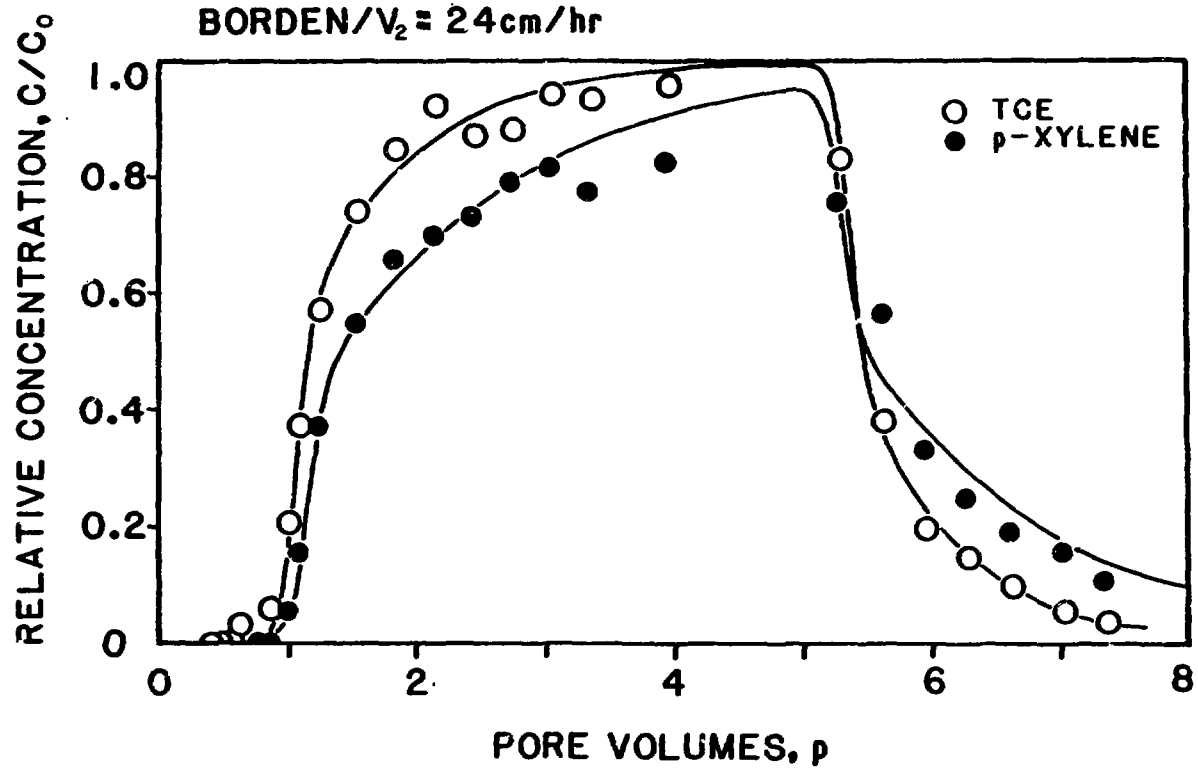

Figure 43. BTC for Displacement of TCE and p-Xylene at High Velocity (v = 24 cm/hr) Through the Borden Column.

nonequilibrium sorption index; k is the first-order sorption rate constant (hr^{-1}) for the nonequilibrium sorption "sites"; and other parameters are as described previously.

Of these dimensionless model parameters, the value of P is known from the ^3H_2O BTC. The unknown values of the other parameters (R_T, β, R_1, and ω), related to sorption on soil, were estimated by fitting the two-site model to the BTC measured at v = 24 cm/hr. A curve-fitting program CFITIM3, based on nonlinear least squares optimization techniques (Reference 13), was used for this purpose. The estimated parameter values are summarized in Tables 19 and 20 and the measured BTC are compared with those curve-fitted in Figures 42 and 43.

Tables 19 and 20 show that the estimated values of the nonequilibrium sorption index (ω) for both solutes in a given column are similar, suggesting that the same process may be controlling the time dependence of TCE and p-xylene sorption. Using these ω values in Equation (47), the values of the first-order sorption rate constant (k) was computed to be about 2.7-5.2 hr^{-1}. Thus, it would appear that in the absence of mobile-immobile soil water regions (as indicated by the ^3H_2O BTC data), sorption nonequilibrium may be attributed to diffusion-controlled accessibility to sorption "sites." Bouchard et al. (Reference 29) arrived at a similar conclusion based on column displacement data for three pesticides. Earlier workers (References 10,42,43) have proposed that solute diffusion within the soil organic matter matrix was the rate controlling step in sorption of hydrophobic organic pollutants by soils. Data presented here support this hypothesis.

The calculated ω (or k) values are somewhat larger than those reported for other sorbents. However, for uniform nonporous media with low organic carbon content, such as the Lula and Borden aquifer materials used here, the diffusion path lengths are likely to be short and hence, rapid diffusion as reflected by larger ω values is expected. A model parameter sensitivity analysis suggests that equilibrium conditions for sorption would prevail when $\omega \geq 2$. Note from Equation (47) that ω is inversely proportional to v, while all other model parameters are independent of velocity. Therefore, ω values estimated from the high velocity experiments were increased by a factor of 4, accordingly, and were used to predict the BTC

TABLE 19. SUMMARY OF SORPTION NONEQUILIBRIUM PARAMETERS ESTIMATED USING THE BTC DATA FOR THE LULA COLUMN.

Parameter	TCE		p-Xylene	
	v_1*	v_2	v_1	v_2
P	94 (79-108)**	94 (79-108)	94(79-108)	94(79-108)
R_T	1.64 (1.50-1.78)	1.61 (1.57-1.64)	2.22 (2.10-2.34)	2.65 (2.52-2.77)
R_1	1.33	1.14	1.40	1.32
p	0.81 (0.72-0.90)	0.71 (0.69-0.72)	0.63 (0.56-0.70)	0.50 (0.47-0.52)
ω	0.70 (*)	0.61 (0.53-0.69)	1.43 (0.71-2.15)	0.93 (0.78-1.08)
F	0.52	0.23	0.33	0.49
T†	3.70	5.11	3.7	5.11

*v_1 = 6 cm/hr; v_2 = 24 cm/hr.

**95 percent confidence limits.

†Pore volumes of solute pulse applied.

TABLE 20. SUMMARY OF SORPTION NONEQUILIBRIUM PARAMETERS ESTIMATED USING THE BTC DATA FOR THE BORDEN COLUMN.

Parameter	TCE		p-Xylene	
	v_1*	v_2	v_1	v_2
P	193 (147-239)**	193 (147-239)	193 (147-239)	193 (147-239)
R_T	1.40 (1.36-1.44)	1.43 (1.38-1.48)	2.01 (1.89-2.13)	2.02 (1.87-2.17)
R_1	0.98	1.05	1.23	1.14
β	0.696 (0.655-0.738)	0.733 (0.707-0.760)	0.601 (0.554-0.65)	0.565 (0.522-0.608)
ω	1.55 (0.93-2.18)	0.64 (0.48-0.80)	1.53 (0.96-2.10)	0.88 (0.66-1.10)
F	(0)	0.11	0.23	0.14
T†	2.53	4.06	2.53	4.06

*v_1 = 6 cm/hr; v_2 = 24 cm/hr.

**95 percent confidence limits.

†Pore volumes confidence limits.

measured at the low velocity. The agreement between measured and predicted BTC (Figures 44 and 45) provides validity to the parameter estimates.

The BTC for the low velocity were also fitted to the two-site model to estimate R_T, R_1, β, and ω values. These estimates are summarized in Tables 19 and 20 and the fitted curves are shown as dashed lines in Figures 44 and 45. Note that the values of R_T, R_1, and β estimated by curve-fitting the low and high velocity BTC are similar; but the ω values estimated by fitting the low velocity BTC are only about 1.5 to 2 times larger than those from the high velocity BTC, and not 4 times as large as expected from Equation (47). As independent estimates of model parameters are preferred, the agreement between measured and predicted BTC for the low velocity experiments is considered satisfactory.

Equations (44), (45), and (46) can be used to derive the following expression for F, the fraction of the total sorption sites that are assumed to attain instantaneous equilibrium during flow:

$$F = (R_1 - 1) / (R_T - 1) \qquad (48)$$

R_1 and R_T values from Tables 19 and 20 were used in Equation (48) to calculate the F values for the measured BTC data. These values, shown in Tables 19 and 20, suggest that about 10 to 50 percent of the sorption sites are readily accessible to permit equilibrium, while sorption on the remaining sites is time dependent. The calculated F values are on the lower end of the range of values reported by earlier workers. Given the uncertainty in estimated values, a discussion of the trends in F values may not be appropriate.

4. Use of Effective Peclet Number

The estimated ω values for the slow velocity experiments are large enough ($\omega > 2$) that the assumption of "local equilibrium" for sorption would be valid in modelling these data. To check this, the estimated values of R_T and an "effective" Peclet number (P_{eff}) were used in the analytical solution to the convective-dispersive (CD) model [Equations (41) and (42)] to predict the TCE and p-xylene BTC measured at the slow velocity. Valocchi (Reference 25) and Parker and Valocchi (Reference 44) have derived the following expression for calculating P_{eff}:

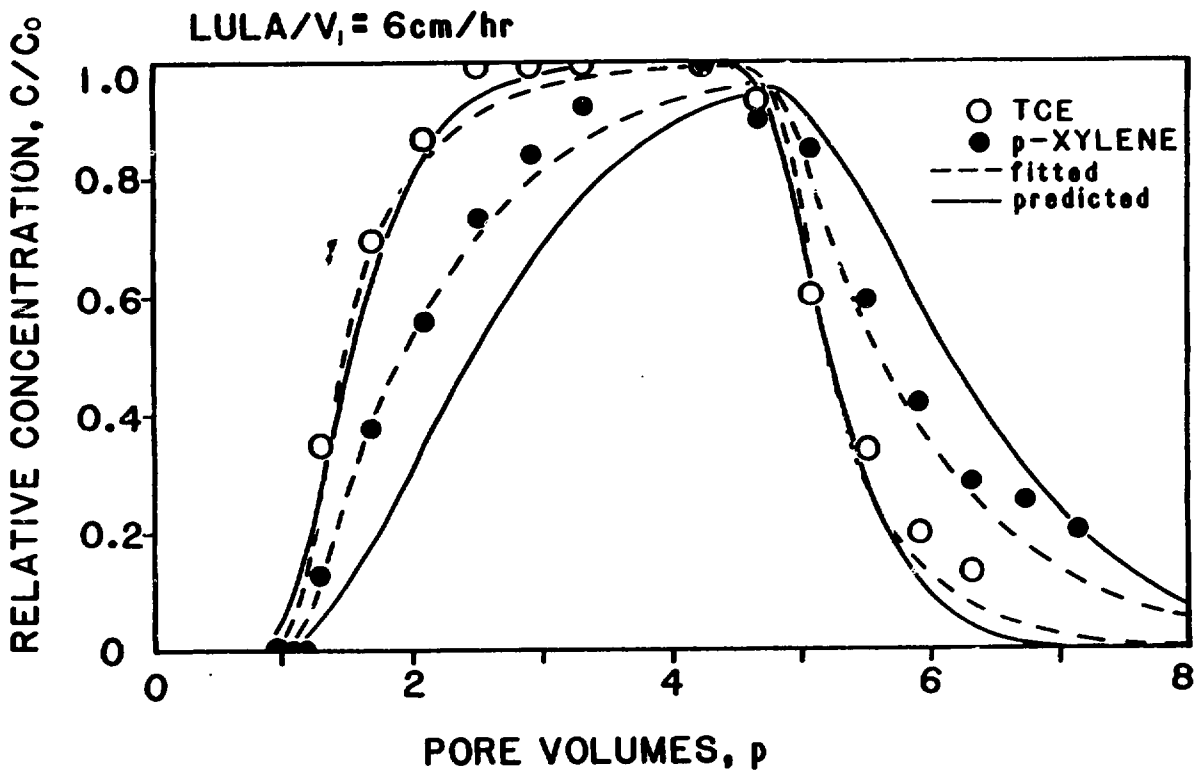

Figure 44. BTC for Displacement of TCE and p-Xylene at Low Velocity (v = 6 cm/hr) Through the Lula Column.

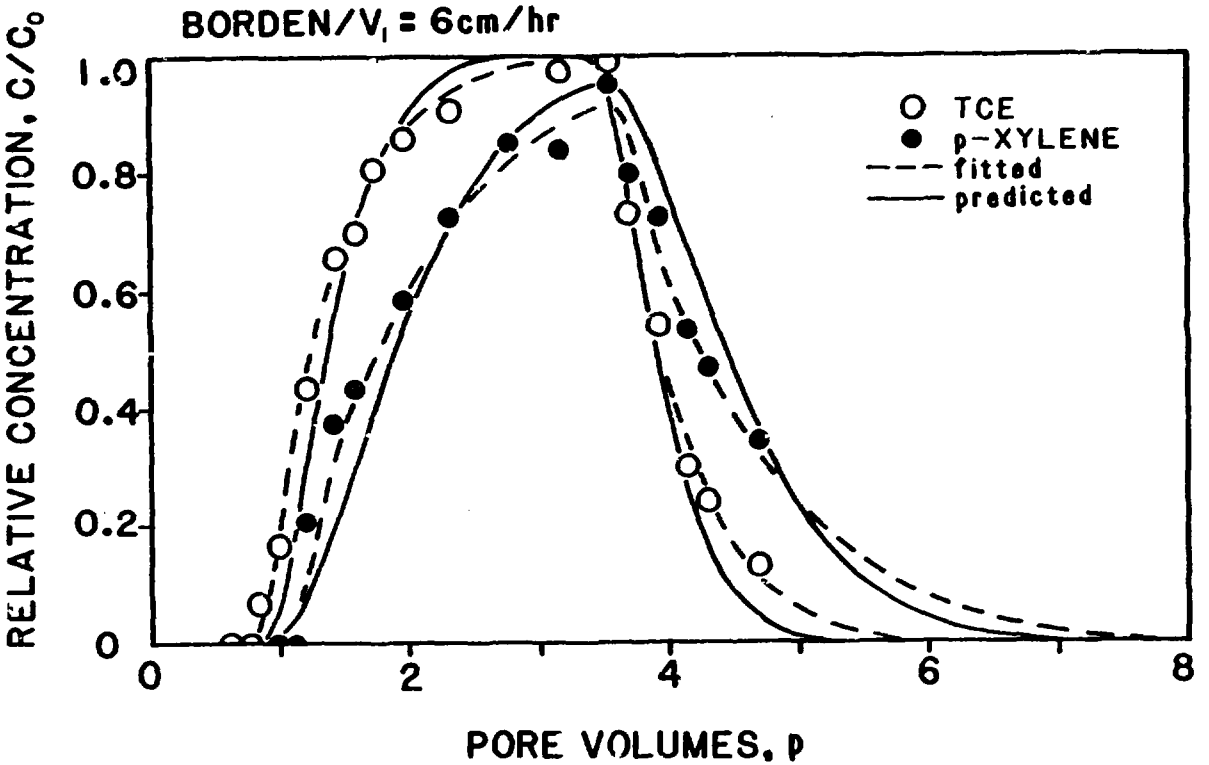

Figure 45. BTC for Displacement of TCE and p-Xylene at Low Velocity (v = 6 cm/hr) Through the Borden Column.

$$1/P_{eff} = (1/P) + (1-\beta)^2/\omega \quad (49)$$

In the above expression, the first term represents hydrodynamic dispersion, while the second term represents the effects of increased dispersion resulting from sorption nonequilibrium.

P values estimated from the tritium BTC (Table 18) and the values of β and ω estimated by fitting the high velocity BTC for TCE and p-xylene (Tables 19 and 20) were used in Equation (49) to calculate P_{eff} values. The BTC predicted using the LEA-based CD model with an effective Peclet number and R_T from the high velocity experiments are compared with measured BTC in Figures 46 and 47. The BTC for p-xylene in Lula is the only case where the agreement is less than satisfactory, and the difference can be attributed to the larger R_T value estimated from the high velocity experiment. Note that a smaller value of R_T (2.22 versus 2.65) was estimated when the two-site model was fitted to the slow velocity BTC (Table 19). The slow velocity BTC were also curve-fitted to CD model. The values of P_{eff} calculated using Equation (49) were generally within the 95 percent confidence limits of the P values estimated from curve-fitting (Table 21). These results suggest that the local equilibrium assumption is, in fact, valid in this case. Apparently, at the slow velocity, sufficient time was available for sorption equilibrium to be attained for both TCE and p-xylene.

TABLE 21. COMPARISON OF PECLET NUMBER VALUES FOR THE LOW VELOCITY (v = 6 CM/HR) BTC DATA.

Column	Solute	Peclet Number (P)	
		Equation (49)	Fitted
Lula	TCE	22.2	25.7 (13.4-37.9)*
	p-xylene	12.8	6.3 (3.7-8.8)
Borden	TCE	30.3	20.8 (13.8-27.7)
	p-xylene	17.0	10.3 (7.8-12.9)

*95 percent confidence limits.

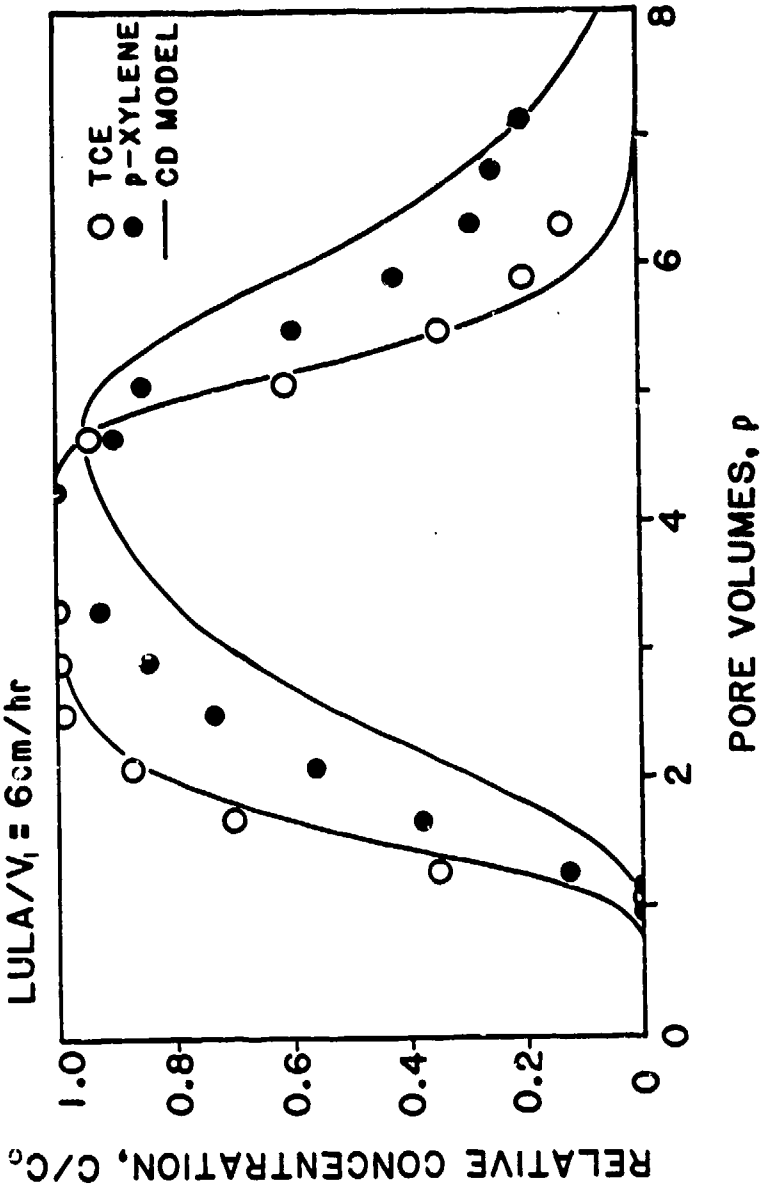

Figure 46. Evaluation of the CD-model to Describe TCE and p-Xylene BTC Obtained at Low Velocity (v = 6 cm/hr) in the Lula Column.

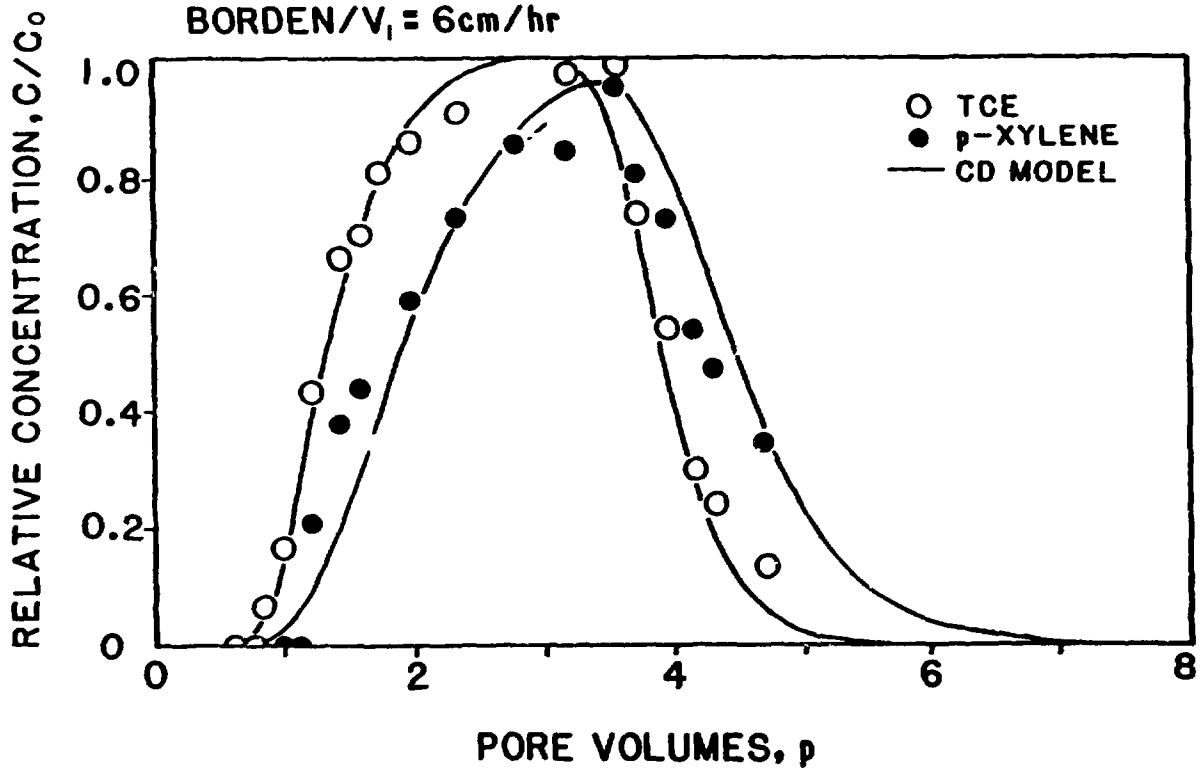

Figure 47. Evaluation of the CD-model to Describe TCE and p-Xylene BTC Obtained at Low Velocity (v = 6 cm/hr) in the Borden Column.

5. Batch- and Column-Measured Retardation Factors

The equilibrium sorption coefficients (K_d) measured using the headspace technique (Figures 38 and 39) and the appropriate values of column bulk density (ρ) and volumetric water content (θ) values (Table 18) were used to calculate the column retardation factor (R_T) values for TCE and p-xylene. These values fall within the 95 percent confidence limits of the R_T values estimated from fitting the the two-site model to the measured BTC data (Table 27). This lends further support to the sorption parameter values estimated from the column studies.

TABLE 22. COMPARISON OF RETARDATION FACTOR VALUES BASED ON EQUILIBRIUM SORPTION ISOTHERMS AND COLUMN STUDIES

Aquifer material	Solute	Retardation Factor (R_T)	
		Batch	Column
Lula	TCE	1.67 (1.52-1.84)*	1.61 (1.57-1.64)
	p-xylene	2.93 (2.83-3.07)	2.65 (2.52-2.77)
Borden	TCE	1.44 (1.09-1.80)	1.43 (1.38-1.48)
	p-xylene	2.01 (1.93-2.11)	2.02 (1.87-2.17)

*95 percent confidence limits.

6. Miscible Displacement of Single Solutes

The BTC data discussed in the previous section have been for miscible displacement of binary mixtures of TCE and p-xylene. To investigate whether competitive sorption did exist additional BTC were measured at the high velocity for single solute displacement. Measured BTC for single and binary solute displacement are identical in all cases investigated (Figure 48). This suggests the absence of competitive sorption between TCE and p-xylene on the two aquifer materials used. These column data are consistent with the batch isotherm data presented in Figures 38 and 39.

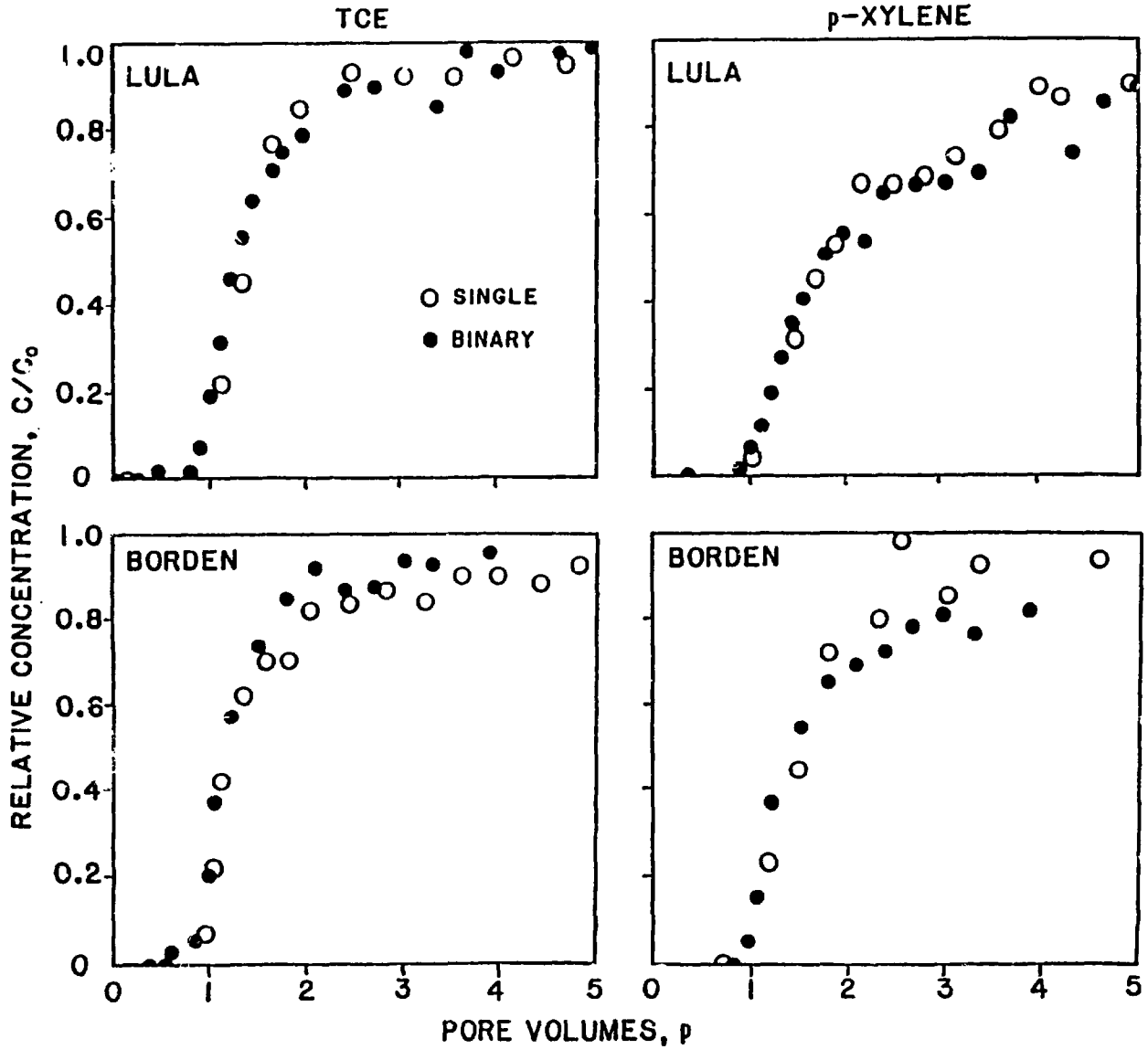

Figure 48. Comparison of BTC Obtained by Displacement of Single Solute (p-Xylene or TCE Alone) and Binary Mixtures (p-Xylene Plus TCE) Through the Lula and the Borden Columns.

D. SUMMARY

Batch equilibrium and miscible displacement studies were conducted to investigate sorption and transport of TCE and p-xylene in two low-OC aquifer materials. The utility of a two-site sorption model to describe the extent of sorption nonequilibrium during transport in saturated columns was evaluated. The model parameters estimated from the BTC obtained at a high velocity (v=24 cm/hr) were used to successfully describe the BTC measured at a lower velocity (v=6 cm/hr). At the lower velocity, the assumption of local sorption equilibrium appeared to be valid, and the measured BTC could be described by an equilibrium sorption model coupled to the convective-dispersive transport model. The values for the column retardation factors estimated by fitting the two-site model to the BTC were comparable to those estimated from equilibrium sorption isotherms. Finally, the BTC measured for displacement of binary mixtures (TCE plus p-xylene) and single-solute (TCE or p-xylene alone) were identical, suggesting no competitive sorption between these two solutes. These column observations were consistent with sorption isotherm data.

E. REFERENCES

1. Wu, S., and Gschwend, P. M., "Sorption Kinetics of Hydrophobic Organic Compounds to Natural Sediments and Soils," 1986, Env. Sci. Tech., Vol. 20, pp. 725-730.

2. Jaffe, P. R., and Ferrara, R. A., "Desorption Kinetics in Modeling of Toxic Chemicals," 1983, J. Env. Eng., Vol. 109, pp. 859-867.

3. Karickhoff, S. W., "Sorption Kinetics of Hydrophobic Pollutants in Natural Sediments," in: Processes Involving Contaminants and Sediments, R. A. Baker (ed.), Ann Arbor Sci. Publ., Inc., MI, 1980, pp. 193-205.

4. McCall P. J., and Agin, G. L., "Desorption Kinetics of Picloram as Affected by Residence Time in the Soil," 1985, Env. Tox. Chem., Vol. 4, pp. 37-44.

5. Oliver, B. G., "Desorption of Chlorinated Hydrocarbons from Spiked and Anthropagenically Contaminated Sediments," 1985, Chemosphere, Vol. 14, pp. 1087-1106.

6. Ball, W. P., and Roberts, P. V., "Rate-limited Sorption of Halogenated Aliphatics onto Sandy Aquifer Material - Experimental Results and Implications for Solute Transport," 1985, EOS, Trans. Amer. Geophys. Union, Vol. 66, pp. 894.

7. Curtis, G. P., Roberts, P. V., and Reinhard, M., "A Natural Gradient Experiment on Solute Transport in a Sand Aquifer: 4. Sorption of Organic Solutes and Its Influence on Mobility," 1986, Water Resour. Res, Vol. 22, pp. 2059-2067.

8. Karickhoff, S. W., and Morris, K. R., "Sorption of Hydrophobic Pollutants in Sediment Suspensions," 1985, Env. Toxicol. Chem., Vol. 4, pp. 469-477.

9. Rao, P. S. C., Davidson, J. M., Jessup, R. E., and Selim, H. M., "Evaluation of Conceptual Models for Describing Nonequilibrium Adsorption-desorption of Pesticides during Steady-flow in Soils," 1979, Soil Sci. Soc. Amer. Jour., Vol. 42, pp. 22-28.

10. Brusseau, M. L., and Rao, P. S. C., "Evaluation of Models for Sorption Nonequilibrium during Transport in Porous Media," 1987, CRC Critical Reviews in Environ. Control, (Manuscript in Review).

11. Selim, H. M., Davidson, J. M., and Mansell, R. S., "Evaluation of a Two-site Adsorption-desorption Model for Describing Solute Transport in Soils," 1976, Proc. Summer Computer Simulation Conf., Washington, D.C.

12. Cameron, D. R., and Klute, A., "Convective-dispersive Solute Transport with a Combined Equilibrium and Kinetic Adsorption Model," 1977, Water Resour. Res., Vol. 13, pp. 183-188.

13. van Genuchten, M. Th., "Nonequilibrium Transport Parameters from Miscible Displacement Experiments," 1981, Research Report No. 119, USDA, US Salinity Lab, Riverside, CA.

14. Rao, P. S. C., Rolston, D. E., Jessup, R. E., and Davidson, J. M., "Solute Transport in Aggregated Porous Media: Theoretical and Experimental Evaluation," 1980, Soil Sci. Soc. Amer. Jour., Vol. 44, pp. 1139-1146.

15. Parker, J. C., and Valocchi, A. J., "Constraints on the Validity of Equilibrium and First-order Kinetic Transport Models in Structured Soils," 1986, Water Resour. Res., Vol. 22, pp. 399-407.

16. Rasmuson, A., "The Influence of Particle Shape on the Dynamics of Fixed Beds," 1985, Chem. Eng. Sci., Vol. 40, pp. 1115-1122.

17. van Genuchten, M. Th., "A General Approach for Modeling Solute Transport in Structured Soils," in: Proc. Hydrogeology of Rocks of Low Hydraulic Conductivity, Memoirs of the IAH Vol. 17 Part 1, 1985.

18. van Genuchten, M. Th., "Solute Transport Processes in Structured Soils," 1985, Joint Proc. Hydrology Days and 14th Annual Rocky Mountain Groundwater Conf., pp. 169-180.

19. Rao, P. S. C., Jessup, R. E., and Addiscott, T. M., "Experimental and Theoretical Aspects of Solute Diffusion in Spherical and Nonspherical Aggregates," 1982, Soil Sci., Vol. 133, pp. 342-349.

20. Rao, P. S. C., Jessup, R. E., and Davidson, J. M., "Mass Flow and Dispersion," in: Environmental Chemistry of Herbicides, Vol. I, R. Grover (ed.), CRC Press, Boca Raton, Florida, 1987.

21. Roberts, P. V., Goltz, M. N., Summers, R. S., Crittenden, J. C., and Nkedi-Kizza, P., "The Influence of Mass Transfer on Solute Transport in Column Experiments with an Aggregated Soil," 1987, Jour. Cont. Hydrol., Vol. 1, pp. 375-393.

22. Koch, D. L., and Brady, J. F., "Non-local Dispersion in Porous Media: Non-mechanical Effects," 1987, Chem. Eng. Sci., Vol. 42, pp. 1377-1392.

23. Crittenden, J. C., Hutzler, N. J., Geyer, D. G., Oravitz, J. L., and Friedman, G., "Transport of Organic Compounds with Saturated Groundwater Flow: Model Development and Parameters Sensitivity," 1986, Water Resour. Res., Vol. 22, pp. 271-284.

24. Hutzler, N. J., Crittenden, J. C., Gierke, J. S., and Johnson, A. S., "Transport of Organic Compounds with Saturated Groundwater Flow: Experimental Results," 1986, Water Resour. Res., Vol. 22, pp. 285-295.

25. Valocchi, A. J., "Validity of the Local Equilibrium Assumption for Modeling Sorbing Solute Transport through Homogeneous Soils," 1985, Water Resour. Res., Vol. 21, pp. 808-820.

26. Lincoff, A. H., and Gossett, J. M., "The Determination of Henry's Constant for Volatile Organics by equilibrium Partitioning in Closed Systems," in: Gas Transfer at Water Surfaces, W. Brutsaert and G. H. Jirka (eds.), D. Reidel Publ. Co., Dordrecht, The Netherlands, 1984, pp. 17-25.

27. Garbarini, D. R., and Lion, L. W., "Evaluation of Sorptive Partitioning on Nonionic Pollutants in Closed System by Headspace Analysis," 1985, Env. Sci. Tech., Vol. 19, pp. 1122-1128.

28. Banerjee, P., Piwoni, M. D., and Ebeid, K., "Sorption of Organic Contaminants to a Low Carbon Subsurface Core," 1985, Chemosphere, Vol. 14, pp. 1057-1067.

29. Bouchard, D. C., Wood, A. L., Campbell, M. L., Nkedi-Kizza, P., and Rao, P. S. C., "Sorption Nonequilibrium during Solute Transport," 1988, Jour. Contaminant Hydrology, (in press).

30. Mackay, D. M., Freyberg, D. L., Roberts, P. V., and Cherry, J. A., "A Natural Gradient Experiment on Solute Transport in a Sand Aquifer: 1. Approach and Overview of Plume Movement," 1986, Water Resour. Res., Vol. 22, pp. 2017-2029.

31. Freyberg, D. L., "A Natural Gradient Experiment on Solute Transport in a Sand Aquifer: 2. Spatial Moments and the Advection and Dispersion of Nonreactive Tracers," 1986, Water Resour. Res., Vol. 22, pp. 2031-2046.

32. Mackay, D. M., Goltz, M. N., Roberts, P. V., and Cherry, J. A., "A Natural Gradient Experiment on Solute Transport in a Sand Aquifer: 3. Retardation Estimates and Mass Balances for Organic Solutes," 1986, Water Resour. Res., Vol. 22, pp. 2047-2058.

33. Roberts, G. P., Roberts, P. V., and Reinhard, M., "A Natural Gradient Experiment on Solute Transport in a Sand Aquifer: 4. Sorption of Organic Solutes and Its Influence on Mobility," 1986, Water Resour. Res., Vol. 22, pp. 2059-1067.

34. Sudicky, E. A., "A Natural Gradient Experiment on Solute Transport in a Sand Aquifer: Spatial Variability of Hydraulic Conductivity and its Role in the Dispersion Process," 1986, Water Resour. Res., Vol. 22, pp. 2069-2082.

35. Roberts, P. V., and Mackay, D. M., "A Natural Gradient Experiment on Solute Transport in a Sand Aquifer," Technical Report No. 292, Dept. of Civil Engineering, Stanford University, Palo Alto, CA, 1986.

36. Stauffer, T. B., "Sorption of Nonpolar Organics on Minerals and Aquifer Materials," Ph.D. Dissertation, The College of William & Mary, Virginia, 1987.

37. Zhong, W. Z., Lemley, A. T., and Wagenst, R. J., "Quantifying Pesticide Adsorption and Degradation during Transport through Soil to Groundwater," 1986, Amer. Chem. Soc. Symp. Series No. 315, pp. 61-77.

38. Karickhoff, S. W., Brown, D. S., and Scott, T. A., "Sorption of Hydrophobic Organic Pollutants on Natural Sediments," 1979, Water Res., Vol. 13, pp. 241-248.

39. Chiou, C. T., Porter, P. E., and Schmedding D. W., "Partition Equilibria of Nonionic Organic Compounds Between Soil Organic Matter and Water," 1983, Env. Sci. Tech., Vol. 17, pp. 227-231.

40. McIntyre, W. G., and deFur, P. O., "The Effect of Hydrocarbon Mixtures on Adsorption of Substituted Naphthalenes by Clay and Sediment," 1985, Chemosphere, Vol. 14, pp. 103-112.

41. Nkedi-Kizza, P., Rao, P. S. C., and Hornsby, A. G., "Influence of Organic Cosolvents on Leaching of Hydrophobic Organic Chemicals through Soils," 1987, Environ. Sci. Techn., Vol. 21, pp. 1107-1111.

42. Rao, P. S. C., and Jessup, R. E., "Sorption and Movement of Pesticides and Other Toxic Substances in Soils," in: Chemical Mobility and Reactivity in Soil Systems, D. W. Nelson, K. K. Tanji, and D. E. Elrick (eds)., Am. Soc. Agron. and Soil Sci. Soc. Spec. Pub. No. 11, Am. Soc. Agron., Madison, WI, 1983, pp. 183-201.

43. Nkedi-Kizza, P., Rao, P. S. C., and Hornsby, A. G., "The Influence of Organic Cosolvents on Leaching of Hydrophobic Organic Chemicals (HOC) through Soil," 1987, Env. Sci. Tech. Vol. 21, pp. 1107-1111.

44. Parker, J. C., and Valocchi, A. J., "Constraints on the Validity of Equilibrium and First-order Kinetic Transport Models in Structured Soils," 1986, Water Resour. Res., Vol. 22, pp. 399-407.

(The reverse of this page is blank)

SECTION V

SPECTROSCOPIC STUDIES OF VOLATILE ORGANICS ADSORPTION

A. EXPERIMENTAL METHODS

1. Clay Mineral Preparation for FT-IR Analysis

The clay mineral samples studied were obtained from the Source Clays Repository located at the University of Missouri and operated by the Clay Minerals Society. The kaolinite sample was the well-crystalline KGa-1 Georgia-kaolinite collected from Washington county, GA, and the montmorillonite sample was the SAz-1 Cheto-montmorillonite collected in Apache county, AZ. A complete description of the physical properties of these clay samples has been given by van Olphen and Fripiat (Reference 1). In addition, Raman and IR spectra of the KGa-1 kaolinite clay have been reported by Johnston et. al. (Reference 2). The colloidal behavior of 1:1 clay minerals (i.e., kaolinite and serpentine group minerals) are fundamentally different from that of the 2:1 clays; therefore, separate clay mineral preparation and purification procedures were used for preparing the KGa-1 and SAz-1 clay materials.

The procedure used to prepare the SAz-1 Cheto-montmorillonite clay sample was similar to that described by Sposito et al. (Reference 3). Sixty grams of the crude reference clay were placed in 1-liter of distilled, de-ionized water and mixed for 2 hours with a mechanical stirrer. The fraction having an equivalent-spherical-diameter (e.s.d.) of < 0.5 μm in suspension was separated by centrifugation, then flocculated by adding 800 mL of a solution containing 0.001 M HCl in 1M NaCl. Because ion-pair formation did not interfere with the FT-IR measurements, a chloride background was substituted for the perchlorate background used by Sposito et al. (Reference 3). The flocculated clay in the NaCl-HCl solution was centrifuged 15 minutes at 5000 rpm on a Sorvall SS-3 centrifuge equipped with a Model GSA. head. After the clear supernatant solution was decanted carefully, the SAz-1 clay plug at the bottom of the centrifuge tube was redispersed manually into a fresh NaCl-HCl solution and the suspension was shaken on tray shaker for 20 minutes. The suspension was centrifuged again as described above. This

washing procedure was repeated about three times until the pH value of the supernatant solution dropped to 3.0. After the final NaCl-HCl wash and centrifugation, the SAz-1 clay plugs were redispersed into a 0.1M NaCl solution and a similar washing procedure was repeated about five times using the 0.1M NaCl solution until the pH of the supernatant solution equaled that of the 0.1M NaCl solution (pH 5.5). After the last wash, the clay was redispersed in 0.1M NaCl and stored in suspension prior to the spectroscopic analysis. A flowchart of the clay preparation procedure is shown in Figure 49.

The clay preparation procedure used for the KGa-1 kaolinite sample was similar to the procedure described by Johnston et al. (Reference 2). Two hundred grams of the the untreated KGa-1 clay were placed in 1 liter of distilled, deionized water and dispersed for size fractionation by adjusting the pH to 9.5 by the addition of small aliquots of 0.01M NaOH. The kaolinite suspension was size-fractionated immediately by centrifugation and the fraction have an e.s.d. of < 2.0 μm was collected. The suspension was then flocculated by the addition of 1 liter of 0.001M HCl in 1.0M NaCl. To separate the supernatant solution from the flocculated clay, the suspension was centrifuged at a relative centifugal force of 700. The supernatant solution then was decanted and its pH measured. The kaolinite samples were redispersed manually into 1 liter of the 0.001M HCl/1.0M NaCl solution, and the washing procedure was repeated until the pH value of the supernatant solution equaled that of the washing solution (pH 3) this objective typically required five washings. At this point in the procedure, the clay was redispersed into 1 liter of 0.01M NaCl, and the above procedure was repeated five more times. The treatment was adequate to raise the pH of the supernatant solution to 5.5. The final step of the procedure consisted of redispersing the clay into 0.01M NaCl and adjusting the volume of the flocculated suspension such that a clay concentration of 20 percent (w/w) was obtained.

2. Bomem DA3.10 Fourier Transform Spectrometer

FT-IR spectra were obtained on a Bomem DA3.10 Fourier transform spectrometer. The DA3.10 spectrometer utilizes a Michelson interferometer with the beamsplitter positioned at a 30 degree angle to the optical axis.

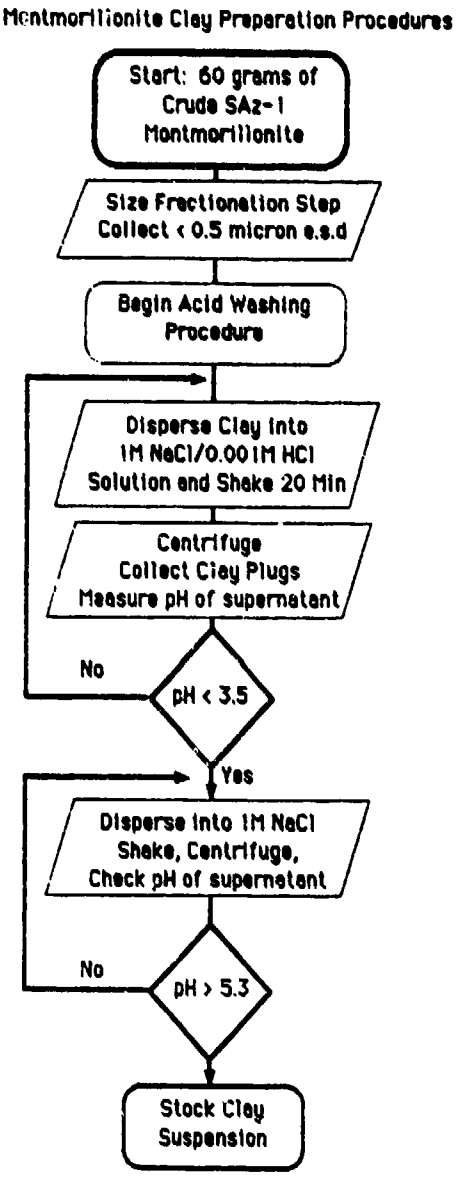

Figure 49. Flowchart of the SAZ-1 Clay Preparation Procedure.

A Digital Equipment Corporation Vaxstation-II based data acquisition system was used to control the DA3.10 spectrometer. A sixty degree field-of-view Infrared Associates broadband, liquid nitrogen cooled, mercury-cadmium-telluride (MCT) detector fitted with a KRS-5 infrared window was used for these FT-IR studies. The size of the detector element was 1.01 mm (width) by 1.01 mm (length); the active area of the detector element was 1.032 mm^2. The measured D* value of the detector was 3.13×10^9 cmHz0.5 and the cutoff wavenumber was 400 cm^{-1} (25 microns). A midinfrared, water-cooled, ceramic silicon carbide source was used for the mid-IR region and a visible quartz tungsten halogen source, mounted inside the spectrometer, was used for sample alignment.

The nominal optical resolution used in these studies ranged between 2.0 and 0.5 wavenumbers. A comparison of several spectra of clay samples obtained at different nominal resolution values showed that the spectra were not instrument limited for nominal resolution values of 0.5, 1.0, 2.0, and 4.0 wavenumbers. The 4.0 wavenumber spectrum of kaolinite was instrument limited; consequently, a spectral resolution of 2.0 cm^{-1} or higher was used in this investigation. The FT-IR spectra of the SAz-1 Cheto-montmorillonite sample were not instrument limited at a resolution of 2.0 cm^{-1}. A Hamming apodization function was used to weight the cosine wave interferograms. Initially, a low-resolution double-sided interferogram was collected and the phase angle deviation from zero of the interferogram was determined using the Forman method (References 4,5,6). The phase correction determined from the double sided interferogram was stored in the HSVP. Subsequently, all single sided, high resolution interferograms were corrected using these stored values. Typically, 16,000 data points were collected per single sided interferogram with approximately 900 data points collected before the centerburst. Programmable low-pass and high-pass analog filters were used to optimize the signal-to-noise ratio. A low-pass cutoff filter of 20 KHz, and a high-pass cutoff filter of 2 Hz (3 db cutoff frequencies). Interferograms were collected with a moving mirror velocity of 0.5 cm/sec which corresponded to a sampling frequency of 15.8 KHz. The dynamic range of the analog-to-digital converter was 16 bits and the word length of the Vaxstation-II computer was 32 bits. One sample point was collected per laser fringe with a resolution of 16 bits per sample. Typically, 256 scans were coadded for the sample and reference files. The total measurement time for

coadding 256 scans was 200 seconds for 1 cm^{-1} resolution and 600 seconds for 0.5 cm^{-1} resolution. No smoothing or interpolation algorithms were used.

The sample compartment of the Bomem DA3.10 can be operated under a vacuum of 0.020 torr, or at 1 atm of pressure using dry N_2 to purge the spectrometer (reduce the spectral interference from H_2O and CO_2 vapors). All of the spectra reported here were obtained using the evacuated sample compartment which virtually eliminated the interference from these atmospheric constituents. Because the sample compartment of the Bomem DA3.10 was operated under a reduced pressure, the sample cover access plates were modified to accommodate two 3/8 inch MDC quick-disconnect vacuum tube feedthroughs which provided a connection through the vacuum wall of the spectrometer from the vacuum manifold to the controlled-environment-transmission (CET) cell in the sample compartment. The position of the CET cell in the sample compartment of the Bomem DA3.10 spectrometer is illustrated in Figure 50.

3. Vaxstation-II Data Acquisition System

The data acquisition system for the Bomem DA3.10 spectrometer was a Digital Equipment Corporation (DEC) Vaxstation-II computer. The Vaxstation-II computer consists of a μVAX-II CPU with a dedicated high-resolution, bit-mapped graphic display terminal. The Bomem DA3.10 spectrometer is connected directly to a proprietary high speed vector processor (HSVP) through a 50-line parallel interface. The Vaxstation-II communicated with the HSVP through a National Instruments General Purpose Interface Bus (GPIB) Card (Model No. GPIB11V-2) which was resident on the Q-bus of the VaxstationII. The initial data acquisition system that was used to collect data from the Bomem was a DEC PDP 11/23 computer (which also supports the Q-bus). The use of the PDP 11/23 was limited for this application because of the 16-bit word-length and address restrictions, limited storage capability, and the extremely slow display output which resulted from the 9600 baud serial-throttle of the VT-240 terminal. The slow display and low resolution of the VT-240 terminal, in particular, were serious limitations of the PDP 11/23.

Figure 51 illustrates the main differences between the Vaxstation-II computer and the PDP 11/23 computer. In terms of overall computational performance, the Vaxstation-II (μVax-II) system is about 20 times faster than the PDP 11/23. Bomem does not support their software on the

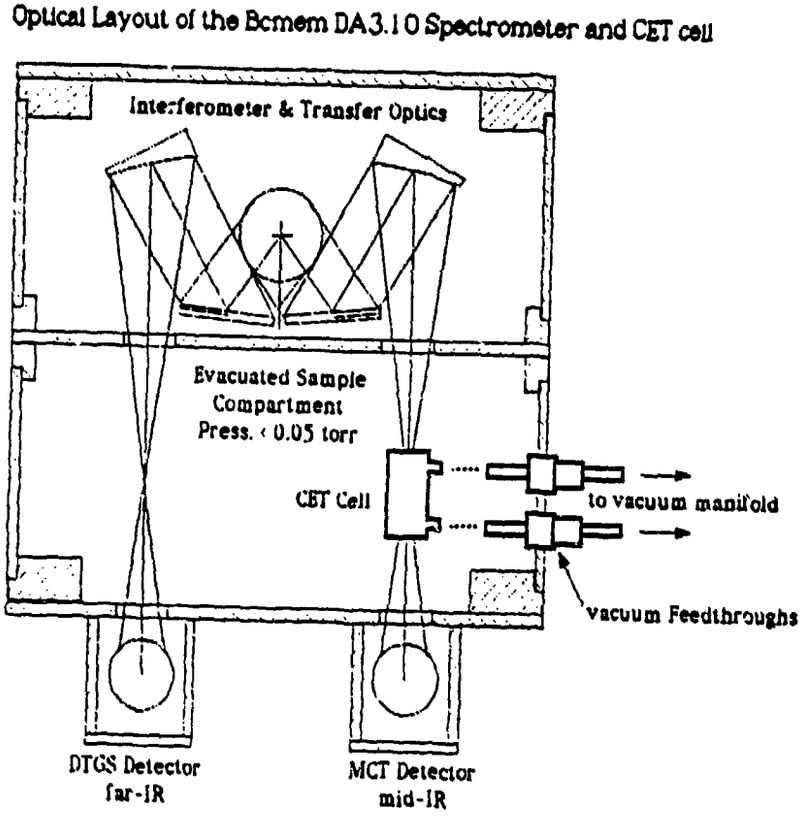

Figure 50. Schematic of the Sample Compartment of the Bomem DA3.10 Spectrometer with the Controlled Environment Transmission Cell.

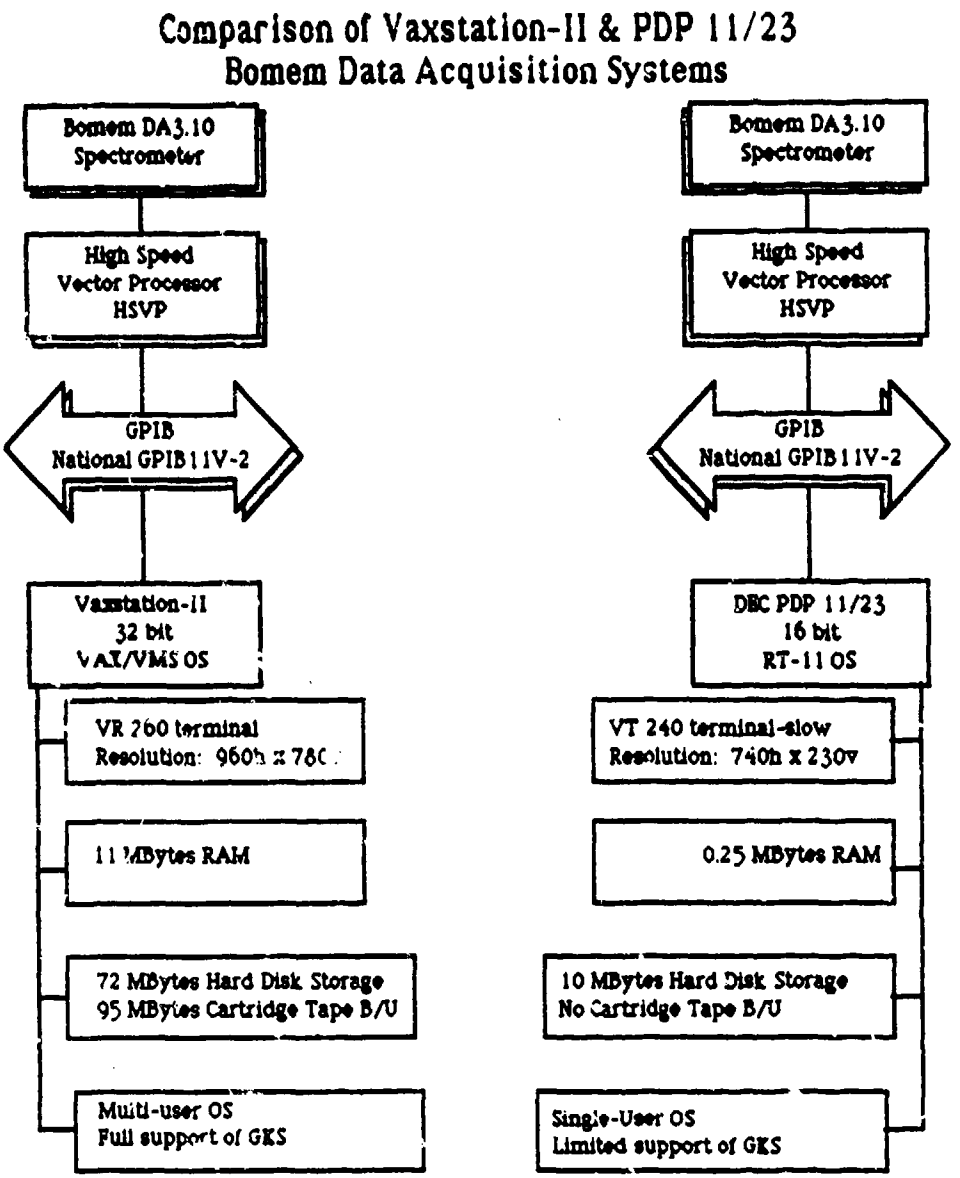

Figure 51. Comparison of the Vaxstation-II Data Acquisition System to the PDP 11/23 Computer.

Vaxstation-II; thus, the Bomem Fortran-77 and assembly-level (Macro-11) codes were modified and transferred to the VaxstationII. Most of the routines could be transferred directly to the VaxstationII with little or no modification; however, the HSVP routines had to be rewritten altogether because of the significant differences between the VAX/VMS and RT-11 operating systems.

In addition to the HSVP routines, new codes were developed to support the VR260 graphic display terminal. The Vaxstation-II software provided two environments for the development of the graphic display codes: the VAX GKS run-time library of graphical functions that are defined by the ANSI X3.124-1985 and ISO 7942-1985 Graphic Kernel System (GKS) standards, or the device dependent MicroVMS Workstation Graphics. The VAX GKS environment was chosen over the latter because GKS is supported on a number of different machines (e.g., DEC, IBM, HP, etc.) and supports a number of different graphic output formats including the Tektronix 4010/4014, DEC VT-125, DEC Vaxstation-II VR260, LVP16, HP7470, HP7475A, LNO3, and GKS Metafile formats. The graphic display codes were developed on the Vaxstation-II operating under the VAX/VMS Version 4.5 operating system using V3.1 of the MicroVMS workstation software. The VAX GKS V2.0 run-time library of graphical functions were called from VAX Fortran-77 V4.

4. Controlled-Environment-Transmission (CET) Cell and Manifold

The controlled-environment-transmission (CE-TR) cell was a modified 10-cm pathlength cell fitted with two Kontes Teflon^{R} stopcocks, and two 49 mm x 3mm ZnSe windows using Viton O-rings (Figure 52). The Kontes Teflon^{R} stockcocks were modified at the glass shop to accommodate two Lab-Crest Model 571190 9 mm Solv-Seal joints. The Solv-Seal joint system, which incorporates a TFE seal with two viton o-rings, can be pumped down to 10^{-8} torr. Clay films were held in place in the CE-TR cell using a TFE holder which allowed the films to mounted at 90 or 60 degree angles of incidence to the modulated IR beam. The CE-TR cell was mounted on a Newport Research Corporation (NRC) Model 460XYZ-DM translation stage which provided precise positioning of the CE-TR cell.

The vacuum system consisted of the following items connected in series on a mobile cart: 195 L/min mechanical pump, 3-angstrom molecular sieve trap, two-way valve, water-cooled Edwards Diffstak 63 oil diffusion pump

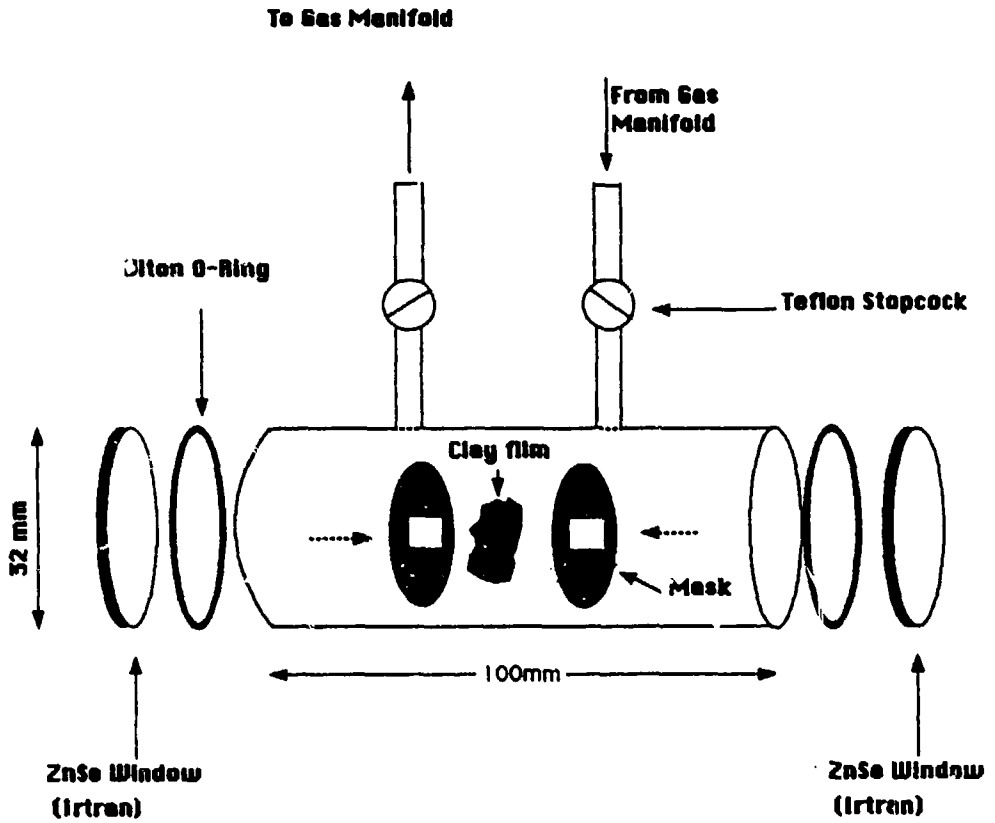

Figure 52. Illustration of the Controlled Environment Transmission Cell

(135 L/sec), Edwards Penning & Pirani gauge head assembly, ISO63 flange to KF40 flange adapter, KF-40 isolation valve, KF16 relief valve, 1 meter KF40 stainless steel bellows, glass liquid nitrogen trap fitted with Lab-Crest Model 571190 15 mm Solv-seal joints, and a five-place Teflon^{R}/glass Airless-ware manifold fitted with Lab-Crest Model 571190 9 mm Solv-Seal joints. Because all of the glass joints were terminated with the Lab-Crest Solv-seal joints, the vacuum manifold was highly modular. An Edwards Model 1005 controller fitted with two Pirani gauge heads and one Penning gauge were used to monitor the pressure in the CE-TR cell and vacuum manifold in the 760 torr to 1 x 10^{-8} torr range. A schematic of the vacuum manifold and CE-TR cell are shown in Figure 53.

B. RESULTS AND DISCUSSION

1. Characterization of the Clay Minerals

a. Comparison of Sample Presentation Methods for Kaolinite

The initial objective of this task was to evaluate the application of Fourier transform infrared (FT-IR) spectroscopic methods to the study of naturally occurring clay minerals. Because of the paucity of reported FT-IR spectra of clay minerals in the literature, a systematic spectroscopic investigation of two representative clay minerals, kaolinite and montmorillonite, was initiated. Published FT-IR spectra of clay minerals in the literature (References 7,8,9) have been restricted to transmission spectra using the KBr pellet method of sample presentation. This technique requires the sample to be diluted in an alkali halide (e.g., KBr or KCl) matrix and compressed under a high pressure (> 7.5 kbar). Although traditionally this has been the most common method of obtaining IR spectra of powders and polycrystalline samples, there are a number of disadvantages associated with this technique. First, the sample must be compressed under a high pressure which can introduce spectral artifacts. Second, the sample must be kept anhydrous because of the hydroscopic behavior of the alkali halide matrix. Third, this method cannot be used for in situ solute adsorption studies because the adsorbate is encapsulated in the alkali halide matrix and is not accessible to the vapor-solid, or liquid-vapor interface. The reported

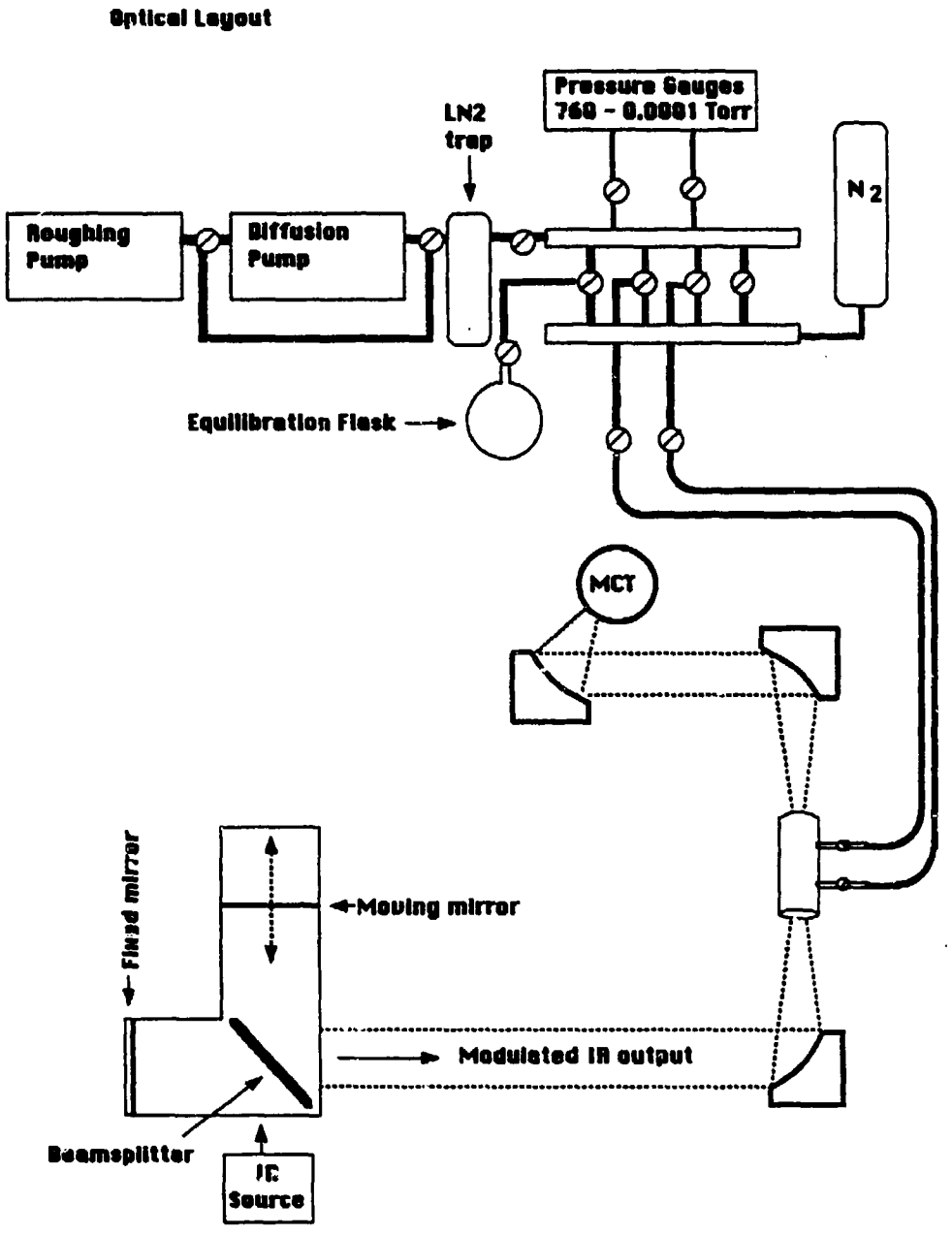

Figure 53. Layout of the Controlled Environment Transmission Cell in Relation to the Vacuum Manifold and Spectrometer.

alkali halide pellet-transmission FT-IR spectra of kaolinite and montmorillonite samples do not show any substantial improvement over similar spectra reported using dispersive infrared spectrometers (Reference 10). Thus, little benefit was realized by the application of Fourier transform (FT) methods over conventional dispersive infrared spectroscopy.

In the present investigation, FT-IR spectra were obtained using three different sample presentation methods: cylindrical internal reflectance (CIR), diffuse reflectance (DR), and transmission (TR) techniques. FT-IR spectra of clay mineral samples obtained using CIR or DR sample presentation methods have not been reported in literature. For the purpose of this comparison, KGa-1 kaolinite was chosen as the reference clay mineral because its infrared and Raman spectra have been reported in the literature. FT-IR spectra of KGa-1 kaolinite obtained using TR, DR, and CIR sample presentation methods at 2 cm^{-1} resolution are presented in Figures 54-57 in the 700 to 4000 cm^{-1}, 700 to 1200 cm^{-1}, and 3500 to 3800 cm^{-1} spectral regions, respectively. In addition, expanded plots of the TR KGa-1 kaolinite spectrum in the 700 to 1200 cm^{-1} and 3500 to 3800 cm^{-1} regions are presented in Figures 57 and 58 showing the position of the bands labeled on the spectra.

In a spectroscopic study of structural disorder among natural kaolinite and dickite samples, Brindley et al. (Reference 7) showed that the spectral resolution and separation of the 3652 and 3669 cm^{-1} bands correlated strongly with the measure XRD structural disorder of the samples (Reference 11). In the present study, these spectral criteria were used to evaluate the sensitivity of the three methods.

As the spectra shown in Figure 56 indicated, the greatest resolution and separation was achieved using TR over the DR, and CIR methods. Overall, the highest signal-to-noise ratio (SNR) was obtained using the TR method and of the three methods used, TR method was considered the most sensitive technique for noninvasive vapor-solid solute adsorption studies. The band positions of the KGa-1 kaolinite obtained here agree well with the reported IR and Raman spectral values, and are tabulated in Table 22 along with their band assignments. One disadvantage of the TR over DR and CIR methods is that TR spectra, in particular, are sensitive to the influence of the Christiansen effect (Reference 12) resulting from the wavelength dependence of the index of refraction of the sample. This interference was minimized in the present study by working with the less that 2 mm particle size fraction (Reference

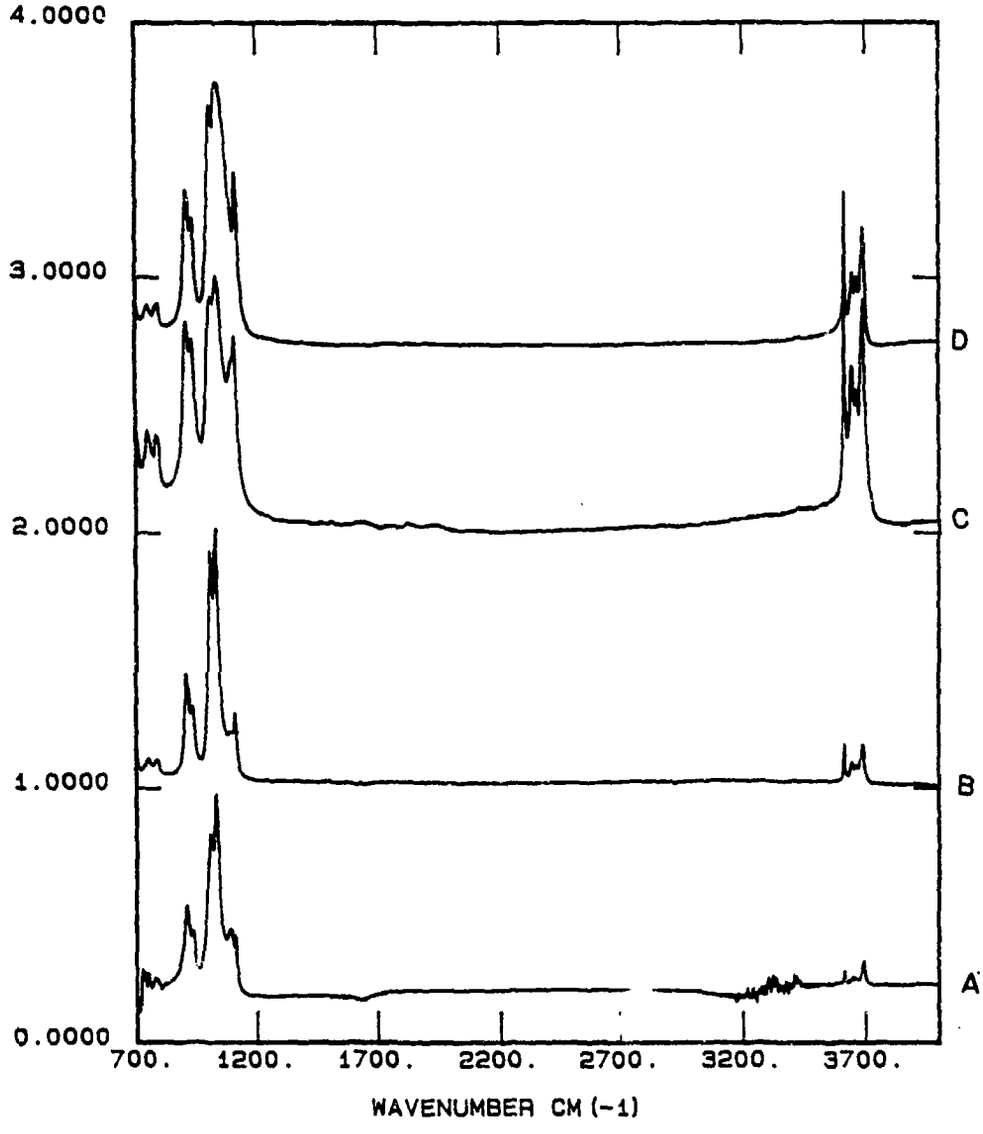

Figure 54. Comparison of FT-IR Spectra of KGa-1 Kaolinite in the 700 to 4000 cm^{-1} Region Obtained Using the Controlled Environment Transmission Cell (D, top), Diffuse Reflectance (C), Cylindrical Internal Reflectance Spectrum Dry (B), and the Cylindrical Internal Reflectance Spectrum Wet (A, bottom).

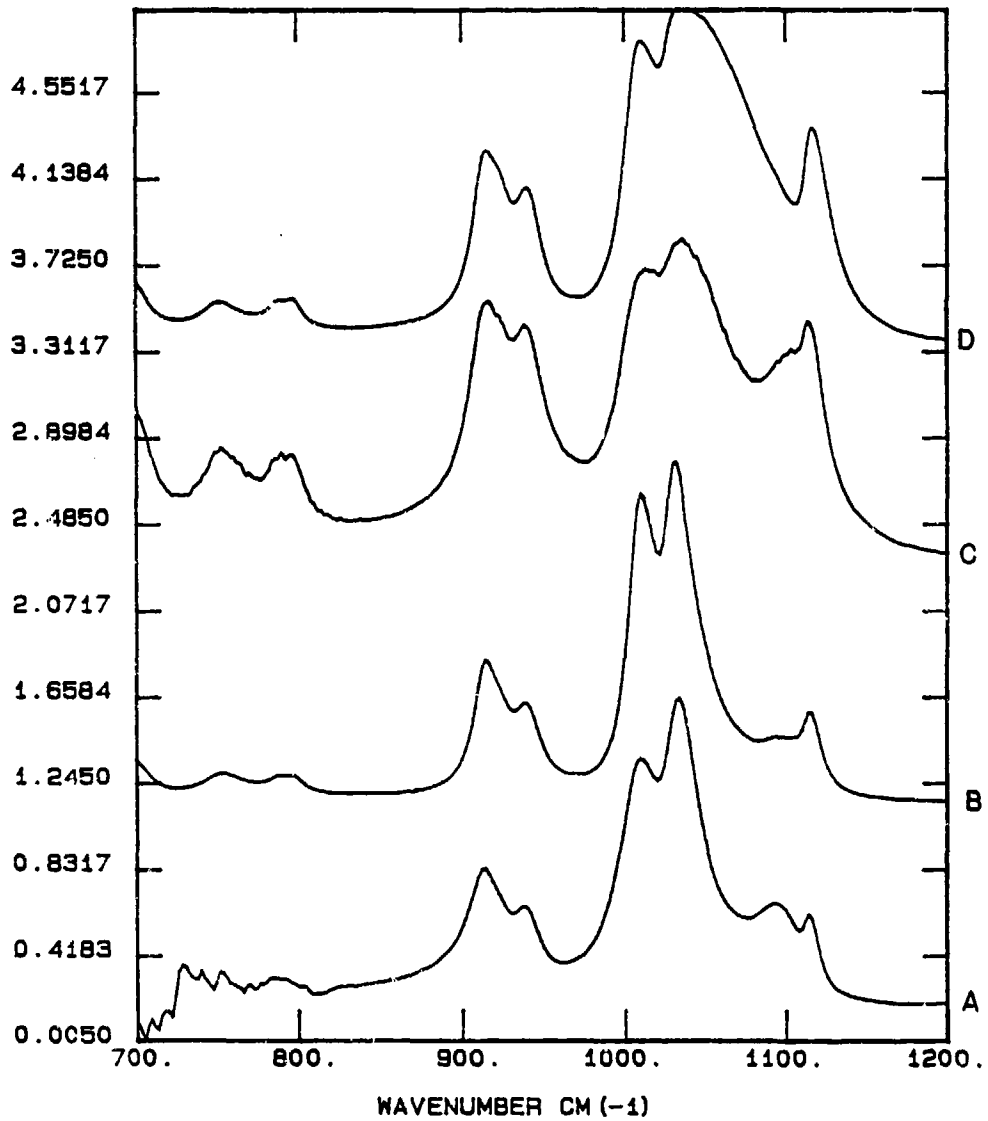

Figure 55. Comparison of FT-IR Spectra of KGa-1 Kaolinite in the 700 to 1200 cm^{-1} Region Obtained Using the Controlled Environment Transmission Cell (D), Diffuse Reflectance (C), Cylindrical Internal Reflectance Spectrum Dry (B), and the Cylindrical Internal Reflectance Spectrum Wet (A, bottom).

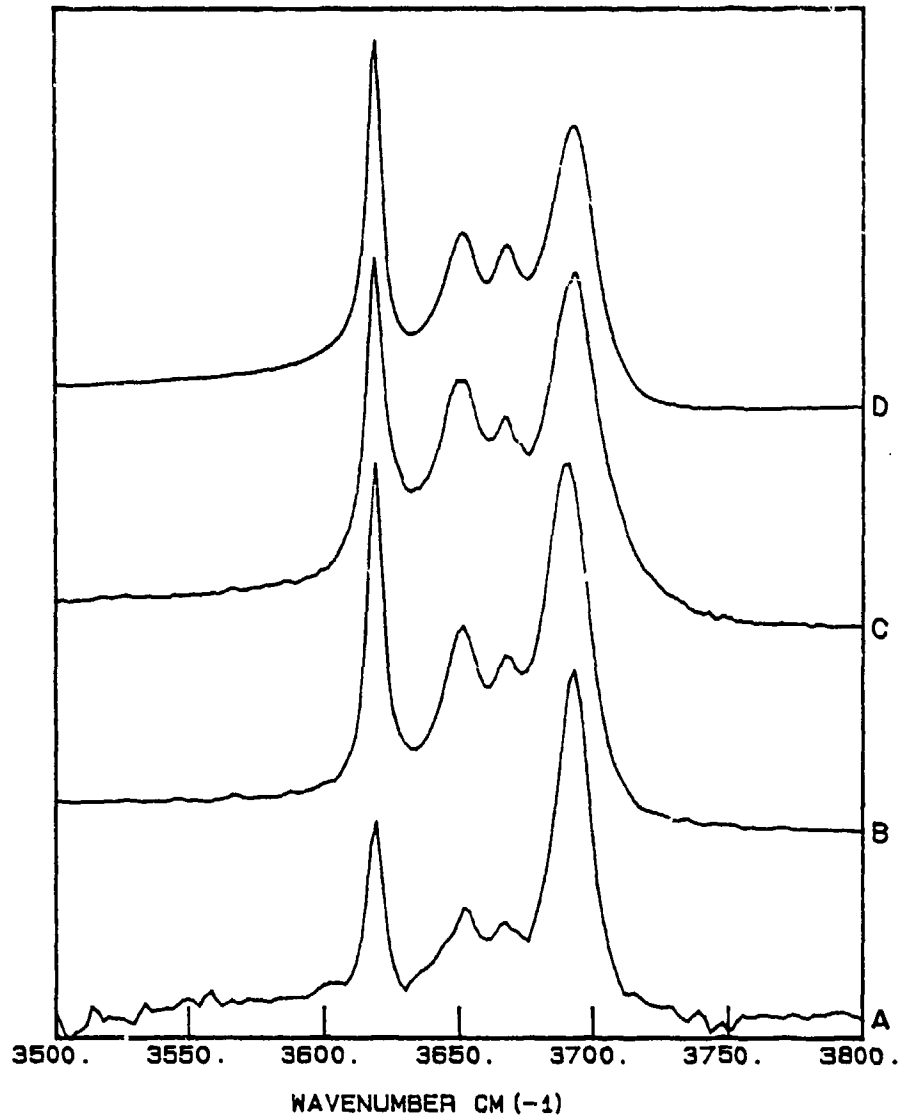

Figure 56. Comparison of FT-IR Spectra of KGa-1 Kaolinite in the 3500 to 3800 cm^{-1} Region Obtained Using the Controlled Environment Transmission Cell (D), Diffuse Reflectance (C), Cylindrical Internal Reflectance Spectrum Dry (B), and the Cylindrical Internal Reflectance Spectrum Wet (A, bottom).

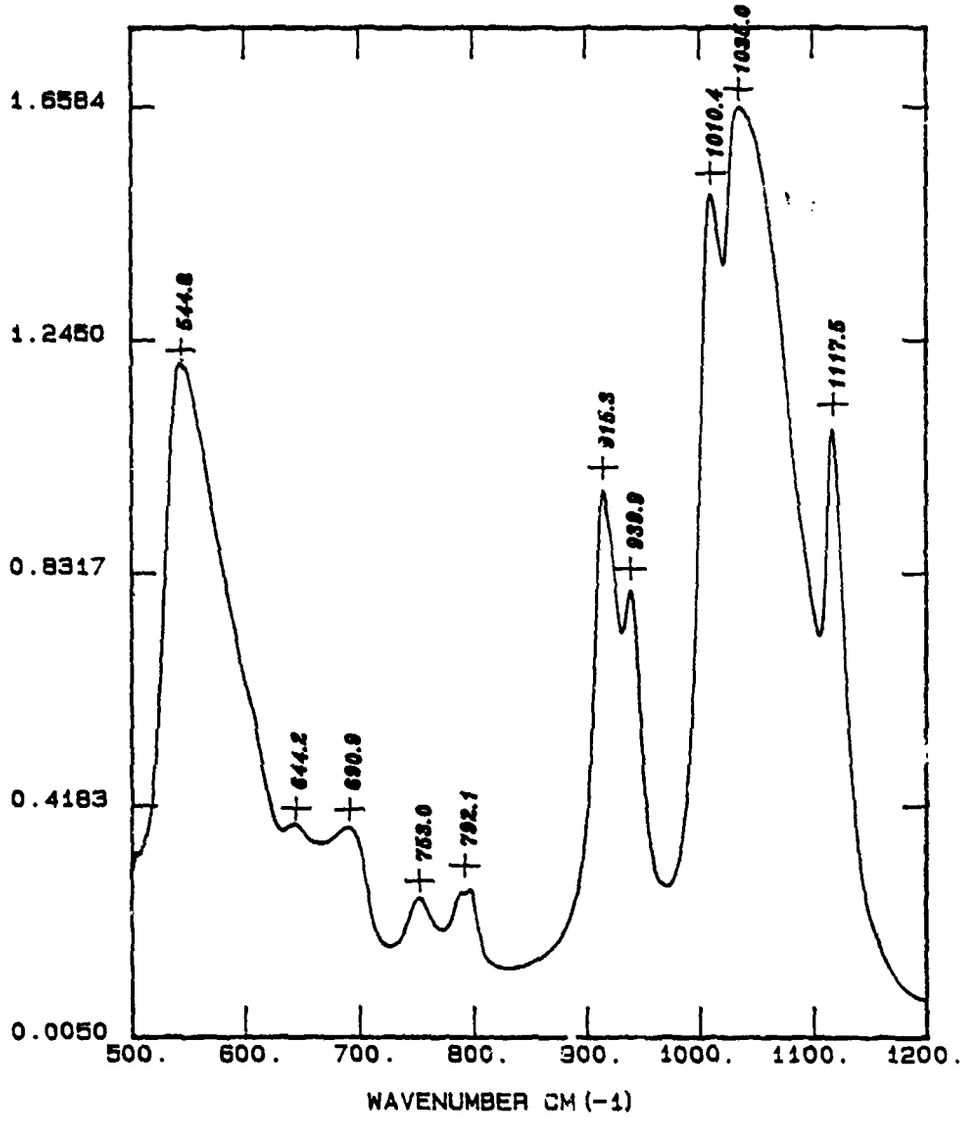

Figure 57. Absorbance FT-IR Spectrum of KGa-1 Kaolinite in the 500 to 1200 cm^{-1} Region Obtained Using the Controlled Environment Transmission Cell.

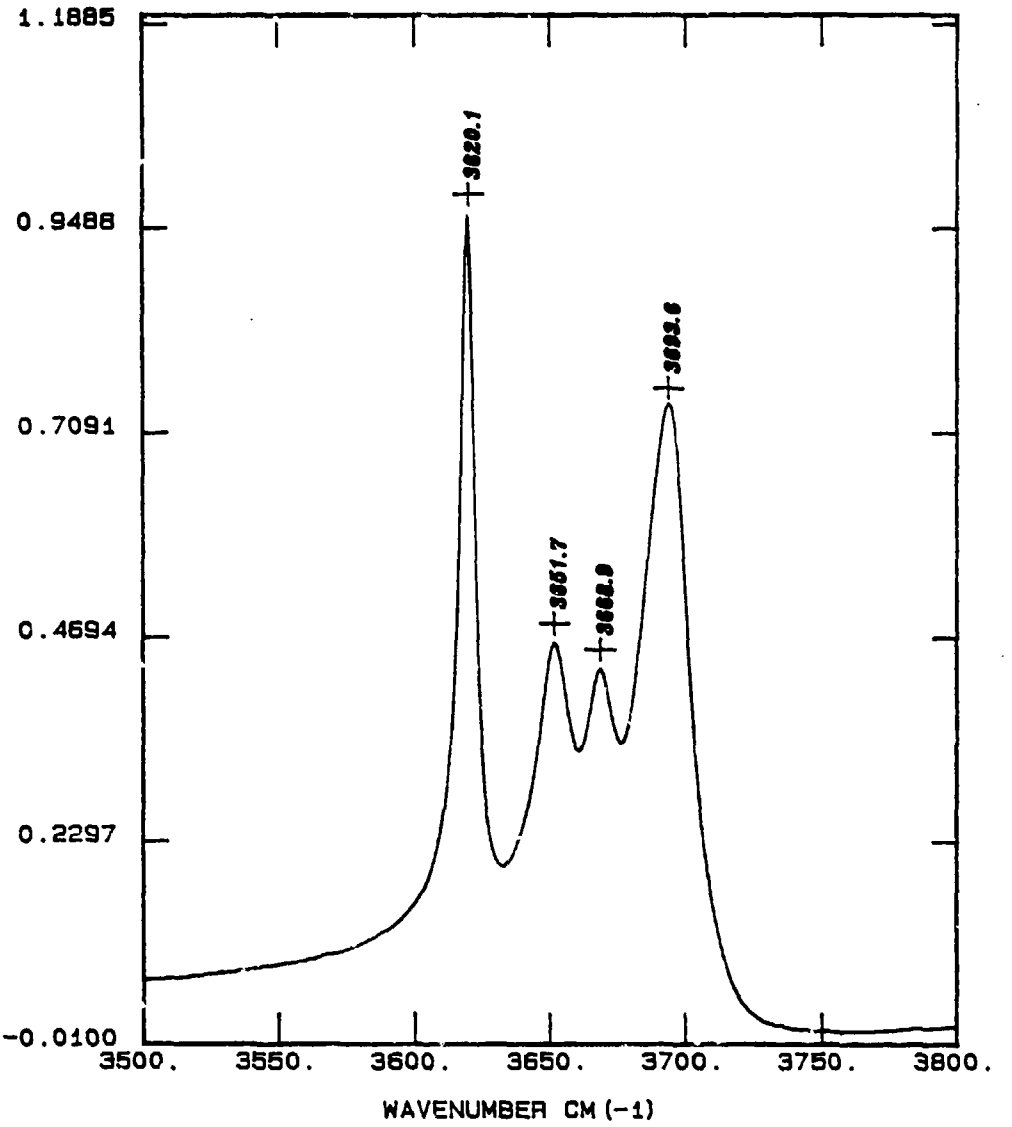

Figure 58. Absorbance FT-IR Spectrum of KGa-1 Kaolinite in the 3500 to 3800 cm^{-1} Region Obtained Using the Controlled Environment Transmission Cell.

13). Evidence for this effect is shown by the small distortion of the baseline in the high frequency TR spectrum of kaolinite (Figure 58). Because this distortion was small, it was concluded that the Christiansen effect did not produce a significant interference in this study.

TABLE 23. BAND ASSIGNMENTS OF KGa-1 KAOLINITE.

Band position	Band assignment
cm^{-1}	
544	Si-O-Al skeletal vibrations
606.0	Si-O-Al skeletal vibrations
643.4	
690.1	-OH deformation - gibbsite layer
787.8	-OH deformation - gibbsite layer
799.7	
915.3	AL-O-H deformation, Inner-Surface Hydroxyl
939.9	AL-O-H deformation, Inner Hydroxyl
1009.6	Si-O Stretch
1034.2	Si-O Stretch
1116.6	Si-O Stretch
3620.1	Al-O-H stretch, Inner hydroxyl group
3652.1	Al-O-H stretch, Inner-Surface hydroxyl group
3668.9	Al-O-H stretch, Inner-Surface hydroxyl group
3693.9	Al-O-H stretch, Inner-Surface hydroxyl group

A relatively new technique, pioneered by Griffiths et al. (References 14,15,16,17) is diffuse reflectance (DR) FT-IR spectroscopy. A complete discussion of this method and several prototypical applications are given in a recent monograph by Griffiths and de Haseth (Reference 18). Diffuse reflectance FT-IR spectra of KGa-1 kaolinite are presented shown as curve C in Figures 54, 56, and 57. Several advantages of DR methods include the lack of interference of the Christiansen effect in DR spectra (Reference 14), and the ease of sample preparation. Very little sample preparation is required in that samples are mixed with a suitable nonabsorbing, highly reflective background matrix material, lightly packed into a sample cup, and placed into the DR cell. Brackett et al. (Reference 19) evaluated a number proposed matrix materials and reported that KCl had suitable properties as a background matrix material. All of the DR reflectance spectra reported here were obtained using KCl as the matrix material. A direct, quantitative

comparison between the band intensities in the TR spectrum to those of the DR spectrum cannot be made because the TR spectra are measured in units of absorbance and the DR are in Kubelka-Munk units. However, the relative intensity of the bands in the hydroxyl stretching region (3500 to 3800 cm^{-1} region) to the lower frequency bands below 1200 cm^{-1} was higher in the DR spectrum than in the TR spectrum (D1D) (Curves C,D; Figure 54). In addition, the relative intensities of the the 690 and 787 bands was greater in the DR spectrum compared to the TR spectrum. The general features of the TR and DR spectra were observed to be very similar.

One disadvantage of DR methods is problems asscciated with spectral reproducibility because this method is very sensitive to the height of the sample cup in the diffuse reflectance cell and to the way the powdered material was packed into the sample cup. During the past few years, several controlled environment (CE) DR cells have become commercially available. These cells permit solutes and adsorbates to be introduced and removed from the sample without disturbing the sample. Consequently, these CE-DR cells provide a solution to the spectral reproducibility problem, and should provide a powerful physical method for observing in situ vibrational spectra of adsorbate-adsorbent interactions.

Cylindrical internal reflectance (CIR) is another relatively new attenuated total reflectance (ATR) method which has become commercially available during the past 3 years (Reference 18). A schematic of the CIR cell used in this study is shown in Figure 59. Although CIR-FT-IR spectra of clay minerals have been not been reported in the literature, several prototypical applications of this method have been reported which include a recent study of the surface chemistry of iron oxides in aqueous suspension (Reference 20) and to several biomedical/protein adsorption problems (References 21,22,23).

A comparison of CIR spectra of KGa-1 kaolinite in aqueous suspension and of dry KGa-1 kaolinite to DR and TR spectra are presented in Figures 54-56. The bottom spectra in Figures 54-57 were obtained for a 1 percent (w/w) aqueous suspension of KGa-1 kaolinite. Initially, the CIR cell was filled with water and a single-beam-energy spectrum (SBES) of water was obtained. The water was removed from the cell was refilled with the 1 percent kaolinite suspension and the SBES of the KGa-1 suspension was obtained. The absorbance spectra presented in Figures 54-56 were obtained by taking the logarithm (base 10) of the ratio of the SBES water spectrum to the SBES

Cylindrical Internal Reflectance Cell For Studying Aqueous Colloidal Suspension

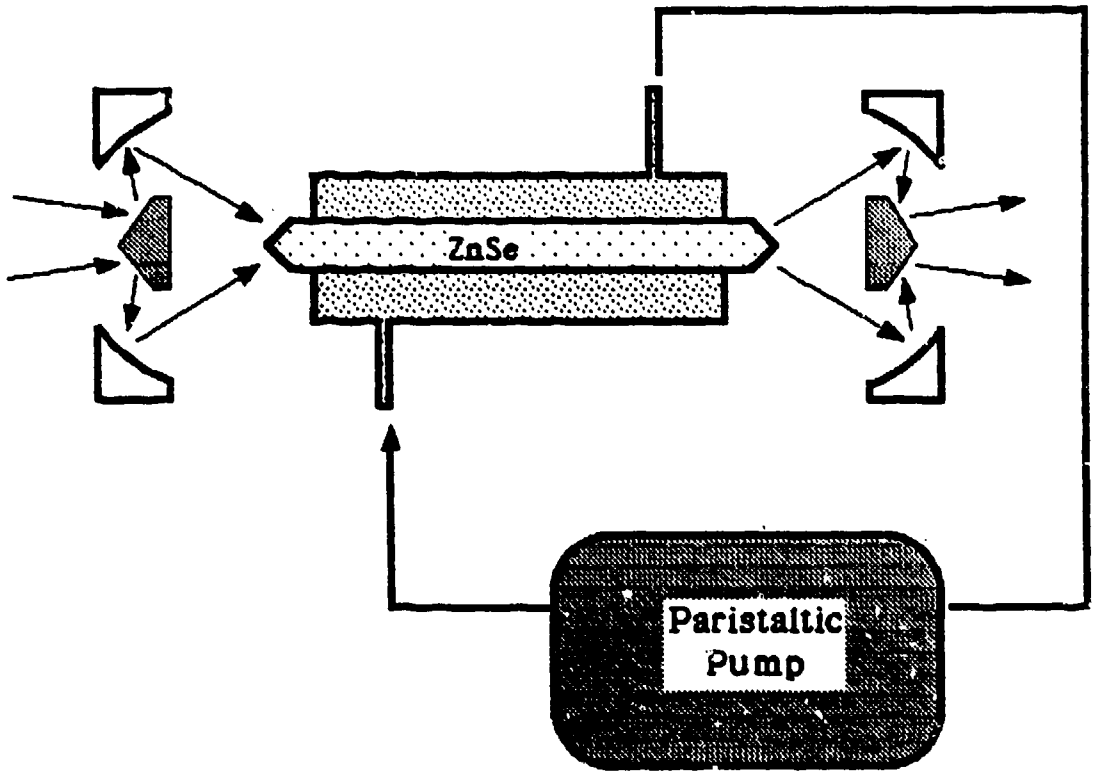

Figure 59. Cell Design of the Spectra-Tech Cylindrical Internal Reflectance FTIR Cell.

KGa-1/suspension spectrum. This procedure is illustrated in Figure 60 where the absorbance spectrum of water in the CIR cell is shown as curve A. This spectrum was obtained as follows:

$$S_{water} = \text{SBES of water (Single beam energy spectrum of water)} \quad (50)$$

$$S_{cell} = \text{SBES of empty CIR cell (Single beam energy spectrum of empty CIR cell)} \quad (51)$$

$$A_{water} = \log_{10} (S_{cell} / S_{water}) \quad (52)$$

$$A_{water} = \text{Absorbance spectrum of water in the CIR cell} \quad (53)$$

where the "sample" spectrum is used in the denominator and the "reference" or "background" spectrum as the numerator.

The absorbance spectrum of KGa-1 kaolinite in aqueous suspension shown in Figure 60 (curve B) was obtained using the following expression:

$$A_{KGa\text{-}1 + water} = \log_{10} (S_{cell} / S_{KGa\text{-}1 + water}) \quad (54)$$

$$A_{KGa\text{-}1 + water} = \text{Absorbance spectrum of KGa-1 kaolinite + water} \quad (55)$$

The "difference" spectrum of the KGa-1 kaolinite sample shown in Figure 60 (curve C) was obtained by using the S_{water} spectrum as the reference in the following expression:

$$A_{KGa\text{-}1} = \log_{10} (S_{water} / S_{KGa\text{-}1 + water}) \quad (56)$$

A detailed comparison of the CIR spectra in the 3550 to 3750 cm^{-1} spectral region is presented at the top of Figure 64 where the absorbance spectra of water (curve D), kaolinite in water (curve E and F), and dry KGa-1 kaolinite (curve G) are presented.

As the spectra shown at the bottom of Figure 60 indicate, water absorbs strongly in the 2800 to 3700 cm^{-1} (ν O-H), and in the 1600 to 1700 cm^{-1} (δ O-H) spectral regions. One of the distinct benefits of FT-IR

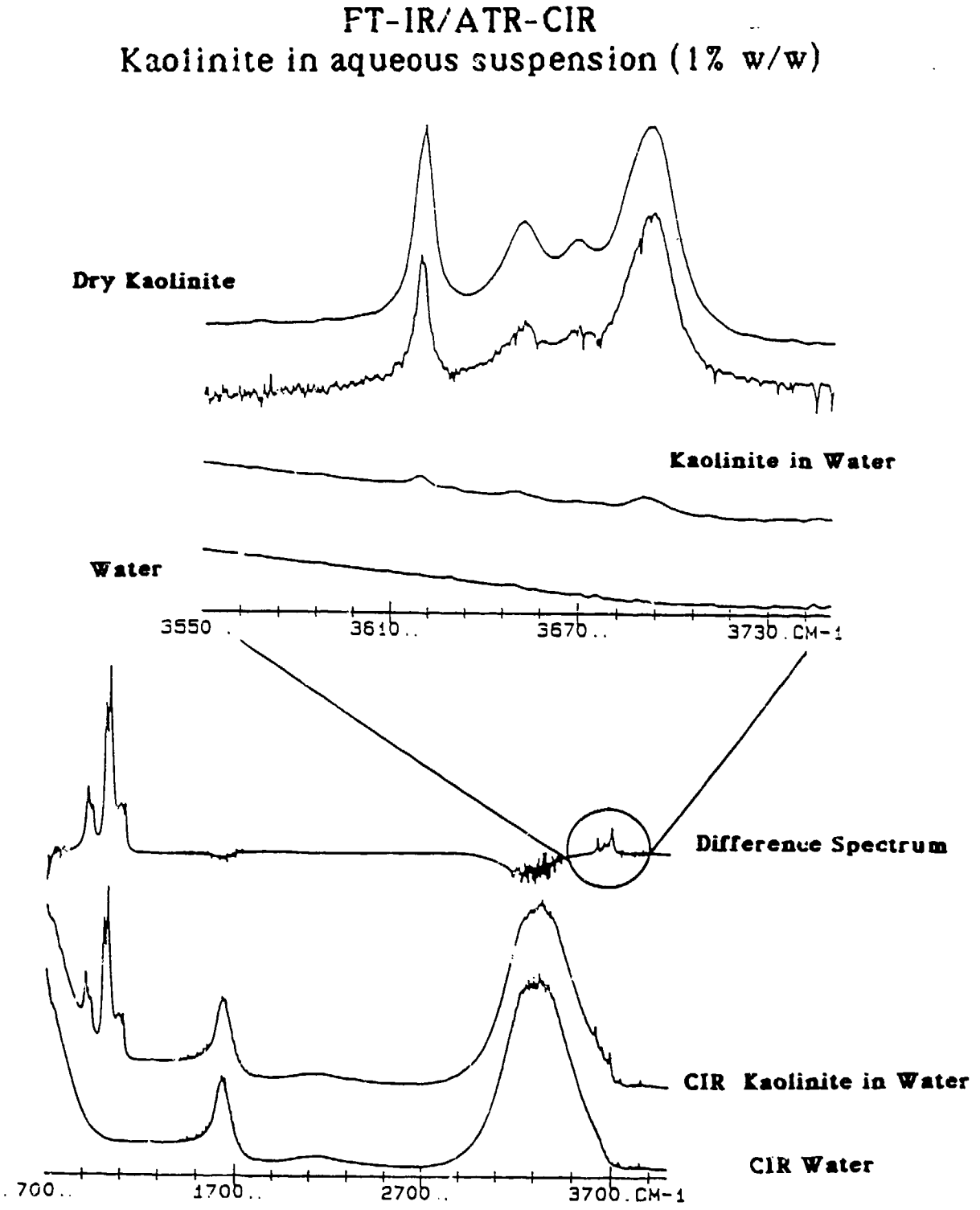

Figure 60. Attenuated Total Reflectance FT-IR Spectra of Water (A.D.), Kaolinite and Water (B.E.), Difference Spectrum of Kaolinite in Aqueous Suspension (C,F), and Dry Kaolinite Obtained Using the Spectra-Tech Cylindrical Internal Reflectance Cell.

spectroscopy, and their associated computerized data acquisition systems, is the ability to ratio out (i.e., subtract) individual spectral components, such as the large spectral contribution of water to the kaolinite spectrum shown as curve E in Figure 60. In this example, the hydroxyl stretching bands in the 3600 to 3750 cm^{-1} region of kaolinite cannot be resolved clearly in Figure 60 because of the strong interference of water. However, after the SBES are manipulated using Equation (56) the hydroxyl stretching bands can be resolved clearly.

These data are the first published CIR FT-IR spectra of kaolinite in an aqueous suspension. The band positions of the hydroxyl stretching modes agree well with reported frequencies of the Raman-active hydroxyl stretching modes of KGa-1 kaolinite in aqeous suspension (Reference 2). Based upon these preliminary results, we conclude that this method has considerable potential for observing the FT-IR spectra natural soil constituents in aqueous suspension.

b. Comparison of KGa-1, AP#7, and Fisher Kaolinite FT-IR Spectra

Because the Fisher-brand kaolin sample was used as one of the adsorbents for the vapor phase studies under Tasks 2 and 3, DR FT-IR spectra of KGa-1 kaolinite (Georgia), AP#7 kaolinite (South Carolina), and Fisher kaolin (Georgia or Florida) were obtained to compare the vibrational spectra of the Fisher kaolin sample to the KGa-1 reference clay mineral. In addition, FT-IR spectroscopy provides a sensitive method to detect impurities which may have been present in the raw clay. DR FT-IR spectra of the three kaolinite samples in the 500 to 1200 cm^{-1} region, and 3500 to 3800 cm^{-1} region are shown in Figures 61 and 62. The low frequency DR FT-IR spectrum of the KGa-1 kaolinite (curve A, Figure 61) is very similar to the Fisher kaolin spectrum (curve B, Figure 61). The O-H deformation modes (δ O-H) modes of the KGa-1 kaolinite sample at 915 cm^{-1} and 939 cm^{-1} are resolved better than those of the Fisher kaolin sample. A similar result was obtained for the O-H stretching modes (v O-H) where the 3652 cm^{-1} and 3669 cm^{-1} modes are poorly resolved for the Fisher kaolin sample (curve B, Figure 62) in comparison to the KGa-1 sample (curve A, Figure 62).

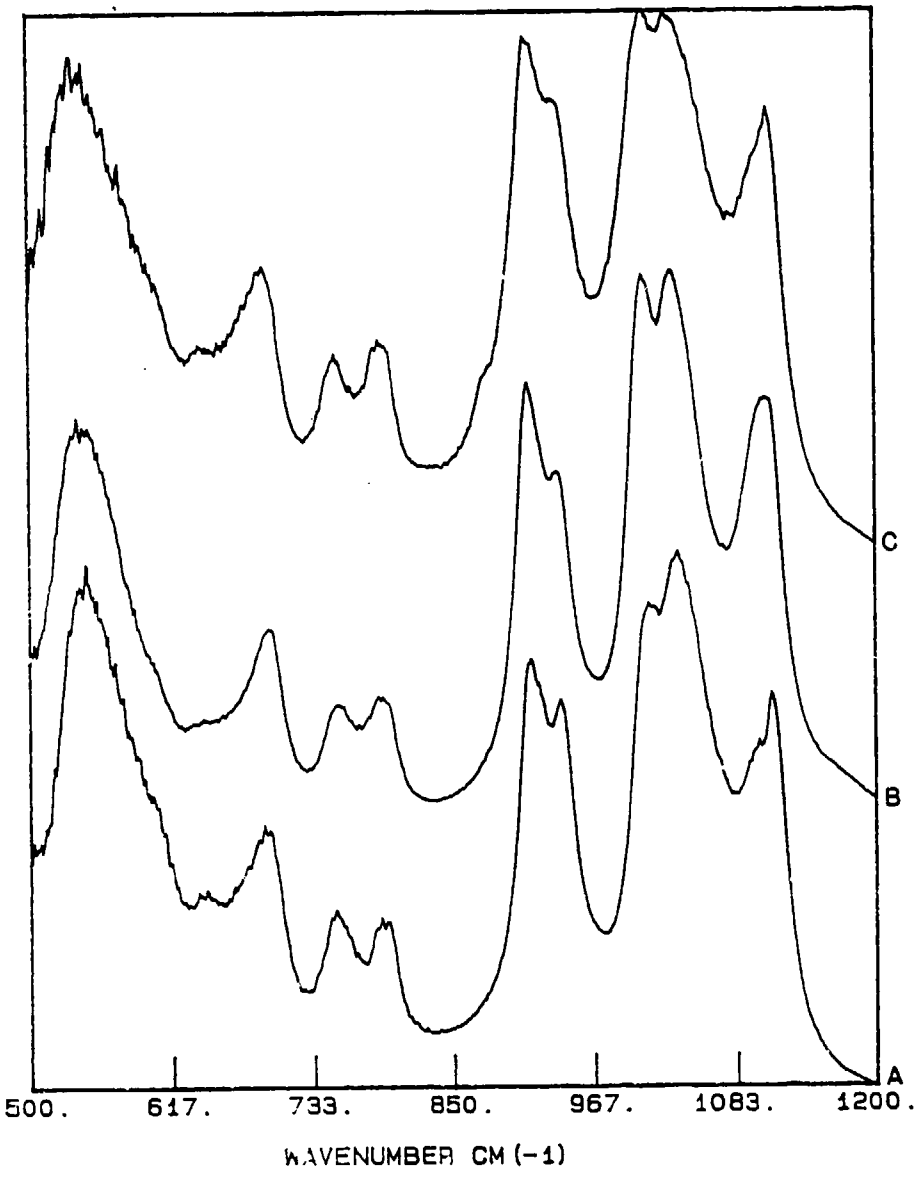

Figure 61. Comparison of Diffuse Reflectance FT-IR Spectra of the KGa-1 Kaolinite (A), Fisher-kaolin (B), and the AP#7 Dixie Pit Kaolinite (C) in the 500 to 1200 cm^{-1} Region.

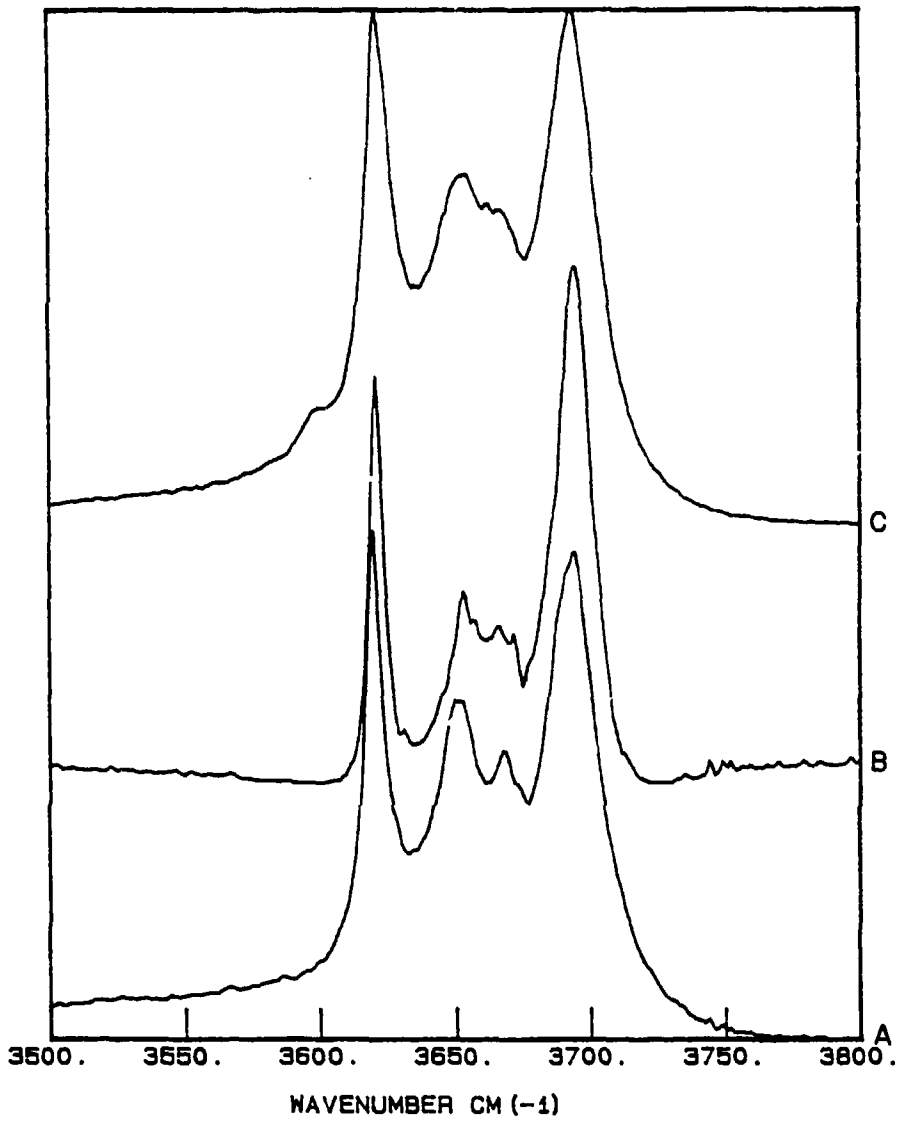

Figure 62. Comparison of Diffuse Reflectance FT-IR Spectra of the KGa-1 Kaolinite (A), Fisher-kaolin (B), and the AP#7 Dixie Pit Kaolinite (C) in the 3500 to 3800 cm^{-1} Region.

These spectral observations suggest that the Fisher kaolin is not as crystalline as the KGa-1 kaolinite. For comparison, DR FT-IR spectra of a poorly crystalline reference clay (AP#7 kaolinite from the Dixie Pit, SC) are shown as curves C in Figures 61 and 62. As the data of this poorly crystalline kaolinite sample indicated, the spectral separation of the δ(O-H) and ν(O-H) modes are less than that observed for either the KGa-1 kaolinite, or the Fisher kaolin. No major impurities were observed in the DR FT-IR spectra of the Fisher kaolin sample, and based upon the FT-IR analysis, the Fisher kaolin sample appears to be slightly less crystalline that the KGa1 kaolinite. It is recommended, however, that the use of this commercial clay be discontinued in future sorption studies because it geologic origin, sample location, and industrial purification procedures are not known.

c. Comparison of Sample Presentation Methods for Montmorillonite

A similar comparison of sample presentation methods was conducted for montmorillonite clay materials in order to evaluate the optimum technique for FT-IR investigations of noninvasive, vapor phase sorption studies on montmorillonite. Survey FT-IR spectra of a Na-exchanged SAz-1 montmorillonite clay sample in the 400 to 4000 cm^{-1} region obtained using TR, DR, and CIR methods are presented in Figure 63. The optical absorbance of the ZnSe crystal does not permit spectral observations to be made below 700 cm^{-1}. A similar restriction applied to the DR spectrum because of the optical transmission properties of the KCl used as the background matrix material.

The highest SNR was observed for the TR spectrum (curve C, Figure 63) in comparison to the DR and CIR spectra. The TR spectrum was obtained by preparing self-supporting clay films of the montmorillonite clay. Initial attempts at preparing the films resulted in films with optical density (OD) values that were too high (OD > 2.5 AU). Upon dilution of the stock clay suspension, thin clay films could be prepared with OD values of less than 2.0 absorbance units (AU). In agreement with the kaolinite results, the TR method resulted in the greatest sensitivity compared to the DR or the CIR methods for vapor phase studies. The spectra are characterized by a broad ν(O-H) band at 3616 cm^{-1}, a structural Si-O and Al-O stretching band centered at about 1040 cm^{-1}, two δ(O-H) modes at 842 $cm^{-1}$and 908 cm^{-1}, and a low frequency structural framework mode at 510 cm^{-1} (observed only in the TR

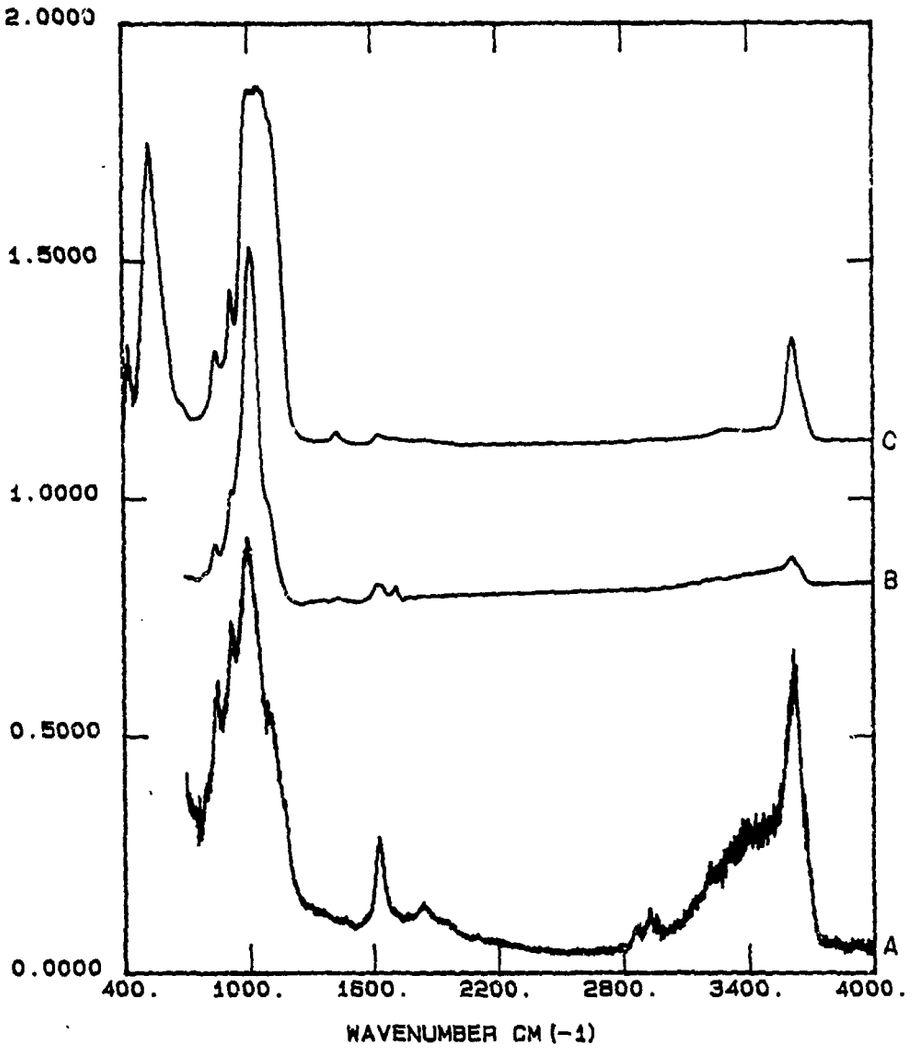

Figure 63. Comparison of FT-IR Spectra of SAz-1 Na-Montmorillonite in the 400 to 4000 cm^{-1} Region Obtained Using the Diffuse Reflectance Cell (A), Cylindrical Internal Reflectance Spectrum of a Thin Self Supporting Clay Film of Montmorillonite in the Controlled Environment Transmission Cell.

spectrum). In addition, the ν(O-H) and δ(O-H) bands of adsorbed water on the Na-exchanged clays were observed at 3280 and 1630 cm^{-1}, respectively. The DR FT-IR spectrum (Curve A, Figure 60) indicated that this sample contained more adsorbed water than the samples used for TR or CIR methods.

The CIR spectrum (Curve B, Figure 63) was obtained by coating the ZnSe internal reflection element with a stock Na-montmorillonite suspension and allowing the suspension to dry which resulted in a thin coating of the montmorillonite clay on the surface of the crystal. In comparison to the TR spectrum, the Si-O and Al-O stretching band is much narrower in the CIR than in the TR spectrum. At present, there is no clear explanation as to why this band is narrower in the CIR spectrum. However, this observation may have an important experimental consequence for adsorbate-clay mineral studies in that adsorbate bands near 1000 cm^{-1} are often obfuscated by the intense SiO-AlO band at 1040 cm^{-1}. Because the intensity of this band is reduced in the CIR spectrum (Curve B, Figure 64), this method may be better for observing adsorbate bands near 1000 cm^{-1} than TR methods. Although the overall sensitivity of CIR is lower than that obtained using TR methods, CIR provides the only suitable method for obtaining FT-IR spectra of solid substrates in aqueous suspension.

The focus of this investigation was to obtain information about the vapor phase adsorbate-surface interactions; consequently, TR sample presentation methods were chosen over CIR and DR methods. At the time of this investigation, a controlled environment diffuse reflectance cell was not available. Several recent articles in the literature, however, have indicated that the sensitivity of CE-DR methods are comparable to that obtained using other methods (References 24,25,26). Because of the spectral reproducibility problems associated with the DR cell, a definitive comparison between the TR and DR methods was not made.

d. Comparison of the SAz-1 Montmorillonite and Fisher Bentonite Spectra

Fisher bentonite was used in Tasks 2 and 3 as one of the mineral absorbents for the vapor phase sorption studies; consequently, one aspect of Task 4 was to compare the FT-IR spectrum of this clay to a reference montmorillonite clay sample. The LR FT-IR spectra of the Fisher bentonite

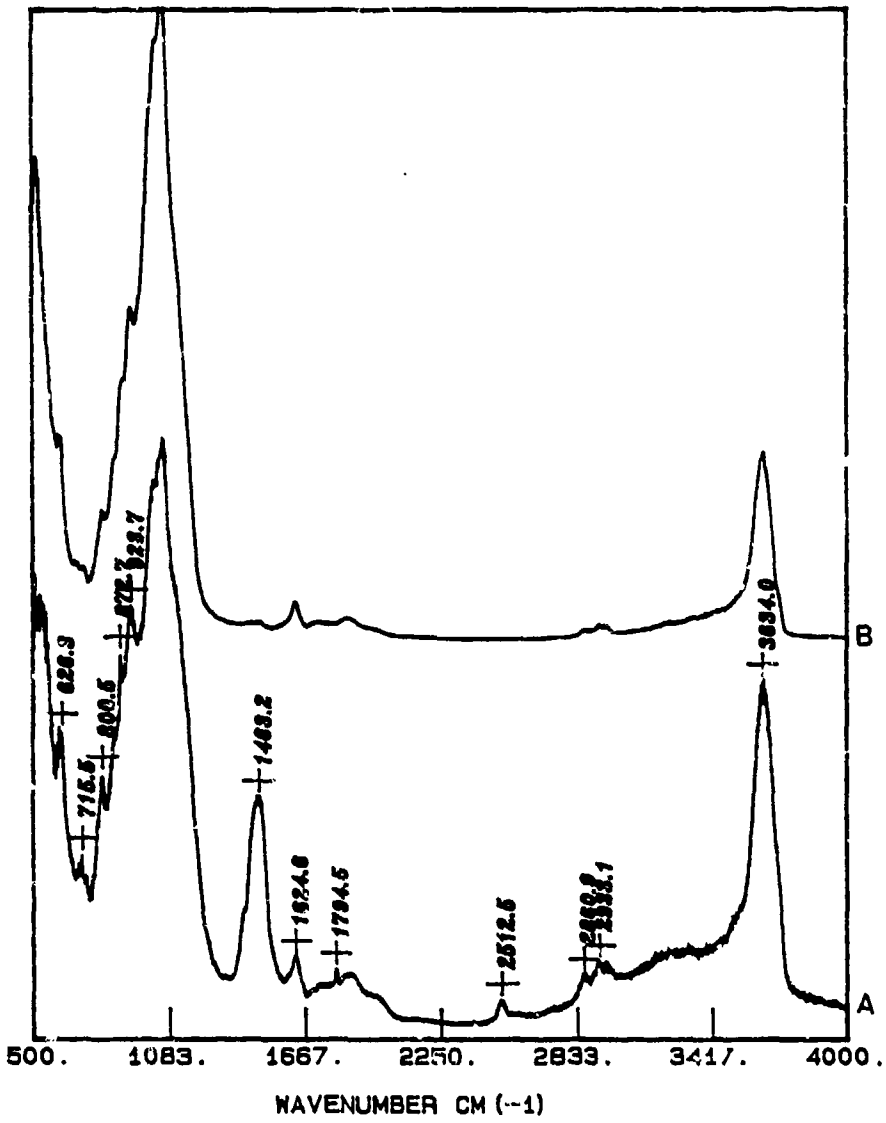

Figure 64. Comparison of Diffuse Reflectance FT-IR Spectra of the SAz-1 Montmorillonite (B) to the Fisher-Bentonite Clay (A) in the 500 to 4000 cm^{-1} Region.

(FB) sample and the SAz-1 sample in the 500 to 4000 cm^{-1} region are compared in Figure 64 (Curves A and B). The spectrum of the SAz-1 montmorillonite is similar to the dispersive IR analysis reported by van Olphen and Fripiat (Reference 1). The band at 1463 cm^{-1} band in the Fisher bentonite spectrum is not observed in the spectrum of the reference montmorillonite and has tentatively identified as a carbonate impurity (Reference 27) . In addition, the Fisher bentonite contains more organic matter evidenced by the v(C-H) bands at 2860, and 2933 cm^{-1}. An additional impurity band was observed in the Fisher bentonite (curve A, Figure 64) at 2512 cm^{-1} which has not been identified.

e. Comparison of Na-, Ca-, and Cu-Exchanged SAz-1 Montmorillonite FT-IR Spectra

Thin, self-supporting clay films (SSCF) were prepared from homoionic clay suspensions containing 0.01M NaCl, $CaCl_2$, $CuCl_2$ salt solutions. FT-IR spectra of the Na-, Ca-, and Cu-exchanged SSCFs (Figures 65-67) were obtained under a vacuum of 10^{-3} torr in order to minimize the interference of adsorbed water from the surface of the clay. The general features of the montmorillonite spectra are in good agreement with the published dispersive IR spectra of montmorillonite samples (References 28,29,30,31). The principal montmorillonite bands occur at 842, 908, 1040, and 3616 cm^{-1}, and the bands of adsorbed water occur at 1630 cm^{-1} and in the 3100 to 3500 cm^{-1} region. The montmorillonite hydroxyl deformation modes (δ(O-H)) occur are observed at 842 and 908 cm^{-1} and have been assigned as Mg-Al-OH and Al_2OH deformation modes, respectively (Reference 10). The low frequency spectra of these three homoionic clay films in the 450 to 1250 cm^{-1} region are very similar (Figure 65). However, significant differences are observed in the TR FT-IR spectra in the 2600 to 3800 cm^{-1} region (Figure 67). The Na-exchanged (Na-X) sample contains much less adsorbed water that the Ca-X or the Cu-X clays. This is consistent with the fact that the hydration energy of Na is much lower than those of Ca^{+2} and Cu^{+2}. In other words, less energy is required to remove water from the Na-X system than for the Ca-X or Cu-X exchangers. Although the integrated intensities of the δ(O-H) band at 1622 cm^{-1} of the adsorbed water on the Ca-X and Cu-X exchangers are approximately equal, which indicated that the amount of water adsorbed by the two clays was about the same, the

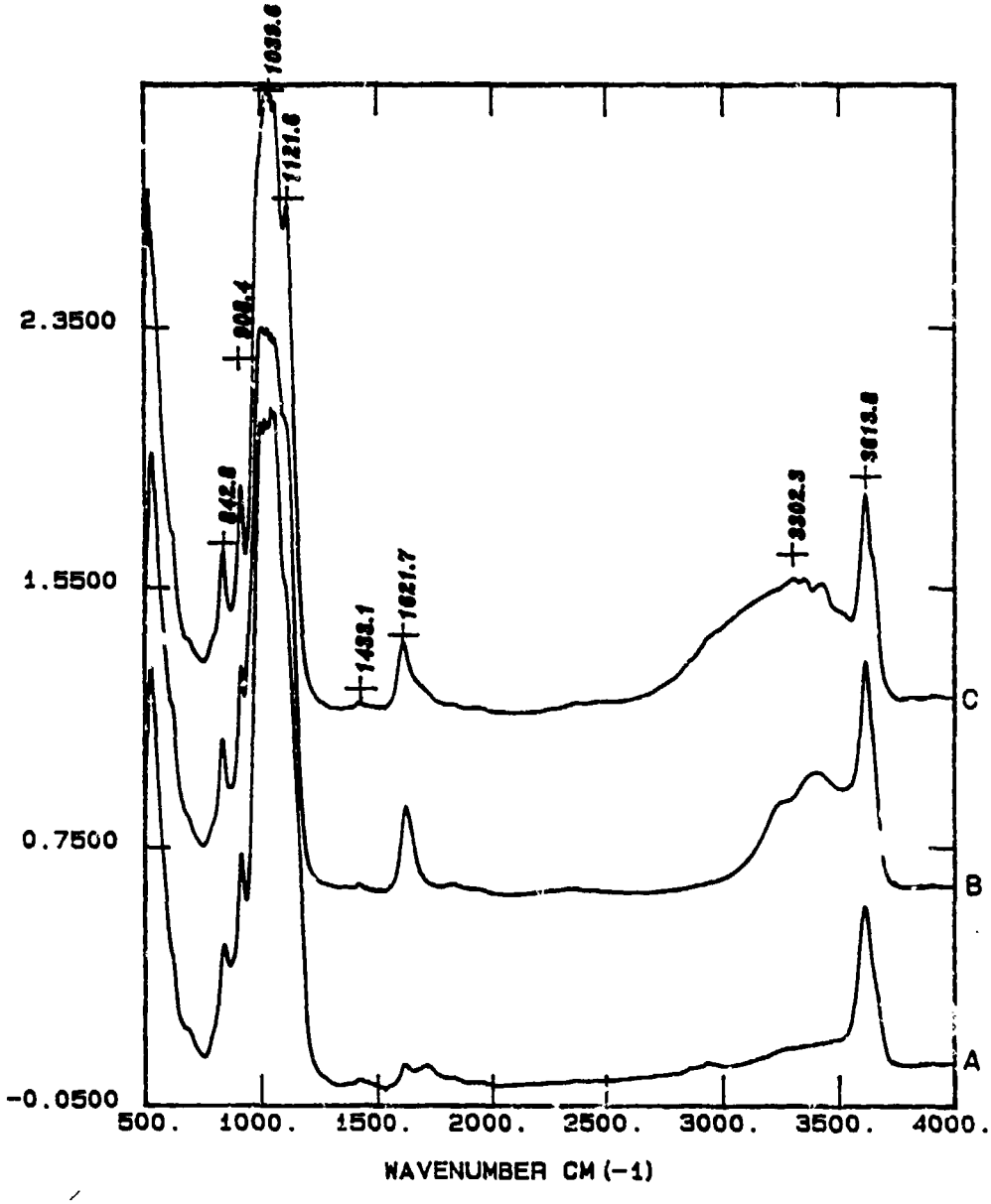

Figure 65. Comparison of Absorbance FT-IR Spectra of Thin Self Supporting Clay Films in the 500 to 4000 cm^{-1} Region of Na-SAz-1 (A), Ca-SAz-1 (B), and Cu-SAz-1 (C).

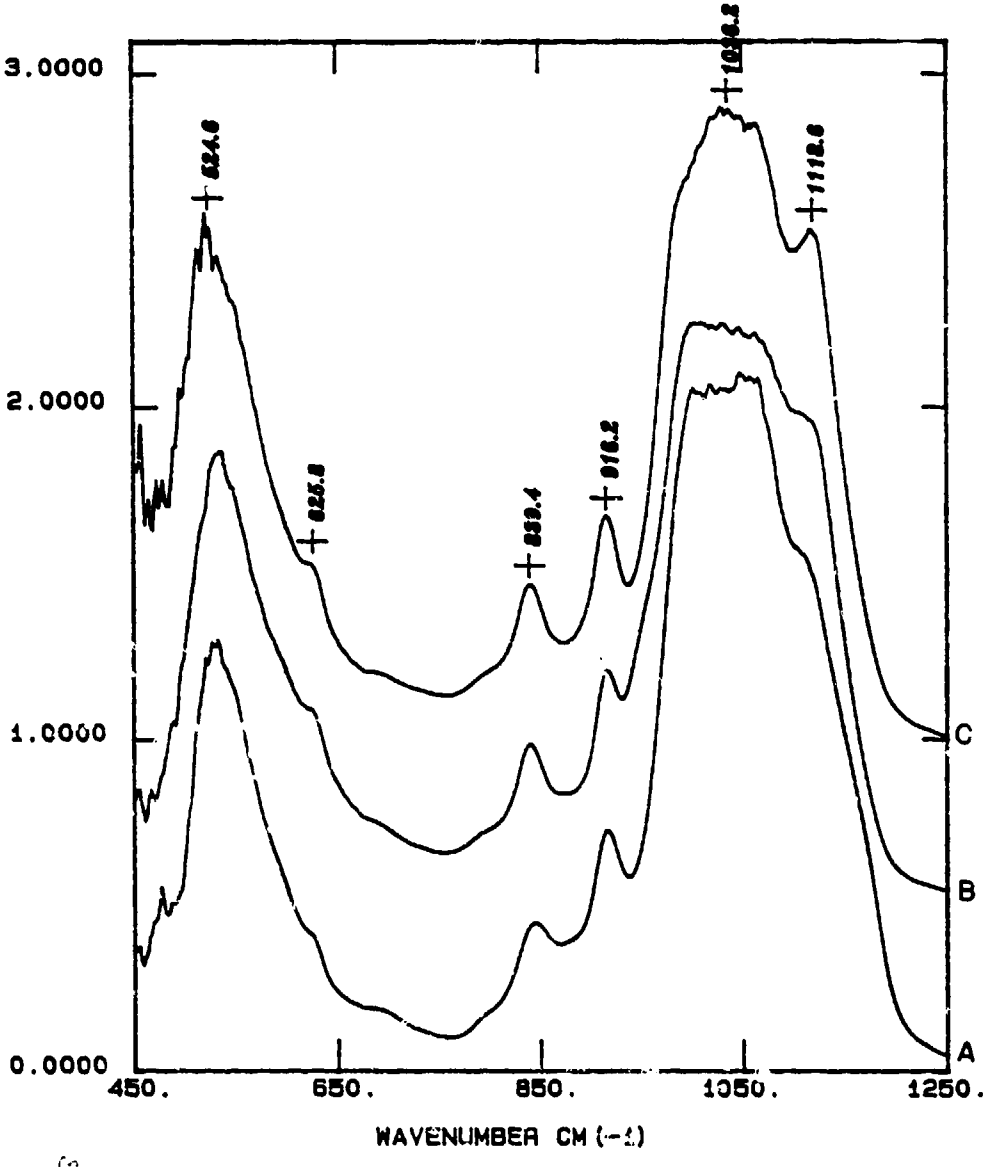

Figure 66. Comparison of Absorbance FT-IR Spectra of Thin Self Supporting Clay Films in the 450 to 1250 cm^{-1} Region of Na-SAz-1 (A), Ca-SAz-1 (B), and Cu-SAz-1 (C).

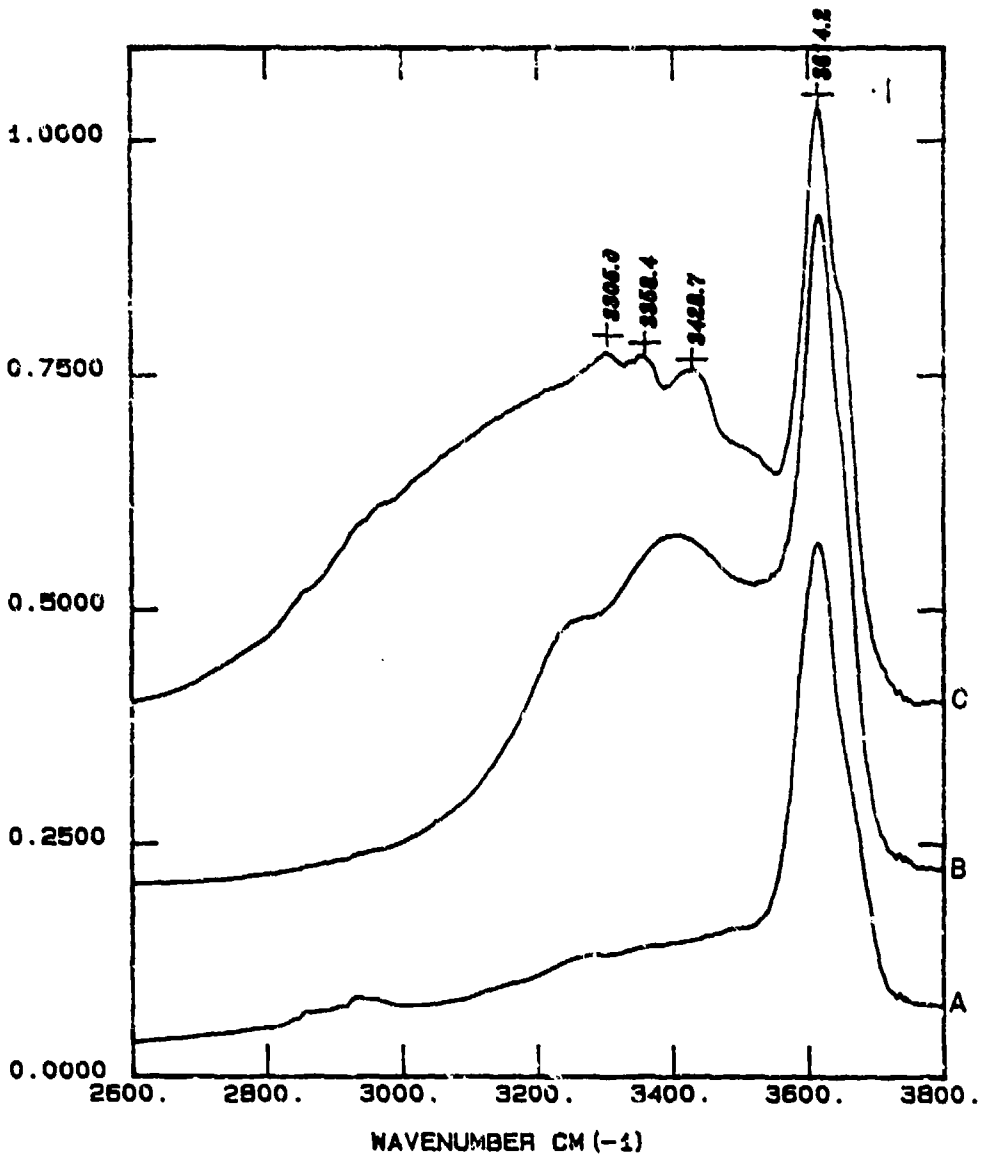

Figure 67. Comparison of Absorbance FT-IR Spectra of Thin Self Supporting Clay Films in the 2600 to 3800 cm^{-1} Region of Na-SAz-1 (A), Ca-SAz-1 (B), and Cu-SAz-1 (C).

vibrational structure in the v(O-H) region of adsorbed water was considerably different (e.g., spectra shown as Curves B and C in Figure 67).

Greater vibrational structure observed for the Cu-X montmorillonite may indicate that the water molecules coordinated to the interlamellar Cu^{+2} ions (aquo complex) are more highly ordered around the metal cation than in the case of the Ca^{+2} - H_2O complex. It has long been recognized (References 32,33,34) that the nature of the exchange complex, i.e., what type of metal cations reside on the surface, strongly influences the behavior of water near the mineral surface. These data support this body of information in that the vibrational spectra of adsorbed water on the surface, and the energy required to remove water from the surface of the clay depend strongly on the type of metal cation on the exchange complex.

The Na-, Ca-, and Cu-X SAz-1 montmorillonite samples investigated in this study were very hydrophillic. Figure 68 shows the TR FT-IR spectra of a dry Cu-X film under a vacuum of 10^{-3} torr in the 400 to 4000 cm^{-1} region (Curve A). The spectrum shown as Curve B in Figure 72 was obtained by exposing the dry film to a 50 percent relative humidity atmosphere for a few minutes. The data indicate clearly that water was adsorbed strongly over a short period of time by the Cu-X montmorillonite as evidenced by the significant increase in the intensity of the adsorbed water bands at 1633 cm^{-1} and 3367 cm^{-1}. The fine structure in the δ(O-H) and v(OH) regions of the spectrum (Curve B, Figure 68) are vibrational modes of water in the vapor phase in contact with the clay. Upon exposing the Cu-X clay film to water vapor, the intensity of structural δ(O-H) modes of the montmorillonite increased substantially relative to the dry spectrum in agreement with a previous IR study of water adsorbed on montmorillonite (Reference 35).

The observed increase in the intensity of structural δ(O-H) modes has been tentatively assigned to the movement of the exchangeable metal cations out of the siloxane ditrigonal cavities on the interlamellar surface of the montmorillonite upon hydration. Upon dehydration of the clay, the interlamellar spacing of the montmorillonite clay decreases from approximately 1.0 nm to less than 0.25 nm. This reduction in the interlamellar d001 spacing forces the metal cations on the exchange complex into the siloxane ditrigonal cavities (Reference 36) which increases the electrostatic repulsion between the structural hydroxyl groups of montmorillonite and the metal cation. It has been proposed (Reference 35) that this increased electrostatic repulsion

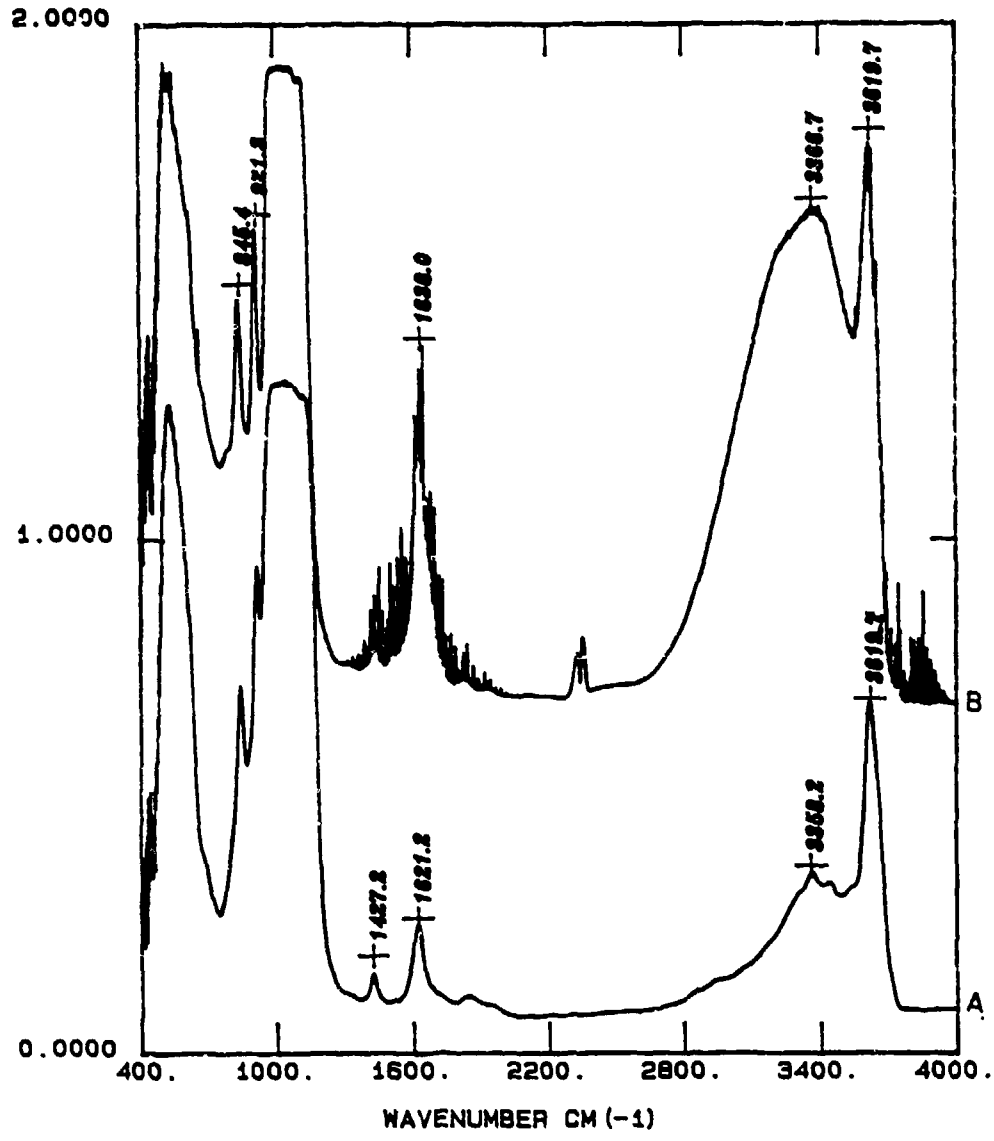

Figure 68. Absorbance FT-IR Spectrum of Thin Self Supporting Clay Films of Evacuated (0.001 torr) Cu-SAz-1 Montmorillonite (A), and the Same Clay Film Exposed to 50 percent Relative Humidity in the 400-4000 cm-1 Region.

results in a decreased the infrared-active cross section of the structural hydroxyl deformation modes. In other words, the induced dipole moment of the O-H bending mode is reduced when metal cations are resident in the siloxane ditrigonal cavity of the dehydrated clay mineral.

In conclusion, the optimum sample presentation method determined from this investigation for noninvasive in-situ vapor phase studies of organic sorption on clay mineral substrates was controlled environment transmission FT-IR spectroscopy. Although the diffuse reflectance (DR) and cylindrical internal reflectance (CIR) methods were shown to provide complementary information, transmission methods were shown to provide the highest spectral resolution and signal-to-noise ratio of the clay mineral samples investigated here.

2. p-Xylene Sorption on Montmorillonite

The final objective of this task was to employ FT-IR spectroscopy to elucidate the chemical mechanisms of p-xylene sorption onto a reference montmorillonite clay mineral. Homoionic clay films of Na-X and Cu-X SAz-1 montmorillonite were prepared with OD values of less than 2.0 AU using the procedures described earlier. Spectral grade p-xylene was used without further purification. Controlled environment (CE) TR FT-IR spectra of p-xylene are shown in Figures 73-75 in the 500 to 4000 cm^{-1}, 700 to 1700 cm^{-1}, and 2800 to 3200 cm^{-1} regions, respectively. The observed band positions of p-xylene (Figures 69-71) agree well the literature values (Reference 37).

The organic adsorbate (p-xylene) was adsorbed onto the clay film by placing approximately 1 mL of p-xylene in the CE-TR cell and allowing the system to equilibrate over a 24 hour period at 1 atmosphere of pressure. Curve A in Figure 72 shows the TR spectrum of a Na-X SSCF prior to the addition of the p-xylene in the 500 to 4000 cm^{-1} region. Curve B in Figure 72 shows the TR spectrum after the clay film was exposed to the organic vapor, plus the residual water vapor in the atmosphere, for a 24 hour period. The broad bands at 1654 and 3471 cm^{-1} indicated that water had been adsorbed on the Na-X sample, in addition, to the organic adsorbate. p-xylene adsorption on the Na-X sample was shown by the p-xylene bands at 793, 1518, 2884, 2993, and 3023 cm^{-1}.

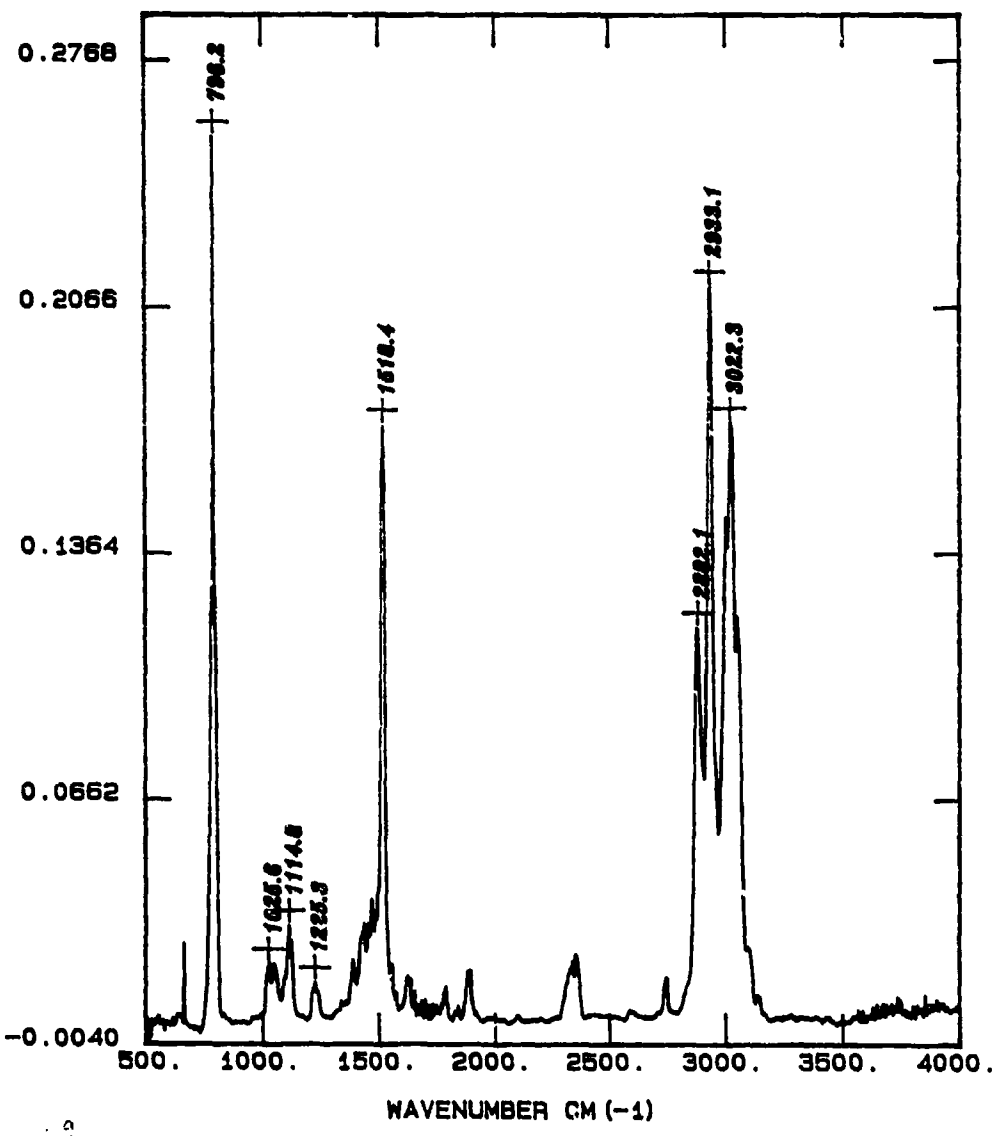

Figure 69. Absorbance Spectra of p-Xylene in the Controlled Environment Cell in the 500 to 4000 cm^{-1} Region.

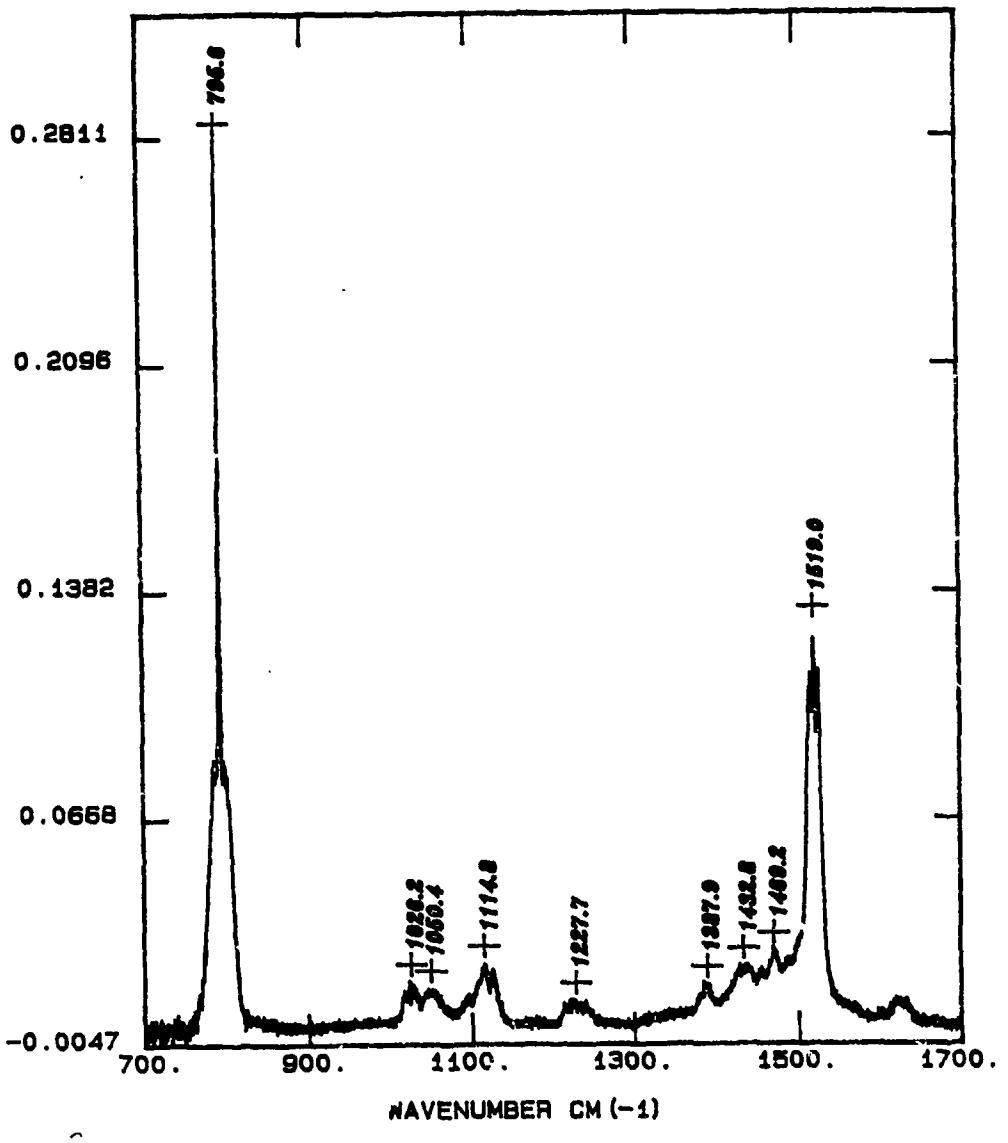

Figure 70. Absorbance Spectra of p-Xylene in the Controlled Environment Cell in the 700 to 1700 cm^{-1} Region.

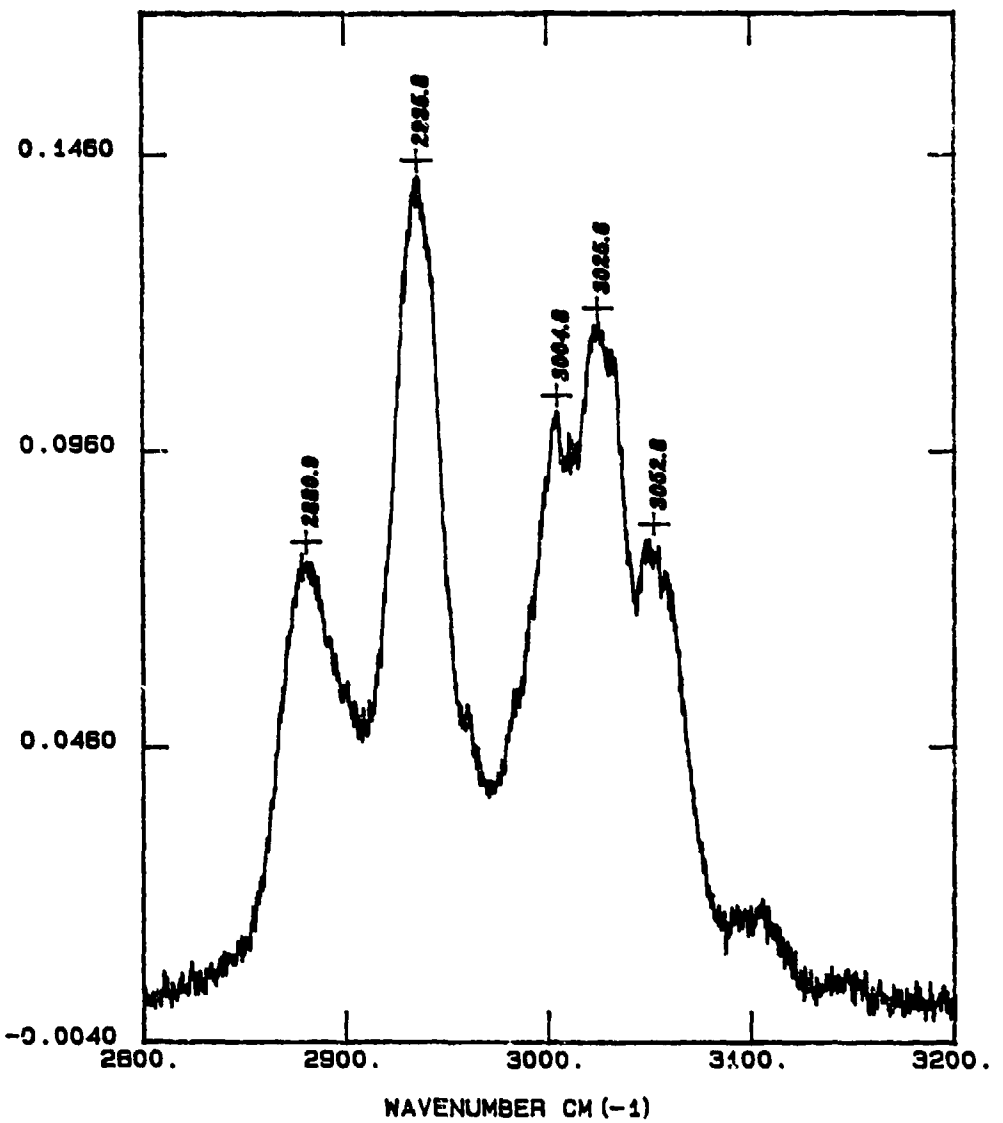

Figure 71. Absorbance Spectra of p-Xylene in the Controlled Environment Cell in the 2800 to 3200 cm^{-1} Region.

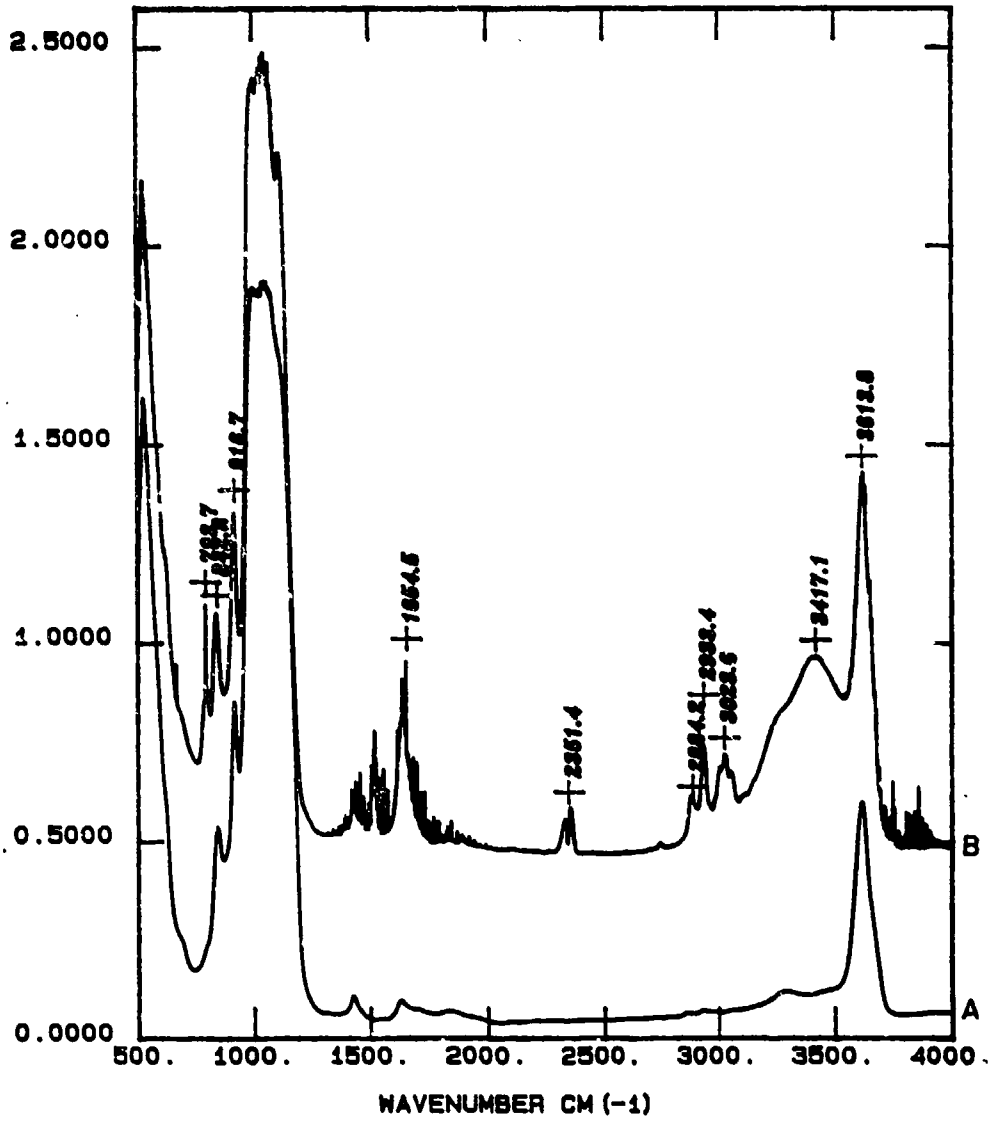

Figure 72. Absorbance Spectra in the 500 to 4000 cm^{-1} Region Obtained in the Controlled Environment Transmission Cell of a Thin Self Supporting Clay Film of Na-SAz-1 Montmorillonite Prior to the Addition of the Organic (A), and the Same Na-SAz-1 Film Exposed to p-Xylene Vapor for 24 Hours (B).

Controlled desorption TR FT-IR spectra of the p-xylene:Na-X complex were obtained by pulling a mild vacuum on the TR cell and allowing the system to come into equilibrium. A stack plot of these spectra are shown in Figure 73 with the equilibrium saturated spectrum shown at the top (Curve J, Figure 73). A successively higher vacuum was applied to the TR cell for each spectrum shown below (Curve J in Figure 73). As a point of reference, the bottom spectrum (Curve A) corresponded to a vacuum of 10^{-7} torr applied to the TR cell for 36 hours. The general features of the controlled desorption study can be summarized as follows:

1. As the pressure decreased in the TR cell, a greater amount of p-xylene was desorbed from the Na-X SSCF.
2. After a prolonged high vacuum was applied to the TR cell, a small amount of the p-xylene remained on the surface of the clay which appeared to be irreversibly adsorbed
3. No evidence for a chemical transformation of the p-xylene on the surface of the Na-X clay was observed. Even after the high vacuum treatment, the chemical identity of the organic adsorbate on the surface of the clay was p-xylene as determined from the TR FT-IR spectra of the adsorbed species.

To illustrate these points, Figure 74 shows the expanded spectral region of three p-xylene:Na-x spectra in the 1300 to 1700 cm^{-1} region: the top spectrum (Curve C) is for the saturated p-xylene:Na-X spectrum shown in Figure 72, the middle spectrum corresponds to the p-xylene:Na-X vacuum exposed to a mild vacuum of 0.1 torr for 1 hour, and the bottom spectrum corresponds to the p-xylene:Na-X complex after the high vacuum treatment of 10^{-7} torr for 36 hours. In other words, the top spectrum (Curve C) corresponded to the beginning, and the bottom spectrum (curve A) shows the clay-organic complex at the end of the experiment. As the bottom TR spectrum indicated (Curve A, Figure 75), a small amount of p-xylene adsorbed on the Na-X clay film remained after the high vacuum treatment which indicates that a small amount of the adsorbate was irreversibly adsorbed. In addition, these spectra also provided clear evidence that a chemical transformation of the adsorbed species did not take place; no "new" bands were observed during or after the high vacuum treatment, and the p-xylene bands of the residual

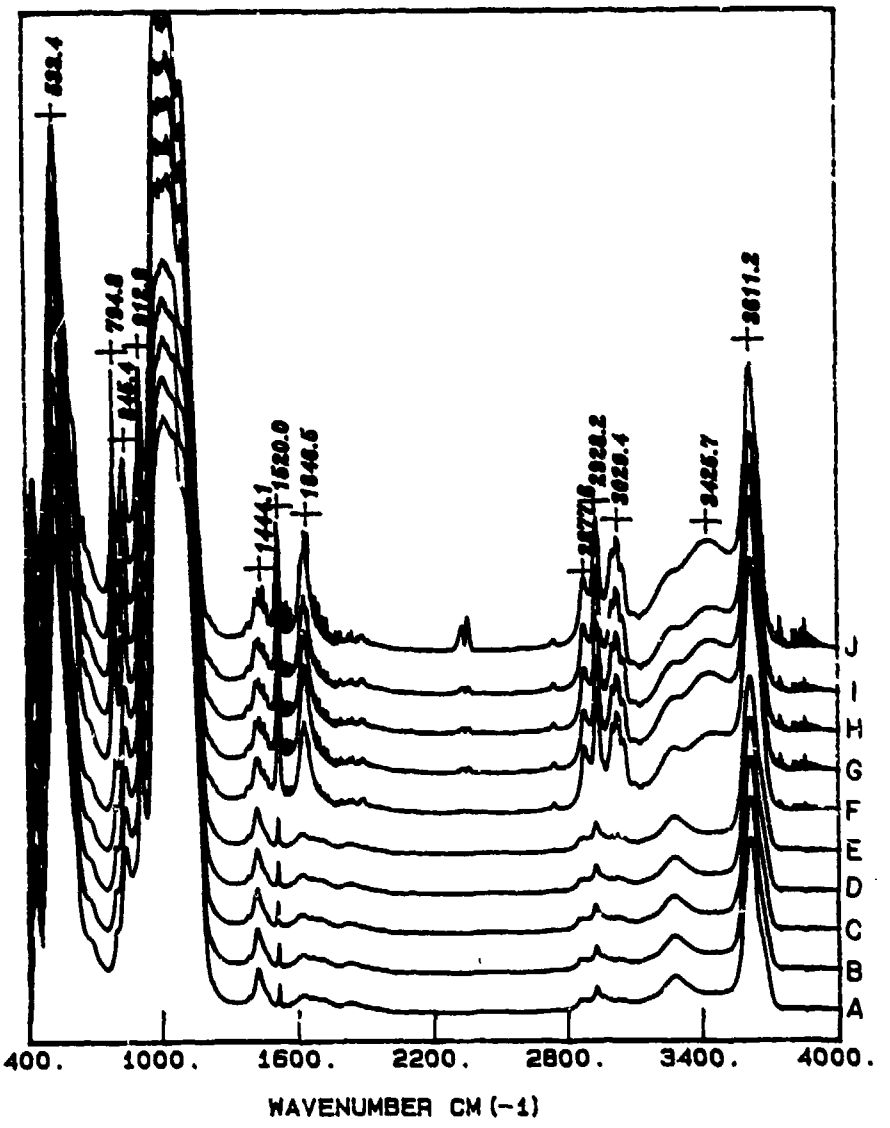

Figure 73. Controlled Desorption Spectra of the p-Xylene: Na-SAz-1 Complex in the 400-4000 cm^{-1} Region. See Text for Complete Description.

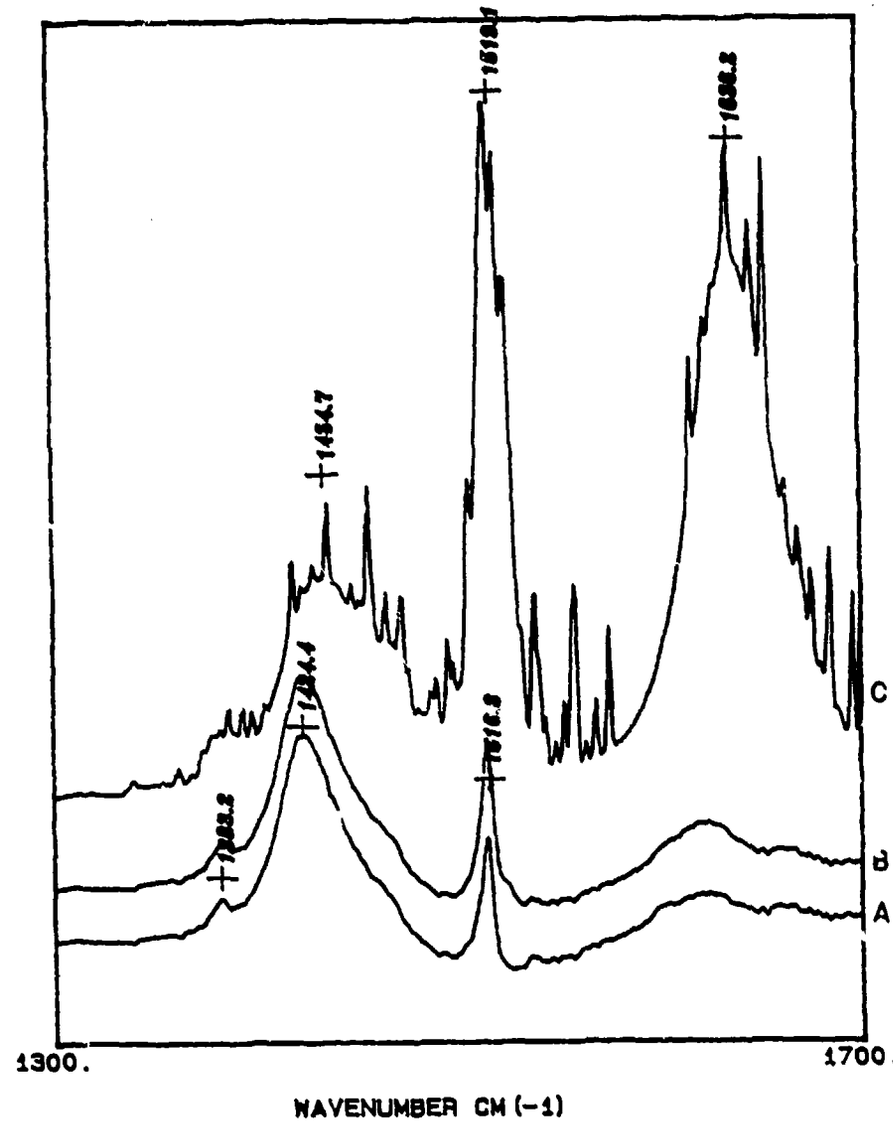

Figure 74. Difference FT-IR Spectra of the p-Xylene:NaSAz-1 Complex Obtained in the Controlled Environment Transmission Cell in the 1300 to 1700 cm^{-1} Region.

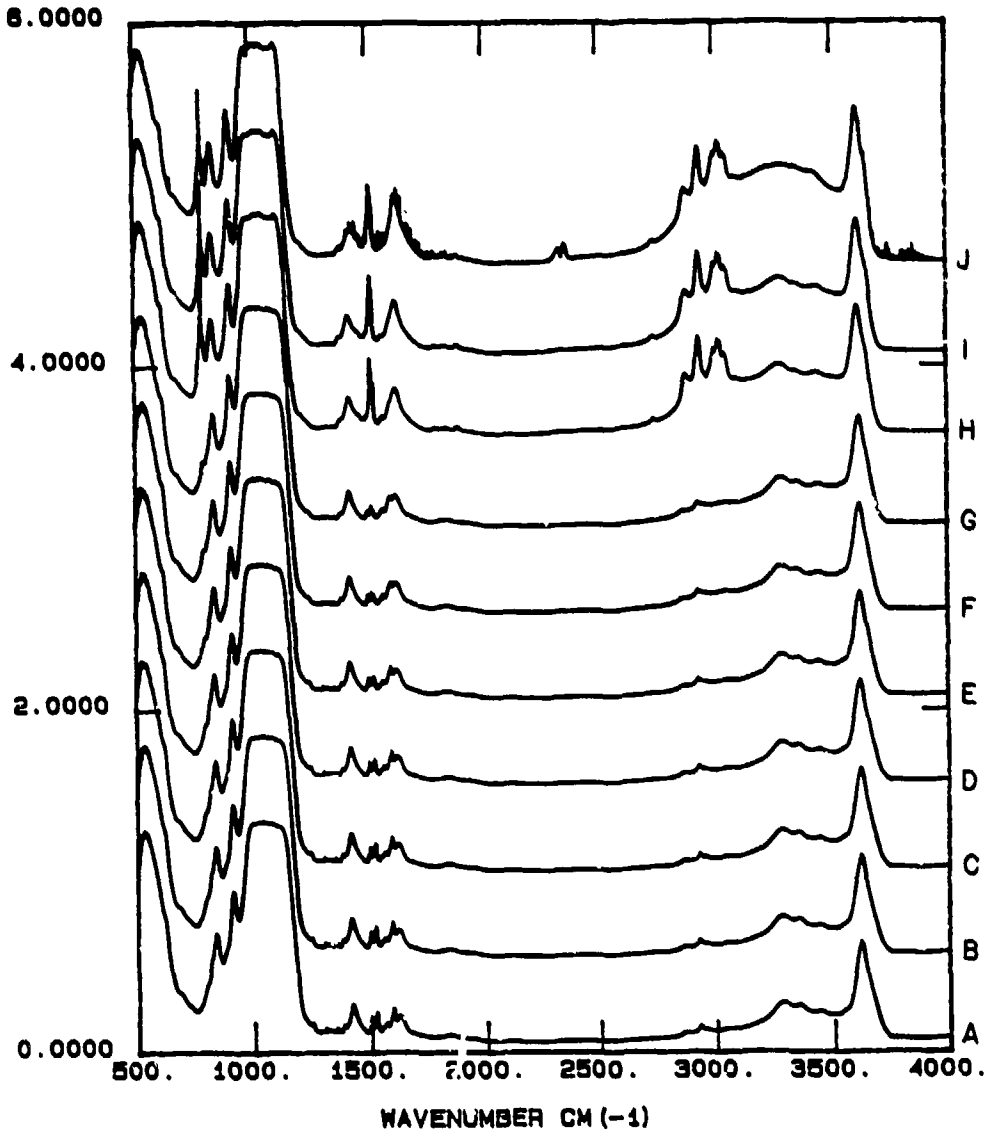

Figure 75. Controlled Desorption Spectra of the p-Xylene: Cu-SAz-1 Complex Obtained in the Controlled Environment Transmission Cell in the 500 to 4000 cm^{-1} Region.

adsorbate were not shifted ignificantly from their initial positions of the physisorbed p-xylene.

A similar controlled desorption study of p-xylene was conducted using a Cu-X SAz-1 SSCF. A stack plot showing the desorption of p-xylene from the Cu-X montmorillonite sample is shown in Figure 75. The data are presented in a similar fashion to the p-xylene:Na-X spectra shown in Figure 73 with the initial scan shown at the top (Curve J) and the final spectrum, after the high vacuum desorption, at the bottom (Curve A). In contrast to the results obtained with the Na-X montmorillonite sample, a chemical transformation of the adsorbed species was observed to occur on the Cu-X film. One obvious indication that a transformation had taken place was the large color change which accompanied the transformation; at the beginning of the desorption study the clay film was translucent with a light blue color, as the end of the desorption study the clay film was opaque and dark brown in color. These observed color changes are in qualitative agreement with previous aromatic adsorption studies on transition metal exchanged montmorillonites (References 38,39,40,41,42).

These spectra are summarized in Figure 76 which compares the spectrum of the initial saturated p-xylene:Cu-X complex at 1 atmosphere (curve C), the final p-xylene:Cu-X spectrum after the high vacuum desorption treatment (Curve B), to the TR spectrum of the Cu-X clay film prior to the addition of p-xylene, i.e., no organic adsorbate present. Upon close inspection of final spectrum (Curve B, Figure 76), a set of "new" bands are present in this spectrum in the 1200 to 1600 cm^{-1} region which were not observed in the p-xylene:Na-X study and that were not present at the outset of this desorption study (i.e., they were not observed in the initial spectrum (Curve C, Figure 76). Based upon this limited evidence, it would appear that the "new" bands resulted from a surface-mediated transformation of the adsorbed p-xylene on the Cu-X montmorillonite sample.

To illustrate these changes more clearly, the single-beam-energy spectra of the controlled desorption study of the p-xylene:Cu-X complex were manipulated using spectral manipulation methods discussed previously. As a point of reference, the absorbance TR spectra (i.e., Ap-xylene on Cu-X) shown in Figure 75 were all ratioed against the SBES empty TR cell (single beam energy spectrum of the empty, evacuated controlled environment cell) according to the following expression:

$$S_{\text{p-xylene on Cu-X}} = \text{SBRS of p-xylene adsorbed on the Cu-X SSCF} \quad (57)$$

$$S_{\text{empty TR cell}} = \text{SBRS of empty, evacuated TR cell} \quad (58)$$

$$A_{\text{p-xylene on Cu-X}} = \log_{10}\left(\frac{S_{\text{empty TR cell}}}{S_{\text{p-xylene on Cu-X}}}\right) \quad (59)$$

To illustrate the appearance of the "new" bands, these same $S_{\text{p-xylene on Cu-X}}$ spectra will now be ratioed against the $S_{\text{Cu-X}}$ spectrum according to the following convention:

$$S_{\text{p-xylene on Cu-X}} = \text{SBES of p-xylene adsorbed on the Cu-X SSCF} \quad (60)$$

$$S_{\text{Cu-X}} = \text{SBES of Cu-X SSCF} \quad (61)$$

$$A_{\text{p-xylene- Dif.}} = \log_{10}\left(\frac{S_{\text{Cu-X}}}{S_{\text{p-xylene on Cu-X}}}\right) \quad (62)$$

Because the vibrational modes of the clay film do not change significantly, this spectral manipulation method highlights only those changes which occur in the vibrational spectra of the adsorbed species. Spectra which have been manipulated according to Equation (62) are presented in Figure 77 in the 1250 to 1750 cm^{-1} region. The top spectrum (curve J) in Figure 77 corresponds to the beginning of the experiment and the observed bands are those of p-xylene. As the p-xylene:Cu-X clay film is exposed to a higher vacuum, a set of "new" bands are observed to grow in intensity as the desorption process proceeds. This observation is in sharp contrast to the p-xylene:Na-X study were no "new" bands were observed during the desorption process and indicates that the Cu^{+2} cation facilitates the chemical transformation.

Detailed FT-IR spectra of aromatic-montmorillonite complexes have not been reported in the literature, however, in a early study of clay-arene complexes by Pinnavaia and Mortland (Reference 43), using dispersive IR methods these authors reported two vibrational modes which were sensitive to the formation of the dark brown complex: the C-C stretch (v19)

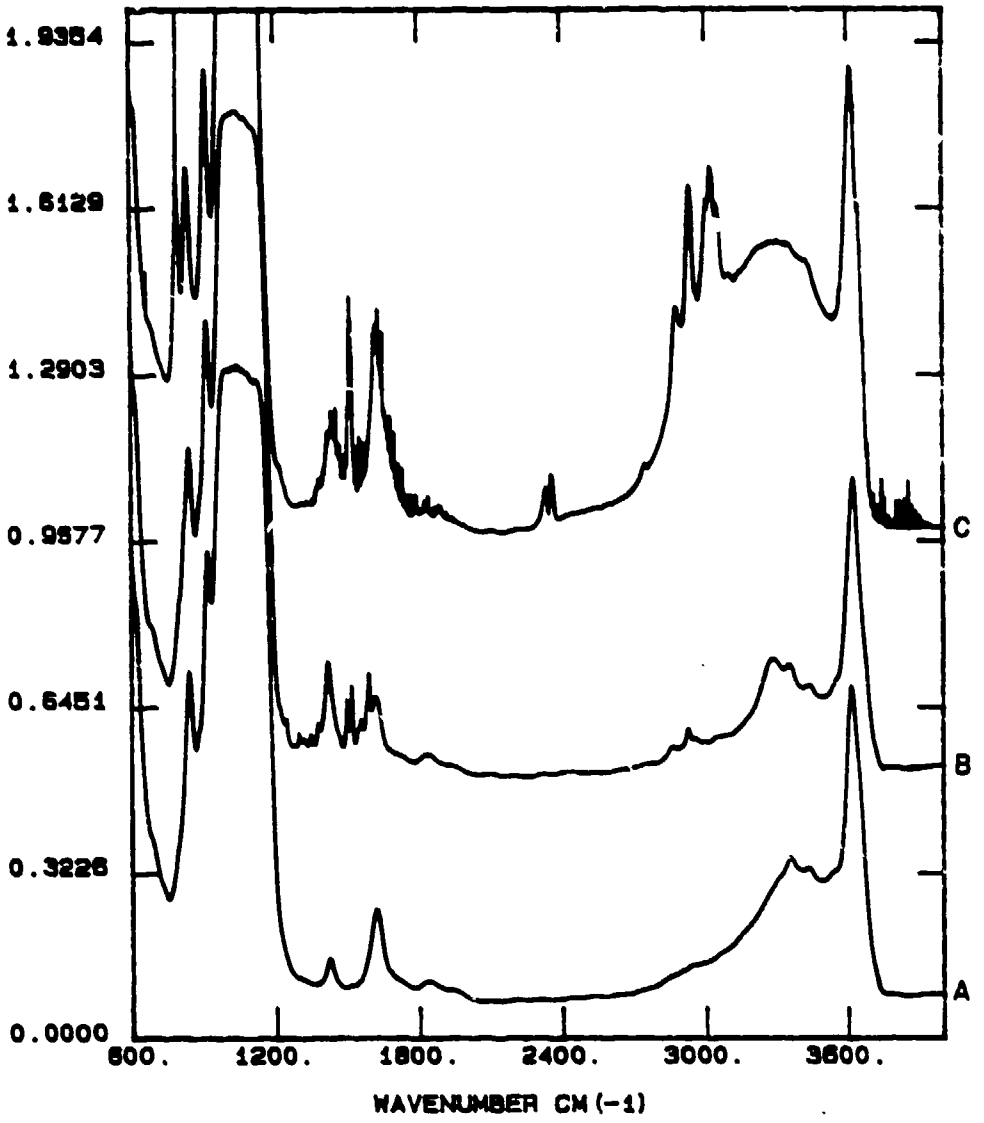

Figure 76. Absorbance FT-IR Spectra of Cu-SAz-1 (A), the p-Xylene:Cu-SAz-1 Complex After the High Vacuum Desorption Treatment (B), and of the p-Xylene: Cu-SAz-1 Complex at 1 atm of pressure (C).

mode p-xylene was reported to shift from 1516 cm^{-1} to 1503 cm^{-1}, and the C-H out-of-plane stretch was observed to shift from 800 cm^{-1} to 817 cm^{-1} upon dehydration of the p-xylene:Cu-X montmorillonite. The results obtained in this investigation of the p-xylene:Cu-X complex are in close agreement with the IR results of Pinnavaia and Mortand (Reference 43). However, in addition to confirming their IR data, a suite of "new" IR-active bands have been observed here which have not been reported previously. This novel observation is attributed to the intrinsically higher sensitivity of FT-IR methods, and to the spectral manipulation capability of FT-IR data acquisition systems.

The bottom spectrum (Curve A) shown in Figure 77 is shown in Figure 78 in the 600 to 1700 cm^{-1} region showing the positions of the residual organic on the surface of the complex after the desorption experiment. In agreement with the results of Pinnavaia and Mortland (Reference 43), "new" bands were observed at 821 and 1501 cm^{-1}. In addition to these bands which confirm the earlier results, a set of new bands were observed at 1248, 1302, 1320, 1354, 1418, 1563, and 1597 cm^{-1}. The chemical identity of the transformed organic adsorbate on the surface of the Cu-X montmorillonite SSCF has not been identified, as yet. However, the application of TR FT-IR methods have provided a sensitive method for observing the formation of the chemisorbed species. The results from the p-xylene:Cu-X study are summarized below:

1. Similar to the p-xylene:Na-X study, water and p-xylene are coadsorbed on the surface of the montmorillonite after the clay film is exposed to p-xylene vapor.
2. A dramatic color change of the clay film occurs as the water is desorbed from the surface of the clay in the presence of the organic vapor. The hydrated p-xylene:Cu-X SSCF is a translucent light blue. Upon dehydration, the film becomes opaque and dark brown in color.
3. A set of new bands in the TR FT-IR spectrum grow in intensity as the desorption process proceeds. The appearance and subsequent growth of these bands accompany the large color change of the SSCF.

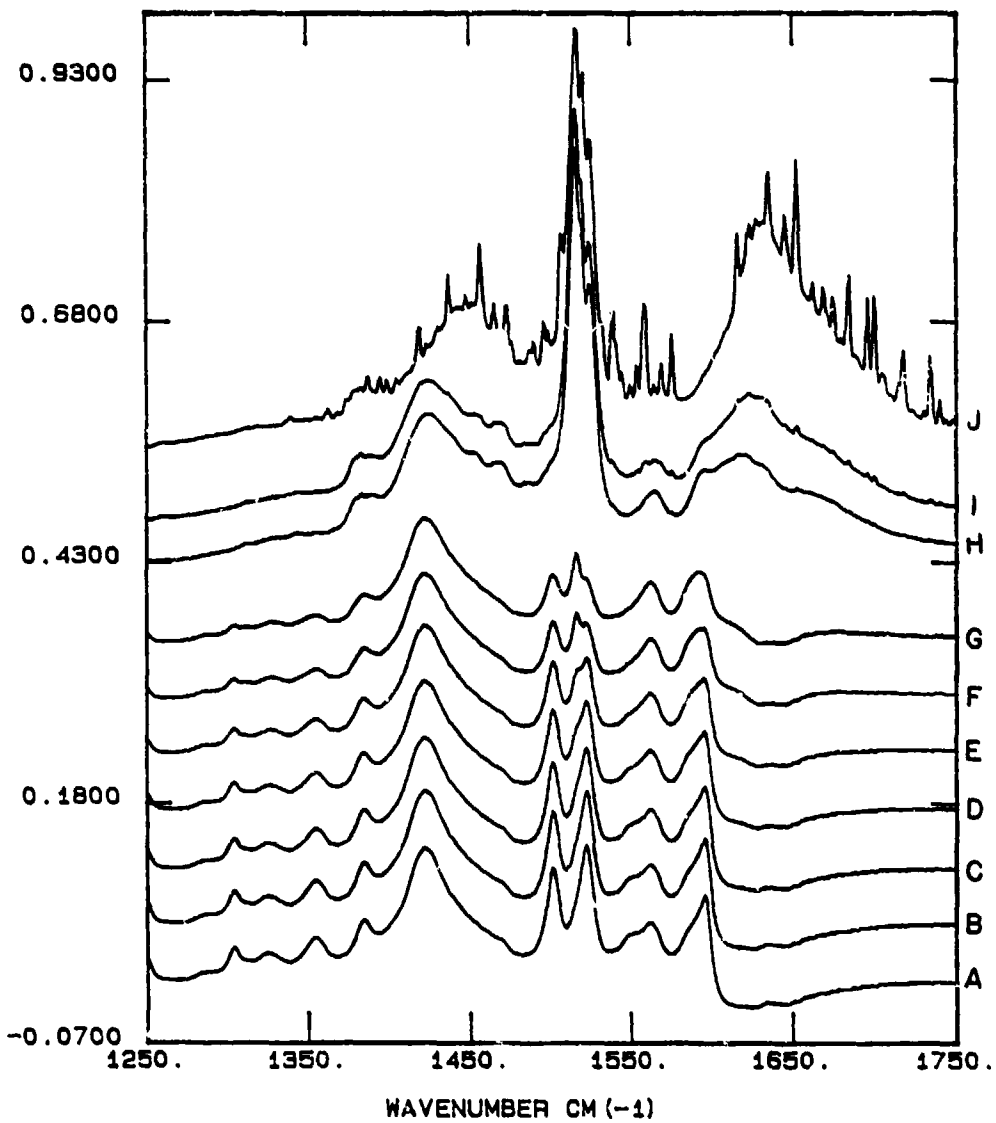

Figure 77. Manipulated Absorbance FT-IR Spectra of the p-Xylene: Cu-SAz-1 Complex Using the Single Beam Energy Spectrum of the Evacuated Cu-SAz-1 Clay Film as the Referenced Spectrum in the 1250 to 1750 cm^{-1} Region.

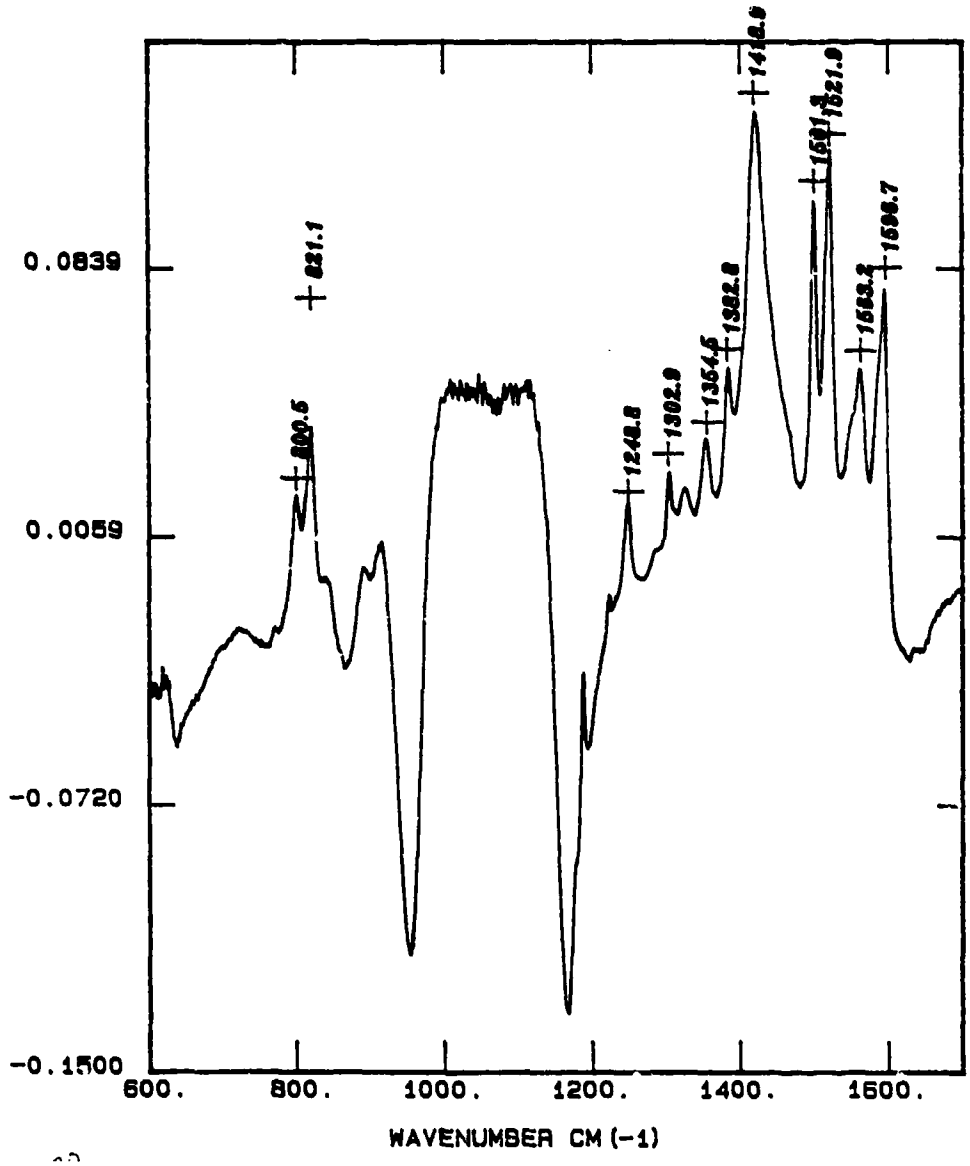

Figure 78. Expanded Manipulated Absorbance FT-IR Spectrum of the Spectrum D23A.

4. The application of TR FT-IR method to the study of the p-xylene complex provided a sensitive in-situ method to observe the surface mediated transformation of the p-xylene on the surface of the Cu-X montmorillonite sample.

In conclusion, these TR FT-IR spectra of p-xylene adsorbed onto Na-X and Cu-X clay films indicated that the role of the transition metal cation on the surface of the clay, and of water in the interlamellar region influenced strongly the adsorption and transformation of p-xylene on mineral surfaces. In the case of the Cu-X clay, a chemical transformation of the p-xylene on the surface of the montmorillonite was observed to take place as water was removed from the system. Although the transformed adsorbate has not been identified as yet, the application of TR FT-IR to this system has resulted in the novel observation of several new bands which have not been reported prior to this study. In contrast to the results obtained for the Cu-X clay, a chemical transformation of p-xylene adsorbed on the surface of the Na-X clay was not observed. Although a small amount of p-xylene was irreversibly adsorbed on the surface of the clay, there was no evidence of a chemical transformation. Thus, the application of FT-IR methods to clay-organic studies appears to have considerable promise with the development of new methods, such as CIR and DR, that are capable of providing noninvasive spectra of natural materials in the presence of liquid water, or water vapor.

C. SUMMARY

Three different Fourier-transform infrared (FT-IR) sample presentation methods were evaluated in order to determine the optimum sampling technique for noninvasive vapor phase adsorption studies on naturally occurring mineral surfaces. FT-IR spectra of clay minerals obtained using diffuse reflectance (DR), cylindrical internal reflectance (CIR), and controlled-environment transmission (CE-TR) presentation methods were compared. It was shown that for noninvasive vapor phase studies of organic sorption on clay mineral substrates the CE-TR method provided the highest signal-to-noise-ratio (SNR) of the three methods. Insofar as these authors are aware, the CIR and DR spectra obtained in this investigation represent the first reported application of these spectroscopic sampling methods to studies of clay minerals or clay-organic complexes. Although the overall sensitivity of the

CIR and DR methods was lower than that obtained using CE-TR, each method was shown to have a unique set of advantages over the other techniques.

CIR FT-IR spectra of kaolinite in aqueous suspension (1 percent w/w) were obtained and compared to the CE-TR, DR, and CIR FT-IR spectra of dry kaolinite. The SNR of the aqueous solution kaolinite spectra were lower than those of the dry kaolinite spectra; however, the specta agreed well with the dry spectra and with previously published Raman and IR data for this clay mineral. In the hydroxyl stretching region the relative intensity of the inner-hydroxyl stretching mode was less for the "wet" kaolinite sample than the "dry" clay. These novel FT-IR spectra of kaolinite in aqueous suspension indicated that this method can be used to observe vibrational modes of natural soil constituents in aqueous suspension.

The DR FT-IR spectra of Fisher-brand kaolin and bentonite clay minerals were compared to those of several reference clay samples of montmorillonite and kaolinite obtained from the Clay Mineral Repository and the American Petroleum Institute. The crystallinity of the Fisher kaolin sample was found to be less than that of the KGa-1 kaolinite sample based upon the spectral resolution of the 3650 cm^{-1} and 3668 cm^{-1} hydroxyl stretching bands. A similar observation was made for the hydroxyl deformations bands at 915 cm^{-1} and 939 cm^{-1}; greater resolution and separation of these bands were observed for the KGa-1 reference clay than for the Fisher kaolin which indicated that the crystallinity of the KGa-1 kaolinite clay was greater than that of the Fisher sample. No major impurities were observed in the Fisher kaolin sample. The DR FT-IR spectra of the Fisher bentonite sample, however, did not agree well with that of the reference SAz-1 montmorillonite clay. Several inorganic impurity bands were reported and the sample was observed to have a higher organic matter content. It was recommended that the use of Fisher clay mineral samples as sorbents be discontinued in future investigations of organic sorption because the information on sample location, genesis, and industrial purification procedures used for these clay minerals were not known. In addition, there is very little information available about the physical properties of these clay minerals such as their cation exchange capacities, chemical analyses, and specific surface area.

In a controlled desorption study of p-xylene from the surface of a Na-exchanged (Na-X) SAz-1 montmorillonite sample, it was shown that a small amount of the adsorbate was irreversibly adsorbed by the montmorillonite clay.

After the initial addition of p-xylene to the CE-TR cell, p-xylene and water vapor were adsorbed on the surface of the montmorillonite clay film. The data indicated that more water was adsorbed by the clay film than p-xylene. Although this material was not removed after pulling a high vacuum of 10^{-7} torr for 36 hours, the CE-TR FT-IR data indicated clearly that the p-xylene was not transformed on the surface. In particular, a significant shift in the ν_{19} (C-C str) mode of p-xylene was not observed.

A similar study was conducted using a Cu-exchanged (Cu-X) SAz-1 clay film instead of the Na-X film. After a mild vacuum was applied to the CE-TR cell, the TR FT-IR data indicated that both water vapor and p-xylene were removed from the surface of the Cu-X clay film. As the water content of the clay film decreased, a drastic change in the clay film color was observed, and, in addition, a suite of new bands appeared that grew in intensity in the CE-TR FT-IR spectra as the desorption process continued. These results were in agreement with the earlier dispersive-IR spectroscopic study of Pinnavaia and Mortland (Reference 43); however, the data presented here showed a number of "new" bands of the adsorbed species that have not been reported previously. This observation was attributed to the fact that FT-IR methods are intrinsically more sensitive than dispersive techniques. The spectral data indicated that a new surface species was formed as evidenced by the new bands in the CE-TR spectra. Although the transformed surface species has not yet been identified, these in situ spectra of the p-xylene: Cu-SAz-1 complex have shown that surface-mediated chemical transformations of adsorbed organic species on mineral surfaces can be obtained using this method in conclusion, the application of noninvasive FT-IR methods, such as CE-TR, DR, and CIR, to the study of organic sorption on naturally occurring mineral surfaces in the presence of liquid water, or water vapor have considerable promise.

D. REFERENCES

1. van Olphen, H., and Fripiat, J. J., Data Handbook for Clay Materials and Other Non-metallic Minerals, Pergamon Press, Oxford, 1979, 346 pp.

2. Johnston, C. T., Sposito, G., and Birge, R. R., "Raman Spectroscopic Study of Kaolinite in Aqueous Suspension," 1985, Clays and Clay Min., Vol. 33, pp. 483-489.

3. Sposito, G., Holtzclaw, K. H., Johnston, C. T., and LeVesque-Mador, C. S., "Thermodynamics of Sodium-copper Exchange on Wyoming Bentonite at 298K," 1981, Soil Sci. Soc. Am. J., Vol. 45, pp. 1079-1084.

4. Forman, M. L., Steele, W. H., and Vanasse, G. A., "Correction of Aymmetric Interferograms Obtained in Fourier Spectroscopy," 1966, J. Opt. Soc. Am., Vol. 56, pp. 59-63.

5. Forman, M. L., "Fast Fourier-transform Technique and Its Application to Fourier Spectroscopy," 1966, J. Opt. Soc. Am., Vol. 56, pp. 978..

6. Forman, M. L., "Spectral Interpolation: Zero Fill or Convolution," 1977, Appl. Opt., Vol. 16, pp. 2081.

7. Brindley, G. W., Kao, C. C., Harrison, J. L., Lipsicas, M., and Raythatha, R., "Relation Between Structural Disorder and Other Characteristics of Kaolinites and Dickites," 1986, Clays and Clay Minerals, Vol. 34, pp. 239-249.

8. Snyder, R. W., Painter, P. C., and Cronauer, D. C., "Development of FT-IR Procedures for the Characterization of Oil Shale," 1983, Fuel, Vol. 62, pp. 1205-1214.

9. Snyder, R. W., Painter, P. C., Havens, J. R., and Koenig, J. L., "The Determination of Hydroxyl Groups in Coal by Fourier Transform Infrared and ^{13}C NMR Spectroscopy," Appl. Spect., 1983, Vol. 37, pp. 497-501.

10. Farmer, V. C., The Infrared Spectra of Minerals, V. C. Farmer (ed.), Mineralogical Soc., London, 1974, 469 pp.

11. Plancon, A., and Tchoubar, C., "Determination of Structural Decects in Phyllosilicates by X-ray Powder Diffraction-I. Principle of Calculations of the Diffraction Phenomenon," 1977, Clays and Clay Min., Vol. 25, pp. 430-435.

12. Barnes, R. B., and Bonner, L. G., "The Christiansen Filter Effect in the Infrared," 1936, Phys. Rev., Vol. 49, pp. 732-740.

13. Prost, R., "The Influence of the Christiansen Effect on IR Spectra of Powders," 1973, Clays and Clay Min., Vol. 21, pp. 363-368.

14. Fuller, M. P., and Griffiths, P. R., "Diffuse Reflectance Measurements by Fourier Transform Spectrometry," 1978, Anal. Chem., Vol. 50, pp. 1906-1910.

15. Willey, R. R., "Fourier Transform Infrared Spectrophotometer for Transmittance and Diffuse Reflectance Measurements," 1976, Applied Spectroscopy, Vol. 30, pp. 593-601.

16. Messerschmidt, R. G., "Complete Elimination of Specular Reflectance in Infrared and Diffuse Reflectance Measurements," 1985, Applied Spectroscopy, Vol. 39, pp. 737-739.

17. Hamadeh, I. M., Yeboah, S. A., Trumbull, K. A., Griffiths, P. R., "Preparation of Calibration Standards for Quantitative Diffuse Reflectance Infrared Spectroscopy," 1984, Applied Spectroscopy, Vol. 38, pp. 486-491.

18. Griffiths, P. R., and de Haseth, J. A., "Fourier Transform Infrared Spectrometry," ACS Monograph Chemical Analysis, Vol. 83, John Wiley and Sons, 1986.

19. Brackett, J. M., Azarraga, L. V., Castles, M. A., and Rogers, L. B., "Matrix Materials for Diffuse Reflectance Fourier Transform Infrared Spectrometry of Substances in Polar Solvents, 1984," Anal. Chem., Vol. 54, pp. 2007-2010.

20. Tejedor, M. I., and Anderson, M. A., "In Situ Attenuated Total Reflection Fourier Transform Infrared Studies of the Goethite- Aqueous Solution Interface," 1986, Langmuir, Vol. 2, pp. 203-210.

21. Winters, S., Gendreau, R. M., Leininger, R. I., and Jakobsen, R. J., Fourier Transform Infrared Spectroscopy of Protein Adsorption from Whole Blood: II. Ex Vivo Sheep Studies," 1982, Applied Spectrosocpy, Vol. 36, pp. 404-409.

22. Kellner, R., and Gotziner, G., "FTIR-ATR Spectroscopic Analysis of the Protein Adsorption on Polymer Blood Contact Surfaces," 1984, Mikrochimica Acta, Vol. 2, pp. 61-74.

23. Gendreau, R. M., "Biomedical FTIR Spectroscopy: Application to Proteins" in: Spectroscopy in the Biomedical Sciences, R. M. Gendreau (ed.), CRC Press, Boca Raton, Florida, 1986.

24. Graf, R. T., Koenig, J. L, and Ishida, H., "Characterization of Silane Treated Glass Fibers by Diffuse Reflectance Fourier Transform Spectroscopy," 1984, Anal. Chem., Vol. 56, pp. 773-778.

25. Culler, S. R., McKenzie, M. T., Fina, L. J., and Ishida, H., "Fourier Transform Diffuse Reflectance Infrared Study of Polymer Films and Coatings: A Method for Studying Polymer Surfaces," 1984, Applied Spectroscopy, Vol. 38, pp. 791-795.

26. Hamadeh, I. M., King, D., and Griffiths, P. R., "Heatable-evacuable Cell and Optical System from Diffuse Reflectance FT-IR Spectrometry of Adsorbed Species," 1984, J. of Catalysis, Vol. 88, pp. 264-272.

27. Nakamot, K., Infrared and Raman Spectra of Inorganic and Coordination Compounds, John Wiley & Sons, New York, 1978, 448 pp.

28. Sposito, G. and Prost, R., "Structure of Water Adsorbed on Smectites," 1982, Chemical Reviews, Vol. 82, pp. 553-573.

29. Sposito, G., Prost, R., and Gaultier, J. P., "Infrared Spectroscopic Study of Adsorbed Water on Reduced Charge Na/Li-montmorillonites," 1983, Clays and Clay Min., Vol. 31, pp. 9-16.

30. Prost, R., "Etude de l'hydration des argiles: Interactions Equ-mineral et Mecanisme de la Retention de l'eau," 1975, Ann. Agron., Vol. 26, pp. 401-461.

31. Farmer, V. C., and Russell, J. D., "Interlayer Complexes in Layer Silicates. The Structure of Water in Lamellar Ionic Solutions," 1971, Trans. Farad. Soc., Vol. 67, pp. 2737-2749.

32. Mooney, R. W., Keenan, A. G., and Wood, L. A., "Adsorption of Water Vapor by Montmorillonite. I. Heat of Desorption and Application of BET Theory," 1952, J. Amer. Cham. Soc., Vol. 74, pp. 1367-1371.

33. Mooney, R. W.c Keenan, A. G., and Wood, L. A., "Adsorption of Water Vapor by Montmorillonite. Effect of Exchangeable Ions and Lattice Swelling as Measured by X-ray Diffration," 1952, J. Amer. Chem. Soc., Vol. 74, pp. 1371-1374.

34. Sposito, G., and Prost, R., "Structure of Water Adsorbed on Smectites," 1982, Chemical Reviews, Vol. 82, pp. 553-573.

35. Sposito, G., Prost, R., and Gaultier, J. P., "Infrared Spectroscopic Study of Adsorbed Water on Reduced Charge Na/Li-montmorillonites," 1983, Clays and Clay Min., Vol. 31, pp. 9-16.

36. Sposito, G., Chapter 1 in The Surface Chemistry of Soils, Oxford University Press, New York, pp. 234.

37. Green, J. H. S., "Vibrational Spectra of Benzene Derivatives, VI p-disubstituted compounds," 1970, Spect. Acta., Vol. 26A, pp. 1503-1513.

38. Fenn, D. B., Mortland, M. M., and Pinnavaia, T. J., "The Chemisorption of Anisole on Cu(II) hHctorite," 1973, Clays and Clay Min., Vol. 21, pp. 315.

39. Moreale, A., Cloos, P., and Badot, C., "Differential Behavior of Fe(III)- and Cu(II)-montmorillonite with Aniline: I. Suspensions with Constant Solid:Liquid Ratio," 1985, Clay Minerals, Vol. 20, pp. 29.

40. Mortland, M. M., and Halloran, L. J., "Polymerization of Aromatic Molecules on Smectite," 1976, Soil. Sci. Soc. Am. J., Vol. 40, pp. 367-369.

41. Pinnavaia, T. J., Hall, P. L., Cady, S. S., and Mortland, M. M., "Aromatic Radical Cation Formation on the Intracrystal Surfaces of Transition Metal Layer Silicates," 1974, J. Phys. Chem., Vol. 78, pp. 994-999.

42. Rupert, J. P., "Electron Spin Resonance Spectra of Interlamellar Copper(II)-arene Complexes on Montmorillonite," 1973, J. Phys. Chem., Vol. 77, pp. 784-789.

43. Pinnavaia, T. J., and Mortland, M. M., "Interlamellar Metal Complexes on Layer Silicates. I. Copper(II)-Arene Complexes on Montmorillonite," 1971, J. Phys. Chem., Vol. 75, pp. 3957-3960.